Universitat de Barcelona

Facultat de Química

Departament d'Enginyeria Química i Metal·lúrgia

REACTIVITY OF ACID GAS POLLUTANTS WITH $Ca(OH)_2$ AT LOW TEMPERATURE IN THE PRESENCE OF WATER VAPOR

Marta Bausach Mercader

Barcelona, April 2005

Programa de Doctorat d'Enginyeria Química Ambiental

Bienni 1998-2000

Memòria presentada per na Marta Bausach Mercader, Llda. en Química.

Marta Bausach Mercader

La present Tesi Doctoral ha estat realitzada en el Departament d'Enginyeria Química i Metal·lúrgia sota la direcció dels Profs. Drs. J.F. Izquierdo Torres i Fidel Cunill i Garcia, qui n'autoritzen la presentació.

Prof. Dr. J.F. Izquierdo Torres Prof. Dr. Fidel Cunill Garcia

Barcelona, abril del 2005

1. Introduction

1.1. AIR POLLUTION LEGISLATION: HISTORICAL EVOLUTION

The demand of higher standard of living, together with the growing population throughout the world has led to a dramatic increase of the industrial activity in recent times. This situation has resulted in a massive rise of the pollutants released to the atmosphere, water and soil, altering their composition, and consequently evolving into many harmful effects on the environment and on human health.

Although environmental problems did not become an important issue of world interest until the last century, some historic events show that the concern for the effect of certain man-made activities on human health began some centuries ago. Under the reigns of Richard II (1377-1399) and Henry V (1413-1422), England took steps to regulate and restrict the use of coal by taxation and regulation of its movement in London. In 1661, a pamphlet entitled *"Fumifugium or The Inconveniences of Air and Smoke"*, written by John Evelyn, was published by the Royal Command of Charles II to propose remedies for London's air pollution problem, such as moving industry to the outskirts of town and establishing green belts around the city. However, none of these proposals were implemented *(Mycock et al., 1995; [www.radford.edu]).*

In the first half of the 20th century, some air pollution episodes were responsible for the death or disease of thousands of people. These facts proved the need to recognize air pollution as a serious environmental problem and to take action against it. In this way, four events should be emphasized: the first large-scale survey of air pollution in the USA (Salt Lake City, 1926); the first air pollution control bureau in the USA (1947); the first international air pollution conference, called *Los Angeles Air Pollution Control District* (1955); and the first Conference on Environment organized by United Nations (Stockholm, 1972) *(Vesilind et al. 1988; Mycock et al., 1995; [www.radford.edu]; [www.ametsoc.org]).* The American Environmental Protection Agency (EPA) in the USA and other environmental institutions in Great Britain and Germany were pioneers in the elaboration of a legislative framework aimed at combating pollution and protecting environment.

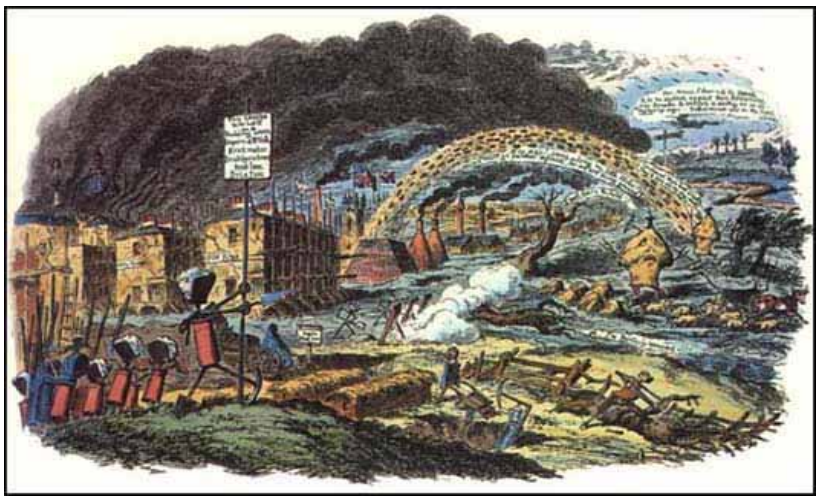

London going out of Town. G. Kruikshank (1829). The caricaturist was opposed to the building of houses on the green fields of Islington and Kilburn.

In 1955, the federal government of the USA decided that legislation dealing with air pollution needed to be implemented at national level. The result was the *Air Pollution Control Act (1955)*, which despite doing little to prevent the air from pollution, it made the nation more aware of the environment. Eight years later, the North-American Congress passed the nation's *Clean Air Act (1963)*, which dealt with a reduction of air pollution by setting emission standards for stationary sources. A further major revision was made later in the *Clean Air Act (1970)*, which established new primary and secondary standards for ambient air quality, set new limits on emissions from stationary and mobile sources, and increased funds for air pollution research. Again, the environmental legislation was revised in 1990 because of the growing political concern on the subject. The *Clean Air Act (1990)* addressed five main areas: air quality standards, motor vehicle emissions and alternative fuels, toxic air pollutants, acid rain, and stratospheric ozone depletion. In many ways, this law set out to strengthen and improve the existing regulations. Consequently, at least every five years, EPA must review the air quality standards with assistance and advice from the EPA's Clean Air Scientific Advisory Committee (*Mycock et al. 1995, Brownell et al., 1998; [www.ametsoc.org]*).

Air pollution became a political concern in the European Union later than in the USA, although some European countries had already individually established some environmental laws. The first significant piece of European air quality legislation was enacted in the early 1980s (*Directive 80/779/EEC* amended by *89/427/EEC*), which covered sulfur dioxide (SO_2) and total suspended particles, as main components of the urban smog (*Colls, 1997*). Limit values of lead (Pb) and nitrogen dioxide (NO_2) were also legislated in the 1980s (*82/884/EEC; 85/203/EEC*). As air pollution became more and more a problem in some European cities and the USA studies provided with alarming results regarding the link between air pollution and health effects, the European Commission developed the framework directive *96/62/EC* on ambient air quality assessment and management. For the first time, the Directive lays down common rules and principles for setting limit values, which are based on WHO guidelines on human health effects, as well as for the assessment and the management of air quality throughout the EU (*[www.eeb.org]*).

Nowadays, slightly over than half of the air pollution comes from the internal combustion engines of cars and other motor vehicles, roughly 25% of it comes from fuel burned at stationary sources such as power-generating plants, and another 15% is emitted from industrial processes (*Mycock et al., 1995*). In recent decades, many efforts have been made to reduce air pollution in the industrialized parts of the world, particularly by improving the technologies. However, many more have to be made in short and medium-term to foresee some factors such as greater industrial production, weak regulations in certain countries of the world, and an increase in the number and annual mileage of cars on the road.

1.2. ACID GAS POLLUTANTS: SO_2, NO_2 AND HCl

Traditionally, both North-American and European air pollution legislation focused significantly on ***acid rain*** or ***photochemical smog***, because of their harmful effects on the environment and on human health. Although acid rain can be originated from the direct emission of strong gaseous acids,

such as HCl, most of it is produced by the atmospheric oxidation of acid-forming gases such as the formation of H_2SO_4(aq) and HNO_3(aq) from sulfur dioxide (SO_2) and nitrogen dioxide (NO_2), respectively. The major contributor to acid precipitation is typically the SO_4^{2-} anion, while the NO_3^- and Cl^- anions present a smaller contribution (*Vesilind et al. 1988; Manahan, 1994*).

On the other hand, the photochemical smog is a photochemically oxidant atmosphere consisting of a mixture of hundreds of different and hazardous chemical compounds (e.g., ozone and Peroxyacetyl nitrate –PAN). Its formation is determined by the presence of NO_x and volatile organic compounds (VOCs) and solar radiation (*Vesilind et al. 1988; Manahan, 1994*).

Photochemical smog and acid gases can cause several damages to human and animal health, as irritation of the respiratory system, eyes and skin. Moreover, they are also responsible for some metabolic miss-functions in plants and for the deterioration of some building materials, as well as a reduction of visibility in polluted cities (*Vesilind et al., 1988; Buonicore and Davis, 1992; [www.epa.gov]*).

1.2.1. SULFUR DIOXIDE (SO_2)

Power stations that burn sulfur-containing fossil fuels (coal and oil) constitute the main source of sulfur dioxide (SO_2) emission. The sulfur content of fossil fuels can be either organically bounded or present in an inorganic form like pyrite. Some industrial processes (e.g., nonferrous smelters, oil refining and pulp for paper manufacture and incinerators) also produce SO_2, although the amount of their emissions is lower than that in power stations.

The increasing use of coal during the 20th century resulted in a dramatic increase of world SO_2 emission, from 4 Mt in 1860 to 160 Mt in 1980, and it is still rising, being currently ca. 200 Mt (*Colls, 1997*). However, as can be seen in Fig. 1.1, the evolution of SO_2 emissions varies from different world regions. Meanwhile SO_2 emissions have been reduced in the USA and Europe in the last decades (by 45% from 1975 to 2002 and 60% from 1980 to 1997, respectively) and tend to level out at present time, those in developing countries are steadily going up (mainly in the Asiatic Pacific countries). According to recent World Bank projections, SO_2 emissions in Asia will be greater than those of North America and Europe combined by the first decade of the XXIst century, unless substantial investments in pollution control equipment are made (*Downing et al., 1997*).

Reductions of SO_2 emissions in the EU and in the USA have been achieved in the last decades by the accomplishment of their respective legislation. In the USA, the current regulation is under *Title IV SO_2 program* (*Clean Air Act, 1990*), which is based on a system of SO_2 emission allowances, which impose a limit on total SO_2 emission from the electric utility industry. An allowance is an authorization, allocated to an affected unit, to emit one ton of SO_2 during a period of time, which can be freely traded among facilities subject to the program. Most of the units that began commercial operation after 1990 had to acquire allowances in the market *(Brownell et al., 1998)* and today the SO_2 allowance market is one of the most active trade markets. In the EU, the emissions of SO_2 were significantly reduced since

the enactment of the Directives *80/779/EEC* and *88/609/EEC*. Higher reductions are expected by the accomplishment of the current Directive *2001/80/EC*, which is specifically restrictive in the limitation of SO_2 emission from large combustion plants (summarized in Table 1.1 for solid and liquid fuels).

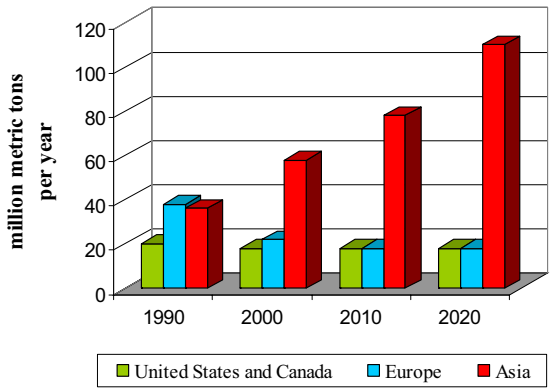

Fig. 1.1: SO_2 emissions in Europe, United States/Canada and Asia (*[www.wri.org]*).

Table 1.1: SO_2 limit emissions for large combustion plants (*Directive 2001/80/EC*).

TYPE OF PLANT	*LIMIT*
Existing solid/liquid-fuel burning plant > 500 MWth	142 ppm
Existing solid-fuel burning plant 50 –700 MWth	710-142 ppm*
Existing liquid-fuel burning plant 50 –500 MWth	603-142 ppm*
New solid-fuel burning plant (excepting biomass) > 100 MWth	71 ppm
New solid-fuel burning plant (excepting biomass) 50-100 MWth	301 ppm
New biomass burning plant	71 ppm
New liquid-fuel burning plant > 300 MWth	71 ppm
New liquid-fuel burning plant 100-300 MWth	142-71 ppm*
New liquid-fuel burning plant 50-100 MWth	302 ppm

* linear decrease

1.2.2. NITROGEN DIOXIDE (NO_2)

A small proportion of the nitrogen dioxide (NO_2) present in the atmosphere is emitted directly from combustion in stationary and mobile sources. The remainder is formed basically in the atmosphere mainly by the photooxidation of NO with ozone. Combustion always produces a mixture of NO and NO_2, collectively known as NO_x, with a typical composition of 90-95% NO and 10-5% NO_2. NO_x are formed in the combustors basically by two ways: the oxidation of atmospheric N_2 at high temperatures (***thermal NO_x***), and the oxidation of chemically bounded nitrogen contained in coal and oil (***fuel NO_x***).

The level of NO_x emitted from stationary sources such as power plant furnaces generally falls within the range of 50-1000 ppm (*Manahan, 1994; Colls, 1997*).

In the 1990s, anthropogenic NO_x in mobile sources constituted the half or more of the total NO_x emitted in developed countries, while electric utilities ranked second, which emissions came basically from coal-fired power plants. Because of a worldwide increasing number of vehicles, a raise on world NO_x emission is expected. In fact, some data provided by the EPA show that since 1970, NO_x constitutes the only of the six priority air pollutants -CO, Pb, NO_x, particulate matter, SO_2 and VOC's- which emissions have increased in the USA, up to 10% until now (*Manahan, 1994; Colls, 1997; [www.epa.gov]; [www.wri.org]*).

The European and North-American legislation against NO_x emissions in large combustion plants are becoming progressively stricter. In the EU, current emission limit values are regulated by the *Directive 2001/80/EC*, while in the USA, the Acid Rain program of the *Clean Air Act Amendments (1990)* provides different emission limits for different types of boilers. The required control technologies by EPA are not generally more stringent than the "low NO_x burner" technology or other ones that are comparable in terms of cost *(Brownell et al., 1998).* Regarding the regulation of mobile source air pollution, both the EU and the USA have specific legislation, which are proceeding down similar courses of increasingly stringent emission standards *(Colls, 1997).*

1.2.3. HYDROGEN CHLORIDE (HCl)

Hydrogen chloride (HCl) is mainly generated from the combustion of chlorinated organic compounds (e.g., polyvinyl chloride (PVC) or polychlorinated biphenyls (PCBs)), although it can be also formed during the combustion of fossil-fuels containing chlorides. High levels of gaseous HCl can therefore be found in waste gases from urban waste combustion -with typical concentrations of 400-1000 ppmdv for uncontrolled emissions-, hazardous waste incineration, and coal-fired boilers *(Buonicore and Davis, 1992; Manahan, 1994; Chisolm and Rochelle, 2000).* HCl emissions in waste incinerators (together with those of other acid gases like SO_2) are restricted by the accomplishment of the "*New Source Performance Standards and Emissions Guidelines for Existing Facilities"* issued by the EPA (1991) under the *Clean Air Act (1990).* In the EU, the accomplishment of the new *Directive 2000/76/EC,* which covers gas emissions of waste incineration plants, is expected to lead to remarkable reduction of acid gases emissions (HCl, NO_x and SO_2).

1.3. ACID GAS EMISSION CONTROL METHODS: AN OVERVIEW

In general terms, pollutant gas emissions from coal-fired boilers are substantially higher than those from oil-fired ones, and natural gas is practically regarded as a clean fuel. Hence, little or no control of the emissions is usually required in natural gas and in small or medium oil power plants. Many of the air-pollution control systems applied in coal-fired boilers can be implemented in waste

incinerators, because of their similarities and the coincidence of the gaseous pollutants involved. The technological alternatives to reduce acid gases from a stationary source can be grouped in the following way:

1. Switching or cleaning the fuel
2. Combustion control methods
3. Post-combustion control methods

Methods 1 and 2 are directed toward solving the problem at the source, namely controlling the generation of the pollutant, while the third option is focused on its retention after its generation.

1.3.1. SWITCHING OR CLEANING THE FUEL

In some cases, switching the fuel has been an efficient alternative for reducing SO_2 emissions, since the amount of SO_2 formed is almost entirely dependent on the sulfur content of the fuel. However, local natural resources -and hence costs- currently dictate the choice of a type of fuel. This fact explains that coal, in spite of its high pollutant potentiality, is still by now one of the most common primary energy sources in the world (25% in 2002). Oil and natural gas contribute, respectively, to a 37 and 24% to the total world consumption as primary energy (*De Nevers, 1998; [www.bp.com]*). An option for using high-sulfur coals is to employ a cleaning process to reduce the sulfur content in the fuel. Although particles with mineral sulfur such as pyrite -FeS_2- can be partially removed by physical separation techniques, the removal of organic sulfur requires chemical processes, which are costly and complex (*Buonicore and Davis, 1992; Manahan, 1994; De Nevers, 1998*).

Switching the fuel is not regarded as an effective option for reducing NO_x emissions, since the amount of fuel NO_x is usually lower compared to thermal NO_x. Moreover, although fuels with different content of organically bounded nitrogen can be found, low-N fuels convert nitrogen into NO_x more efficiently than high-N fuels *(Buonicore and Davis, 1992; Colls, 1997*).

1.3.2. COMBUSTION CONTROL METHODS

On contrary to NO_x emissions, SO_2 and HCl emissions are generally neither affected by burner design nor by boiler operation *(Buonicore and Davis, 1992)*. However, coal gasification is an available technology that reduces SO_2 emissions, since sulfur is transformed into hydrogen sulfide (H_2S), which can be captured by means of specific technologies *(De Nevers, 1998; [fossil.energy.gov]).*

1.3.3 POST-COMBUSTION CONTROL METHODS

Several different methods have been developed in the past to remove SO_2 from combustion gases before they are exhausted to atmosphere. Nowadays, a great number of scrubbing systems, referred in the literature as ***Flue Gas Desulfurization*** processes **(FGD)**, are well-established technologies that can be found in coal-fired industrial boilers, coke calciners and catalyst regenerators. Furthermore, their use is currently extended towards the retention of other gaseous acid pollutants such as HCl, so that scrubbing processes can be also installed in incinerators, aluminum furnaces fluxed with chlorine and regenerators for chlorinated solvent drums *(Brown, 1998)*. Although NO_2 can be also effectively retained by these technologies, the amount of NO removed by them is negligible. Since the predominant nitrogen oxide species in stack gases is NO, scrubbing systems are not feasible to control NO_x, at least in their basic forms.

Scrubbing systems to remove SO_2 and HCl from flue gases take advantage of the acid character of these compounds to retain them. All of them are based on the addition of alkaline solid sorbents, so that neutralization of the acid compounds takes place with the formation of solids as reaction products. The solid products -sulfites, sulfates and chlorides- have a much lower pollutant capacity than that of their precursors (SO_2 and HCl). As the neutralization reaction is enhanced by the presence of water, many of these flue gas cleaning technologies also introduce it in the process.

In Fig. 1.2, the main units of a power plant or incinerator is indicated together with the typical temperatures: (1) furnace, where the temperature is kept in the range of 1050-1450 K; (2) particulate collector, usually fabric filters or electrostatic precipitators, where fly-ashes are collected, as well as unreacted reagents and reaction products in case of using FGD technologies; (3) waste flue gas duct, which lead exhaust gases from the furnace to the chimney being cooled along it until 343-353 K. The different FGD processes, which can be broadly classified into wet and dry scrubbing, can be implemented at different parts of a plant (see Fig. 1.2). A summary of the most significant features of each of them is collected in Table 1.2.

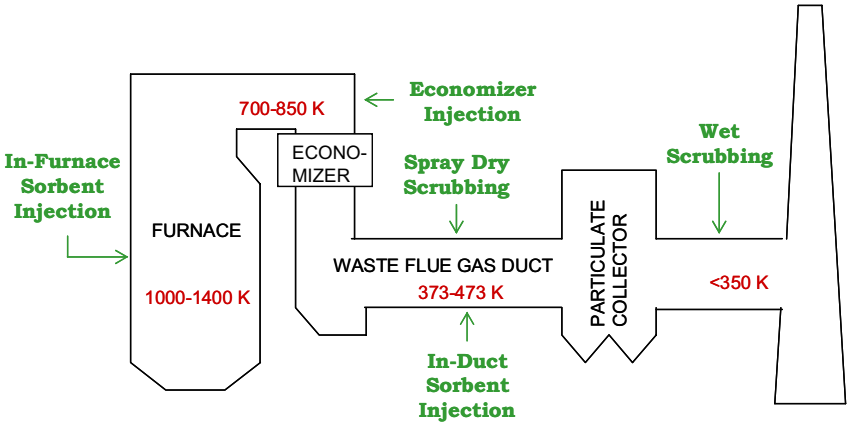

Fig. 1.2: Scheme of a power plant (*Golesworthy, 1999*).

1.3.3.1. Wet scrubbing

Wet scrubbing is usually regarded as an *absorption* process, in which the acid gas is dissolved in a solution, usually alkaline, or in a slurry that typically contains ca. 10 wt.% of an alkaline sorbent. In conventional wet scrubbers, a large vessel placed downstream the particulate collector (see Fig. 1.2) is generally used to put in contact the gas with the sorbent. In refuse incinerators, wet scrubbing includes typically two-stage scrubbers, the first of which (water absorber) is used for HCl removal, while the second one (alkaline solution) is used for SO_2 removal (*Buonicore and Davis, 1992; [www.worldbank,org/.../aqsowet]; Maziuk and Kumm, 2002*).

The most common sorbent employed in large wet scrubbers is limestone (constituted basically by $CaCO_3$), because of its low price and high abundance. Slaked lime -constituted basically by $Ca(OH)_2$- can be alternatively used, because it is more reactive than $CaCO_3$ and it is not costly. Lime (CaO) is also a feasible sorbent, although it involves a first step for its conversion into $Ca(OH)_2$. Since these Ca-based sorbents are not highly soluble in water, their use involves the formation of slurries. As reaction products, mixtures of $CaSO_3 \cdot (1/2)H_2O$ and $CaSO_4 \cdot 2H_2O$ are obtained. Calcium sulfite, which is hard to dewater, has no market value, so it is frequently landfilled after stabilization, typically with fly-ash. On the contrary, calcium sulfate is easy to dewater and can be used to manufacture wallboard. Nevertheless, its formation is undesirable because it creates scale in the scrubber equipment (*Brown, 1998; De Nevers, 1998*). In Table 1.2, the use of other sorbents is indicated.

1.3.3.2. Dry scrubbing

According to *Muzio and Offen (1987), Dahlin et al. (1992)* and *Golesworthy (1999)*, dry scrubbing processes may fall into different categories:

- ***Spray dry scrubbing*** (temperatures up to 450 K): It is based on the injection of an atomized alkaline sorbent slurry into a spray drying vessel upstream of the particulate collector. The dryer is designed to ensure that there is sufficient time for the water to evaporate before the flue gas enters the particulate collector *(Coll, 1997)*.

- ***Circulating fluidized bed reactor (CFB)***: The flue gas passes through a circulating fluidized bed of material composed of fresh hydrated and recycled limes and fly ash either in slurry form or as a dry sorbent with humidification. It is similar to spray drying, except for two significant differences: high solid recirculation, which provides additional gas/solid contact time and high solid concentration, and lower approach to the adiabatic saturation temperature (*Brown et al, 1998; Ollero et al., 2001*).

- ***In-duct sorbent injection*** (temperatures up to 450 K): It involves the injection of an alkaline sorbent either as slurry (*in-duct spray drying*) or as dry powder with humidification (*in-duct sorbent injection with humidification*) into the existing flue gas ductwork. The water is added to increase the flue gas humidity -or to reduce the approach to the adiabatic saturation temperature- as a means to

enhance the sorbent performance. It can be done either upstream or downstream the sorbent injection. The entrained particles and the gas are then conveyed to a particulate-collection device, where they are collected. Various corporations have developed specialized forms of in-duct spray drying such as ***Bechtel's CZD*** process, ***GE IDS*** or ***EPA's E-SO$_x$***. Specialized forms of dry sorbent injection with humidification include ***Dravo's HALT, Conoco's Coolside*** (see Fig. 1.3), and ***EPRI*** processes (*Dahlin et al., 1992*).

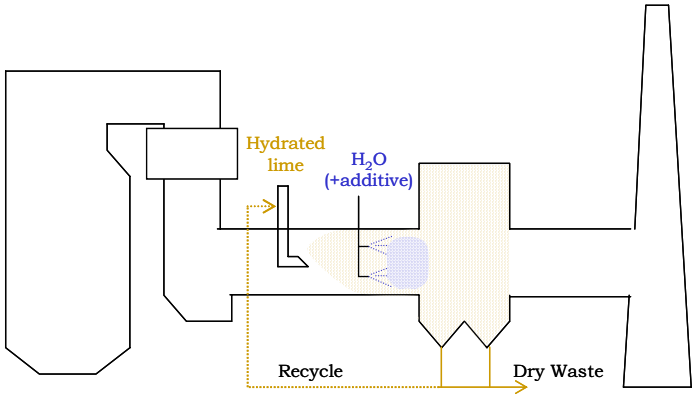

Fig. 1.3: Coolside Process (*Dahlin et al., 1992*).

- ***In-furnace sorbent injection*** (1000-1400 K): The sorbent (usually $Ca(OH)_2$ or $CaCO_3$) is directly injected to the furnace as a fine powder. Alternatively, the sorbent may be injected before the economizer, where the gas temperature is approximately 700-850 K *(Economizer Injection)*.

In low temperature processes, the particulate collector is regarded as an integral part of the FGD system, since the flue gas desulfurization and dechlorination takes place partially in it. For instance, in a commercial spray drying technology, the SO_2 removal in the particulate control device can contribute up to 20% of the total SO_2 removal for the system (*Peterson et al., 1989; Buonicore and Davis, 1992*). Respect to the kind of particulate collector, various laboratory and pilot-scale investigations have shown that fabric filters have a greater ability to remove acid gases than electrostatic precipitators, in addition to a higher solid conversion. This difference could be attributed to an improvement in gas-particle contact when the flue gas is forced through the sorbent particle layer and to the longer residence time in the baghouse, from several minutes to up to one hour (*Li et al., 1998; Maziuk and Kumm, 2002*).

Table 1.2: SO_2 and HCl scrubbing technology comparison (*Brown, 1998; De Nevers, 1998; Golesworthy, 1999; Sedman, 1999; Maziuk and Kumm, 2002*).

Scrubbing Technology		***Sorbent (Physical form)***	***Product***	***Efficiency***		***Capital cost***	***Reagent cost***	***Complexity***	***Present situation***
				Acid gas capture levels	***Reagent utilization***				
Wet		$CaCO_3$ (slurry)	$CaSO_3$, $CaSO_4$ $CaCl_2$	>90%	++	+++	+	+++	Mature technology. Typical process for large systems
		$Ca(OH)_2$ (slurry)					++		The higher reactivity of $Ca(OH)_2$ than $CaCO_3$ does not offset higher sorbent cost. Therefore, it is less widespread
		NaOH, Na_2CO_3, $NaHCO_3$ (solutions)	Na_2SO_3, Na_2SO_4 NaCl		+++	++	+++	++	Effective for smaller systems. As sodium salts are water soluble, the product deposition may become problematic
Dry	Spray-dry scrubbing	$Ca(OH)_2$ (atomized slurry)	$CaSO_3$, $CaSO_4$ $CaCl_2$	- 80-90% in coal combustors - 90-95% in incinerators	++	++ (20-30% lower than wet)	++	++	Widely used in combustion units burning coal with sulfur content of 2 wt.% or less, in industrial applications, cogeneration plants and waste-to-energy plants
	Circulating fluid. bed reactor	$CaCO_3$ $Ca(OH)_2$ (dry particle + water)	$CaSO_3$, $CaSO_4$ $CaCl_2$	Slightly higher than spray-dry scrubbing	++/+++	++	++	++	Relatively novel dry desulfurization technology. It can be used for burning coal with higher sulfur content than in spray-dryers
	In-duct injection with humidification	$Ca(OH)_2$ (fine powder + water)	$CaSO_3$, $CaSO_4$ $CaCl_2$	- 40-80% in coal combustors - 90-95% in incinerators	+	+	++	+	Successful in special circumstances such as low space availability, waste water treatments economically unviable, requirement of low process complexity
	In-furnace injection	$CaCO_3$ $Ca(OH)_2$ (fine powder)	$CaSO_4$ $CaCl_2$	30-60%	+	+	+	+	It is most suited to large furnaces, where the flue gas residence time is long

The almost dry solid waste product from dry Ca-based systems typically contains mainly a mixture of calcium sulfite and calcium sulfate, normally with higher amounts of the former. It can be landfilled, but the unreacted reagent in the waste product might result in a leachate with a high pH (*Brown, 1998*). Regarding the product formed when HCl is retained, a mixture of highly hygroscopic mono- and dihydrate $CaCl_2$ seems to be formed which tend to agglomerate causing problems of solid deposition in the ductworks and equipments. Furthermore, the product has to be kept away from a cold and/or humid environment due to its high melting temperatures (*Buonicore and Davis, 1992*). Open dumping should be precluded, due to the risk of leaching and run off to surface and ground water (*Karlsson et al., 1981*).

1.3.3.3. Advantages and disadvantages of the post-combustion control methods

In general terms, a trade-off between collection efficiency and costs has to be established. The experience to date has shown that wet scrubbers are the most efficient, which remove over 90% of the SO_2 present in the flue gas. As HCl is soluble in water, it is fast retained, achieving 99% of removal efficiencies in incinerators. NO_2 can be also absorbed, particularly with an alkaline scrubbing solution (*Zamansky et al., 1996*). Although design and operation methods of wet limestone scrubbers are continuously improving, they are still expensive and problematic, they generate huge quantities of solid waste, and their landfill can be an issue. However, at least in large systems, the low reagent cost usually offsets its high operation cost (*Vesilind, 1988; Buonicore and Davis, 1992; De Nevers, 1992; Brown, 1998; Golesworthy, 1999*). For small systems, wet soda ash (Na_2CO_3) or caustic soda (NaOH) are often cost-competitive on a weight basis, since the higher efficiency of these sorbents on acid gas capture usually offsets their higher costs. Furthermore, as neither slurries nor solids are handled, the complexity of the systems is lower (*Brown, 1998*).

In comparison to wet scrubbers, dry technologies have fewer problems of corrosion and scaling-up. Furthermore, wastewater treatment is not required and solid products are quite or completely dry, being therefore easily handled. Nevertheless, acid gas captures are generally lower than those achieved with wet scrubbers.

Among dry scrubbers, *spray dry scrubbers* constitute the most successful system, with more than 80% of acid gas capture levels in coal combustors when the solid residue is recycled. This technology is widely used for industrial applications (*Brown, 1998*), showing high removal efficiencies for all acid gases in refuse incinerators -99% of HCl and 95% of SO_2 (*Buonicore and Davis, 1992*) and significant quantities of NO_2 (*O'Dowd, 1994*)-. Although the operation costs are lower than those of wet scrubbers, they are relevant due to the slurry handling, which can cause technical problems such as solid deposition on the walls of the ductworks, plugging of the atomizers and premature deterioration of the devices or ducts due to abrasion. *In-duct spray drying* shows analogous problems (*Peterson et al., 1989; Ruiz-Alsop and Rochelle, 1987*).

CFB is a relatively new acid-gas control technology similar to spray drying in terms of capital costs and efficiency. However, as solids circulate at high rate, the possibility of solid deposition becomes reduced. Furthermore, higher reagent utilization and higher SO_2 removal can be obtained and therefore lower reagent costs (*Brown, 1998*). Some of the advantages of *in-duct sorbent injection with humidification* in comparison to *spray dry scrubbing* or *CFB* are operational simplicity, smaller space requirement, and lower energy and capital costs, since neither filter, thickeners nor mix tanks are needed. Furthermore, compared to *spray dry scrubbing*, waste solids are drier, and hence previous treatments for their disposal into landfills are not required.

However, the drawbacks involved in in-duct processes with humidification have deterred its spread. Acid gas capture levels are generally between 40-80%. Moreover, the solid utilization or conversion is quite low, generally lower than 40% (*Muzio and Offen, 1987; Chu and Rochelle, 1989; Golesworthy, 1999*). In contrast, efficiencies up to 90% and 50%, respectively, for HCl and SO_2 removal can be achieved in refuse incinerators in dry conditions and at high stoichiometric ratios of alkali added per equivalent of acid (2-4). These ratios can be reduced to 1-2 by humidifying the gases (*Buonicore and Davis, 1992*).

The comparison between the solid conversion for SO_2 removal obtained in some *in-duct sorbent injection with humidification* and *in-duct spray drying* processes is shown in Fig. 1.4 (*Peterson et al., 1989*). Although all the values are fairly low, it appears that at similar operational conditions -approach to saturation, sorbent type, calcium to sulfur [Ca/S] molar ratios, inlet flue gas temperature-, slurry injection leads to better solid conversion. As [Ca/S] molar ratios are similar, it can be also concluded that the desulfurization efficiency in slurry processes is higher than that of injection of dry solids with humidification.

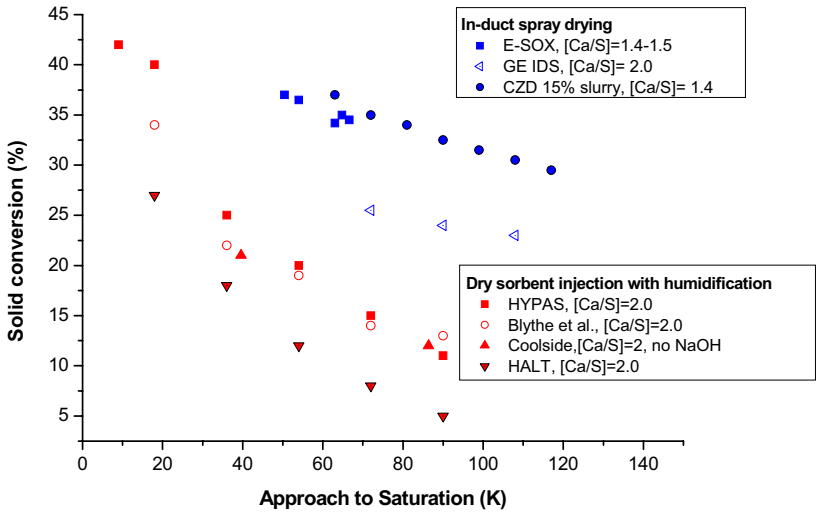

Fig. 1.4: Comparison of solid conversion in in-duct injection processes (*Peterson et al. 1989*).

In-furnace sorbent injection is an interesting technology from the point of view of its low space requirement and its simplicity of operation. Although this technology is in principle suitable for both

new and retrofit applications, the addition of solids in the combustion area leads to boiler power reduction. Therefore, it is not a desirable option for old plants. Furthermore, the experience shows that SO_2 removal is only between 30-60% -with a [Ca/S] of 2:1. The low efficiency of the process leads to the use of higher amounts of sorbent, which involves not only higher reagent costs, but also the possible saturation of the particulate collectors and generation of higher amounts of waste solids to dispose *(De Nevers, 1998; [www.worldbank,org/.../aqsosoij]*).

1.3.3.4. Development of in-duct sorbent injection with humidification processes

Wet scrubbing is a mature technology widely used in large coal combustors, which has shown essentially good retentions of SO_2 and HCl. However, a trend towards "no liquid effluent" has made dry scrubbing technologies attractive options not only for small and medium coal combustion facilities but also for incineration applications (*Golesworthy, 1999; Sedman, 1999*). Among dry technologies, in-duct sorbent injection with humidification is especially attractive in the following circumstances (*Maziuk and Kumm, 2002*):

- Old plants with lack of space for other FGD set-up or with limited remaining boiler life.
- Wastewater discharges cannot be permitted or are uneconomical to treat.
- Local electric power rates are high.
- Moisture saturated exhaust gas or a visible steam plume are unacceptable.
- The complexity of other scrubbers is incompatible with the knowledge of operators.
- The process is not large enough to make spray-dryers or Na-sorbents wet scrubbers economically viable.

Despite all these favorable situations, this technology is not so widely spread as wet and spray dry scrubbers for SO_2 removal applications, basically because of its low sulfur removal capacity (*Peterson et al., 1989; Rochelle and Jozewicz, 1990*). An increase of the amount of solid reagent added to the ductwork does not solve this drawback. Although there is a positive effect of increasing the Ca/S ratio on SO_2 removal, it is progressively reduced until a value beyond which no significant influence is observed. This effect may be explained considering that the fraction of the total sorbent particles that interact with water droplets may be smaller at a higher sorbent particle loading. On the other hand, a raise of the Ca/S ratio obviously leads to higher sorbent costs and to disposal and overloading problems, which could be a major drawback for the existing particulate collectors.

Since the 80s, some strategies have been developed to improve the performance of this technology. In this way, Consol Corporation developed an ***Advanced Coolside Process***, which is a modification of the Coolside process. Over 60% of solid conversion and over 90% of SO_2 removal can be achieved, but capital and operational costs are significantly increased. The key of the process is a gas/liquid contacting device downstream of the air preheater, which serves two purposes: to nearly

saturate the flue gas with water and to remove most of the coal fly ash from the flue gas, which allows high sorbent recycle levels (*Whitum et al., 1995)*.

Another alternative is the use of high reactive sorbents obtained by hydration of mixtures of fly ash and $Ca(OH)_2$ (*Martinez et al., 1991*). However, these sorbents are more expensive and more difficult to produce than normal Ca-based reagents (*Jozewicz et al., 1986; Chang and Sedman, 1988*). Some studies at laboratory scale carried out by *Krammer et al. (2002)* and at pilot plant scale by *Gutiérrez and Ollero (2003)* also showed an enhance in the sorbent conversion by the recirculation of the partially spent sorbent after being reactivated by putting it into contact with liquid water (or seawater) or a gas with a high relative humidity.

Numerous studies at laboratory scale have shown the effect of the surface area of limes on solid conversion. *Blythe et al. (1986)* and *Yoon et al. (1985)* found that the SO_2 removal increased linearly from 7% to 60% and from 12% to 45% as the sorbent specific surface area was increased, respectively, from 5 to 75 m^2g^{-1} and from 8 to 40 m^2g^{-1} (see Fig. 1.5). It should be mentioned that the positive effect of the surface area on the SO_2 removal might only occur when the solid is not in a slurry form, that is in bag filters or in ductworks after water evaporation. The surface area is not relevant when a lime excess is present in the slurry droplet, because the overall rate of reaction is limited by the bulk mass transfer of SO_2 to the droplet surface *(Karlsson and Klingspor, 1987)*.

The use of soluble additives to the water sprayed has been also a strategy to improve SO_2 capture efficiencies. In that way, *Yoon et al. (1988)* obtained SO_2 removals up to 85% with NaOH as additive in Coolside pilot tests. A drawback of this process is that it produces waste products that contain a significant amount of Na-based compounds, which are water soluble.

In addition to SO_2 removal applications, in-duct technologies appear to be a suitable technology for HCl removal applications and even for HCl and SO_2 simultaneous removal, for instance in incinerators plants.

Much research has been done both at pilot and laboratory scale, which has provided much information concerning the parameters affecting the solid conversion and SO_2 removal capabilities, such as relative humidity, temperature, SO_2 concentration, solid loading, and sorbent surface area. However, less information is available in the literature dealing with the effect of the parameters on reaction rates. Nowadays, the characterization of the reactions is still far from being completed, and so, fundamental research is still needed to improve the understanding of the overall process.

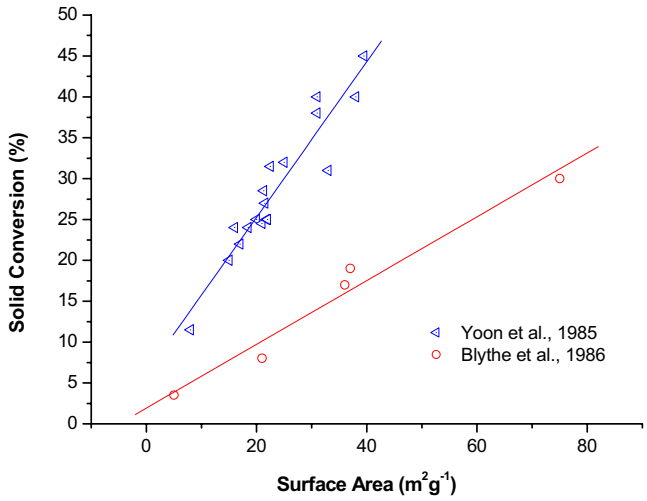

Fig. 1.5: Effect of sorbent surface area on reactivity for Bench-Scale Experiments.

1.4. CHEMICAL REACTIVITY OF SO_2, NO_2 AND HCl WITH $Ca(OH)_2$ IN DRY SCRUBBERS AT LOW TEMPERATURE

The chemistry of the system constituted by one acid gas that is in contact with Ca-based solutions, slurries or dry solids, including solids with adsorbed water, is generally quite simple. Both the mechanisms and the kinetics of the reactions involved in wet systems are generally well understood and described. In contrast, major gaps in the understanding of the basic chemistry involved at dry conditions are still present. The kinetics of the acid gas-solid reaction, the identification and quantification of the competitive reactions when more than one acid gas is simultaneously present and the outstanding role of the water in these systems at low temperature constitute major aspects that require more research.

1.4.1. CHEMICAL REACTIVITY OF SO_2 WITH $Ca(OH)_2$

The overall reaction that takes place in FGD scrubbers operating at low temperature using lime as active agent is the following one (*Manahan, 1994*):

$$Ca(OH)_2 + SO_2 \xrightarrow{H_2O(aq/vap)} CaSO_3 \cdot (1/2)H_2O + (1/2)H_2O\,, \qquad (1.1)$$

where part of sulfite can be oxidized to sulfate if oxygen is present. For FGD processes that use alkaline slurries, it has been proposed that reaction (1.1) consists of three consecutive steps, which are intimately linked to the drying stages of the slurry droplets *(Ruiz-Alsop and Rochelle, 1987; Strömberg, 1992)*:

1. Constant rate period: it lasts until the droplet shrinks to the extent that the alkali particles touch each other. The reactions are the same as those that occur in wet scrubbers:

- Absorption of SO_2: $SO_{2(g)} \xleftrightarrow{H_2O} SO_{2(aq)}$ (1.2)

- Dissolution of the sorbent in the droplet:

$$Ca(OH)_{2(s)} \xleftrightarrow{H_2O} Ca^{2+}_{(aq)} + 2OH^-_{(aq)} \quad (1.3)$$

- Reaction: $SO_{2(aq)} + H_2O_{(l)} \leftrightarrow HSO^-_{3(aq)} + H^+_{(aq)}$ (1.4)

$$HSO^-_{3(aq)} \leftrightarrow SO^{2-}_{3(aq)} + H^+_{(aq)} \quad (1.5)$$

- Sulfite oxidation: $SO^{2-}_{3(aq)} + \frac{1}{2}O_{2(aq)} \leftrightarrow SO^{2-}_{4(aq)}$ (1.6)

- Precipitation: $Ca^{2+}_{(aq)} + SO^{2-}_{3(aq)} + \frac{1}{2}H_2O_{(l)} \leftrightarrow CaSO_3 \cdot (1/2)H_2O_{(s)}$ (1.7)

$$Ca^{2+}_{(aq)} + SO^{2-}_{4(aq)} + 2H_2O_{(l)} \leftrightarrow CaSO_4 2H_2O_{(s)} \quad (1.8)$$

During this period, residence time is low, although it is significantly higher in processes that use spray dryers than in others that inject the slurry into the ductworks -approximately 10 s versus 0.5-3 s, respectively, according to *Peterson et al. (1989)*.

2. Falling rate period: the evaporation of water is limited by its diffusion through the pores of the agglomerate.

3. Dry period: particles have reached their equilibrium water content, which is dependent on the relative humidity (RH). During this period, there is still reaction, but the mechanism must be different from that in the wet period. This period corresponds to the reaction between SO_2 and the spray-dried particles while they are still suspended in the flue gas and while they are fixed in the particulate collector device.

In in-duct processes that humidify the flue gas prior to the solid injection, since the water evaporates before the entrance of the solid, only a single period must be expected. It should be analogous to that of the dry period mentioned above, which would be, in principle, characterized by a gas-solid reaction. When the humidification is done downstream of the solid injection, part of the water will be evaporated before impacting the sorbent particles. Consequently, the first or at least the second period may also occur at very short times. Once the water is evaporated, the mechanism must be equal to that of the dry period.

It is well-known that many reactions involving solids as reagents can be kinetically enhanced in wet-phase. Water may provide an environment to dissolve the solid, so that reagents can interact more easily than in dry conditions. This fact might explain the different efficiencies obtained by different scrubbing processes. Wet scrubbers are more efficient than spray-dryer systems, which at the same time

are more efficient than in-duct injection slurries due to the higher drying time for the slurry droplets. Furthermore, in-duct injection with downstream humidification provides better efficiencies than upstream humidification, as should be expected by considering the involving periods explained above (*Peterson et al., 1989; Stouffer et al., 1989*).

The great importance of the approach to saturation temperature on the amount of SO_2 captured has been shown in many pilot-plant studies (see Fig. 1.4). Furthermore, the research carried out at laboratory scale which is focused on the study of the reaction between $Ca(OH)_2$ and SO_2 at typical conditions of in-duct dry technologies have shown that the solid conversion and SO_2 captures, as well as reaction rates, are strongly dependent on the RH. The only differences have been observed at short reaction times. Meanwhile *Yoon et al. (1985)* detected a positive effect of RH on the initial solid reactivity, *Rochelle and Jozewicz (1990)* observed only a slight effect at very short times and *Krammer et al. (1997)* found no influence at the initial stage of the reaction. A summary of the main results reported in the literature regarding the effect of the RH on the reaction is shown in Table 1.3.

Table 1.3: Effect of RH on the reaction between SO_2 and $Ca(OH)_2$.

Reference	***RH (%)***	***T(K)***	***C_{so_2} (ppm)***	***Results***
Yoon et al. (1985)	<60	333-353	1000	Initial solid activity↑, X_S↑
Damle et al. (1986)	0-50	343		X_S↑ at long time.
Jorgensen et al. (1987)	10-80	338	500-1000	X_S↑(1h)*. Exponential trend**.
Ruiz-Alsop and Rochelle (1987)	19-70	338	2000	X_S↑(1h)*. Higher effect of RH in the range 19-50% than in 50-70%.
Rochelle and Jozewicz (1990)	24-85	339	450-1800	X_S↑(1h)*. Reaction rate↑
Aichinger et al. (1995)	15-75	353	3500	X_S↑(1h)*
Krammer et al. (1997)	22-75	353	3500	X_S↑ (1h-2h). Reaction rate↑, except for short reaction times.
Karatepe et al. (1999)	25-90	338	5000	X_S↑(10min-1h)*
Garea et al. (2000)	40-95	327-343	1000	X_S↑(1h). Linear trend** in the range 40-70% of RH and stronger influence beyond 70%.

* Solid conversion at 1 hour of exposure time.

** Linear or exponential trend are referred to the obtained trend when X_s vs RH are represented graphically.

The outstanding effect of the RH on the reaction appears to indicate that physically adsorbed water onto the internal and external surfaces of the porous reagent might play a key role in the reaction. The amount of physically adsorbed water in particles of $Ca(OH)_2$ (or $CaCO_3$) as a function of RH at 343 K is represented in Fig. 1.6, which shows that the amount of water adsorbed in equilibrium onto the

particle surface strongly increases with the RH. From the water adsorption isotherm on $Ca(OH)_2$, water amounts of 0.45, 0.87, 1.43 and 1.80 wt.% with respect to dry sorbent at RHs of 10, 50, 80 and 90%, respectively, were found.

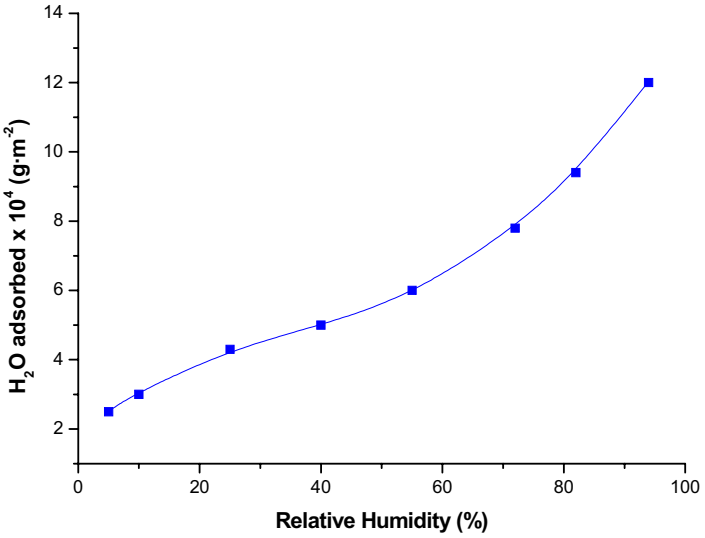

Fig. 1.6: Water isotherm adsorption for hydrated lime/limestone at 343 K (BET surface area = 2.0-25.5 m^2g^{-1}) (*Klingspor et al., 1984*).

Although a linear correlation between the amount of water adsorbed and the SO_2 removal seems to be observed according to *Yoon et al. (1987)*, the effect of adsorbed water on SO_2 removal is not completely understood. Several researchers have suggested different roles of water according to the reaction mechanism that they proposed. Thus, *Rochelle and Jozewicz (1990)* suggested the formation of a solid product layer onto the reagent surface, whose characteristics and diffusivity of species across it might be modified by the total amount of water adsorbed. Furthermore, *Damle et al. (1986)* and *Weinell et al. (1992)* proposed an enhancement of the reaction with the amount of water adsorbed due to an increase of $Ca(OH)_2$ dissolution, proceeding then the reaction in a similar manner as would occur in wet-phase. Finally, *Klingspor et al. (1984)* suggested an stabilization SO_2 molecules onto the surface of the reagent due to the action of adsorbed water by the formation of Ca-S complexes.

In contrast to the great effect of the RH on the reaction, the effect of the temperature is not very remarkable and certain disagreement can be found between the reported results. Meanwhile *Rochelle and Jozewicz (1990)* and *Krammer et al. (1997)* found no significant influence of the temperature on the reaction rate, *Jorgensen et al. (1987), Ruiz-Alsop and Rochelle (1987), Aichinger et al. (1995)* and *Ho et al. (2002)* found a weak or moderate positive influence on solid conversion. The most relevant results concerning with the effect of the temperature found in the literature are summarized in Table 1.4.

Table 1.4: Effect of T on the reaction between SO_2 and $Ca(OH)_2$

Reference	*RH (%)*	*T (K)*	C_{SO_2} *(ppm)*	*Results*
Jorgensen et al. (1987)	40-70	327-347	500	When T raises 10 K, X_S increases 20-30% (relative).
Ruiz-Alsop and Rochelle (1987)	74	303-337	500	When T raises from 303 to 337K, X_S increases ≈ 20% (relative)
Yoon et al. (1985)	<60	323-353	1000	$X_S \neq f(T)$
Rochelle and Jozewicz (1990)	30-60	323-345	2000	Reaction rate$\neq$f(T) at t<5s. $X_S(1h)^* \neq f(T)$
Aichinger et al. (1995)	70	325-353	5000	When T raises from 325 to 353K, X_S increases ≈ 40% (relative)
Krammer et al. (1997)		343-363		Reaction rate$\neq$f(T)

*Solid conversion at 1 hour of exposure time.

In general terms, the SO_2 concentration has a slight or null influence on the reaction, as can be seen in the results listed in Table 1.5. Most of the studies show no influence of the SO_2 concentration both on the solid conversion and on the reaction rate at one hour of reaction. *Ruiz-Alsop and Rochelle (1987)* pointed out that the effect after one hour of reaction depends mainly on the RH, so it is practically null at values of 70% and 50% at SO_2 concentrations in the range 2000-4000 ppm, but it is positive at lower concentrations. These results seem to be in contradiction with those reported by *Aichinger et al. (1995)*, who suggested a weak positive influence of the SO_2 concentration beyond 3500 ppm at a 50% of RH. On the other hand, *Krammer et al. (1997)* proposed that its effect might be rather linked to the solid conversion. In this way, according to their data, reaction only seems to depend on the SO_2 concentration at low conversions, which appears to be in correspondence with the results reported by *Seeker et al. (1986)* and *Rochelle and Jozewicz (1990)*, while at just initial reaction time and higher conversions, the influence seems to be null.

Table 1.5: Effect of SO_2 concentration on the reaction between SO_2 and $Ca(OH)_2$

Reference	*RH (%)*	*T (K)*	*C_{SO_2} (ppm)*	*Results*
Damle et al. (1986)	0-75	343	300-550	$X_S \neq f(C_{SO_2})$ at long time.
Seeker et al. (1986)	High RH	335	2000-5000	$n=1^{**}$ at t<5min
Jorgensen et al. (1987)	20-80	338	500-1000	$X_S(1h)^* \neq f(C_{SO_2})$.
Ruiz-Alsop and Rochelle (1987)	50-70	339	1000-4000	- RH: 70%: $X_S(1h)^* \neq f(C_{SO_2})$; $n=0^{**}$ - RH: 50%; 2000-4000ppm: $X_S(1h)^* \neq f(C_{SO_2})$; $n=0^{**}$ - RH: 50%; 1000-2000ppm: $X_S(1h)^* = f(C_{SO_2})$; $n=1^{**}$
Rochelle and Jozewicz (1990)	50-60	339	450-1800	- Reaction rate=$f(C_{SO_2})$ at t<5s. - $X_S \neq f(C_{SO_2})$ at long time
Aichinger et al. (1995)	55	353	1000-6500	Weak positive influence, particularly above 3500ppm
Krammer et al. (1997)	50	353	270-15000	- Initial reaction rate$\neq f(C_{SO_2})$ - Reaction rate=$f(C_{SO_2})$ at short time. - $X_S(1h) \neq f(C_{SO_2})^*$

*Solid conversion at after one hour of exposure time.
**Reaction order with respect to SO_2 concentration

1.4.2. CHEMICAL REACTIVITY OF NO_2 (+SO_2) WITH $Ca(OH)_2$

NO_2 can be absorbed in aqueous solutions. According to *Schriver et al. (1994)*, in alkaline solutions, NO_2 may disproportionate into NO_2^- and NO_3^-, while in acid conditions, NO_2^- may further disproportionate to form NO_3^- and gaseous NO. Both reactions are the following ones:

$$2NO_{2(aq)} + 2OH^-_{(aq)} \leftrightarrow NO^-_{2(aq)} + NO^-_{3(aq)} + H_2O_{(l)} \quad (1.9)$$

$$3NO^-_{2(aq)} + 2H^+_{(aq)} \rightarrow NO^-_{3(aq)} + 2NO_{(g)} + H_2O_{(l)} \quad (1.10)$$

At temperatures in the range 294-413 K, NO_2 is in equilibrium with its dimmer N_2O_4, which can be further hydrolyzed in an aqueous system in an analogous manner as NO_2 (*Sharpe, 1992*).

The aforementioned reactions would be involved in a wet-scrubber to retain NO_2. However, reactions seem to be more complex in a wet-scrubber for simultaneous NO_2 and SO_2 removal. Several researchers (*Kobayashi et al., 1977; Takeuchi et al., 1977; Cliffton et al., 1988; Littlejohn et al., 1993*) studied the reactions involved in the system $NO_{2\,(g)}$ / aqueous solution in the presence of SO_3^{2-}/HSO_3^-. Their results appear to indicate that a redox reaction is produced between the hydrolyzed NO_2 and the

sulfite ions. Moreover, *Kobayashi et al. (1977)* investigated the capability of several inorganic reagents in an aqueous solution to remove NO_x and found that the removal of NO_2 increases with the redox potential of the reagent system. Na_2SO_3, with the highest redox potential of all the tested species, has been found to be the most efficient one. *Takeuchi et al. (1977)* carried out some kinetic studies related to the absorption of NO_x in sodium sulfite aqueous solutions and concluded that the absorption is accompanied by some competitive reactions involving the reactions of NO_2 with sulfite ions and water. *Rosenberg and Grotta (1980)* worked in a laboratory-scale scrubbing system, and found that NO_2 tends to act as a promoter of the oxidation of $CaSO_3$. The overall reaction scheme that has been suggested for this reaction, which is consistent with all the experimental results aforementioned, could proceed as follows *(Cliffton et al., 1988)*:

$$2NO_{2(g)} + SO_{3(aq)}^{2-} + H_2O_{(l)} \leftrightarrow 2NO_{2(aq)}^{-} + SO_{4(aq)}^{2-} + 2H^{+}{}_{(aq)} \ , \qquad (1.11)$$

which is thermodynamically favorable according to the values of redox standard potential of the couples SO_4^{2-}/SO_3^{2-} and N_2O_4/HNO_2 (-0.94 and 1.065 V, respectively) (*Shriver et al., 1994*). *Littlejohn et al. (1993)* carried out some studies concerning the reactivity of aqueous sulfite solutions in the presence of NO_2 at pH 5-14. They found nitrites, sulfates and dithionate ions as products of the reaction by using Raman spectroscopy and ion chromatography. According to their results, they suggested that reaction (1.11) could proceed via the formation of sulfite radical:

$$NO_2 + SO_3^{2-} \rightarrow NO_2^{-} + SO_3^{\bullet -} , \qquad (1.12)$$

where in its turn, the radicals might recombine in the following way:

$$SO_3^{\bullet -} + SO_3^{\bullet -} \rightarrow SO_3^{2-} + SO_3 , \qquad (1.13)$$

and the SO_3 produced might generate sulfate ions by the reaction:

$$SO_3 + H_2O \rightarrow 2H^{+} + SO_4^{2-} \qquad (1.14)$$

The existence of the $SO_3^{\bullet -}$ radical is well-established by its ultraviolet absorption and electron spin resonance spectra *(Deister and Warneck, 1990)*. Reactions (1.13) and (1.14) were previously proposed by *Eriksen (1974)* in their study of the reaction mechanism of deoxygenated aqueous solutions of SO_2 under pulse irradiation. *Waygood and McElroy (1992)*, who studied the kinetics of the evolution of the $SO_3^{\bullet -}$ in aqueous solution, also proposed reaction (1.13) as feasible.

When O_2 is present (at least 3%), a mechanism involving several radical chain reactions has been suggested by *Littlejohn et al. (1993)*, where many sulfite ions might be oxidized by only one absorbed NO_2 molecule, as was previously discussed by other researchers *(Hayon et al., 1971; Deister and Warneck, 1990)*.

On the other hand, very few studies have been conducted regarding the chemistry of the system NO_2+$Ca(OH)_2$ and SO_2+NO_2+$Ca(OH)_2$ in the presence of water vapor. *Nelli and Rochelle (1998)* carried out some experiments in a fixed-bed reactor to determine SO_2 and NO_2 removal using $Ca(OH)_2$

and Fly Ash ADVACATE sorbent at a RH of 60%. They assumed that at RHs higher than 50%, a multilayer of water covered the surface, which provided enough water to absorb NO_2 and SO_2, which would further react in a similar manner as they would do in an aqueous solution.

Furthermore, *O'Dowd et al. (1994)* carried out some analyses of the solid product obtained in a spry dryer/baghouse system. The results showed that, with and without the injection of SO_2, nitrites were the predominant species containing nitrogen. They also observed that, by increasing the ratio NO_2/SO_2, the sulfite ion concentration decreased, meanwhile the sulfate ion concentration increased. On the opposite, the studies of *Nelli and Rochelle (1998)* showed the presence of nitrate species -but not nitrites- by using Fly Ash ADVACATE as solid reagent, whose chemistry is similar to that observed with $Ca(OH)_2$. The absence of nitrite species was explained by considering the acidification of the external surface of the alkaline sorbent due to the formation of a product layer onto it in such a way that reaction (1.10) would take place.

From the point of view of the desulfurization capture, the kinetic behavior of the $SO_2+NO_2+Ca(OH)_2$ system at typical conditions of in-duct injection with humidification technologies is not predictable. On the one hand, the acid character of SO_2 and NO_2 and the higher aqueous solubility of the latter suggest that NO_2 should be considered as a chemical competitor to the desulfurization reaction, namely reactions (1.9) or (1.10) would have similar or higher reaction rates than reaction (1.1). On the other hand, the formation of nitrites and nitrates might enhance SO_2 retention, since they are hygroscopic species. Regarding this field, *O'Dowd et al. (1994)* found that the presence of NO_2 seems to enhance the baghouse SO_2 removal by $Ca(OH)_2$, but they did not found any influence in a spray dryer. *Nelli and Rochelle (1998)* reported that both SO_2 and NO_x captures by calcium hydroxide are increased when increasing NO_2 concentration in a fixed-bed reactor at 343 K and 60% RH and concluded that an increase of RH -or decreasing the approach to the adiabatic saturation temperature- enhances both SO_2 and NO_2 removal. They also showed that the presence of O_2 tends to lower the amount of NO_2 and SO_2 removed after 30 minutes of reaction.

Because not many studies have been issued in this field and some discrepancies seem to be found regarding the solid products formed, more studies are needed to elucidate the chemistry of the $SO_2+NO_2+Ca(OH)_2$ system and to describe the effect of the operation variables on the desulfurization yield. Future prospects of this study could be the possible application of the scrubbers for simultaneous removal of SO_2 and NO_x. This alternative seems to be feasible if NO is first oxidized to NO_2. The investigation carried out by *O'Dowd et al. (1994)* in a spray dryer/baghouse system showed that, with solid load ratio of $Ca/(SO_2+0.5NO_x)=1.25$, 40-50% of NO_x of flue gases containing 560 ppm of NOx (420 ppm of NO_2) and 2050 ppm of SO_2 can be removed. Although direct oxidation of NO with O_2 to NO_2 is too slow to be converted in a FGD system (*Zamansky, 1996; De Nevers, 1998*), this conversion could be achieved by the addition of methanol or other hydrocarbons into the flue duct at an optimum temperature (*O'Dowd et al., 1994; Nelli and Rochelle, 1998*).

1.4.3. CHEMICAL REACTIVITY OF HCl WITH $Ca(OH)_2$

Millikan (1918) stated that the overall reaction between HCl and $Ca(OH)_2$ in an aqueous systems is the following one:

$$Ca(OH)_{2(s)} + 2HCl_{(aq)} \rightarrow CaCl_{2(s)} + 2H_2O_{(l)} \qquad (1.15)$$

Since then, most of the studies reported in the literature both at high and at low temperatures *(Karlsson et al., 1981; Weinel et al.l, 1992; Fonseca et al., 1998)* assume that reaction (1.15) takes place in flue gas HCl scrubbing systems, and therefore calcium chloride $CaCl_2$ or $CaCl_2{\cdot}2H_2O$ is the final product of the dechlorination reaction. However, only few data are available in the literature dealing with the identification of final products and mechanistic pathways of the system HCl+$Ca(OH)_2$ (*Daoudi and Walters, 1991; Jozewicz and Gullet, 1995; Allal et al., 1998*). *Weinell et al. (1992)*, *Fonseca et al. (1998)* and *Chisholm and Rochelle (1999)* reported a final conversion at a ratio of 1 to 2 based on Cl/Ca indicating that at least a fraction of the product consists of $CaCl_2$ working at temperatures between 323 and 493 K and in the presence of water vapor. These results confirmed the previous results from *Karlsson et al. (1981)*, who reported that the final conversion is reached at a ratio close to 1.1.

Furthermore, *Daoudi and Walters (1991)* carried out solid analyses and found that $CaCl_2$ was the only final product when calcined $CaCO_3$ -i.e. CaO- was employed at temperatures between 583-943 K. They also verified that the maximum weight increase corresponded to full conversion of CaO to $CaCl_2$. Later, *Jozewicz and Gullet (1995)* also did solid analyses of reacted $Ca(OH)_2$ that had been in contact with HCl for 1 minute at 773 K and dry conditions, and detected not only $CaCl_2{\cdot}2H_2O$, but also Ca(OH)Cl as chlorinated product. However, they only found Ca(OH)Cl at 473 K, which was also reported by *Allal et al. (1998)* for a residence time of 0.5 seconds at 523 K and dry conditions.

The comparison between Ca(OH)Cl and $CaCl_2$ indicates that both compounds are formed by the substitution of one and two hydroxyl groups in $Ca(OH)_2$, respectively. This fact suggests that reaction (1.15) could take place via the intermediate Ca(OH)Cl, as was already pointed out by *Jozewicz and Gullet (1995)* in the following way:

$$Ca(OH)_{2(s)} + HCl_{(g)} \leftrightarrow Ca(OH)Cl_{(s)} + H_2O_{(ads)} \qquad (1.16)$$

$$Ca(OH)Cl_{(s)} + HCl_{(g)} \leftrightarrow CaCl_{2(s)} + H_2O_{(ads)}\,, \qquad (1.17)$$

Reaction (1.17) is also reported by *Gmelin (1956)*. *Allal et al. (1998)* estimated the free enthalpy of formation of Ca(OH)Cl and evaluated the equilibrium constants of the reactions (1.15), (1.16) and (1.17) in the range from 373 to 1000 K. They concluded that these reactions can occur in the range of temperatures studied.

The stoichiometry of the reaction with respect to chloride in the solid product seems to be undecided, although this information is essential when considering the characteristic data of total conversion -i.e. maximum uptake of chloride by the sorbent. Depending on the kind of reaction product,

the chemical stability is also an issue when considering its disposal in landfills, as has been also referred in section (1.3). Moreover, the amount of freely movable liquid, which is a measure for the tendency of the particles to agglomerate, can depend upon the kind of reaction product. $CaCl_2$ is a well-known compound, and therefore its behavior in HCl scrubber applications is also well-known. In contrast, Ca(OH)Cl is not widely known and consequently, its behavior in landfills and in ductworks and equipment of HCl scrubbers is not predictable.

1.5. MECHANISMS AND KINETIC MODELS

1.5.1. GAS-SOLID NON-CATALYTIC REACTIONS

In general terms, the physical and mathematical description of the mechanisms and kinetic models involved in heterogeneous reactions are more complex than those of homogeneous reactions. Moreover, among the reported heterogeneous reactions, those related to the gas-solid non-catalytic kind are usually the most. The apparent complexity of these reactions is usually ascribed to intrinsic aspects related to their nature, some of which are listed below (*Doraiswami and Kulkarni, 1987; Froment and Bischoff, 1990*):

1. The overall reaction is the result of several elemental steps, both physical and chemical, which include: external mass transfer, internal mass transfer or intraparticle diffusion, adsorption of the reactants, diffusion through the product layer, surface reaction and desorption of the products (see Fig. 1.7). These steps take place consecutively and simultaneously and one or more might be rate limiting. The role played by them usually depends on the particle size, temperature, structural properties of the solid, gas flow rate and gas concentration.

2. As the solid is a reactant and therefore it is continuously consumed, the system as a whole shows an essentially non-steady nature, and the controlling regime might continually change with time. As a result, kinetic equations are in principle dependent on the reaction time, and their form might completely change as the reaction progresses. However, gas-solid systems are often simplified by considering pseudo-steady states (*Carberry, 1976*).

3. Structural properties of the solids (e.g., pore size distribution, particle size and surface area) have a strong influence on the reaction rates and on the rate limiting step. As the solid reacts, structural changes of the solid such as pore shrinkage or closure, swelling or cracking can occur. Consequently, the complexity of the kinetic models that include such changes might be notably increased.

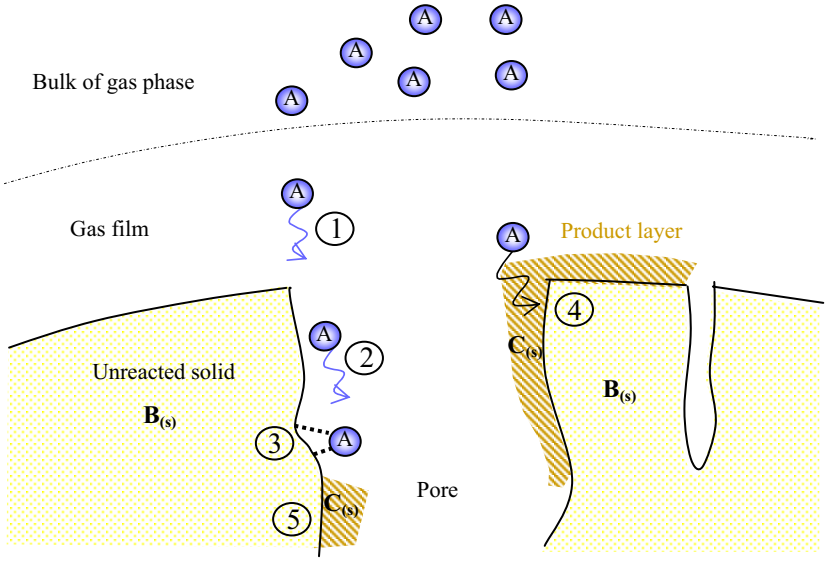

Fig. 1.7: Schematic representation of a gas-solid reaction $A_{(g)}+B_{(s)}\rightarrow C_{(s)}$. (1) external mass transfer; (2) intra-particle diffusion of the gas reagent; (3) adsorption of the reactant gas; (4) diffusion through product layer; (5) reaction and formation of the product.

Moreover, it should be emphasized that the mechanistic and kinetic description aforementioned only takes place in a single particle. When a fixed-bed reactor is involved, for instance, the description of the behavior of the system becomes even more complex, because the kinetics in each particle can be strongly influenced by its own microenvironment, and at a given time, different rate limiting steps might be controlling at different positions in the reactor.

1.5.2. KINETIC MODELS FOR THE REACTION BETWEEN Ca-BASED SORBENTS AND SO_2 AT HIGH TEMPERATURE

The reaction of Ca-based sorbents with SO_2 at common furnace temperatures (950-1400 K) underwent in the past extensive and fundamental research. It was observed that the simplest kinetic model developed for the description of non-catalytic gas-solid reactions, the so-called ***Shrinking Core Model (SCM)***, is generally unsuitable for the explanation and simulation of kinetic experimental data. Because this reaction is relevant in desulfurization processes, many efforts have been made since the 70's to find an appropriate kinetic model and by now, some models and empirical correlations are available in literature.

The mechanistic and kinetic description of this reaction is highly influenced by the high ratio -ca. 3- between the molar volume of the solid product ($CaSO_4$) and that of the reagent (CaO[1]). This difference in molar volumes leads to important structural changes during the course of reaction, such as particle swelling and reduction of particle porosity or pore size, which at the same time can increase the pore diffusion resistance. The progressive decrease of the reagent porosity with the conversion may fast

[1] Common Ca-based sorbents -$CaCO_3$, $Ca(OH)_2$- tend to generate CaO at high temperature, which acts as the active species in the desulfurization reaction with SO_2.

reduce the reaction rate and, depending on the particle size, it can cause pore mouth plugging and/or small-pore filling as the final step of the reaction.

On the other hand, in a similar manner as it happens in other non-catalytic gas-solid reactions, the progression of the reaction results in the formation of a product shell, which can inhibit further contact of the reactants with SO_2 and thus to an incomplete conversion of the reagent. In fact, experimental conversions lower than 40% are generally found, unless the starting material is very porous and the particle size very small. Another characteristic of this reaction is that solid conversion depends on the initial porosity and on the initial pore size distribution of the solid reagent (*Doraiswamy and Kulkarni, 1987; Hartman and Coughlin, 1976; Bathia and Perlmutter, 1981; Simons et al. 1987; Doğu and Doğu, 1993*).

The models applied to the reaction at high temperature fall into the following categories: (1) grain, (2) pore and (3) deactivation models, most of which incorporate mathematical equations to consider structural variations. The models are described as follows:

1. **Grain model**: A porous particle is regarded as an assemblage of non-porous spherical CaO grains of uniform size surrounded by intergranular voids (see Fig. 1.8), and each grain is modeled by the SCM. One relevant application of this model was carried out by *Hartman and Coughlin (1976)*, who took into account a reduction in the effective diffusion coefficient of SO_2 with the progressive reduction of the reagent porosity as a means to describe the evolution of the reagent pore structure. Furthermore, *Georgakis et al. (1978)* and *Hartman and Tranka (1980)* proposed modified versions of a grain model that included grain expansion and porosity changes. Later, *Sotirchos and Yu (1988)* developed the so-called ***overlapping grain model***, which visualizes the solid reagent as a population of overlapping grains that react in a shrinking core fashion. Their results revealed strong effects of the type of the grain size distribution and of grain overlapping on the reactivity.

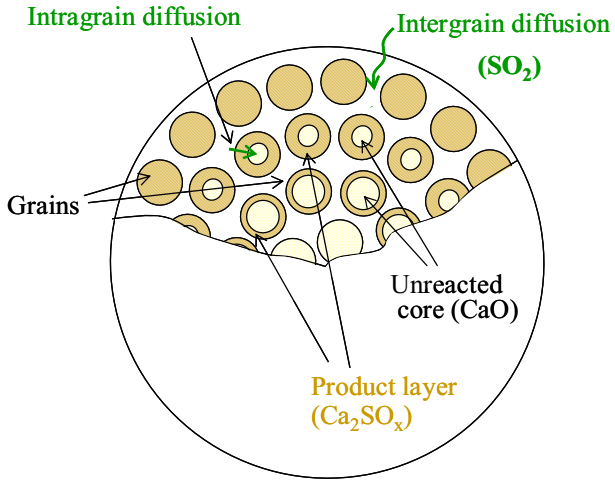

Fig. 1.8: Schematic representation of the grain model (*Sohn and Szekely, 1972*)

2. **Pore model**: Reagent particles are regarded as a solid continuum penetrated by pores. The reaction is initiated on the pore boundaries, which results in a set of growing surfaces at each radial position within the particle. The product accumulates in the space between the growing reaction surfaces and the pore boundaries offering a diffusional resistance to the gas flow. One initial application was carried out by *Ramachandran and Smith (1977b)*, who regarded the total porosity of the overall pellet as a representative single pore, which size is reduced in the course of the reaction (see Fig. 1.9). This model was later extended by *Christman and Edgar (1983)* by considering pore size distribution. *Bhatia and Perlmutter (1981)* developed the random pore model to take into account the intersections among pores as well as changes in pores structure. Their results indicated that a solid reagent with a wide pore size distribution would be more reactive than another one with uniform pores. Finally, *Simons et al. (1987)* fitted experimental data to a ***pore tree model***, which regards the pore structure as a set of various sizes which trunks are located at the particle surface.

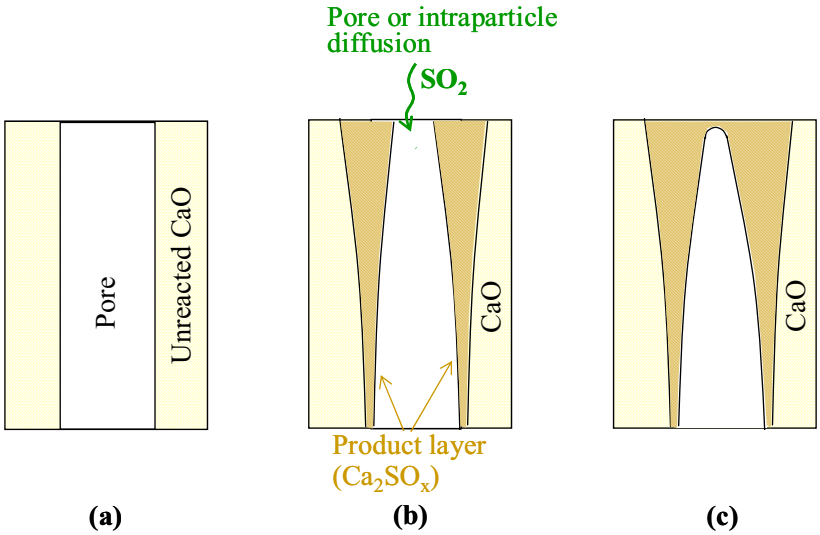

Fig. 1.9: Schematic representation of the single-pore model for Vm(product)>Vm (reagent) with pore-mouth plugging. (a) unreacted particle (b) partially plugged porous (c) plugged porous (*Modified from Ramachandran and Smith, 1977*).

3. **Deactivation model (DM):** This model includes a solid activity factor in the reaction term, which takes into account that changes in the pore structure, in active surface area and in active site distribution can cause significant ***deactivation*** of the solid reagent, and thus a reduction in the reaction rate. *Doğu (1981)* assumed that the activity of the solid (CaO) decreases with time due to changes in surface area and to the formation of product layer ($CaSO_4$) over the reactive surface. They considered the simplest version of the model, which assumes that the rate of temporal change of the activity is proportional to the activity itself, and considered only pore diffusion and kinetics as controlling regimes. Although the DM is simpler than the random pore and grain model, it has been less applied to the desulfurization reaction.

In general terms, all kinetic models described could in principle consider all the typical steps in a gas-solid reaction. However, if some considerations are taken into account, some mass transfer

resistances can be neglected, or some steps can become rate limiting. In this way, external mass transfer can be easily rejected from the kinetic model working at high flow rates of the gas. Intraparticle diffusion can be also neglected, but this simplification is usually limited to small particle sizes (order of a few microns). On the contrary, intraparticle diffusion can become important at higher temperatures and short reaction times and for larger particles. Generally speaking, for non-catalytic gas-solid reactions, it can be considered that small particles are controlled by the kinetics of the surface reaction, while larger ones are more influenced by intraparticle diffusion at least at low conversions (*Simons et al. 1987; Doğu and Doğu, 1993*). Furthermore, at higher conversions, the diffusion of SO_2 through the developing product shell onto the solid reagent could be proposed as the rate limiting step. In this way, the applied models commonly treat the kinetics of the reaction under study by taking into account the three following consecutive steps:

1. Diffusion of SO_2 through the intergranular voids or pore structure (intraparticle diffusion).

2. Reaction at the grain -or pore- surface, which can be kinetically controlled by either the chemical reaction or the product-layer diffusion, except for a DM.

3. Plugging of the porous structure by filling the pores, by pore-mouth closure or by coalescence of grains.

According to *Borgwardt and Bruce (1986)*, even though the kinetic models pointed out accurately describe the self-limiting effects on ultimate conversion in large particles, the temporal evolution of conversion for smaller ones (few microns) might be described by the simplest version of a grain model that assumes no coalescence and product-layer diffusion control. Their results suggest that, although the pores in large particles become plugged, further sorbent sulfation can continue by diffusion through the product layer.

1.5.3. KINETIC MODELS FOR THE REACTION BETWEEN $Ca(OH)_2$ AND SO_2 AT LOW TEMPERATURE

The reaction between $Ca(OH)_2$ and SO_2 at low temperature in the presence of water vapor has undergone in the past intensive research, as it has been explained in the section 1.4.1. This reaction is characterized by an incomplete solid conversion and by a sharp decrease of the reaction rate with solid conversion (data reported by *Krammer et al. (1997)* employing a thermogravimetric balance show that reaction rate decreases ca. two orders of magnitude when the solid conversion reaches 5% operating at 50% of RH). Moreover, experimental data reported at a RH higher than 70% appear to show that the reaction does not cease at long times (after 1 hour), even though the reaction rate has already dramatically decreased (*Ruiz-Alsop and Rochelle (1987), Aichinger et al. (1995) and Krammer et al. (1997)*).

Only few studies concerning the kinetics and the mechanism of the reaction have been surveyed. As the experimental kinetic behavior cannot be described by means of the simplest form of the SCM

(Damle et al., 1986), several attempts have been made to develop empirically improved versions of this model. In this way, *Karatepe et al. (1999)* introduced a diffusion coefficient which decreased exponentially with the solid conversion. Another empirical correlation was proposed by *Ruiz-Alsop and Rochelle (1987),* which included a decrease in roughness as the reaction progresses.

Irabien et al. (1992) proposed a model based on the adsorption of SO_2 on the solid surface as the rate limiting step, where the adsorption activation energy was assumed to depend linearly on the surface coverage. More recently, *Ho et al. (2002)* fitted their experimental data obtained by means of a differential fixed-bed reactor to a DM, which assumed that the reaction is controlled by the surface reaction and that the surface reaction only takes place on the reactive surface, namely not yet covered by product.

Krammer et al. (1997) suggested the presence of four stages during the reaction: (1) the formation of a product monolayer, mainly determined by both the SO_2 concentration and the RH; (2) the formation of consecutive product layers, depending mostly on the RH; (3) a product layer diffusion, becoming the rate-limiting step with a reaction rate only affected by the RH and a reaction product that is thought to be built up in a cluster-like form at a high RH, which could result in a better accessibility of the still unreacted material; (4) pore closure, which could explain the significant drop of the reaction rate at high conversions. *Klingspor et al. (1984)* proposed a reaction mechanism based on the adsorption of SO_2 on adsorbed water layers, where the formation of a hydrated complex of SO_2 could be the rate-limiting step, and a higher RH would involve the formation of more stable compounds.

Due to the importance of the structural properties of the solids on the reaction rate and on the maximum solid conversion in non-catalytic gas-solid reactions, the influence of the surface area and the evolution of the structural properties has also been the aim of some studies. The analysis of the structural properties of the solids at different reaction times carried out by *Ortiz et al. (1993)* allowed them to conclude that the region of 9-200 nm is the effective pore size for the desulfurization reaction. They also found a linear decrease of the surface area and the pore volume of the solid with conversion, since the molar volume of the product is higher than that of the reagent (in a ratio of 1.5). This result was later confirmed by *Ho et al. (2002)*. Furthermore, *Krammer et al. (1997)* and *Ho et al. (2002)* found that conversion per BET unit area was irrespective of particle size in the diameter range between 50-120 μm and 10-96 μm, respectively.

1.5.4. IONIC SOLID-STATE DIFFUSION

Although it has been traditionally thought that the diffusion step aforesaid in section 1.5.2. took place by means of SO_2 transfer, *Hsia (1993, 1995)* found evidence of an outward solid-state diffusion of Ca^{2+} ions through the product layer rather than a transfer of SO_2 molecules. They used two different techniques, one based on the use of platinum markers, and the other was a "two-stage" sulfation technique using $^{32}SO_2$ and $^{34}SO_2$. The second technique consisted of carrying out the reaction between SO_2 and sintered CaO tablets in 2 consecutives stages at the same conditions, but using $^{32}SO_2$ in the first stage and a mixture of $^{34}SO_2$:$^{32}SO_2$ (3:1) in the second one. A subsequent analysis of the reacted CaO

tablets by secondary ion mass spectrometer allowed them to find an enrichment of ^{34}S at the surface, which was consistent with an outward ionic diffusion.

In general terms, the lattice of real crystals always contains imperfections, which are, indeed, responsible for ionic solid-state diffusion. The most current imperfections are the following ones (*Girifalco, 1964; Gottstein, 1999; Rao and Gopalakrishnan, 1997*):

1. **Point defects**: They are irregularities of atomic dimensions in the crystal lattice that can be present both in metals and ionic materials. The most typical point defect in a crystal are ***vacancies*** and ***interstitial***, based on, respectively, the presence of unoccupied positions in the crystalline lattice that should be occupied by missing atoms or ions, and on the occupation of interstitial voids by atoms or ions from the lattice. In case of ionic crystals, the different defects have to be balanced electrically to keep electroneutrality within it. Thus, positive ion vacancies can be neutralized either by negative ion vacancies or by positive ion interstitials, leading to the so-called *Schottky* and *Frenkel* defects.

2. **Grain boundaries**: They are regions that separate two single crystals of different atomic orientation. Crystalline materials usually consist of aggregates of grains, each of which being a single crystal and being separated from adjacent grains by grain boundaries. This region has a thickness of several atomic diameters and most of the atoms in it are distributed in such a way that their average interatomic distances are greater than those in the sinus of the crystal. This inference is significant for diffusion, since it leads to expect that atomic migration rates are greater in grain boundaries than in single crystals or within grains.

3. **First and second order defects**: They consist of dislocations, stacking faults and crystallographic shear planes.

Because of the important role of imperfections on ionic solid-state diffusion, the chemical reactivity of the reactions controlled by this process is determined more often by the crystal and defect structure of solids rather than by the intrinsic chemical reactivity of the constituents (*Rao and Gopalakrishnan, 1997*). When more than one defect is present, the prevailing mechanism for the ionic solid-state diffusion is the one that provides the highest ionic migration. Because of the much lower activation energy of boundary diffusion, it is dominant at lower temperatures. However, as the temperature is raised, bulk diffusion rates increase rapidly, until, for high temperatures, grain-boundary diffusion contributes a negligible amount to the overall process (*Girifalco, 1964*).

One outstanding characteristic related to ionic solid-state diffusion coefficients is their small values, usually thousands of times lower than those between two species in a liquid or gas phase. A second important characteristic is the huge range of values reported. In gases and ordinary liquids, most ranges fall within a power of 10, while for solids, ionic solid-state diffusion coefficients can differ by more than 10^{10}. Other important characteristic is that their temperature dependence is sharp and non-linear, a characteristic of chemical reactions, which suggests that ionic solid-state diffusion might be regarded as a chemical rate process (*Cussler, 1987).*

2. Objectives

This study has been focused on the following aspects:

1. Evaluation of the influence of the relative humidity, temperature and SO_2 concentration on the ability of $Ca(OH)_2$ to retain SO_2 in the ranges 313-353 K, 0-70% of RH, 2000-8000 ppm of SO_2.

2. Study of the reacting system $NO_2 + SO_2 + Ca(OH)_2$ in the presence of water vapor: evaluation of the influence of the presence of 75-250 ppm of NO_2 on the ability of $Ca(OH)_2$ to retain SO_2 (2000 ppm) in the ranges 343-353 K and 30-70% of RH. Proposal of a mechanistic pathway for the systems $NO_2/Ca(OH)_2$ and NO_2-$SO_2/Ca(OH)_2$.

3. Study of the reacting system $HCl + Ca(OH)_2$ in the presence of water vapor: determination of the final products of reaction and their stability, the amount of water adsorbed during the reaction, and the remaining water after a drying period. Proposal of a mechanistic pathway.

4. Determination of a kinetic model to describe kinetic experimental data of the system SO_2 ($+NO_2$) $+ Ca(OH)_2$ in the presence of water vapor. Evaluation of the effect of the RH on the kinetic parameters of the kinetic equation.

5. Study of the role of water vapor on the reaction between SO_2 and $Ca(OH)_2$ by Atomic Force Microscopy (AFM).

6. Proposal of a mechanism of the reaction between SO_2 and $Ca(OH)_2$ in the presence of water vapor.

3. Experimental set-up and procedures

3.1. SYSTEM SO_2 (+NO_2) + $Ca(OH)_2$

3.1.1. DETERMINATION OF EXPERIMENTAL BREAKTHROUGH CURVES

3.1.1.1. Experimental set-up

The experiments were carried out in the apparatus depicted schematically in Fig. 3.1, which consists basically of four main parts:

1. ***Feeding system***: Synthetic flue gas to simulate gas emitted by power plants was obtained by injecting the appropriate amounts of pure gases (SO_2 and N_2) or mixtures (air and N_2/NO_2 mixtures) from gas cylinders, employing four mass flow controllers (supplied by Brooks, 5850S, The Netherlands). The steam was fed into the reactor from a ***liquid-injection system*** (Bronkhorst Hi-Tec, L1-FA-22-0, The Netherlands), where liquid water contained in a pressurized reservoir was mixed with a carrier gas (N_2) and later vaporized in a mixer chamber. Liquid water flow was controlled by means of a liquid flow valve. The RH was measured upstream the reactor (Vaisala , HMP 235, Finland), together with temperature and total pressure as it is indicated in Fig. 3.1. To prevent from water condensation inside the ducts, the tubes downstream the evaporation chamber were wiped up by an electric resistance.

2. ***Reaction system***: The reaction took place in an isotherm fixed-bed reactor with a downward flow, which consisted of a jacketed Pyrex tube (450 mm height, 12 mm i.d.) with a porous plate to hold the solid sorbent. The reactor was thermostated by pumping water from an external thermostatic bath. The pressure drop along the reactor was measured by means of two pressure transmitters (Bourdon, E713). Several PT-100 thermopars were used to measure the temperature of the ducts. The isothermicity of the bed was checked in some experiments by inserting a thermocouple in its sinus.

3. ***Analytical system***: SO_2 and O_2 concentrations were measured by means of an infrared equipment and a paramagnetic measuring cell, respectively (Maihak, Multor610). An electrical gas cooler was placed before the analyzer system to separate water, which was removed by the means of a peristaltic pump.

4. ***Personal computer (PC)***: The system was provided with a PC for continuous data acquisition concerning temperature, pressure, gas concentrations, gas flows and relative humidity, which were displayed on-line by means of a Lab View software. Moreover, the computer was provided with a programmed alarm system in order to stop the set-up in case of overcoming a critical value of pressure, SO_2 concentration or temperature.

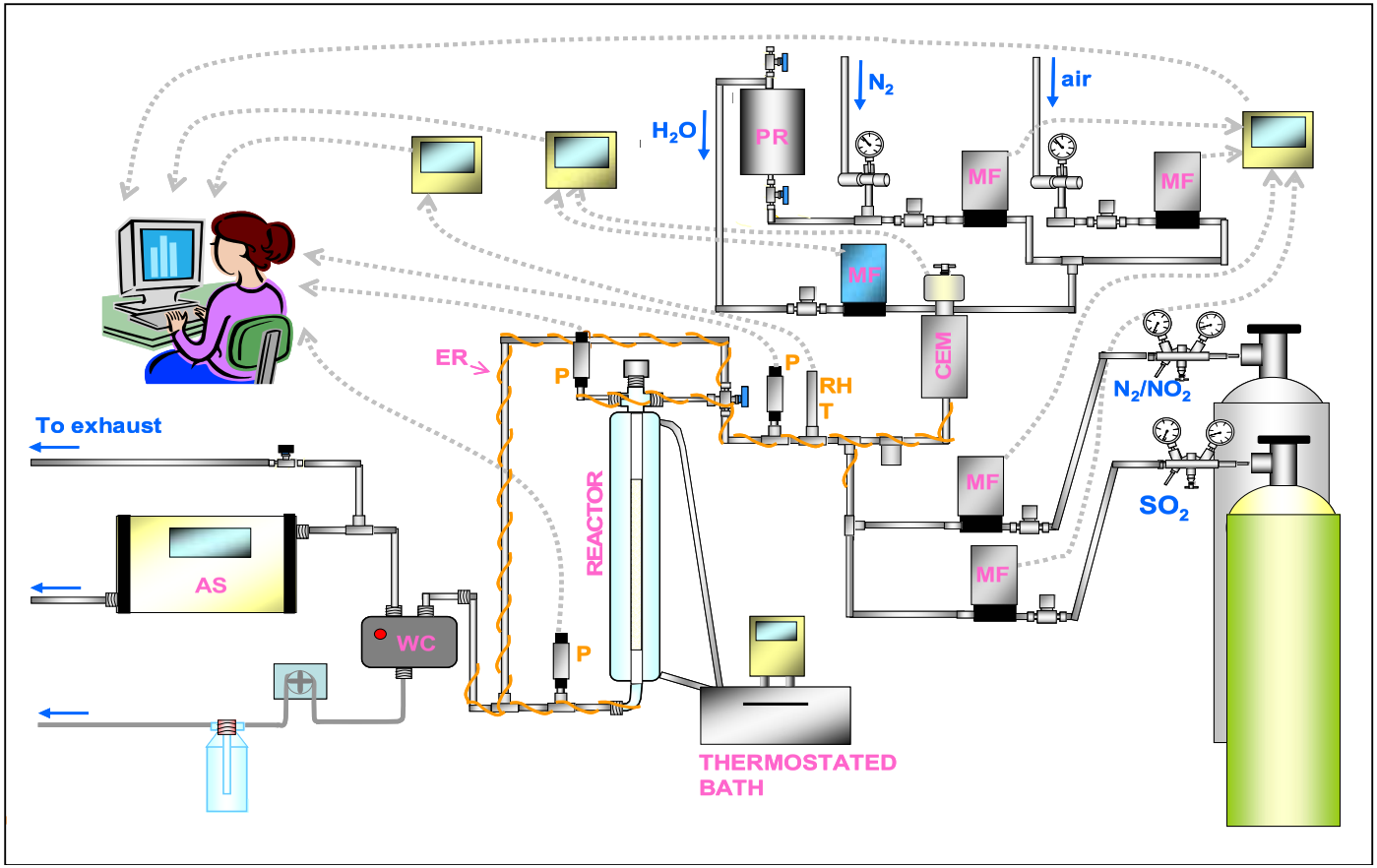

Fig. 3.1: Experimental set-up for SO_2 ($+NO_2$) study. AS: analytical system; CEM: evaporator mixer chamber; ER: electric resistance; MF: mass flow-meter; P: pressure transmitter; PR: pressurized reservoir; RH: relative humidity sensor; T: temperature sensor; WC: water condenser.

3.1.1.2 Experimental procedure

The following procedure was used to carry out each experiment in the aforementioned set-up:

1. ***Warming the system:*** The desired values of temperature both in the resistance and in the thermostatic bath and evaporation chamber were selected. The flow of N_2 was usually kept at 1.5 L(STP) min^{-1}.

2. ***Loading the reactor:*** A mixture of powder $Ca(OH)_2$ (1 g) (commercial reagent supplied by Ciaries Co., Spain) and commercial seasand (Fluka, Germany) as inert solid was introduced in the reactor. The seasand was employed to avoid the channeling of the gas and to assure isothermal conditions. An apparent porosity of the bed of 23% was previously determined.

3. ***Feeding water vapor flow*** after reaching the desired temperatures in all points of the reactor.

4. ***Bed pre-humidification***: Once the system was stabilized, the gas stream was led through the reactor during five minutes. Preliminary experiments were done to check that preconditioning time did not affect the experimental results.

5. ***Reaction period***: The required flow of the rest of the species was supplied to the reactor and data began to be recorded by the computer.

6. ***Bypass of the gas stream out of the reactor*** before the end of each experiment in order to measure the composition of the feeding stream.

7. ***Removal of the whole bed from the reactor***: The reacted solids to be analyzed were dried during 12 hours at 373 K and sieved to separate reacted from inert particles, except for those to be analyzed by ionic chromatography, which were rapidly introduced in a glass with distilled water without a previous separation.

After each experiment, reaction breakthrough curves of SO_2 concentration in the gas stream leaving the reactor were plotted. Blank breakthrough curves of SO_2 were also obtained from experiments performed with the same procedure, but replacing $Ca(OH)_2$ with a grinded inert solid (3 g).

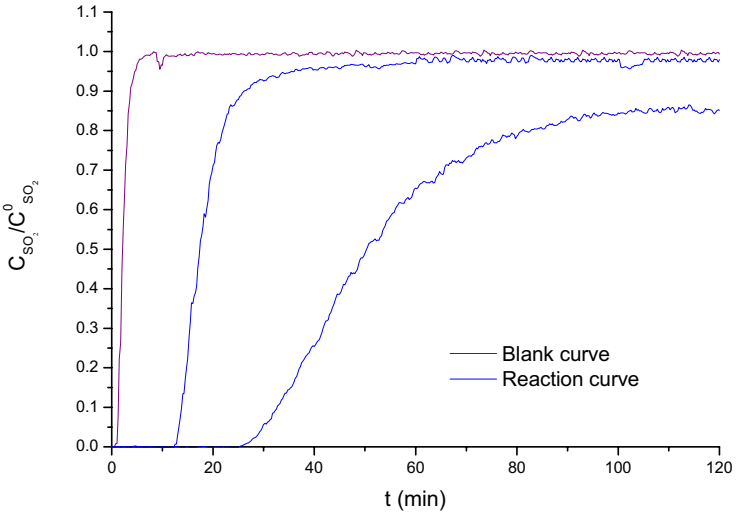

Fig. 3.2: Experimental breakthrough curves

Some examples of reaction and blank breakthrough curves are shown in Fig. 3.2, where $C^0_{SO_2}$ and C_{SO_2} correspond, respectively, to the SO_2 concentration at the inlet (feeding stream) and outlet of the reactor [ppm]. Thus, when all the SO_2 that enters the reactor is retained, the ratio $C_{SO_2}/C^0_{SO_2}$ becomes zero. In the same way, when $C_{SO_2}/C^0_{SO_2}$ tends to one, no reaction can be expected. On the other hand, the total amount of SO_2 removed from the flue gas was evaluated from the area between blank and reaction breakthrough curves. The amount of SO_2 retained per mole of Ca is given by:

$$\text{mol SO}_2\text{ retained / mol Ca} = \left(A_{bl} - A_{exp}\right) C^o_{SO_2}\, 10^{-6}\, \frac{\phi_v}{22400}\, \frac{M_{Ca(OH)_2}}{m_{Ca(OH)_2}} \qquad (3.1)$$

where A_{bl} and A_{exp} correspond to the areas drawn, respectively, by the blank and reaction breakthrough curves [s], and ϕ_V, $M_{Ca(OH)_2}$ and $m_{Ca(OH)_2}$ indicate, respectively, the volumetric total flow in the bed [mL s^{-1}], the molecular weight of $Ca(OH)_2$ [g mol^{-1}] and the amount of $Ca(OH)_2$ introduced in the reactor [g]. A detailed calculation of the amount of SO_2 retained per mol of Ca can be found in appendix A. For experiments carried out without the presence of NO_2, the solid conversion (X_S) was directly calculated from the stoichiometry of reaction (1.1), as it is indicated below:

$$X_S = \frac{\text{mol SO}_2\text{ retained}}{\text{mol Ca}} \text{x100} \qquad (3.2)$$

Some preliminary experiments were carried out to evaluate the effect of the dilution of the solid sorbent on the breakthrough curves. A selected dilution ratio of 1:30 was chosen, because beyond this ratio the breakthrough curves did not depend on it (see Fig. 3.3). The effect of dilution on the flow pattern of the fixed-bed reactor is discussed in section 4.3.1.1.

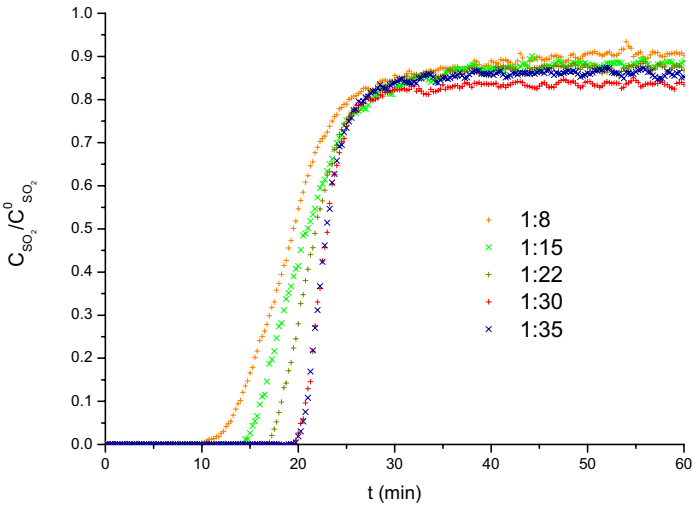

Fig. 3.3: Effect of dilution on experimental breakthrough curves (1 g of $Ca(OH)_2$ for all dilution ratios)

3.1.2. ATOMIC FORCE MICROSCOPY (AFM) STUDIES

In heterogeneous reactions where crystals are involved, the surface of the crystal usually plays a relevant role in the development of the reaction. The study of surfaces can require the use of microscopy techniques with a high resolution. Some preliminary tests showed that, among them, Atomic Force Microscopy (AFM) appeared to be suitable to study the reaction between SO_2 and $Ca(OH)_2$. Since AFM analyses require uniform and smooth surfaces of a large size (~ 1 mm^2 or larger) and good quality $Ca(OH)_2$ crystals were not available in the market, a few $Ca(OH)_2$ single crystals were prepared in our laboratory.

3.1.2.1. Synthesis of $Ca(OH)_2$ single crystals

$Ca(OH)_2$ single crystals were prepared by means of the so-called ***diffusion method*** (*Brauer, 1958*), which consisted of the following steps:

1. Preparation of $CaCl_2$ and NaOH precursor solutions in two different glass beakers by dissolving, respectively, 30 g of $CaCl_2$ and 24 g NaOH in 100 mL distilled water. A small amount of $Ba(OH)_2$ was added to the latter to retain CO_2 in the course of crystallization by the precipitation of $BaCO_3$.

2. Introduction of the glass beakers containing the precursor solutions in another one of 2000 mL, as it is indicated in Fig. 3.4.

3. Addition of distilled water to the 2000 mL glass beaker until the water level reaches approximately 1 cm over the top of the glass beakers of the precursor solutions in order to get them into contact.

4. Crystallization during 4 weeks.

5. Filtration of the crystals, washing with methanol and drying at 383 K during 10 minutes.

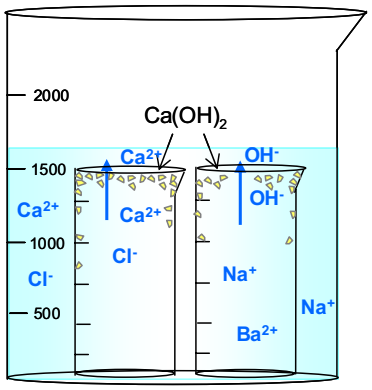

Fig. 3.4. Preparation of $Ca(OH)_2$ single crystal by the diffusion method.

3.1.2.2. Experimental set-up for sample preparation prior to AFM analyses

A scheme of the experimental set-up used for carrying out the reaction between $Ca(OH)_2$ single crystals and SO_2 in the presence of water vapor is shown in Fig. 3.5. The feeding system to generate N_2, SO_2 and H_2O streams was the same as that used to obtain breakthrough curves and already described in section 3.1.1.1. $Ca(OH)_2$ single crystals were placed in a glass reactor immersed in a thermostated bath. A 3-way valve (1) and an on/off valve (2) were placed, respectively, at the inlet and outlet of the reactor to allow its isolation with a desired atmosphere (composition, pressure and RH) during each experiment. The relative pressure in the reactor was controlled by means of a manometer (range 0-1 ± 0.05 bar).

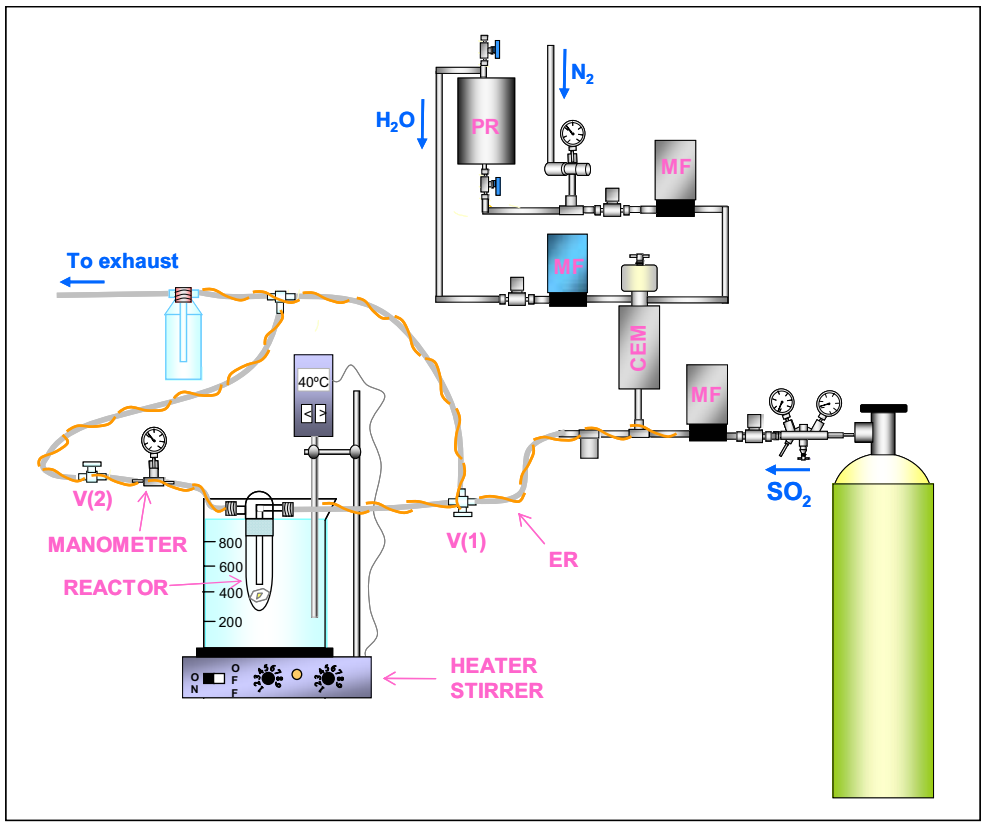

Fig. 3.5: Experimental set-up for AFM experiments. CEM: evaporator mixer chamber; ER: electric resistance; MF: mass flow-meter; PR: pressurized reservoir; V: valve.

3.1.2.3. Experimental procedure

The procedure conducted for AFM studies consisted of the following three consecutive steps:

3.1.2.3.1. Cutting of $Ca(OH)_2$ crystals and exploration of its surface

In the beginning of each AFM experiment, $Ca(OH)_2$ single crystals were cut with a sharp blade to obtain a clean, flat and smooth surface. The crystals were easily cleaved because of their layered structure *(Moreno et al. 1984)*.

3.1.2.3.2. Sample preparation

Once the crystals had been cut, they were supported on a Teflon base. A polymer was employed to fix the crystal to the base. Immediately afterwards, the fresh cut surfaces were explored by AFM to check that they were smooth and uniform to assure that further changes could be ascribed exclusively to

the reaction. The surfaces were characterized by its **surface roughness Rms** (root mean square roughness) parameter, which is defined as follows:

$$Rms = \left(\left(\frac{1}{N-1} \right) \sum_{i}^{N} (X_i - X_m)^2 \right)^{0.5} \quad (3.3)$$

where **i** is the number of measurement, X_i is the height at point **i**, N is the number of data points and X_m is the height average, which is given by

$$X_m = \left(\frac{1}{N-1} \right) \sum_{i}^{N} X_i \quad (3.4)$$

3.1.2.3.3. Reaction between cut crystals and SO_2 in the presence of water vapor

Each sample was prepared by means of the set-up described above according to the following procedure:

1. ***Warming the system:*** The temperature in the reactor was kept at 313 K for all the experiments. The electric resistance was set at a temperature beyond 323 K to prevent the system from any water condensation, and the evaporation chamber was turned up to generate the required amount of water vapor.

2. ***Loading the reactor****:* A cut crystal was introduced in the reactor

3. ***Feeding reacting gases:*** The desired flows of water vapor, SO_2 and N_2 were supplied to the system, and the resulting feeding stream bypassed the reactor.

4. ***Reaction period***: Once the system was stabilized, the feeding stream was directed to the reactor and the experiment started. After one minute of continuous feeding, valve (2) was closed, and when the pressure in the reactor reached the exact value of 1.2 bars, valve (1) was closed to allow the feeding stream to bypass the reactor, and thus it remains isolated. The SO_2 and water supply was stopped.

5. ***Inertization of the reactor:*** After 30 minutes, pure N_2 was fed to the reactor to stop the reaction. Finally, it was isolated again with an inert N_2 atmosphere and it was removed from the system. The reacted crystal was maintained inside the reactor until the AFM analyses were done to prevent its reacted surface from any further change due to the action of atmospheric humidity.

3.1.2.3.4. Study of the morphology of the reacted surfaces by AFM

The reacted crystals were imaged by tapping mode AFM (TM-AFM) to obtain a representative morphology of the surface just reacted. Preliminary essays showed that tapping mode is not destructive to both $Ca(OH)_2$ and $CaSO_3(1/2H_2O)$ and that the surface does not change substantially during the exploration time at room conditions (ca. 30 minutes). After the reaction and further exploration of the crystal surface by AFM, some studies were carried out to provide an insight into the effect of water on

the reacted crystals. The crystal samples were exposed to a humid atmosphere by means of three different procedures:

1. ***Short time addition at high water vapor pressure:*** The reacted crystal was placed in the reactor again and it was humidified at 313 K and at a controlled RH for 2 hours, after which the surface was newly imaged.

2. ***Long time addition at room conditions:*** The reacted crystal was left at room temperature for some days. During this period, the surface was explored several times, until no significant changes were observed. The RH was measured three times per day, showing that it was quite high (60-80%) during all the period. The temperature varied from 288 to 298 K.

3. ***In-situ humidification:*** The crystal sample and the AFM scanning unit were placed inside a controlled humidified chamber and the crystal surface was continuously imaged. The procedure consisted of:

    1. Placing the crystal sample on the AFM support

    2. Placing the AFM with the crystal sample in the chamber

    3. Closing the chamber and feeding a high flow of N_2 until the RH was lower than 15% (about 5 min were required).

    4. Starting AFM imaging (one image every 2.5 min)

    5. Humidification of the chamber by bubbling N_2 in liquid water. At room temperature, a RH of 75% was achieved.

Owing to the fact that consecutive explorations of all samples required their removal from the AFM apparatus, some marks were done on their Teflon base. These marks enabled to explore approximately the same surface region each time the samples were imaged. In order to show that the changes on the surface are ascribed to the product instead of the reagent, some experiments with an un-reacted sample of $Ca(OH)_2$ were done by procedures (2) and (3). Furthermore, in order to check that the changes on the reacted sample were actually due to the effect of water, some reacted crystals were leaved for some days in a dessicator, and afterwards were newly imaged by AFM.

3.2. SYSTEM HCl + $Ca(OH)_2$[1]

3.2.1. SYNTHESIS OF $Ca(OH)_2$

[1] This study was done at the Institut für Apparatebau, Mechanische, Verfahrenstechnik und Feuerungstechnik of the Technische Universität of Graz (Austria).

The $Ca(OH)_2$ reagent used to study its reaction with HCl was prepared in the laboratory. The raw material used was a commercially available limestone (Bad Ischler limestone, Austria) containing 5% inert and 95% $CaCO_3$. The limestone was sieved to obtain particles of a diameter range of 50-63 micron, which were further used to prepare Ca-based reagent. The preparation included the following steps:

1. Calcination of the limestone, so that CaO is formed according to its thermal decomposition as follows:

$$CaCO_3 \rightarrow CaO + CO_2 \qquad (3.5)$$

2. Cooling of the sample

3. Hydration of CaO to form $Ca(OH)_2$ by dispersing the former on a surface and slowly moistening it by pouring water droplets on it. This gentle procedure was chosen to prevent particle fragmentation. The reaction of hydration proceeded as follows:

$$CaO + H_2O \rightarrow Ca(OH)_2 \qquad (3.6)$$

3.2.2. EXPERIMENTAL SET-UP

The experiments were carried out in a thermogravimetric analyzer (TGA), whose schematic diagram is presented in Fig. 3.6. A microbalance *(Sartorius M 25D)* with an accuracy of 0.01 mg was placed at the top. The sample holder was connected to the balance via a chain, which position was adjusted with an electrically driven winch system. The temperature of the sample was measured directly underneath the sample holder. Both the sample holder and the sample holder chain were made of inconel, which is inert when exposed to an acid environment. A sample lock, where the temperature remained low, was placed between the reactor and the microbalance.

The HCl required in the experiments was supplied as a gas mixture (HCl/N_2) from a gas cylinder employing a mass flow controller (Bronkhorst Hi-Tec, F-201C-FAC-22-E, The Netherlands) and the water vapor was produced by means of a steam generator that expanded liquid water through a sintered metal block (HPLC pump, Biotronik, BT 8100). The resulting stream was mixed with pure N_2 at the entrance of the reactor to achieve the desired HCl concentration and RH. The gases were heated before the reactor. Furthermore, a balance purge and a protective purge flows were used to avoid reacting gases approach the microbalance and to protect the steel wall of the TGA of corrosive gases as HCl, respectively. In the course of an experiment, the sample mass, the temperature of the sample and the total pressure were continuously measured and recorded.

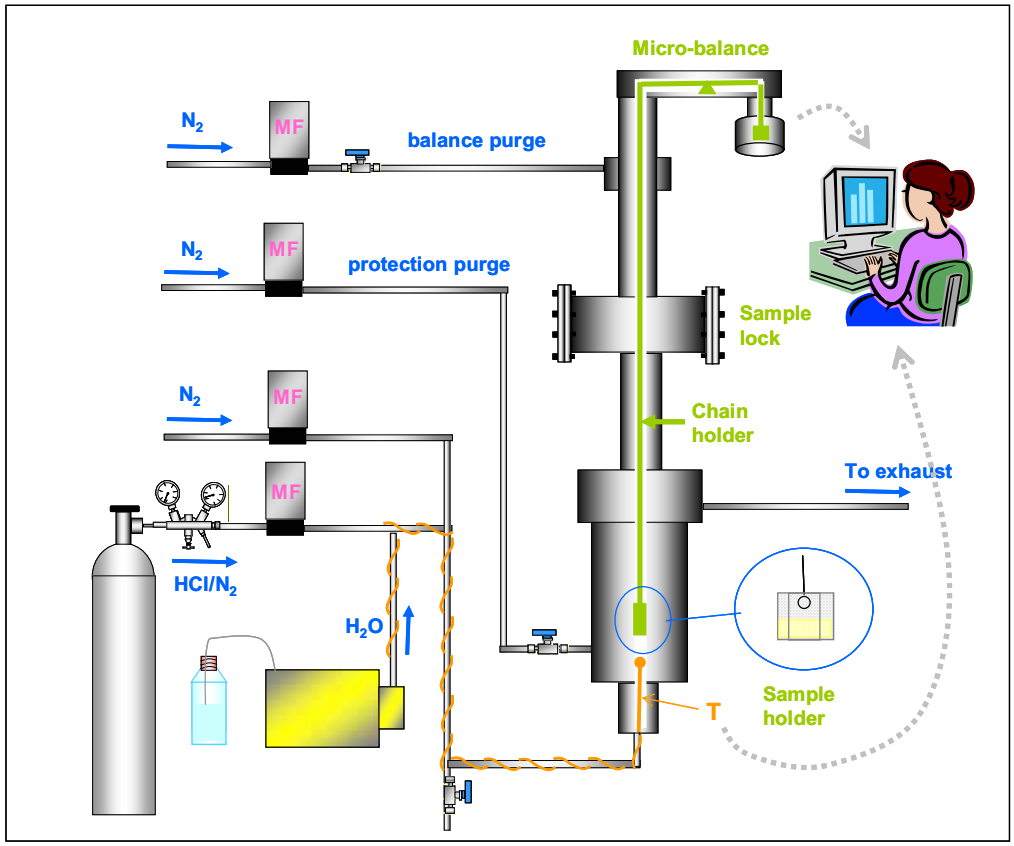

Fig. 3.6: Schematic representation of a TGA for HCl study

3.2.3. EXPERIMENTAL PROCEDURE

The procedure of each experiment consisted of the next steps:

1. ***Drying period*** by circulating pure N_2 over the sample until constant weight (1500 s).

2. ***Warming*** the pipes upstream the reactor and the reaction zone until 393 K and turning on the purge and protective flows (2 and 0.5 L(STP) min^{-1}, respectively).

3. ***Loading the reactor***: Setting the solid reagent (3.2 mg, except for solid analyses, where 1 g was used) in the sample holder and further introducion in the cold sample lock and lowering to the reaction zone, where the sample remained hanging during the following steps.

4. ***Reaction period***: Supply of the feeding stream and start of the reaction for a desired reaction time (always shorter than 2000 s). All the experiments were undertaken at a temperature of 393 K, 18% of RH, 240 ppm of HCl concentration and a total flow of 0.9 L (STP) min^{-1}.

5. ***Product drying period***: The sample was dried again by circulating pure N_2 over it with the same flow that was employed in the first period, until the total weight became constant (about 3 minutes).

6. ***Removal of the reacted solid from the TGA***: The samples to be chemically analyzed, namely Cl analyses, were quickly suspended in distilled water.

In Fig. 3.7, a typical experimental curve of the total weight change during reagent drying, reaction and product drying periods is shown. The weight change when comparing the reaction and the drying periods, indicated as "b" in Fig. 3.7 is caused by the different gas atmosphere employed during each period, that is to say the different buoyancy.

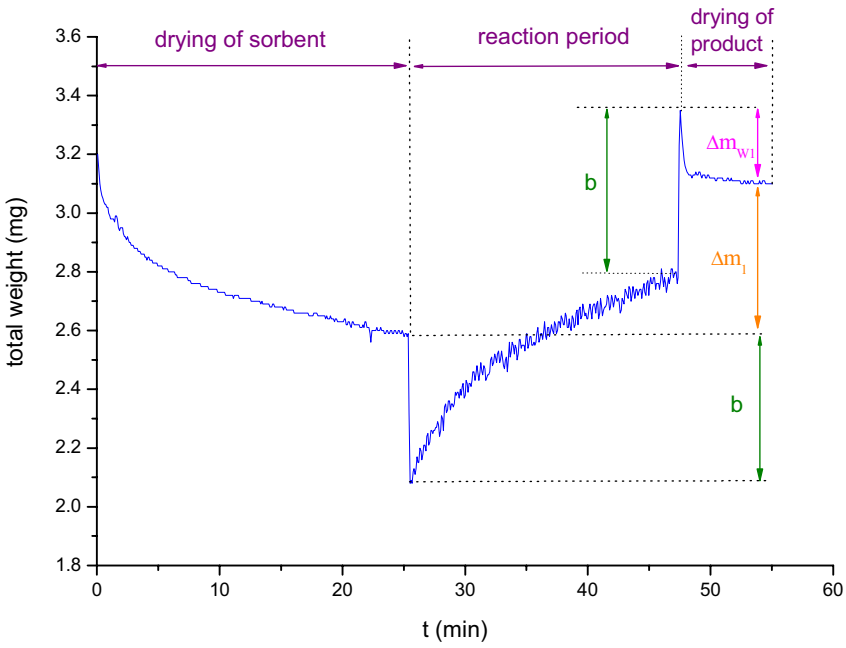

Fig. 3.7: Scheme of total weight change during TGA experiment. Results unaccounted for different buoyancy.

Some preliminary experiments showed that the total weight of a sample was reduced considerably when the sample was dried, which reflected the hygroscopic character of the products formed. The variation of the total weight during each experiment was ascribed to two different contributions: (1) the reaction of Ca-based sorbent with HCl, and (2) the retained water. As the TGA experiments only provided the total weight change, additional solid analyses (described in section 3.3) were required to determine the actual retention of HCl by the sample, that is, the conversion. The actual amount of water retained was calculated by taking into account the total weight change (obtained by TGA experiments) and the conversion of the sample (obtained by solid analyses), as it is detailed below.

The moisture content in the samples during the reaction can be divided into two parts: (1) one fraction that can be easily removed by a short drying period, and (2) another one that remains after this period, which is more strongly bound to the solid. The fraction of water strongly linked to the crystal was determined from the weight difference between the final dried product and the weight of the unreacted sample (indicated as Δm_1 in Fig. 3.7), where Δm_1 is the sum of the strongly bound water

Δm_{Ws} and the increase due to the HCl uptake according to reaction (1.16), in agreement with the results of XRD analyses of reacted samples (described in section 4.2.3.1). As a result, the following expression can be proposed:

$$\Delta m_{Ws} = \Delta m_1 - n_{Cl}\left(M_{Ca(OH)Cl} - M_{Ca(OH)_2}\right) \qquad (3.7)$$

where M denotes the molecular weight and n_{Cl} the moles of Cl in the solid sample. On the other hand, the amount of loosely bound water, Δm_{Wl}, can be determined directly from weight decrease during the drying step of the product (see Fig. 3.7). The total amount of water that is taken up by the sorbent is given by

$$\Delta m_W = \Delta m_{Wl} + \Delta m_{Ws}\,. \qquad (3.8)$$

The reproducibility of the results was in the range of 8-16% (standard deviation with 95% confident interval), which made a large number of experiments necessary at the same conditions. The low sample weight and critical gas species of H_2O and HCl caused surprisingly large data fluctuations.

In order to evaluate whether TGA experiments are appropriate to do kinetic studies of the reaction between HCl and $Ca(OH)_2$, some experiments were carried out changing the amount of sample from 1 to 10 mg. The results (not shown) revealed that both the amount of HCl retained and the reaction rates obtained decreased when the amount of sample was increased. This clearly indicates that the TGA set-up used here did not provide differential conditions. Also compaction and channelling might have occurred in the sample. Amounts lower than 1 mg were not checked, because of the limits of accuracy of the TGA balance. Furthermore, because the start of the reaction coincided with the change of buoyancy, the initial step of the reaction was difficult to be determined. Hence, accurate initial reactions rates could not be obtained. Appropriate geometries of the sample holder were also tested to eliminate external mass transfer resistance which could, however, not be excluded for the results presented here. Consequently, it was concluded that no accurate kinetic data could be obtained from TGA experiments, at least for the set-up used.

3.3. SOLID CHARACTERIZATION

The following techniques were used to carry out different analysis concerning the solid reagents and reacted solids used in this work:

1. X-ray diffraction (XRD)

Qualitative analysis of reagents and reacted solids were done to identify the phases present in the samples. Even though XRD is a qualitative technique, it was also used to obtain a rough quantitative approximation of the purity of the commercial $Ca(OH)_2$ reagent. The interpretation of the obtained

patterns were done by comparison with data published by the "Joint Committee of Powder Diffraction Standards (2002)"

- *Equipment used*: Diffractometer (Simens D-500, Germany) using Cu Kα radiation and a secondary graphite monochromator.

2. X-ray fluorescence (XRF)

This technique allows to do semi-quantitative analyses of 78 elements of atomic weight larger or equal to boron. It was used for two purposes:

a. To obtain the amount of impurities of the $Ca(OH)_2$ reagent in a Ca base.

b. To verify the reliability of the calculated values of the retention of SO_2 by $Ca(OH)_2$ from the breakthrough curves (section 3.1.2).

- *Equipment used*: X-ray spectrophotometer Philips PW 2400 equipped with UniQuant v. 2.53 software for semi-quantitative analyses.

3. Laser diffraction granulometry

This technique was used to determine the size particle distribution of the $Ca(OH)_2$ reagent and the seasand that was used to build up the fixed-bed reactor.

- *Equipment used*: Microtrack SRA 150.

4. Ion chromatography (IC)+UV/VIS analysis

Some exploratory analyses were performed by means of IC to check whether nitrite and nitrate ions are formed when the reaction takes place in presence of NO_2.

- *Equipment used*: pump Waters 515 HPLC, column IC-PAC anions, detector UV/VIS Kontron.

5. Ion chromatography (IC) + chlorine potentiometry

Standard methods based on both techniques were used to determine the amount of HCl captured by $Ca(OH)_2$ at different times of exposition (TGA experiments). Some chemical analyses of the final product were performed before and after the drying period to find out whether the final drying step would alter the amount of Cl^- retained.

6. BET surface area

This technique was used to determine BET specific surface areas, total porosities and pore size distribution of the solid reagent.

- *Equipment used*: Porosimeter Micrometrics ASAP 2000 using liquid N_2 (77 K).

7. Helium picnometer

An helium picnometer was used to check the real density of the sorbent reagent

- *Equipment used*: Helium picnometer Accupic 1330.

8. Scanning electron microscopy (SEM)- Energy dispersive spectroscopy (EDS)

The surface morphology of the reagent and reacted particles was observed with SEM. Furthermore, some elemental microanalyses by EDS were also carried out to check the presence of sulfur on the surface of the reacted particles.

- *Equipment used*: Hitachi S-2300 (10-15 kV) and Jeol JSM-840 (10-15 kV).

10. Atomic force microscopy (AFM)

This technique provides 3D topographical maps of surfaces with a resolution range extended from the millimeter down to the nanometer or subnanometer. The information is digitally registered, and subsequently, the roughness, and the form and distribution of the features on the surface can be determined (for more information concerning this technique see Appendix B).

- *Equipment used*: Extended Multimode microsope controlled by a Nanoscope IIIA electronics (Digital Instruments). The AFM probes were ultrasharp silicon tips (NT-MDT, Russia), manufactured in monocrystalline silicon with a nominal tip radius of about 10 nm, pyramidal shape, a spring constant of approximately 35 N/m and a resonant frequency of about 300 KHz. The AFM scanning unit could be introduced inside a control humidity chamber.

4. Results

4.1. CHARACTERIZATION OF THE SOLID REAGENTS

4.1.1. CHARACTERIZATION OF COMMERCIAL SOLID REAGENT

The XRD pattern of the solid reagent is shown in Fig. 4.1. As can be seen, the solid was quite crystalline, being $Ca(OH)_2$ the main species. $CaCO_3$ was also found, but at much lower proportion, and $CaSO_4$ and Na_2SO_4 were present at very small quantities. A quantitative analysis of the pattern provided the following rough composition: 99% $Ca(OH)_2$ and 1% $CaCO_3$.

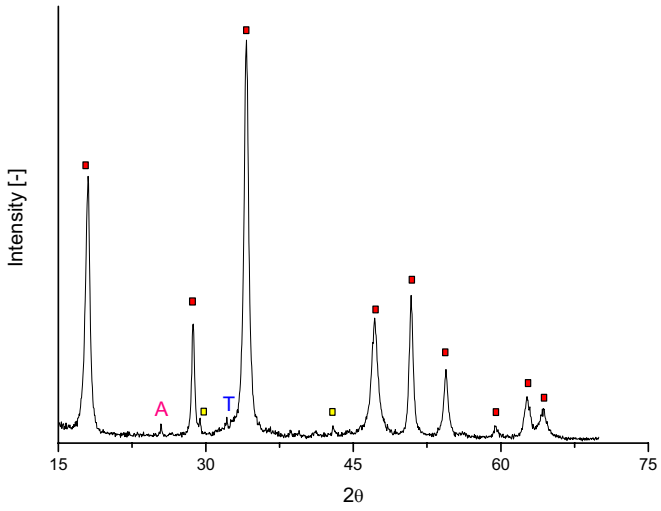

Fig. 4.1: XRD pattern of the solid reagent.

■ - Portlandite ($Ca(OH)_2$), □ - Calcite ($CaCO_3$),
T - Thenardite (Na_2SO_4), A - Anhydrite ($CaSO_4$)

The quantification of other minor elements contained in the solid reagent was done by XRF. The results revealed the presence of Si, Mg, Al, S, K, Fe, Na and P, all of them as trace elements, and hence, the solid could be considered as highly pure.

The main physical properties of the $Ca(OH)_2$ commercial crystals used in this work are summarized in Table 4.1. As can be seen, the apparent density was found to be 2.37 g cm^{-3}, very similar to that found in the literature, 2.24 g cm^{-3}. The mean size of the $Ca(OH)_2$ crystals was 9.4 μm, while that of the inert solid used as diluent was 308 μm.

Table 4.1: Physical properties of $Ca(OH)_2$ commercial crystals.

Property	*Value*
Density[1] (apparent) (g cm^{-3})	2.37
Crystal size[2] (mean - d_p-) (μm)	9.4
Crystal size[2] (90% of volume occupied) (μm)	20.3
BET specific surface[3] (m^2g^{-1})	13.8 ± 0.1
Pore volume[3] (cm^3 g^{-1})	0.060
Porosity[3] (%)	14
Pore diameter[3] (mean) (nm)	17.5

[1] Determined by an He picnometer.

[2] Determined by laser diffraction granulometry.

[3] Determined from N_2 adsorption by BET technique.

Moreover, the pore size distribution of the commercial crystals (see Fig. 4.2) was determined from N_2 adsorption by means of the BET technique. Most of pores lie in the range 3.6-19.6 nm, which indicates that the porous are basically mesoporous, while the amount of microporous is practically negligible (lower than 3%).

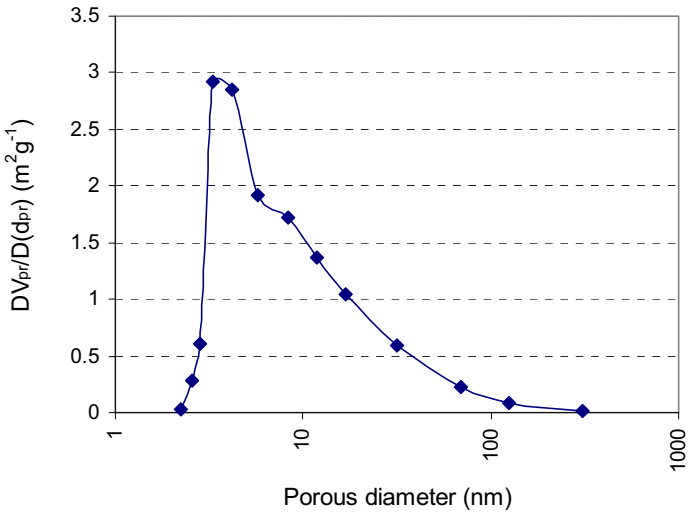

Fig. 4.2: Pore size distribution of $Ca(OH)_2$ commercial crystals
V_{pr} and d_{pr} denote the volume and diameter of porous.

The SEM micrographs of some $Ca(OH)_2$ commercial crystals are displayed in Figs. 4.3 (a-d). It can be seen that the crystals are irregular shaped and two kinds of morphologies seem to be distinguished. First, some agglomerates of a size around 10 μm built of small 1 μm subcrystals can be observed. In fact, this size is in agreement with the mean crystal size obtained by laser diffraction (see

Table 4.1). Some crystals seem to be laminar-shaped. Furthermore, some individual crystals of higher size can be also observed (see Fig. 4.3d), but they are less frequent.

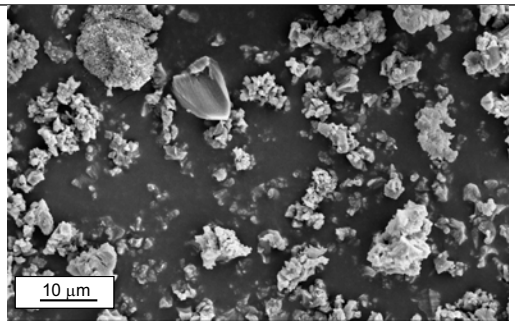

Fig. 4.3a: SEM micrograph of $Ca(OH)_2$ crystals.

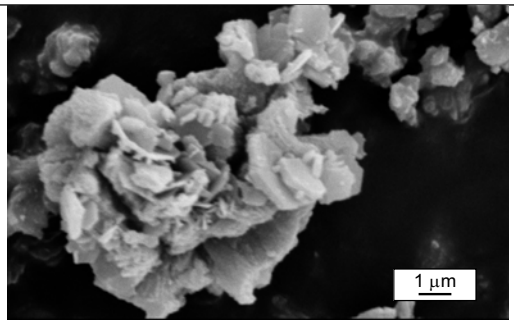

Fig. 4.3b: SEM micrograph of a $Ca(OH)_2$ agglomerate.

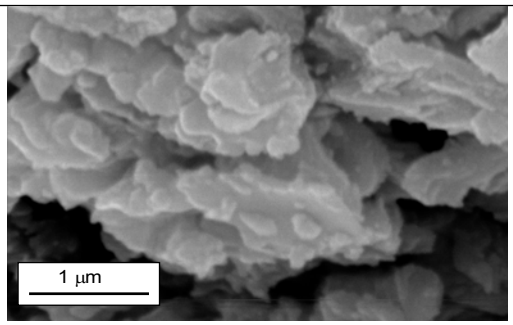

Fig. 4.3c: SEM micrograph a $Ca(OH)_2$ agglomerate.

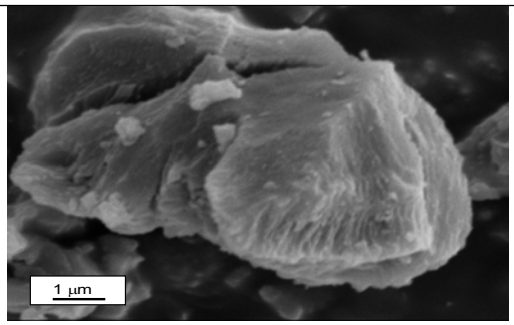

Fig. 4.3d: SEM micrograph of one particle of $Ca(OH)_2$.

4.1.2. CHARACTERIZATION OF SINGLE CRYSTALS PREPARED BY THE DIFFUSIONAL METHOD

The diffusional method described in section 3.1.2. allowed to obtain crystals up to 2-5 mm after 4 weeks of crystallization. A photograph of selected crystals is shown in Fig. 4.4.

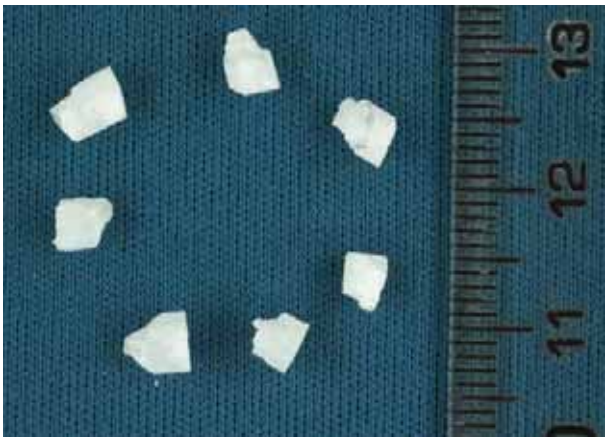

(a)

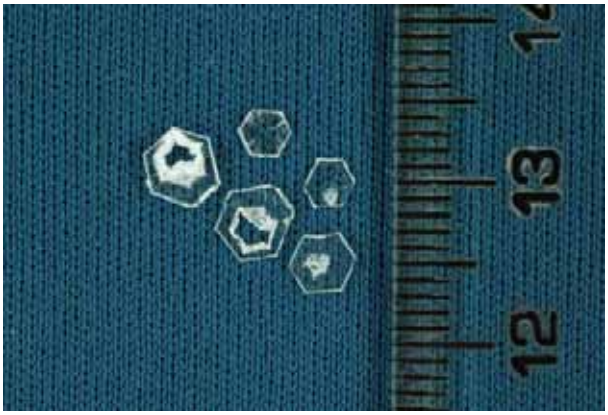

(b)

Fig. 4.4: Crystals of $Ca(OH)_2$ obtained by a diffusion method (length scale in cm) (a) Crystals after preparation; (b) Cleaved crystals.

Some cleaved crystals are shown in Fig. 4.4(b). As can be seen, they were perfectly transparent to visible light and hexagonal-shaped. The larger crystals showed an inner hexagonal hole which might be ascribed to two different and crystalline growing profiles. After a few days of preparation of the precursor solutions, some additional water was added to the 2000 mL beaker to maintain its level constant, since it had been slightly reduced due to evaporation. The addition of water might have changed the concentration of the precursor ions, which could have altered the growing profile and promoted the growth of a new surrounding crystal.

The surface of different freshly cleaved $Ca(OH)_2$ crystals was viewed by AFM (see Figs. 4.5 and 4.6). The images reveal that all the surfaces were quite regular and smooth (roughness < 0.3 nm). The smooth terraces were interrupted by steps of height about 0.5 nm, which corresponds to the **c** lattice parameter of the unit cell of $Ca(OH)_2$, as it is explained in the following section.

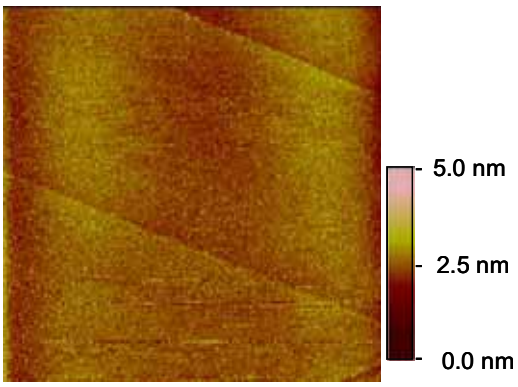

Fig 4.5. 20 x 20 μm^2 AFM image of a freshly cleaved surface of $Ca(OH)_2$. Rms: 0.3 nm.

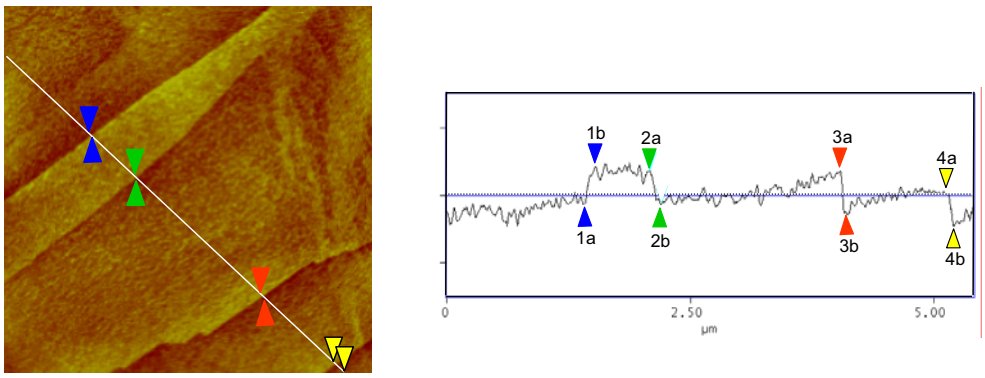

Fig 4.6. 4 x 4 μm^2 AFM image of a freshly cleaved surface of $Ca(OH)_2$ and image profile where it can be seen that the step height corresponds to the **c** lattice parameter of the unit cell of $Ca(OH)_2$.
Step height: 1a-1b: 0.501 nm; 2a-2b: 0.474 nm; 3a-3b: 0.594 nm; 4a-4b: 0.499 nm. Rms: 0.195 nm.

4.1.3. CRYSTAL STRUCTURE OF $Ca(OH)_2$

$Ca(OH)_2$ crystallizes in the hexagonal space group $P\bar{3}m1$ (*Pauling, 1960; Moreno et al. 1984*). The main data concerning the lattice parameters and atomic distances are summarized in Table 4.2. A unit cell of the lattice and a projection of the (0001) plane are schematically depicted, respectively, in Figs. 4.7(a-b). The calcium ions lie in the (0001) planes and the planes containing the hydroxyl ions are parallel to the (0001) planes at 0.233C and -0.233C away from it. As a result, the hydroxyl ions are alternately above and below the planes containing the calcium ions. Moreover, in Fig. 4.7(c), a diagrammatic view of the layered lattice structure is shown. The layers are supposed to be held together by weak secondary forces occurring between the neighboring HO^- ions layers. It has been established that, at low temperatures, the hydroxyl ions are oriented parallel to the C-axis as it is shown in Fig. 4.7(c).

Table 4.2: Lattice parameters and atomic distances of $Ca(OH)_2$.

Property		*Value*
Lattice parameters (Å)	a	3.5918
	b	3.5918
	c	4.9063
Atomic distances (Å) [1]	O-H	0.984, 2.665
	Ca-O	2.371
	O-O	3.592 (in basal plane) 3.333 (the other edges of the CaO_6 octahedron) 3.095 (the H-containing O_4 tetrahedron)

[1] Determined by neutron diffraction (*Pauling, 1960*).

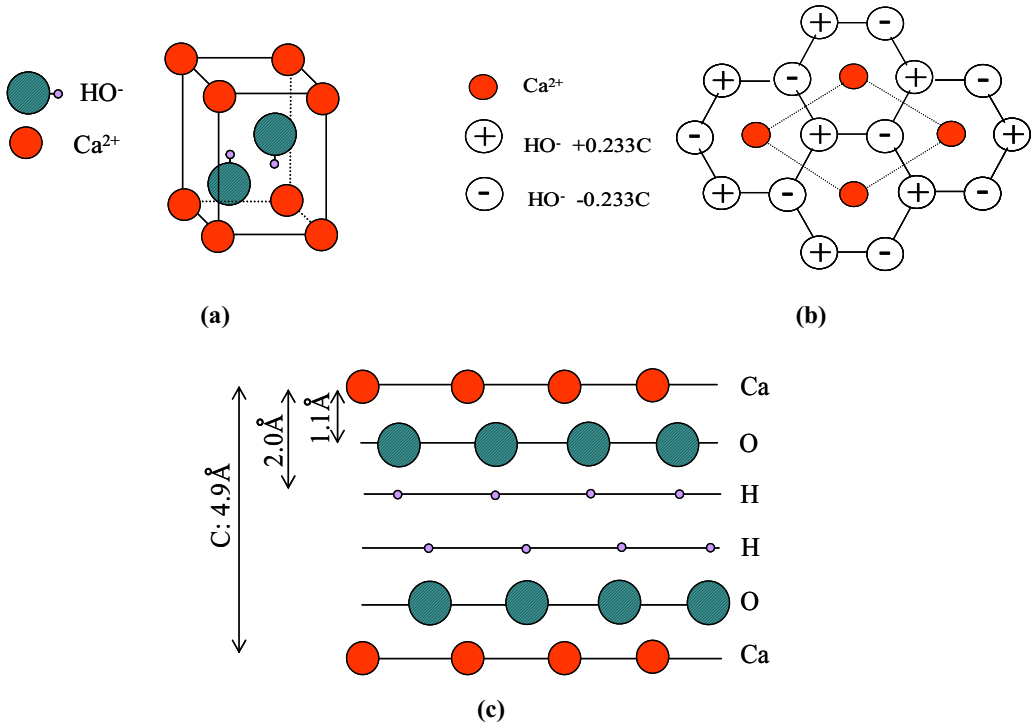

Fig. 4.7: Hexagonal lattice of $Ca(OH)_2$. (a) Unit cell; (b) Projection on the (0,0,0,1) plane; (c) View of the layered structure (*Moreno et al. 1984; Chaix-Pluchery et al., 1987*).

4.2. CHEMICAL REACTIVITY OF SYSTEMS SO_2 (+NO_2) / HCl + $Ca(OH)_2$

4.2.1. SYSTEM SO_2 + $Ca(OH)_2$

The study of the reaction between SO_2 and $Ca(OH)_2$ has been performed in the ranges 0-70% of RH, 313-353 K, 2000-8000 ppm of SO_2 concentration and 0-21% (molar) of O_2 concentration. The

obtained values of the amount of SO_2 captured by the solid sorbent after 1 hour of reaction at all tested conditions are indicated in Table 4.3.

From the data presented in Table 4.3, it can be pointed out that solid conversions after one hour of reaction time are lower than 30% for all tested conditions. Low solid conversion was already found in some studies carried out both at laboratory scale *(Damle et al. 1986, Ruiz-Alsop and Rochelle, 1987, Aichinger et al. 1995, Karatepe et al. 1999)* and at pilot scale (see Fig. 1.4). In fact, the low reactivity of $Ca(OH)_2$ towards SO_2 retention is one of the major drawbacks of in-duct injection with humidification technologies.

Table 4.3: SO_2 retained after 1 hour of reaction at all experimental conditions tested.

C_{SO_2} (ppm)	T (K)	RH (%)	mol SO_2/mol Ca
2000	313	0	0.028
		30	0.071
		50	0.144
		70	0.263
	333	0	0.028
		30	0.083
		50	0.163
		60	0.170
		70	0.270
	353	0	0.021
		30	0.112
		50	0.170
		70	0.222
5000	313	30	0.060
		50	0.115
		70	0.293
	333	30	0.077
		50	0.136
		70	0.287
	353	30	0.100
		50	0.144
		70	0.211
8000	313	30	0.051
		50	0.079
		70	0.210
	333	30	0.067
		50	0.100
		70	0.209
	353	30	0.093
		50	0.126
		70	0.156

Some experimental breakthrough curves obtained in this work are shown in Fig. 4.8. Although reaction rates cannot be directly found from these curves because the fixed-bed did not work at differential conditions, their shape can provide valuable information concerning the progress of the reaction:

1. Since the differences between the blank and the reaction breakthrough curves during the first 30 minutes of reaction are much larger than those at longer times, an initial period where most of the overall reaction takes place can be suggested.

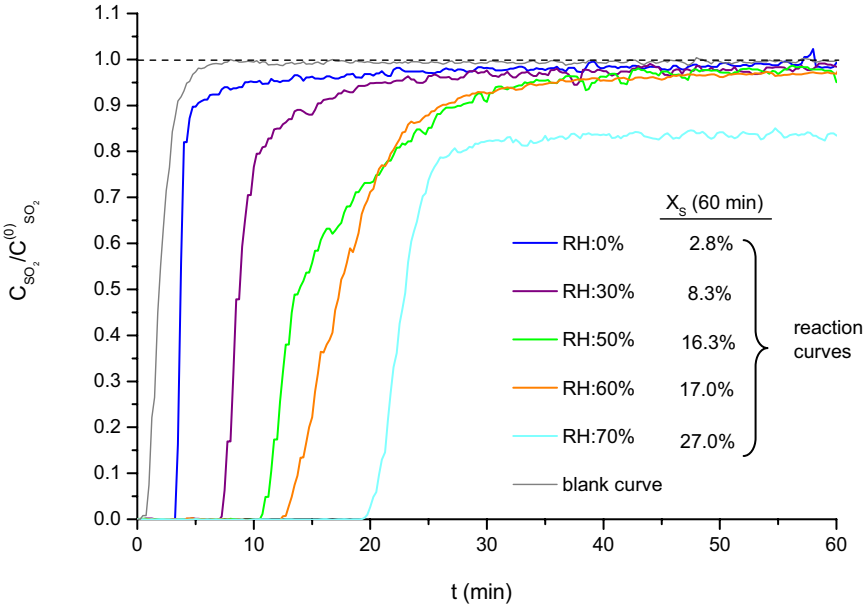

Fig. 4.8: Experimental breakthrough curves obtained at 333 K and 2000 ppm of SO_2.

2. This initial period seems to terminate with a sharp decrease of the reaction rate, according to the steep slope usually observed, which is in agreement with the results previously found by other researchers (see section 1.5.3).

3. Finally, it should be mentioned that the ratio $C_{SO_2}/C^0_{SO_2}$ does not strictly reach values of 1 for all the curves after 1 hour of reaction, especially in those corresponding to experiments undertaken at high RH (70%), which indicates that complete conversion has not been achieved. After a period of a steep decrease of the reaction rate, the reaction would not stop and could go on at a very low reaction rate.

In order to give new insight in the evolution of the reaction at times longer than 1 hour, two experiments were undertaken, respectively, at 50% of RH during 4 hours and at 70% of RH during 6 hours. The results obtained for solid conversion (X_s) vs. time (see Fig. 4.9) seem to confirm that the reaction goes on after 1 hour. Furthermore, as the trend obtained is practically linear for times beyond 1 hour, a constant rate step after the sharp decrease of the reaction rate could be proposed. In fact, a

constant rate step was previously mentioned by *Damle et al. (1986)* for a reaction carried out at 70% of RH and 343 K. Moreover, the results obtained by *Aichinger et al. (1995)* and *Krammer et al. (1997)* in a thermobalance also show a low but monotonic increase of the sample weight after 20-30 minutes of reaction at RH of 70% or higher, which could be also related to a constant rate step. Given that for 1 hour of reaction the solid conversion of the entire bed increases ca. 2.4% and 4.0% (absolute values) operating at 50 and 70% of RH (see Fig. 4.9), respectively, this period can be characterized by a very low reaction rate and by a high dependence on the RH.

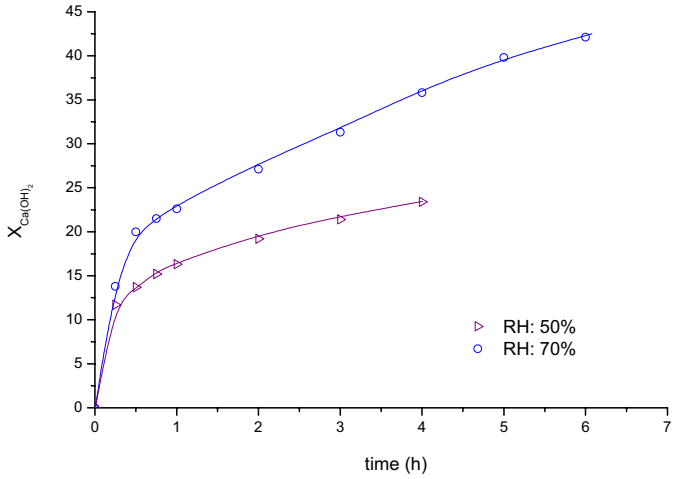

Fig. 4.9: Solid conversion at 333 K and 2000 ppm of SO_2 concentration.

4.2.1.1. Influence of the RH on SO_2 retention

The effect of the RH on the desulfurization reaction was studied at 1 hour of exposure time. The amount of SO_2 retained by the solid sorbent at 2000, 5000 and 8000 ppm of SO_2 concentration, respectively, is shown in Figs. 4.10(a-c).

From the results obtained, a great effect of RH on the ability of the sorbent to capture SO_2 can be observed, which agrees with the studies reported in the literature. Although this effect is observed for all the temperatures and SO_2 concentrations tested, it seems that it is more remarkable at 313 and 333 K than at 353 K. Despite the lack of more RH conditions tested, an exponential trend between the amount of SO_2 captured and RH at 313-333 K could be suggested, while at 353 K, a linear trend might be more appropriate. This behavior does not essentially differ from that observed by *Garea et al. (2000)* and *Jorgensen et al. (1987)*, since the former proposed a lineal trend in the range of 337-343 K at 40-70% of RH and the latter suggested an exponential trend at 338 K in the range of 10-80% of RH (see Table 1.3). In contrast, *Ruiz-Alsop and Rochelle (1987)* found a stronger influence of the RH on the SO_2 retention at lower values of RH than at higher ones.

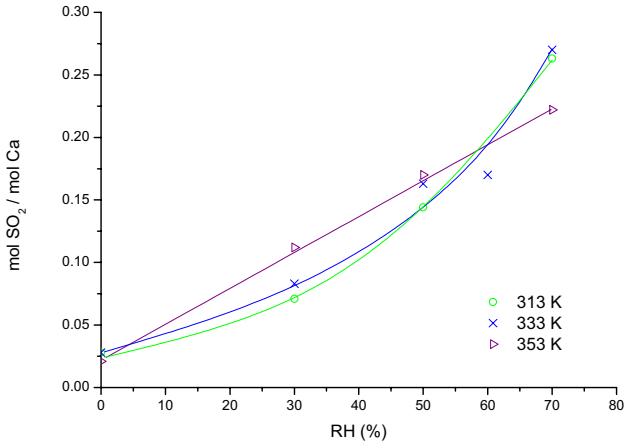

(a)

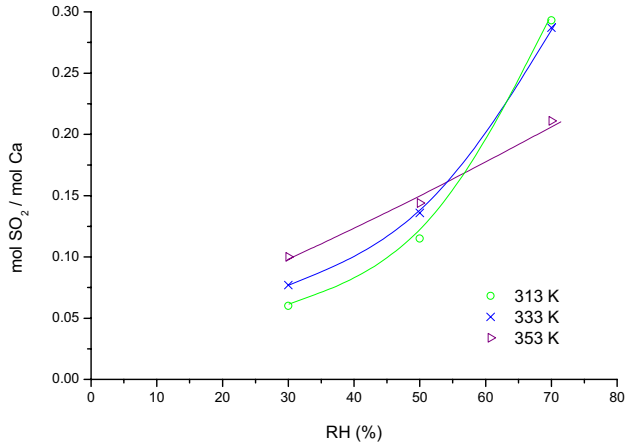

(b)

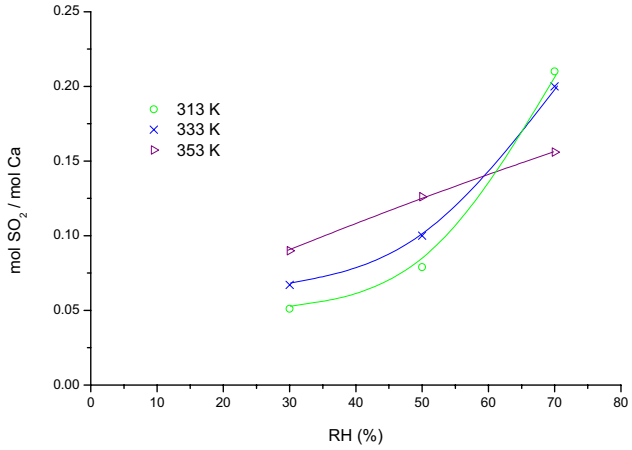

(c)

Fig. 4.10: Effect of the RH on SO_2 retention after 1 hour at: (a) 2000 ppm; (b) 5000 ppm; and (c) 8000 ppm SO_2.

4.2.1.2. Influence of temperature on SO_2 retention

The effect of temperature on the ability of $Ca(OH)_2$ to retain SO_2 can be also observed in Figs. 4.10(a-c). As can be seen, the influence of the temperature is much less significant than that of RH, which is in correspondence with the majority of the results reported in the literature (see section 1.4.1). In addition, it appears that the effect of temperature after 1 hour of reaction varies depending on the RH. In general terms, at 30% of RH, the influence of temperature is slightly positive, while at 50% its effect is practically negligible, which is in agreement with most of the results found in the literature (see Table 1.4). Finally, at 70% of RH, no influence of temperature on the SO_2 retention is observed in the range 313-333 K, but an increase until 353 K has a slight negative effect, which seems to differ somewhat from the literature. The fact that the effect of temperature on the reactivity is quite low could account for the differences found.

4.2.1.3. Influence of SO_2 concentration on SO_2 retention

Concerning the effect of SO_2 concentration on the amount of SO_2 captured by the solid after 1 hour of exposure time, different behaviors can be observed depending on the RH (Fig. 4.11). A null influence is found at 30% RH, because the SO_2 uptake for different SO_2 concentrations lies within experimental error range. This result is in agreement with those reported by several researchers (*Ruiz-Alsop and Rochelle, 1987; Krammer et al., 1997; Karatepe et al. 1999*). However, a slight negative effect is found beyond 30% of RH.

4.2.1.4. Influence of O_2 concentration on SO_2 retention

Some experiments were also conducted to determine the effect of oxygen on the SO_2 removal. The study was done at 70% RH, 333 K, 2000 ppm of SO_2, varying the O_2 concentration from 2.5 to 21% (molar). It was found that the effect of O_2 on the SO_2 breakthrough curves is practically negligible, which might indicate that, despite its oxidant character, it does not appear to change neither the reaction rate nor the capability of $Ca(OH)_2$ to capture SO_2 (experimental breakthrough curves are not shown here).

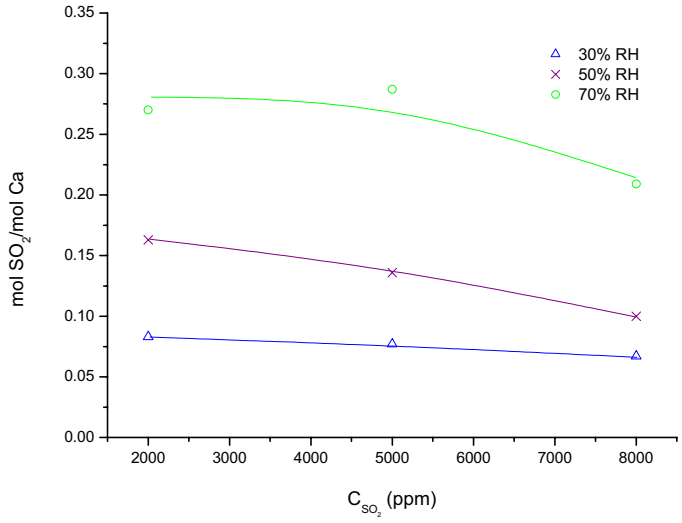

Fig. 4.11: Effect of SO_2 concentration on SO_2 retention after 1 hour at 333 K.

4.2.1.5. Verification of the experimental method to calculate SO_2 retentions

Semi-quantitative elemental analyses of reacted solids by X-ray fluorescence (XRF) were performed to verify the reliability of the method to evaluate the SO_2 retained by the solid from the experimental breakthrough curves, that is, by gas phase-analysis (see Appendix A). As can be seen in Table 4.4, the results obtained by means of both analytic methods are in fairly good agreement. Furthermore, the last two data corresponding to experiments carried out at 70% of RH and at 1 and 2 hours of reaction time, respectively, confirm that the SO_2 uptake goes on after one hour of reaction.

4.2.1.6. Reproducibility of the amount of SO_2 retained

The reproducibility of the experimental data was determined by repeating some experiments at the same conditions at least 4 times, including also replicates of some blank breakthrough curves. The chosen conditions, as well as the results, are shown in Table 4.5. It is noticeable that, in all cases, the experimental error was lower than 12% (confidence level 95%) despite the complexity of the experimental set-up.

Table 4.4. SO_2 retention determined from gas phase analyses and solid analyses.

RH (%)	C_{so_2} *(ppm)*	*Reaction time (h)*	*mol SO_2/mol Ca (by IR)*	*mol SO_2/mol Ca (by XRF)*[1]
60	1100	1	0.1216±0.0061	0.1284±0.0051
60	1100	1	0.1358±0.0057	0.1451±0.0089
60	2000	1	0.225±0.013	0.2017±0.0062
70	2000	1	0.254±0.016	0.2035±0.0096
70	2000	2	0.302±0.016	0.2643±0.0089

All the experiments have been done at 333K. Standard deviation with 95% confidence level.

(1) Error includes only fluorescence analysis error.

Table 4.5: Experimental error determined from experimental breakthrough curves at 1 hour of reaction time.

C_{so_2} *(ppm)*	*RH (%)*	*T (K)*	*Nr of replies*	*mol SO_2/mol Ca (average)*	*σ (%)*
2000	70	333	4	0.270	3.6
8000	30	333	4	0.067	12.3
2000	30	353	4	0.112	2.3
8000	70	353	5	0.156	8.9

Standard deviation with 95% confidence level (relative values).

4.2.2. SYSTEM SO_2 +NO_2 + $Ca(OH)_2$

4.2.2.1. Effect of NO_2 presence on SO_2 retention

In Table 4.6, data concerning the experiments performed to quantify the influence of the presence of NO_2 on the capability of $Ca(OH)_2$ to retain SO_2 are shown. In the first row of each subdivision, experiments without NO_2 are detailed as a reference. The ratio of SO_2 retained in the presence of NO_2 to that in the absence of NO_2 is shown in the last column.

Table 4.6: Effect of NO_2 on SO_2 capture. Experimental conditions and results.

Nr	*T (K)*	*RH (%)*	*C_{SO_2} (ppm)*	*C_{NO_2} (ppm)*	*C_{O_2} (%)*	*Reaction time (h)*	*mol SO_2/mol Ca* [1]	*Ratio*
1	333	70	2000	0	0	2 / 3	0.260 / 0.294	
2				175		2 / 3	0.738 / 0.823	2.84 / 2.80
3				75		3	0.762	2.59
4				275		3	0.865	2.94
5	333	60	2000	0	0	0.5/ 2	0.1702 / 0.189	
6				175	0	0.5 / 1 / 2	0.2696 / 0.453 / 0.565	1.58(0.5h) / 2.99(2h)
7				175	2.5	1 / 2	0.416 / 0.561	0.92 / 0.99 [2]
8				175	5	1 / 2	0.402 / 0.562	0.89 / 1.00[2]
9				175	10	1 / 2	0.395 / 0.550	0.87 / 0.97[2]
10				175	18	1 / 2	0.410 / 0.544	0.90 / 0.96[2]
11	333	50	2000	0	0	1.5 / 2	0.1714 / 0.1718	
12				175	0	1.5 / 2	0.336 / 0.387	1.96 /2.25
13				75	0	1.5	0.312	1.82
14				275	0	1.5	0.357	2.08
15	333	30	2000	0	0	2	0.1241	
16				175	0	2	0.179	1.44
17	353	60	2000	0	0	2	0.200	
18				175	0	2	0.554	2.77

[1]Calculated at the reaction time indicated on the left column.

[2]The ratio is calculated respect the experiment nr. 6 done in absence of O_2 and presence of NO_2.

As can be seen in Table 4.6, the presence of NO_2 enhances greatly the capability of $Ca(OH)_2$ to capture SO_2 for all the conditions tested, with an increase up to 200% after 2 or 3 hours of reaction. This positive effect was also observed by *O'Dowd et al. (1994)* in a spray dryer/baghouse system and by *Nelli and Rochelle (1998)* in a fixed-bed reactor. Moreover, the effect observed by the latter when working at similar experimental conditions is of the same order of that found in this study. A good agreement is observed when comparing the effect of the addition of NO_2 to the gas stream on the experiments performed at 60% of RH and 0.5 hours of reaction. Meanwhile in this study SO_2 retentions increased ca. 58% when 175 ppm of NO_2 were added to the system, *Nelli and Rochelle (1998)* found an increase of 30% and 88% when 55 and 227 ppm of NO_2 were added. Furthermore, although absolute captures found in this study are higher than those reported by *Nelli and Rochelle (1998)*, the apparent differences might be explained by comparing the surface areas of the solids employed in both studies.

The ratio of the SO_2 retained in the presence to that in the absence of NO_2 at 60% of RH at 333 K - 0.170 (Table 4.6) / 0.120 (in *Nelli and Rochelle, 1998*) = **1.4**- is very close to the ratio of surface areas of the $Ca(OH)_2$ -13.84 m^2/g (Table 4.1) / 8.76 m^2/g (in *Nelli and Rochelle, 1998*) =**1.6**.

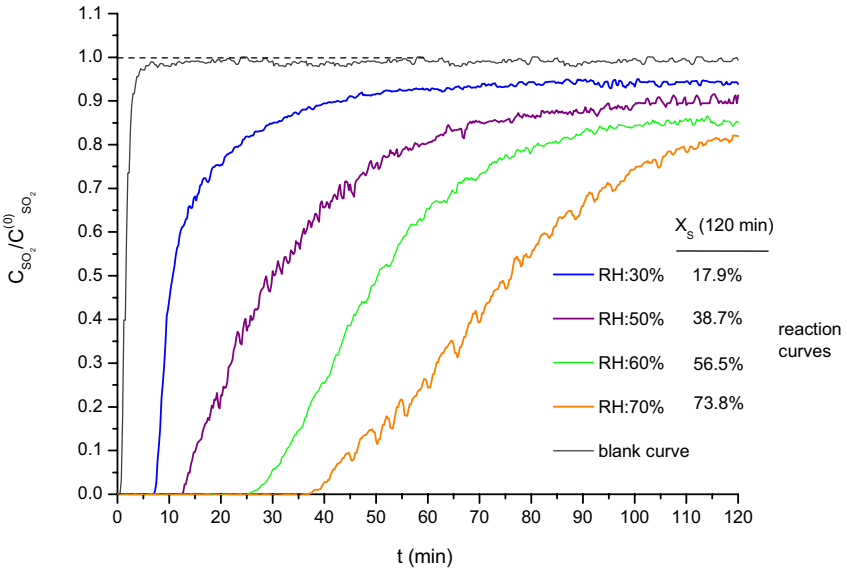

Fig.4.12: Experimental breakthrough curves obtained at 333 K, 2000 ppm SO_2 and 175 ppm NO_2.

Regarding the shape of the experimental breakthrough curves, some of which are plotted in Fig. 4.12, two aspects should be emphasized. To begin with, the slope of the curves are at almost all conditions less steep than those without NO_2, which might be interpreted as a more gradual or softer reduction of the reaction rate in comparison to that suggested in the absence of NO_2. Moreover, the constant rate step mentioned in section 4.1.1. is also observed, but it appears to take place at higher reaction rates. In the presence of NO_2, the solid conversion of the entire bed for 1 hour of reaction is 7.5% and 8.5% at 50% and 70% of RH, respectively, while for experiments carried out in absence of NO_2, they are 2.4% and 4.0% (see section 4.2.1.). Consequently, the presence of NO_2 seems to boost the progress of the reaction at longer times in the range of conditions described above.

Analogously to the study of SO_2 in absence of NO_2, some solid analyses have been also done to evaluate the reliability of the experimental procedure. The obtained results, collected in Table 4.7, also show a reasonable agreement between both data. Thus, it could be concluded that the selected analytical method provides good measurements.

Table 4.7: SO_2 retention determined from gas phase analyses and solid analyses.

RH (%)	C_{SO_2} *(ppm)*	C_{NO_2} *(ppm)*	*Reaction time (h)*	*mol SO_2/mol Ca (by IR)*	*mol SO_2/mol Ca (by XRF)*[1]
30	2000	175	1	0.1319±0.011	0.1367±0.0058
50	2000	175	2	0.3265±0.018	0.3218±0.0094
50	2000	175	2	0.3677±0.020	0.3394±0.0093
60	2000	175	2	0.537±0.020	0.486±0.011

All the experiments have been done at 333K. Standard deviation with 95% confidence level.

[1]Error includes only fluorescence analysis error.

4.2.2.2. Influence of NO_2 concentration, RH, temperature and O_2 presence on SO_2 retention

The effect of NO_2 concentration has been determined in the range of 0-275 ppm at 70 and 50% of RH (see Table 4.6, runs 1-4 and 11-14). As can be seen in Figs. 4.13 (a-b), a raise in the SO_2 uptake is observed when NO_2 concentration increases from 0 to 175 ppm. Moreover, it seems to be practically independent beyond 175 ppm, since the small differences lie within the experimental error. However, SO_2 retention remains almost unchanged with NO_2 concentration as time elapses. This result seems to indicate that an increase of NO_2 concentration (up to 175 ppm) involves an increase in SO_2 capture rate, while the maximum uptake of SO_2 by mol of $Ca(OH)_2$ might not be influenced by NO_2 concentration.

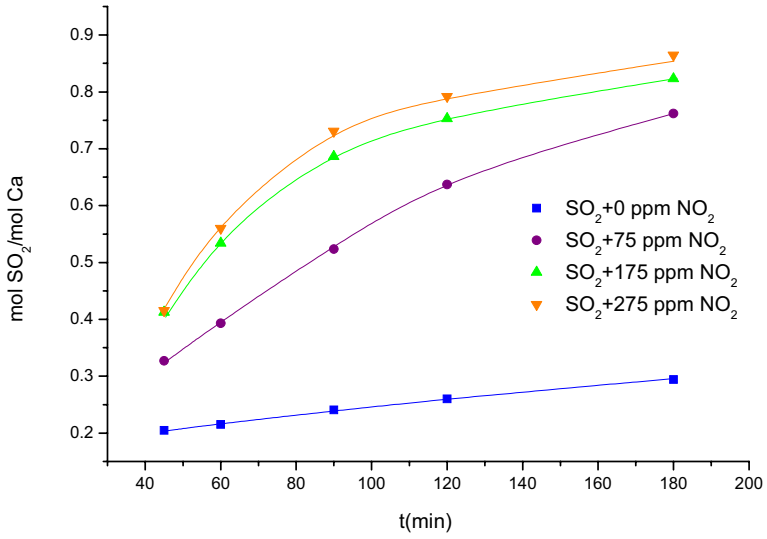

(a)

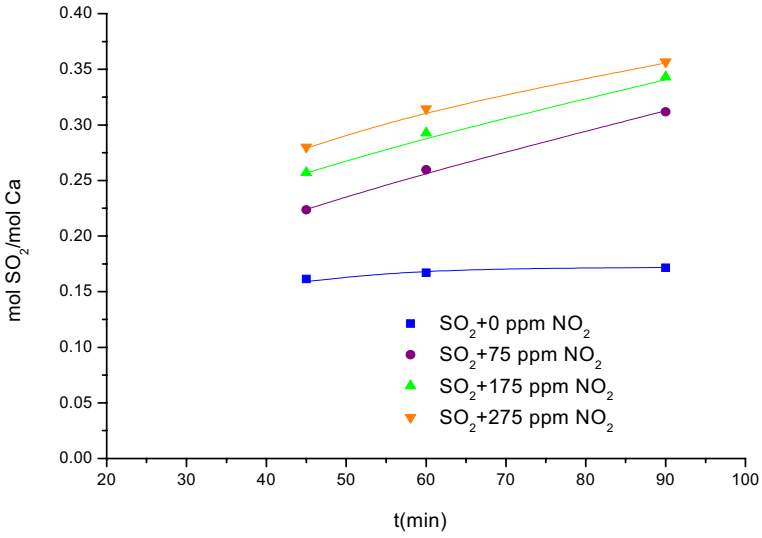

(b)

Fig. 4.13: Effect of NO_2 concentration on SO_2 uptake at 333 K and 2000 ppm SO_2, (a) 70% RH, (a) 50% RH.

The influence of the RH on SO_2 capture has been studied at 333 K. The results obtained, which are plotted in Fig. 4.14, indicate that the strong influence of RH on the capability of $Ca(OH)_2$ to retain SO_2 is boosted when NO_2 is present. For instance, after two hours of reaction, a raise of RH from 30% to 70% (run 15 respect to 1) involves a SO_2 uptake increase of 117% in the absence of NO_2, while in the presence of NO_2 (run 16 respect to run 2), it raises to 311% (see Table 4.6). Furthermore, as can be seen in Fig. 4.14, an exponential trend could be suggested, similar to that proposed for the system without NO_2.

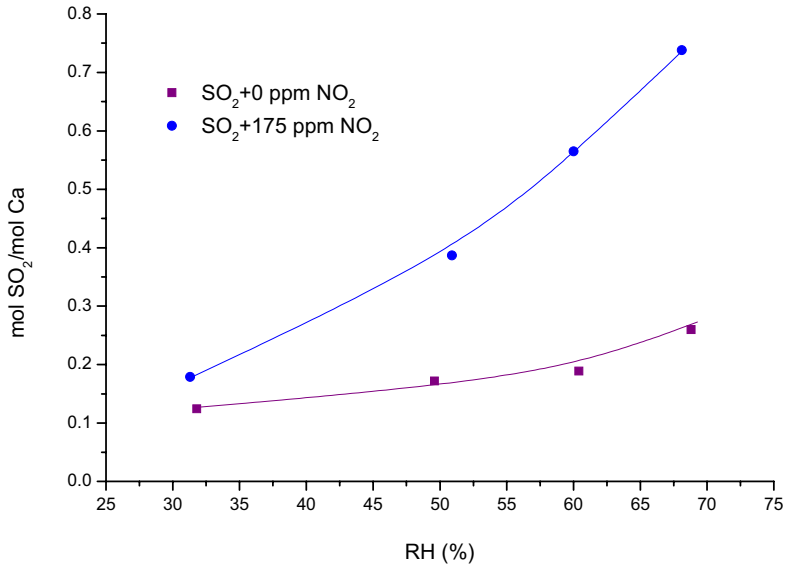

Fig. 4.14: Effect of RH on SO_2 uptake after 2 hours of reaction at 333 K and 2000 ppm SO_2.

The effect of temperature has been studied in the range 333-353 K. From the experimental results (see Table 4.6), it can be concluded that when both pollutants coexist (run 18 respect to 6), the influence of temperature at constant RH is not significant on the capability of $Ca(OH)_2$ for SO_2 capture. This observation agrees with that found in the previous study in the absence of NO_2. (see section 4.2.1.4.) Therefore, the temperature does not seem to play a key role in the desulfurization process in the studied range.

The effect of O_2 concentration on SO_2 removal has been studied in the range 0-18% and keeping the rest of variables constant at the following conditions: 60% RH, 333 K, 2000 ppm of SO_2 and 175 ppm of NO_2. The values obtained for SO_2 retention are included in Table 4.6, while the experimental breakthrough curves are depicted in Fig. 4.15. From the results shown, it can be suggested that the addition of O_2 involves a slight reduction of SO_2 removal per mol of calcium (runs from 7 to 10) for 1 h reaction time. Furthermore, this effect seems to be independent of O_2 concentration, which agrees with the results reported by *Nelli and Rochelle (1998)* at 30 min. However, when the reaction progresses, the total amount of SO_2 retained appears to be unaffected by the presence of O_2, as can be seen in experiments 7 to 10 for 2 h of reaction (Table 4.6). In fact, different breakthrough curves are obtained, respectively, in the absence and in the presence of O_2, which appears to indicate that O_2 plays a role in the reaction especially at short times by inhibiting the retention of SO_2, although it does not seem to modify it at longer times.

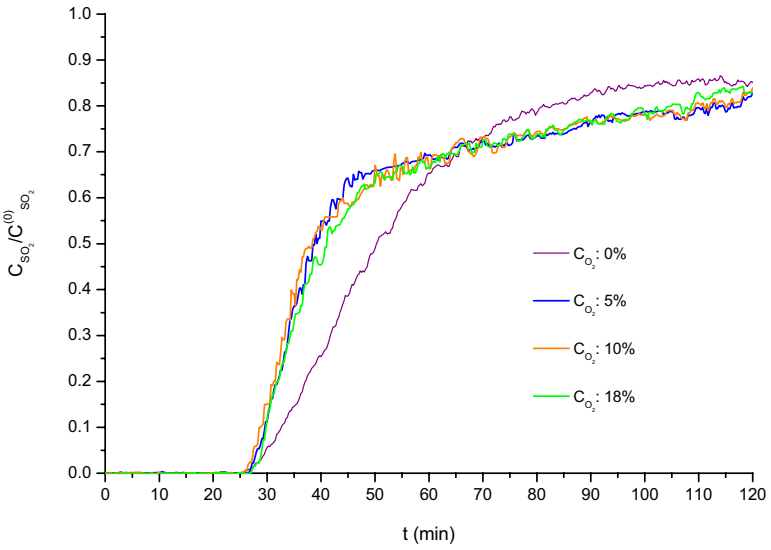

Fig. 4.15: Effect of O_2 concentration at 333 K, 60% RH, 2000 ppm SO_2 and 175 ppm NO_2.

4.2.2.3. Solid analyses and mechanistic pathway

The results obtained for XRD solid analyses are summarized in Table 4.8 and some XRD patterns are shown in Fig. 4.16. XRD analyses indicate the effect of the nature of the gas reactants on the oxidation state of the sulfur species in the reacted product. In this way, independently of the RH values

tested, when SO_2 is the only reactive gas species, $CaSO_3 \cdot (1/2)H_2O$ is the only crystalline structure detected as reaction product. When a 5% O_2 is added, even though the amount of SO_2 uptake does not significantly change, a fraction of the product is oxidized to $CaSO_4$.

Table 4.8: X-Ray diffraction of reacted product. Experimental conditions and results.

RH (%)	C_{SO_2} *(ppm)*	C_{NO_2} *(ppm)*	C_{O_2} *(%)*	*Reaction time (h)*	*Results*
30	2000	0	0	1	$CaSO_3 \cdot (1/2)H_2O$
75	2000	0	0	1	$CaSO_3 \cdot (1/2)H_2O$
60	2000	0	5	1	$CaSO_3 \cdot (1/2)H_2O$, $CaSO_4$
70	2000	175	0	1.5	Main peak: $CaSO_3 \cdot (1/2)H_2O$ Small peaks: $CaSO_4(1/2)H_2O$. $CaSO_4 2H_2O$
70	2000	175	10	1.5	$CaSO_4(1/2)H_2O$. $CaSO_4 2H_2O$

When SO_2 and NO_2 are simultaneously present in the feed, a main peak of $CaSO_3 \cdot (1/2)H_2O$ and appreciably lower peaks of sulfates have been detected as crystalline species. In this case, the presence of sulfates could be explained by means of the redox reaction (4.1), which is analogous to that reported in solution (reaction 1.11):

$$2NO_{2(g)} + CaSO_{3(s)} + Ca(OH)_{2(s)} \leftrightarrow Ca(NO_2)_{2(s)} + CaSO_{4(s)} + H_2O_{(ads)} \qquad (4.1)$$

Although this reaction involves two solids as reactants, which is generally kinetically disadvantageous, the reaction could be feasible in the presence of calcium nitrites and nitrates. Because these species are highly hygroscopic, an adsorbed water layer might be formed on their surface, where the reaction could take place more easily as the involved ions HO^-, SO_3^{2-} and Ca^{2+} could react more freely. Furthermore, if this reaction is considered, the results reported by *O'Dowd et al. (1994)* related to an increase in the ratio sulfate/sulfite with the ratio NO_2/SO_2 could be as well explained.

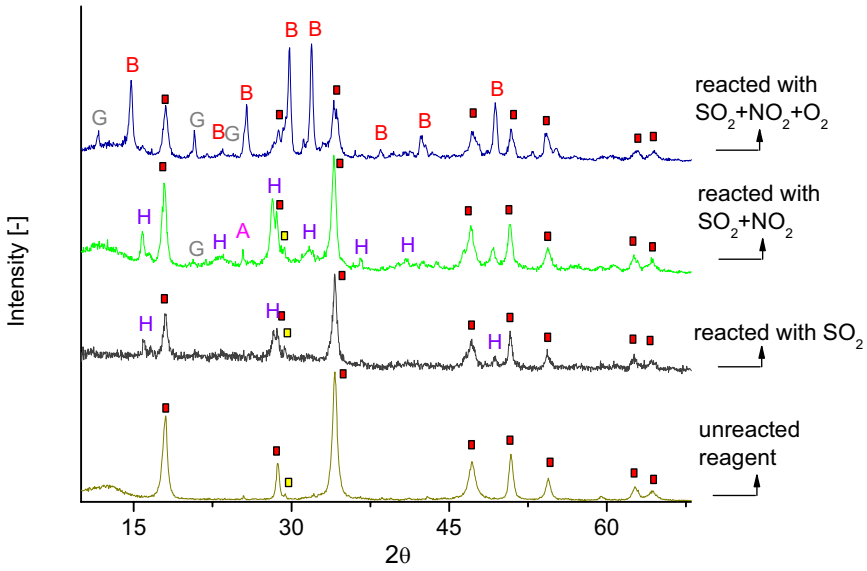

Fig. 4.16: XRD patterns obtained at 333 K and 70-75% of RH.

■ - Portlandite (Ca(OH)$_2$), □ - Calcite (CaCO3), H - Hannebachite (CaSO$_3$·(1/2)H$_2$O), A - Anhydrite (CaSO$_4$), G - Gypsum (CaSO$_4$·2H$_2$O), B - Bassanite (CaSO$_4$·(1/2)H$_2$O)

Finally, when O_2 coexists together with SO_2 and NO_2, no peaks corresponding to sulfite species have been detected (see Table 4.8), which indicates that the addition of O_2 involves a complete oxidation of sulfur species. This effect might be explained by means of the mechanism proposed by *Littlejohn et al. (1996)* for the analogous reaction in aqueous solution, which involves an increase of the ratio of sulfite consumed by NO_2 retained when O_2 is present. It should be mentioned that the preponderance of sulfates with respect to sulfites appears to be interesting from an environmental point of view, because calcium sulfate can be revalorized, while the only alternative for sulfites seems to be their disposal in landfills (see section 1.3.3.1.).

The analyses of the species containing nitrogen (ionic chromatography) indicated the presence of nitrites and nitrates both in the absence and presence of SO_2 (see Fig. 4.17). The presence of nitrates is inconsistent with reaction (4.1), and, in addition, this reaction is obviously inconsistent with the system only constituted of NO_2. This gives rise to propose reaction (4.2), which is analogous to reaction (1.9) for aqueous solution, which could take place both in the absence and in the presence of SO_2:

$$4NO_{2(g)} + 2Ca(OH)_{2(s)} \leftrightarrow Ca(NO_2)_{2(s)} + Ca(NO_3)_{2(s)} + 2H_2O_{ads} \qquad (4.2)$$

Nevertheless, according to Table 4.8, the ratio nitrate/nitrite tends to decrease for all the RHs tested when SO_2 is present in the reactor, which suggests that reaction (4.1) could also play a role together with reaction (4.2).

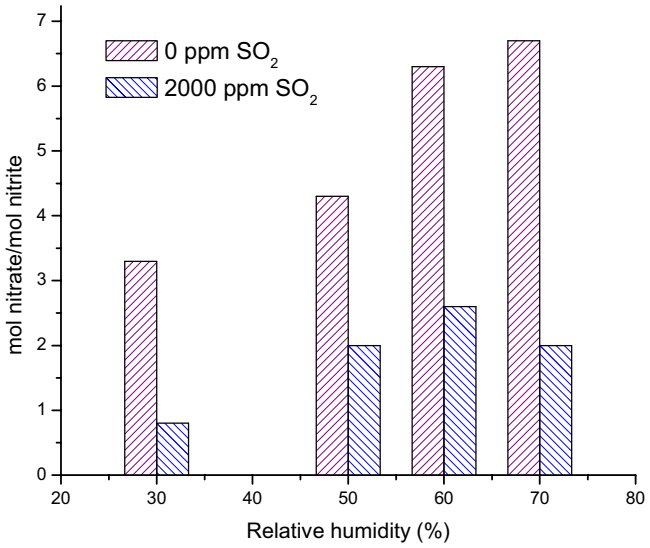

Fig. 4.17: Ratios NO_3^-/NO_2^- obtained at 333 K and 175 ppm NO_2 after 2 h of reaction. Effect of RH.

According to their stoichiometry, only reactions (4.1) and (4.2) would lead to ratios nitrate/nitrite up to one. However, the results shown in Fig. 4.17 reveal ratios higher than one. This evidence gives rise to propose a possible role of reaction (4.3), which would be analogous to reaction (1.10) in aqueous solution:

$$3Ca(NO_2)_{2(s)} + 2H_2O_{(ads)} \leftrightarrow Ca(NO_3)_{2(s)} + 4NO_{(g)} + 2Ca(OH)_{2(s)} \qquad (4.3)$$

This reaction could remove the nitrite species generated by reactions (4.1) and (4.2) by means of their disproportionation to nitrate species and NO. Compared to the reaction in aqueous phase (1.10), the reaction for solid-phase (4.3) does not seem to require acid conditions. Nonetheless, according to its stoichiometry, it appears to be promoted by the presence of adsorbed water. Furthermore, this fact might explain the positive trend of the ratio nitrate/nitrite with the RH (see Fig. 4.17).

Nevertheless, no clear explanation has been yet given in the literature concerning the positive effect of NO_2 on SO_2 uptake pointed out in section 4.2.2.1-2. In a first attempt, reaction (4.1) might account for this observation. In this way, sulfate formation might shift this reaction, thus enhancing sulfur retention. However, by taking into account its stoichiometry and the results of SO_2 retention in Table 4.6, this reaction cannot solely explain the extraordinary influence of NO_2 in its retention. For instance, a ratio of 0.74 S/Ca was found after 2 h of reaction at 70% of RH and 175 ppm of NO_2 for run 2. As the ratio S/Ca obtained at the same conditions in the absence of NO_2 is 0.26 for run 1, this difference (0.74-0.26=0.48 S/Ca) should be at least ascribed to reaction (4.1) being it responsible for the increase of SO_2 retention. This would lead to inconsistent values of Ca conversion (e.g. 0.26 $CaSO_3$/Ca + 0.48$CaSO_4$/Ca + 0.48$CaNO_3$/Ca > 100%Ca!!).

Another possible explanation for the increase on SO_2 uptake could be again related to the formation of nitrite and nitrate species. Because $Ca(NO_3)_2$ and $Ca(NO_2)_2$ are highly hygroscopic species, their presence might cause an effect similar to an increase of the RH in the gas flow. In order to evaluate this effect, an experiment using $Ca(NO_3)_2$ as additive of $Ca(OH)_2$ -4% of $Ca(NO_3)_2$ in the mixture- and SO_2 as the only gaseous reactant was undertaken at 333 K, 70% RH and 2 h of reaction. The result showed a retention of 0.504 mol SO_2 / mol Ca, which is in the order of the retentions determined without the additive but in the presence of 175 ppm of NO_2. The promotion of water adsorption owing to the presence of nitrite and nitrate species is in agreement with the results reported by *Goodman et al. (2000)*, who determined adsorption isotherms of water vapor over particles of $CaCO_3$ reacted with HNO_3 in the presence of water from FTIR spectra. Their results revealed that the amount of water adsorbed on the reacted particles, which contained some amounts of $Ca(NO_3)_2$ as a product of reaction, was sensibly higher than that adsorbed on the surface of $CaCO_3$ particles.

4.2.3. SYSTEM HCl + $Ca(OH)_2$

4.2.3.1. Final product and stability

The X-ray diffraction pattern of a reacted sample at 393 K and 18% of RH is shown in Fig. 4.18. As can be seen, the only product detected was Ca(OH)Cl, which was analyzed immediately after the sample was produced. Another sample was prepared at the same reaction conditions and was left in contact with the atmosphere (RH: 66% ± 10%, T around 293 K) for 24 hours, and afterwards was analyzed. The XRD obtained is also depicted in Fig. 4.18. Both patterns are basically identical, thus indicating that the solid formed is a stable product at ambient conditions for at least 24 hours.

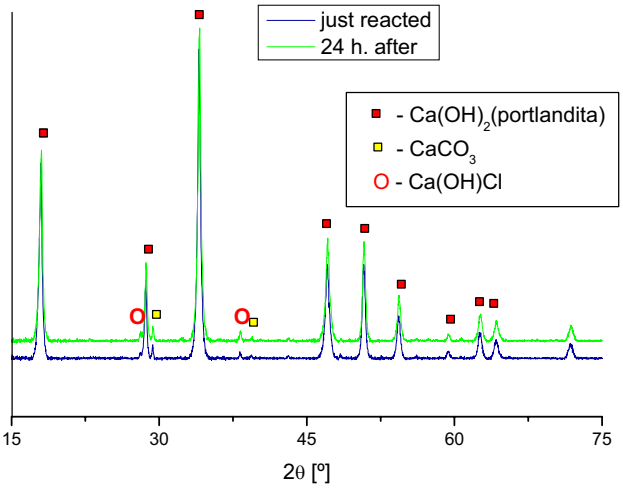

Fig. 4.18. XRD patterns of two samples from TGA experiment, one immediately after reaction and the other after 24 hours, with only Ca(OH)Cl as a product.

The presence of Ca(OH)Cl was already found in previous studies carried out at higher temperature (*Jozewicz and Gullet, 1995* and *Allal et al., 1998* at 773 K and 523 K, respectively). This reaction product implies a stoichiometric coefficient of at most one based on Ca and Cl which is, however, in contradiction to *Chisholm and Rochelle (1999), Weinell et al. (1992), Fonseca et al. (1998)* and *Mura and Lallai (1994),* who reported ratios of Cl/Ca beyond one. Furthermore, local EDXS analyses of Ca and Cl of cross sections of single crystals reacted for more than 2 hours at 393 K and RH of 18%, clearly show that the ratio of Cl/Ca is locally higher than one though at other locations in the particle it is below one (*Koch, 2004*). This apparent discrepancy between the different results might be solved by considering the proposed mechanistic pathway described later in section 4.2.3.4.

In order to confirm the long-term stability of Ca(OH)Cl, a sample of Ca(OH)Cl was left in contact with the atmosphere at room temperature for 8 days before it was analyzed by X-ray diffraction. Since Ca(OH)Cl is not commercially available, the sample was prepared by mixing chemically grade $CaCl_2$ with $Ca(OH)_2$ (20% of $CaCl_2$ at room temperature in air with moderate humidity). The mixture proceeds according to reaction (4.4), which was previoulsy proposed by *Jozewicz and Gullet (1995)* and *Allal et al. (1998)* after having identified the compounds of the mixture by XRD:

$$Ca(OH)_{2(s)} + CaCl_2 \cdot 2H_2O_{(s)} \leftrightarrow 2Ca(OH)Cl \cdot H_2O_{(s)}, \qquad (4.4)$$

This reaction was found to be thermodynamically viable at the range of temperatures from 373 to 1000 K (*Allal et al., 1998*). Fig. 4.19 shows the XRD patterns of two samples, one of the mixture just prepared and the other 8 days after being prepared. From the comparison of both patterns, it can be suggested that the solid mixture is quickly converted to a mixture of $Ca(OH)_2$ and Ca(OH)Cl, since the analyses of the first sample were carried out only around 10 minutes after the preparation of the mixtures. Moreover, the XRD patterns show that only $Ca(OH)_2$ and Ca(OH)Cl, but no $CaCl_2$ was present in the sample. As purely solid-solid reactions tend to be quite unlikely, the reaction of $CaCl_2$ and $Ca(OH)_2$ seems only to be feasible if $CaCl_2$ picks up water from the air to create a liquid phase where the formation of Ca(OH)Cl is occurring quickly. Finally, because the peaks of Ca(OH)Cl remain unchanged irrespective of the time of exposure, the stability of the product seems to be confirmed.

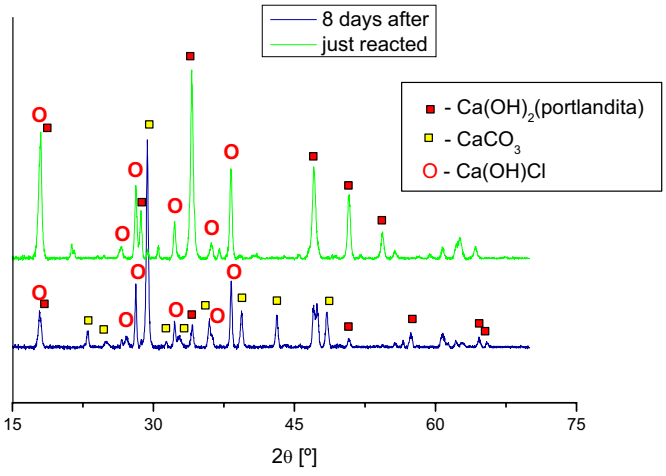

Fig. 4.19: XRD patters of a sample prepared by mixing $Ca(OH)_2$ and chemically grade $CaCl_2$ at ambient conditions just after preparation and after 8 days.

The purity of the $CaCl_2$ employed to prepare Ca(OH)Cl was also checked. Since a fast hydration of $CaCl_2$ was expected, a sample was analyzed by XRD just immediately after being taken out from the jar. A first analysis of the range 19 to 20 of 2θ, which corresponds to a typical peak of $CaCl_2$, was done, which confirmed the presence of $CaCl_2$. Just afterwards, complete analyses in the range 6 to 70 of 2θ was done, which indicated the only presence of $CaCl_2 \cdot 2H_2O$, thus confirming the fast hydration of the $CaCl_2$.

Besides, the stability of the sample during the drying period of the TGA experiments (see Fig. 3.7) was checked. The results of the amount of Cl^- found from solid analyses before and after the drying period (3 minutes at 393 K) are approximately the same considering the experimental error. Hence, the amount of HCl that could be driven out during the drying period can be considered negligible. Since no HCl is liberated during this period, reverse reactions (1.16) and (1.17) might not occur, but the possibility that reaction (4.4), i.e. $CaCl_2$ forms Ca(OH)Cl during drying, cannot be entirely excluded. This is, however, unlikely as will be discussed below (see section 4.2.3.4).

4.2.3.2. HCl retention

As it is explained in section 3.2, the HCl retained at different reaction time was determined by chemically analyzing the Cl^- content of liquid samples of the reacted solid sorbent. Only some of the samples were chemically analyzed, since an excellent correlation was found between the total increase of the weight of the sample after the drying period (Δm_l in Fig. 3.7) and the amount of Cl^- determined (see Fig. 4.20). This correlation was employed to determine the Cl^- content for the rest of experiments.

Fig. 4.21 shows the amount of HCl retained by mol of $Ca(OH)_2$ vs. reaction time. The obtained values are significantly lower to some of the literature at similar operating conditions. *Fonseca et al. (1998)* after 1200 s of reaction at 400 K and 4.4% of RH found values of ratio mol Cl^-/mol Ca around 0.6. *Chisholm and Rochelle (2000)* obtained retentions of 1.4 mol Cl^-/mol Ca working at 393 K and RH of 19% after 2700 s of exposure time. However, these differences might be explained by taking into account that external mass transfer limitation in TGA experiments was likely present (see section 3.2.3.). Consequently the reaction rate was lower, which in turn could have an influence on the kind of reaction product, according to the mechanism discussed in section 4.2.3.4.

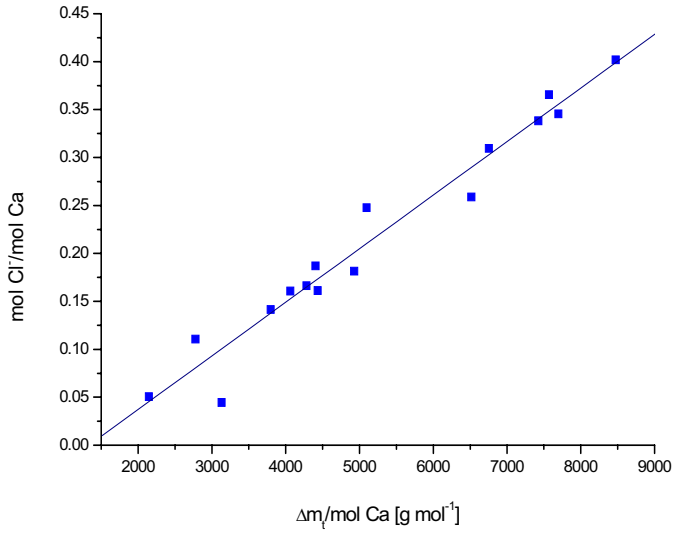

Fig. 4.20: Correlation between the total increasing weight of the sample after the drying period (Δm_l) and the amount of Cl^- determined in the liquid samples (mol Cl^-). Experiments were carried out at 393 K, RH of 18 % and 240 ppm HCl.

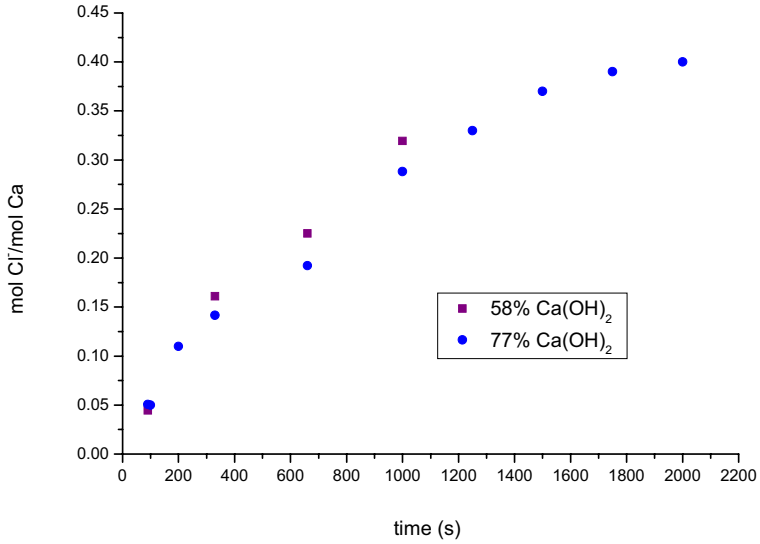

Fig. 4.21: Transient HCl retention by lime with different $Ca(OH)_2$ content at 393 K, RH of 18% and 240 ppm HCl.

The use of calcium hydroxide re-carbonated to different levels (77% and 58% of $Ca(OH)_2$) for HCl retention experiments did not show any significant difference, which can also be seen in Fig. 4.21.

For the desulfurization reaction, *Klingspor et al. (1984)* pointed out that the reaction rate is governed by the surface area irrespective whether $Ca(OH)_2$ or $CaCO_3$ is present. If this were true also for the HCl removal, the re-carbonation reaction would not cause a significant change of the surface area at least at the low reaction rates present when CO_2 is picked up by $Ca(OH)_2$ from the air.

The influence of HCl concentration was studied in the range 150-350 ppm. The results are shown in Fig. 4.22, which indicates that the amount of HCl retained follows an approximately linear trend with respect to HCl concentration. This result could be in agreement with the results reported by *Fonseca et al. (1998)* and *Chisholm and Rochelle (1999)* for experiments conducted at low temperature and in the presence of water vapor. They claimed that at HCl concentrations up to 1000 ppm, the rate of absorption is first-order with respect to HCl concentration, except for early reaction times, where *Chisholm and Rochelle (1999)* proposed a pseudo-second reaction order.

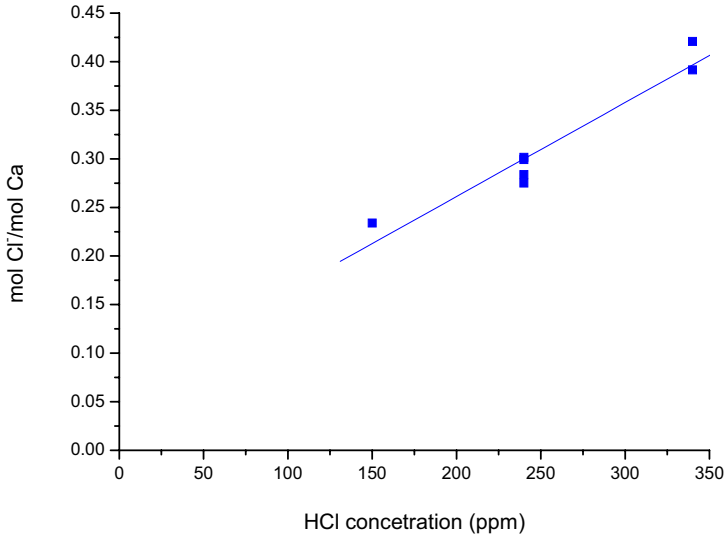

Fig. 4.22: Effect of HCl concentration on HCl retention after 1000 seconds at 393 K and RH of 18%.

4.2.3.3. Water retention

In Fig. 4.23, the total amount of H_2O that is taken up during the reaction and the respective fractions are displayed together with their linear trend lines. Both fractions increase with the conversion with almost the same slope (0.6 mol H_2O/mol Cl^- for strongly bound water and 0.4 mol H_2O/mol Cl^- for loosely bound water). The trend lines have a positive value at the intersection with the ordinate, i.e. when no Cl is taken up. This intersection is much higher than the amount of adsorbed water of pure $Ca(OH)_2$, which is lower than 0.07 mol H_2O/mol Ca for RHs up to 90% according to the water adsorption isotherm (Fig. 1.6). This could indicate that a very small amount of Cl could alter

considerably the surface chemistry to allow a much higher uptake of water. Since the trend line for loosely bound water raises with the conversion, this H_2O uptake cannot only be attributed to an effect of the size of the surface area, but also to changing surface adsorption capacity.

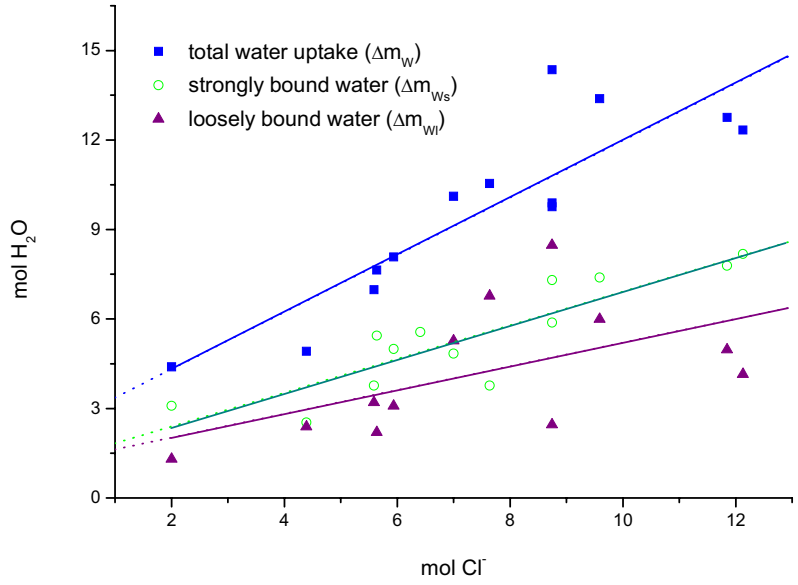

Fig. 4.23: Water retained at various levels of HCl uptake. The retained water is divided into a loosely bound fraction i.e. that can be removed during drying at 393 K and a fraction that cannot be removed during this drying procedure.

Finally, the ability of Ca(OH)Cl, $Ca(OH)_2$, and $CaCl_2$ samples to pick up water from the atmosphere was roughly compared. The samples of commercially available $Ca(OH)_2$, and chemically grade $CaCl_2$ were pure, but the sample of Ca(OH)Cl was prepared by mixing 20% $CaCl_2$ with $Ca(OH)_2$. After some days having left the samples in contact with the atmosphere at room temperature, the amount of water retained by $Ca(OH)_2$ was practically negligible, while Ca(OH)Cl was shown to be hygroscopic (can retain around 2 mol H_2O/mol Ca(OH)Cl). Finally, $CaCl_2$ took up 9 mol H_2O / mol $CaCl_2$, thus indicating its highly hygroscopic feature, which was also reported in the literature (*Ullmann's, 2003*). These results allow to conclude that if Ca(OH)Cl is formed, an excess of water in the solid product in in-duct technologies implies less operation problems than when $CaCl_2$ is formed. Moreover, deposition in landfills might be less problematic when Ca(OH)Cl is preferentially generated. However, the maximum theoretical retention of $Ca(OH)_2$ if Ca(OH)Cl is formed is half of that achieved in case of $CaCl_2$ formation.

4.2.3.4. Mechanistic pathway

Three possible routes concerning the mechanistic pathways consistent with the formation of Ca(OH)Cl could be in principle proposed, which are schematically represented in the Fig. 4.24:

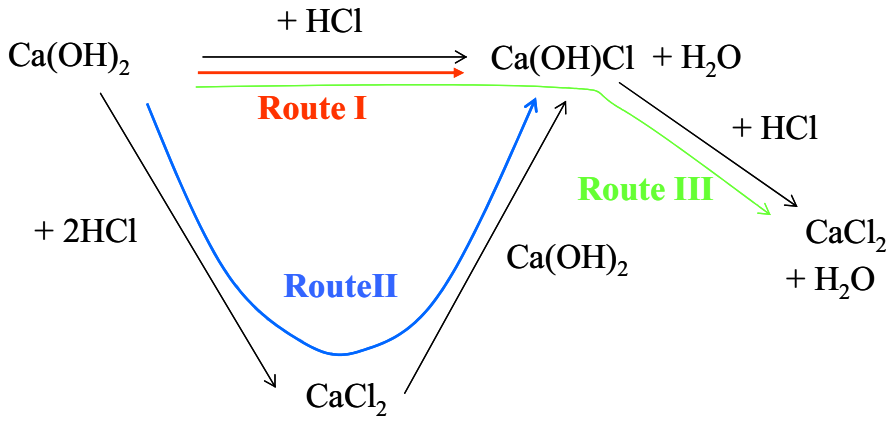

Fig. 4.24: Proposed mechanistic pathways concerning the reaction of HCl with $Ca(OH)_2$. Routes I and II are inconsistent with the experimental results.

- **Route I:** Elementary reaction between $Ca(OH)_2$ and HCl (reaction 1.16). However, this reaction is inconsistent with the results reported by *Chisholm and Rochelle (1999), Weinell et al. (1992), Fonseca et al. (1998)* and *Mura and Lallai (1994)*, who found stoichiometric ratios of Cl/Ca beyond one or who stated $CaCl_2$ as the reaction product.

- **Route II**: Formation of $CaCl_2$ by elementary reaction (1.15) and a consecutive reaction of $CaCl_2$ with the remaining $Ca(OH)_2$ (reaction 4.4) to finally generate Ca(OH)Cl. According to *Allal et al. (1998)*, all these reactions are possible from a thermodynamic prospective, though the reaction tends to be irreversible at low temperature. This pathway, where $CaCl_2$ is considered to be an intermediate product, requires that the formation of $CaCl_2$ is the rate limiting step, because no $CaCl_2$ was reported to be formed by *Jozewicz and Gullet (1995)* and by *Allal et al. (1998)* at very short reaction times. The fact that at longer reaction times only $CaCl_2$ was formed *(Daoudi and Walters, 1991)*, reverse reaction (4.4) should be possible, which is however thermodynamically not favored.

- **Route III:** Consecutive reactions (1.16) and (1.17) can represent the reaction schema. Nevertheless, making the premise that Ca(OH)Cl is the only product found in the present study, it requires the constraint that reaction (1.16) will only occur if $Ca(OH)_2$ is lacking, at least locally. Such a situation will intrinsically be present if all the available $Ca(OH)_2$ is used to form Ca(OH)Cl, which might explain the results presented by *Chisholm and Rochelle (1999)*, and *Weinell et al. (1992)* at short times. Under the hypothesis that during the reaction a product layer is formed in the particle which proceeds towards the center, $Ca(OH)_2$ can be missing locally when transport is reaction limiting.

This will occur preferentially at higher reaction rates, especially at higher temperatures or higher HCl concentrations. This schema would also allow to explain the results from *Daoudi and Walters (1991)* and *Jozewicz and Gullet (1995)*. Furthermore, from a kinetic point of view, bimolecular reactions involved in this mechanistic pathway might be more favored than termolecular ones. A schematic representation of the proposed mechanistic pathway in a reagent particle is presented in the Fig. 4.25.

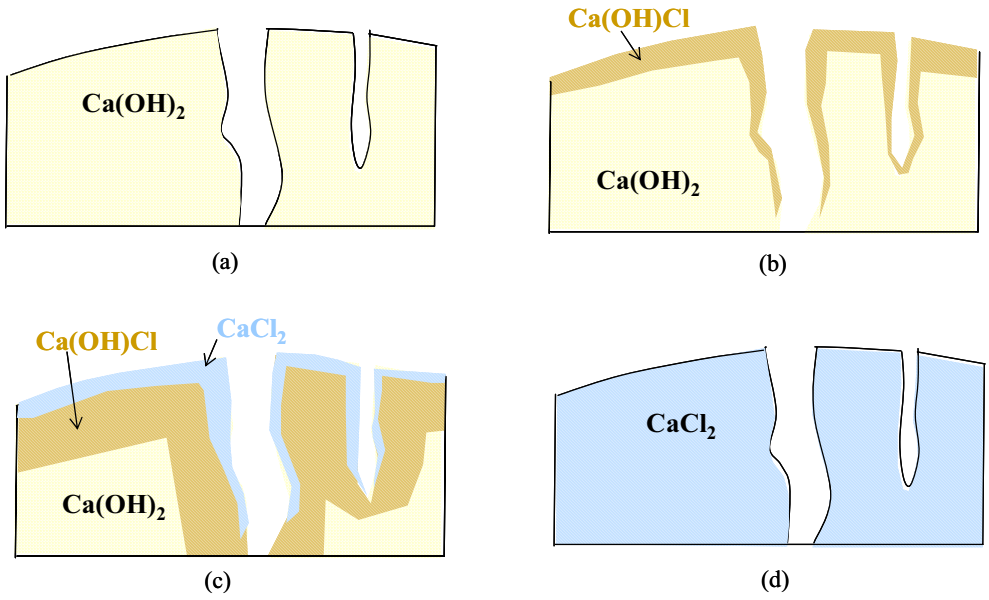

Fig 4.25: Schematic representation of the mechanistic pathway based on reactions (1.16) and (1.17). (a) Conversion = 0; (b) $Ca(OH)_2$ available in all particle; (c) no available $Ca(OH)_2$ locally; (d) $Ca(OH)_2$ completely consumed.

4.3. KINETIC MODELING OF THE SYSTEM SO_2 (+ NO_2) + $Ca(OH)_2$

The experimental breakthrough curves obtained from a fixed-bed reactor are the result of the reaction taking place in the whole bed. As reaction rates can vary with the position and time in the bed, no direct correlation between experimental data and a kinetic model can be established. Consequently, a kinetic study carried out by means of an integral fixed-bed reactor requires the following steps:

1. ***Proposal of a kinetic model***

2. ***Reactor modeling***: Introduction of the kinetic model in the microscopic mass balance of each reactant and integration of the differential equations through the entire bed to obtain the predicted breakthrough curves.

3. ***Model fitting***: Comparison of theoretical and experimental breakthrough curves with an optimization method to adjust the parameters of the proposed kinetic model.

4. ***Checking the goodness of the fitted kinetic model***.

4.3.1. REACTOR MODELING

In order to model a fixed-bed reactor, a mathematical function of the variables that describe their evolution with the position must be found. In addition, as the nature of a gas-solid non-catalytic reaction is non-steady, the reactor operates under non-steady state, and hence the variables are also time dependent. Finally, temperature gradients and hydrodynamics can also make more intricate the resolution of the bed.

4.3.1.1. Flow model

In general terms, several phenomena that might occur altogether in a fixed-bed reactor have to be taken into account in the modelling of its flow model. However, the hydrodynamics become simplified if an idealized plug flow can be assumed. Most of the typical effects that cause deviations from the idealized plug flow are described in the literature, as well as some criteria or well-established recommendations based on experience to assure that they are negligible or at least to reduce their contribution (*Rase, 1977*). The main effects are the following ones:

- *Velocity gradients normal to the flow direction because of wall effects*

  The turbulence in an empty tube tends to promote the presence of an idealized plug-flow or flat velocity profile over a cross section (see Fig. 4.26(a)). The turbulence in a tube can be increased due to the presence of particles (fixed-bed reactor) and thus, a flat velocity profile can be attained at lower velocities. However, a peak velocity is usually observed at about one particle diameter from the wall (see Fig. 4.26(b)). According to *Schwartz and Smith (1953)*, the velocity profile of a fixed-bed reactor does not tend to deviate more than 20% from the flat profile when $D_b/d_p>30$, where D_b and d_p correspond, respectively, to the bed diameter and to the mean particle size. Because this condition is fulfilled by the fixed-bed reactor used in this work (D_b= 12 mm and d_p= 0.308 mm for inert particles, since the fraction of reagent particles is negligible for dilution ratios of 1/30) (see sections 3.1.1. and 4.1.1.), no significant deviation from a flat profile can be assumed.

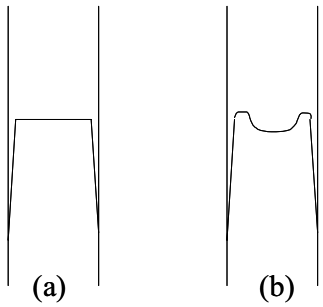

Fig. 4.26: Velocity profiles in cylindrical reactors (a) Idealized plug-flow; (b) Flow through packing (*Rase, 1977*).

- *Axial dispersion*

  The axial dispersion in a fixed-bed reactor is attributed to stream splitting, acceleration, deceleration and trapping (*Rase, 1977*). The axial dispersion may be neglected for gases with Peclet Number (N_{Pe}) of 2 for a ratio $L_b/d_p \geq 100$, where L_b is the bed length (*Rase, 1977*). The application of this criterion to the fixed-bed reactor used in this work (see Appendix C for more detailed information) leads to reject the presence of axial dispersion in the flow pattern.

- *Velocity gradients caused by poor distribution of reactants*

  A poor distribution of reactants over an entire cross section of a tubular reactor is a common problem of large reactors. However, in short tubular reactors, the presence of elbows or valves placed immediately upstream of the reactor, as well as changes in pipe diameter, tends to perturb the uniformity of the flow. This problem can be saved by a straight length of at least 10 diameters of the pipe before the reactor. This criterion is accomplished by the reactor used in this work, because the length of the tube of the reactor that remains empty before the bed inlet is approximately 15 cm, which is longer than ten times its diameter.

- *Radial temperature and concentration gradients*

  In a tubular reactor, radial mass transfer might be caused by two main effects: (1) *wall effect*, which is deterred by the action of the particles in the bed, and (2) *concentration gradients* due to a chemical reaction. This second aspect could be remarkable for systems with a high ratio of reaction heat to heat dissipation capacity, where a higher temperature at the center of the reactor could lead to faster reactant depletion and product generation. This effect can be neglected in our fixed-bed reactor because it operates under isothermal conditions (see section 3.1.1.1.)

- *Channeling and shortcuts*

  The presence of very small particles and with a high tendency to become adhesive and to stick together can lead to local variations of porosity, which might cause channelling through the bed. In addition, a fraction of the particles become inaccessible to the gas stream, which might cause a decline in solid conversion. These effects are especially significant in the present study, not only owing to the small crystal size of the reagent used (9.4 μm, see Table 4.1), but also due to the use of water vapor, which promotes particle agglomeration. This inconvenience can be overcome by mixing the reagent particles with seasand, namely by diluting the bed. The effect of dilution on the overall conversion has been already shown in Fig. 3.3, where the curves appeared at longer times with an increase of the dilution ratio.

  In principle, an excess of the degree of the dilution could promote the formation of shortcuts, which could be detected by the shape of the breakthrough curves. However, the breakthrough curves obtained from our reactor do not suggest the presence of shortcuts.

In addition to the effect of dilution on the flow pattern (bed dimensions, channeling, shortcuts, and so on), it also plays a role in the distribution of reagent particles throughout the bed. As the mixture of reagent and inert particles is not complete, each time the bed is packed, different particle distributions are obtained, which might lead to different solid conversions (*Van den Bleek, 1969*). As a result, the experimental error of solid conversion rises with the degree of dilution. The following criterion determines the degree of dilution that allows one to neglect this effect on solid conversion for an assumed experimental error:

$$\frac{f \times d_p}{\varepsilon_r \times L_{wd}} \leq 4x10^{-3} \qquad (4.5)$$

where **f** is the fraction of inert solid [-], d_p is the crystal size of the reagent [m], L_{wd} is the bed length without dilution [m] and ε_r is the relative error of the solid conversion [-]. Taking into account a ε_r of 5%, the application of this criterion to our experimental data leads to conclude that whatever dilution is allowable.

In conclusion, because all criteria aforementioned that assure plug-flow model in a fixed-bed reactor are fulfilled by the reactor used in this work, this flow model will be assumed for its further modeling.

4.3.1.2. External and internal mass transfer

External and internal mass transfer (EMT and IMT, respectively) have been evaluated to determine their influence in the kinetics of the reaction under study by means of an integral fixed-bed reactor.

- *External mass transfer (EMT)*

The reaction rate for EMT control can be described by the following equation:

$$r_g = k_g A_p C_{SO_2} \qquad (4.6)$$

where k_g is the EMT coefficient [m s^{-1}], A_p is the external particle surface [m] and C_{SO_2} is the SO_2 concentration in the bulk of the gas phase [mol m^{-3}]. The comparison of the reaction rates calculated from eq. (4.6) with the experimental values would determine whether this step is or not controlling. This comparison cannot be done in our reactor, since an integral fixed-bed reactor does not directly provide reaction rates. However, a rough analysis can be done to find out if EMT is not controlling:

1. The resistance of the gas film can be reduced by increasing the velocity of the gas and by reducing particle sizes. In this work, both gas velocity is very high (22 cm s^{-1} and 79 cm s^{-1} of superficial and interstitial velocity, respectively –see Appendix C) and the particles are very small (see Table 4.1).

2. Assuming that the particles are spherical, the time to achieve 100% of solid conversion ($\sigma_{100\%}$) of one particle under external mass transfer control can be estimated from equation (4.6) by the following expression:

$$\sigma_{100\%} = \frac{\rho_S (d_p/2)}{3 k_g C_{SO_2}} \qquad (4.7)$$

where ρ_S and d_p are the density and the mean size of the $Ca(OH)_2$ commercial crystals respectively. The EMT coefficient, k_g, was estimated by means of three different empirical correlations (see appendix D), which provided values in the range 25-720 cm s^{-1}, respectively. Taking into account these values, the calculated time to achieve complete conversion ($\sigma_{100\%}$) is extremely short (0.1-0.3 s at 2000 ppm of SO_2 concentration for a temperature and RH ranges 313-353 K and 30-70%, respectively), much shorter than what is suggested from the experimental breakthrough curves obtained in this study. Hence, the assumption that the reaction between $Ca(OH)_2$ and SO_2 is not controlled by EMT seems to be reasonable.

3. *Ruiz-Alsop and Rochelle (1987)* found no contribution or control of EMT for the reaction under study in a fixed bed-reactor built with spherical particles and with a k_g of 544 cm s^{-1}.

- *Internal mass transfer (IMT)*

The degree of influence of the internal mass transfer (IMT) on the reaction rate can be experimentally determined by varying the particle size. The studies carried out by *Krammer et al. (1997)* and *Ho et al. (2002)* with particles sizes in the range 50-125 μm and 10-96 μm, respectively, showed that the reaction between SO_2 and $Ca(OH)_2$ is not influenced by the particle size, which

indicates that internal mass transfer is not controlling. It can be also assumed in this study, since the particles employed (see Table 4.1) are practically in the same range of size, or even smaller.

4.3.1.3. Modeling of a fixed-bed reactor

An integral fixed-bed reactor can be modeled through the microscopic mass balance of each reactant in the gas and solid phase in the reactor. The following assumptions have been taken into account:

1. Plug-flow for the gas-phase, which was verified for the experimental conditions considered in this work (see section 4.3.1.1.)

2. Isothermal operation, which was experimentally checked (see section 3.1.1.1.)

Considering these assumptions, the following set of equations is obtained:

- Gas phase balance:

$$\frac{\partial(\varepsilon_b C_g)}{\partial t} = -\frac{\partial(\Phi_v C_g)}{A_b \partial z} - \rho_S (1-\varepsilon_b) r_g \qquad (4.8)$$

- Solid phase balance:

$$\frac{1}{M_S}\frac{dX_S}{dt} = r_S \ , \qquad (4.9)$$

Initial conditions: $t = 0, \ \forall z \rightarrow C_g = 0, \ X_S = 0$

Boundary condition: $z = 0, \ \forall t \rightarrow C_g = C_g^0$

where ρ_S, M_S and X_S correspond to the density [g m^{-3}], the molecular weight [g mol^{-1}] and the conversion of the solid reagent [-], respectively; A_b and ε_b are the area [m^2] and porosity [-] of the bed, respectively; Φ_v is the volume flow rate of the gas flow [m^3 s^{-1}]; C_g and C_g^0 are the gas concentration (i.e., SO_2 concentration) in the bed and at the inlet [mol m^{-3}], respectively; and r_g and r_S indicate the reaction rate of the gas and solid reagents [mol g^{-1} s^{-1}], respectively, which are related stoichiometrically by eq. (1.1).

The reactor model has been solved numerically by using a finite difference technique, which is based upon a spatial and temporal discretization (see Appendix E). A least-square non-linear optimization method based on the Levenberg-Marquardt algorithm has been employed to adjust the kinetic parameters of each tested model. The confidence interval of the fitted kinetic parameters has been calculated by means of a standard method for non-linear models, which is explained in the Appendix F (*Himmelblau, 1970*).

The number of position intervals (200) and time intervals (1200) (position and time mesh size, respectively) has been chosen to avoid any dependence of the optimized curves on them. The

independence of the optimized values of the fitted parameters respect to their initial values has also been checked.

4.3.2. KINETIC MODELING

4.3.2.1. Insight into the reaction mechanism

The description of the kinetics of a gas-solid non-catalytic reaction usually comprises a number of physical and chemical steps. In this way, a sequence of the steps involved in the reaction between $Ca(OH)_2$ and SO_2 in the presence of water vapor will be proposed. This first scheme not only takes into account typical steps involved in gas-solid reactions, but it also constitutes a first approximation to describe the relevant role of water vapor in the kinetics of the reaction. External and internal mass transfer contributions to the kinetics of the reaction have been neglected (see section 4.3.1.2.). The following steps have been considered:

1. Adsorption of water on the solid surface (pores and external), which can be described by eq. (4.10):

$$H_2O_{(v)} \xleftrightarrow{K_{ads}^{H_2O}} H_2O_{(ads)} \qquad (4.10)$$

The hydrophilic nature of $Ca(OH)_2$ surface was studied by *Klingspor et al. (1984)*, who determined experimentally the water adsorption isotherm of different hydrated limes and one calcium carbonate at 343 K (with BET surface areas of 14.4-25.5 $m^2\ g^{-1}$ for the hydroxides and 6.7 $m^2\ g^{-1}$ for the carbonate) (see section 1.4.1.). Their results show that the sorption capacities per BET surface area are equal for all the sorbents tested, which suggests that their water adsorption isotherm is appropriate for the $Ca(OH)_2$ commercial reagent employed in this study (BET surface area of 13.8 $m^2\ g^{-1}$ -see Table 4.1). According to the BET classification, water adsorption follows a Type II isotherm, which indicates the formation of a water multilayer *(Anderson and Bourdart, 1981)*. The number of water monolayers adsorbed on the sorbent surface or water coverage (θ) can be estimated by fitting the water adsorption isotherm of $Ca(OH)_2$ to the equation given by *Brunauer et al. (1938)*. Water coverages about 1.0, 1.3, 1.5, 2.0 and 3.0 for 20, 30, 50, 70 and 90% RH, respectively, have been found. Moreover, according to the shape of the isotherm (see Fig. 1.6), it seems that a deliquescence point should be expected beyond 90% of RH.

The physical state of water thin layers at a molecular level seems to be of relevant importance to understand and describe the role of water on the reaction. Although water thin films have been rarely studied for the system $H_2O_{(v)}/Ca(OH)_2$, some studies reported in the literature concerning the description of water thin films on NaCl could provide a valuable information. It is expected that the interaction between water adsorbed molecules and the solid substrate for sub-monolayer coverages might be different for NaCl and $Ca(OH)_2$. However, the interactions between water molecules at higher coverages should not differ widely, because water interactions might be less influenced by the substrate.

The results found in several experimental studies (*Peters and Ewing, 1997; Foster and Ewing, 2000*) and simulation works (*Engkvist and Stone, 2000*) seem to suggest that at coverages from 2-2.5 to 3.5, the water is adsorbed onto the surface of NaCl(100) forming a liquid-like thin film, that is, the bonding pattern of the layer is characterized by an isotropic hydrogen bonding network resembling that in liquid water. One marked result found by *Peters and Ewing (1997)* is that film coverages near 2 produce infrared spectra essentially indistinguishable from those of saturated salt solutions, which appears to indicate that Na^+ and Cl^- ions can be drawn into the water layer. Of course, at lower coverages, water molecules are strongly bonded and more ordered, meanwhile at high coverages, NaCl crystals deliquesce to form a saturated salt solution.

2. Hydration of SO_2 with adsorbed water molecules on the solid surface

In the presence of water, both in gas phase (*Loerting et al., 2000*) and liquid phase (*Greenwood and Earnshaw, 1986*), SO_2 can be hydrated forming $SO_2 \cdot zH_2O$ species with different **z** values. Hence, it seems reasonable to propose that SO_2 might be hydrated with the adsorbed water molecules on the surface of $Ca(OH)_2$, in the same way as was suggested by *Klingspor et al. (1984)* according to reaction (4.11):

$$SO_2 + zH_2O_{(ads)} \overset{k_C}{\longleftrightarrow} SO_2 \cdot zH_2O_{(ads)} \qquad (4.11)$$

This suggestion might be reinforced by the expected quasi-liquid nature of water thin layers on the hydrophilic surface of $Ca(OH)_2$, especially for high RHs, as has been above pointed out.

3. Reaction of $SO_2 \cdot zH_2O$ with $Ca(OH)_2$ and formation of the reaction product according to the reaction:

$$SO_2 \cdot zH_2O + Ca(OH)_2 \longrightarrow CaSO_3 \cdot (1/2)H_2O + (z + 1/2)H_2O \qquad (4.12)$$

4. Once a product layer is built on the solid reagent, a diffusion step might be hypothesized. Taking into account the crystalline structure of $Ca(OH)_2$, the lattice parameters of its unit cell and the BET surface area, the ratio between surface and inner Ca^{2+} or HO^- ions can be roughly estimated. In this way, solid conversions of only 1.5% would be attained if only the most superficial $Ca(OH)_2$ reacted. However, as higher conversions are experimentally obtained, inner solid reagent should also react. Moreover, because the molar volume of the solid product ($CaSO_3$) is slightly higher than that of $Ca(OH)_2$ reagent (ratio of 1.6), it seems reasonable to consider that a non-porous product layer will be formed, which might be crossed by diffusion by at least one of the reactants (SO_2 or Ca^{2+} and HO^- ions) to go on with the reaction.

All the kinetic models proposed to describe experimental data of the reaction under study are based on one or more of the above stages. The first step of the present study has consisted of evaluating the suitability of different kinetic models, most of which have been already applied by other researchers,

to the experimental data. In the second step, the most suitable kinetic model tested has been improved by a new performance.

4.3.2.2. Evaluation of kinetic models

4.3.2.2.1. Description of the kinetic models tested

- ***Shrinking core model (SCM)***

  The SCM, originally developed by *Yagi and Kunii (1961)*, is a theoretical model that considers the beginning of the reaction at the outer surface of the particle and the formation of a reaction front which moves towards the center of the particle -$Ca(OH)_2$ in our case-, leaving backwards a product layer as the reaction progresses. The model takes into account the following assumptions:

  1. Spherical and non-porous particles

  2. The kinetic equation of the chemical reaction is first order with respect to SO_2 concentration

  3. Pseudo-stationary state with respect to the profile of SO_2 concentration in the product layer

  From these assumptions, the kinetic equation of the SCM which considers diffusion of reactive gas through the product layer and chemical reaction on the core surface is:

$$r_{S,p} = \frac{4\pi R_p^2 C_g \left(1 - X_S\right)^{2/3}}{\frac{1}{k_S} + \frac{R_p \left(1 - X_S\right)^{1/3}}{D_g^P}\left[1 - \left(1 - X_S\right)^{1/3}\right]} \qquad (4.13)$$

  where $r_{S,p}$ is the reaction rate of the solid phase per unit particle [mol s^{-1} $particle^{-1}$], C_g is the gas concentration in the bulk gas phase [mol m_g^{-3}], R_P and X_S correspond to the radius of the particle [m] and to the solid conversion [-], respectively. The parameters to be fitted are k_S and D_g^P, which are the rate constant [$m_g^3 m_S^{-2} s^{-1}$] and the diffusion coefficient of the gaseous reactant through the product layer [$m_g^3 m_S^{-1} s^{-1}$], respectively. To obtain r_S [mol s^{-1} g^{-1}], the following relation for spherical particles is used:

$$r_S = r_{S,p} \frac{1}{(4/3)\,\pi\, R_p^3 \rho_S} \qquad (4.14)$$

  where ρ_S is the density of the solid reactant [kg m^{-3}].

- ***SCM + empirical correlation which accounts for a decrease of diffusion coefficient as reaction progresses (Karatepe et al., 1999)***

This model assumes that the diffusion coefficient (D_g^P) decreases exponentially with X_S. The following expression is proposed:

$$D_g^P = D_{g,0}^P \exp(-aX_S) \qquad (4.15)$$

where D_g^P is the diffusion coefficient at $X_S = 0$, and **a** is a fitting parameter [-]. For the calculations, eq. (4.15) is directly substituted into eq. (4.13), where now **a**, k_S and $D_{g,0}^P$ are the fitting parameters.

- ***SCM + empirical correlation which accounts for a decrease in particle roughness as reaction progresses (Ruiz-Alsop and Rochelle, 1987)***

This model takes into account that real particles have a rough surface, so their surface area is much higher than that of spherical particles of the same volume. The roughness of the particles is supposed to decrease as the reaction progresses. To take into account this contribution, the SCM is modified with the following empirical expression:

$$\sigma^p = 1.0 + \exp[a(1 - X_S) + b] \qquad (4.16)$$

where **a** and **b** are parameters [-] and σ^P is the roughness parameter [-], which is defined as the ratio between the actual surface area of the particle (A_r) and that of spherical particles of equal mass (A_ϕ):

$$\sigma^p = \frac{A_r}{A_\phi} \qquad (4.17)$$

When $X_S = 0$, A_r is the BET surface area of the $Ca(OH)_2$, and consequently, parameters **a** and **b** are related according to the following expression:

$$\frac{A_{BET}}{A_\phi} = 1.0 + \exp[a + b] \qquad (4.18)$$

The final kinetic equation used is equation (4.13) with the numerator corrected with the roughness parameter σ^p, where the relations (4.16) and (4.18) are taken into account. Hence, the fitting parameters are **a**, k_S and D_g^P.

- ***Adsorption model (Irabien et al. 1992)***

Irabien et al. (1992) proposed that the adsorption of SO_2 on the surface of $Ca(OH)_2$ is the rate determining step of the reaction under study. Therefore, the kinetic equation of the overall process is given by the following expression, which corresponds to the rate of adsorption of a gas on a particle surface:

$$r_S = \frac{\varepsilon_b}{\rho_S(1-\varepsilon_b)} \int k_{ads}\, C_g (1-\theta)\, d\theta\,, \qquad (4.19)$$

where θ is the surface coverage [-],k_{ads} is the kinetic constant of adsorption [s^{-1}] and ε_b denotes the bed porosity [-]. Taking into account a non-ideal surface, the adsorption activation energy (E_{ads} [J mol^{-1}]) can be assumed to depend linearly on θ:

$$E_{ads} = E^{\circ}_{ads} + \gamma\,\theta \qquad (4.20)$$

where E°_{ads} is the adsorption activation energy for an ideal surface [J mol^{-1}] and γ is a parameter related to non-ideality [J mol^{-1}]. As a consequence, the kinetic constant of adsorption for a non-ideal surface (k_{ads} [s^{-1}]) is:

$$k_{ads} = A \exp[-(E^{\circ}_{ads} + \gamma\,\theta)/RT] \qquad (4.21)$$

Assuming that θ and X_S are linearly related and that a maximum conversion (X_M) is achieved, the substitution of eq. (4.21) into eq. (4.19) and further integration yields:

$$r_S = \frac{\varepsilon_b}{\rho_S(1-\varepsilon_b)} k_{ads} \frac{1}{a} C_g \left[\exp(-aX_S) - \exp(-aX_M)\right], \qquad (4.22)$$

where **a** is defined as

$$a = \frac{\gamma}{RT} \qquad (4.23)$$

Thus, k_{ads} and **a** are the fitting parameters of the adsorption model. As any experiment has been carried out to obtain whether a maximum conversion, X_M is or not ultimately achieved, the results found by *Irabien et al. (1992)* have been employed as a first approximation. They undertook some experiments at 8 hours, 325 K and SO_2 concentrations in the range 2.5 -100.0% SO_2 and obtained a X_M of 0.62. This model has been tested to fit our experimental data with a collection of different X_M values higher than 0.40, which corresponded to the conversion value obtained after 6 hours of reaction (see Fig. 4.9).

- ***Avrami model***

Nucleation models have become successful in describing the kinetic behavior of some gas-solid reactions that present a sigmoid curve when solid conversion is plotted vs. time, such as the reduction of metallic oxides. Nucleation models describe the kinetics of a reaction by means of three periods: (1) generation of nuclei, (2) subsequent growth of nuclei and (3) overlapping thereof (see Fig. 4.27) *(Doraiswamy and Kulkarni, 1987; Rao and Gopalakrishnan, 1997)*. The so-called ***Avrami model***, which considers that nucleation occurs randomly and isolated nuclei grow one, two

or three-dimensionally (*Avrami, 1940*), was the first nucleation model suggested. This model proposes the following expression that relates the solid conversion with time:

$$X_S = 1 - \exp(-at^N), \tag{4.24}$$

where N takes the values 1-4 depending on how many nuclei grow and when they are formed, and **a** is the rate constant. The derivation of eq. (4.24) with time yields the following kinetic equation:

$$r_S = \frac{1}{M_S} aNt^{N-1} \exp(-at^N) \tag{4.25}$$

which is fitted to the experimental data to determine **a** [s^{-N}].

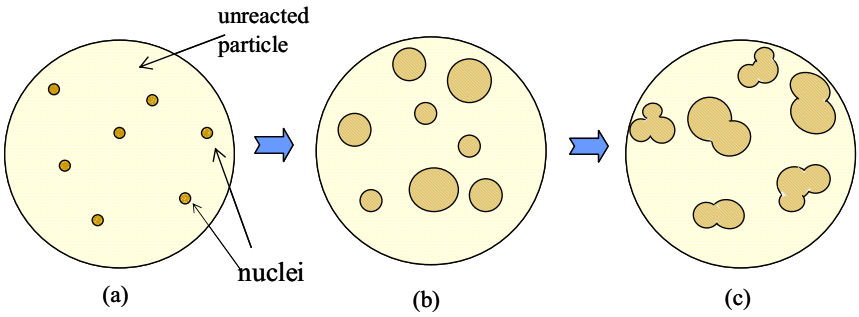

Fig. 4.27: Representation of a nucleation model. (a) formation of nuclei; (b) growing of nuclei; (c) coalescence.

- ***Deactivation model (DM)***

A deactivation model assumes that the reaction between the gas molecules and the solid reagent depends mainly on the concentration of the gas on the solid surface and on the so-called active surface (a_S), that is, the ratio of active surface of unreacted solid and the initial solid surface. As the reaction progresses, the solid product deposits on the surface of the reagent and the solid activity becomes reduced. Thus, the reaction rate can be expressed in the same manner as it is reported by *Doğu and Doğu (1993)*:

$$r_S = \frac{\varepsilon_b}{\rho_S(1-\varepsilon_b)} k_S C_g^n a_S , \tag{4.26}$$

where k_S and **n** indicate, respectively, the rate constant [$m^{3(n-1)}mol^{(1-n)}s^{-1}$] and the reaction order with respect to the gas concentration [-]. Furthermore, the rate of reduction of active surface -or deactivation rate- is thought to depend on the activity of the solid and on the gas concentration in a way as it is commonly proposed for the deactivation of catalysts (*Levenspiel, 1999*) as follows:

$$\frac{da_S}{dt} = -\beta C_g^m a_S , \tag{4.27}$$

where **m** is the order of the deactivation process with respect to the gas concentration, with typical values of 0 or 1 *(Doğu and Doğu, 1993)*, and β is the deactivation rate constant. The integration of eq. (4.27) for **m**=0 and for **m**≠0 but C_g^m constant with the initial condition t=0, $a_S = 1$ and its subsequent combination with eq. (4.26) yields the following general expression:

$$r_S = \frac{\varepsilon_b}{\rho_S(1-\varepsilon_b)} k_S C_g^n \exp\left(-\beta C_g^m t\right), \qquad (4.28)$$

which indicates that at long times, when the activity of the solid becomes zero, the reaction rate also tends to zero, because no active surface area is left. In case **m**≠0 for C_g^m not constant, no analytical expression for the r_S can be found and the concentrations and active surface must be calculated separately. As in any case the SO_2 concentration in the fixed-bed reactor is constant, the employed equations to fit experimental data have been:

- For **n**=0 or **n**=1 and **m**=0 $\Rightarrow$ Eqs. (4.28)

- For **n**=0 or **n**=1 and **m**=1 $\Rightarrow$ Eqs. (4.26) + (4.27), which have been solved numerically by using a finite difference technique, which is based upon a discretization of a_S.

4.3.2.2.2. Results and discussion of model fitting

As an instance of the obtained results, two experimental breakthrough curves are shown in Figs. 4.28(a-b), together with the fitted curves for the different kinetic models tested. As can be seen, it seems that the SCM in its simplest form cannot describe the experimental data. In contrast, the introduction of an empirical correlation that considers an exponential reduction of the D_g^P with the solid conversion provides much better results. However, it must be noted that the initial period of experimental breakthrough curves cannot be well fitted by this model. Furthermore, the SCM appears to fail in interpreting other experimental results regarding the effect of SO_2 concentration on the reaction. Previous reported studies (see Table 1.5) showed that SO_2 concentration did not exert a significant influence on the reaction rate at long times (after a few minutes) at low temperature and in the presence of water vapor. This observation is not consistent with a diffusion limiting step, which is the final situation predicted by the SCM, since it predicts a lineal trend with SO_2 concentration. Moreover, a diffusion of SO_2 through the product layer seems to be unlikely, since hydrated SO_2 is a very large molecule (kinetic diameter of SO_2=2.3 Å) and the product of similar desulfurization reactions at high temperatures are usually non-porous (*Doğu G and Doğu T, 1993*), which makes it difficult the diffusion of hydrated SO_2 through the product layer.

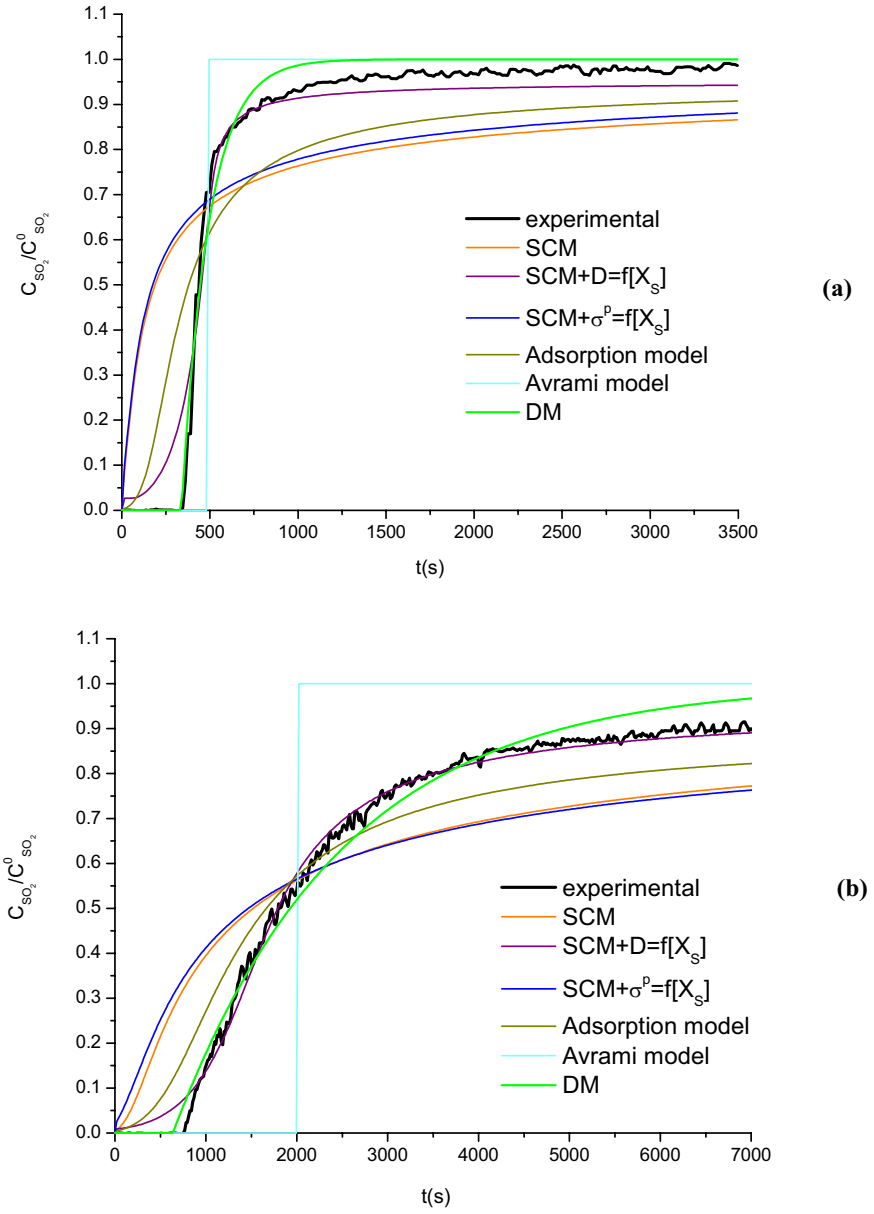

Fig. 4.28: Experimental and simulated breakthrough curves fitted to the tested kinetic models at 333 K, 30% of RH, 2000 ppm SO_2. (a) without NO_2; (b) with 175 ppm NO_2.

The adsorption model and, more clearly the Avrami model, seem to be far to predict experimental data. The adsorption model has been fitted for different values of X_M, which did not lead to better results. Likewise, the Avrami model has been evaluated for values of N from 1 to 4, but no significant differences of the best fitted curve have been found. As can be observed in Figs. 4.28, neither the initial period nor the slopes nor the final period of the curves are well fitted.

With respect to the DM, it appears to be the most feasible model to describe the experimental data. The initial period and slopes are reasonably well fitted. However, at the final period of the curves, it can be observed that predicted values of $C_{SO_2}/C^0_{SO_2}$ are higher than the experimental ones, which indicates that the kinetic model underestimates the reaction rate and solid conversion at long times. *Ho*

et al. (2002) also found quite good results fitting a DM to their experimental data obtained by a differential reactor, but they did not study the validity of the model at long times. According to our fittings, it seems reasonable to propose the introduction of a further kinetic step to the DM to describe more accurately our experimental data at long times.

4.3.2.3. Deactivation model combined with an inverse shrinking core model (DM-ISCM)

4.3.2.3.1. Description of the DM-ISCM

The DM only takes into account the contribution of the remaining active surface area of the solid reagent to the reaction rate. However, one can assume that other parallel pathways might take place simultaneously with the deactivation of the surface. While the reaction goes on and a thin layer of the solid product covers partially the reactant surface, further reaction controlled by a slow diffusional process in this layer may be suggested, as follows below.

As it has been explained above, the diffusion of SO_2 across the product layer should not account for the progression of the reaction. However, an outward solid-state diffusion of hydrated Ca^{2+} and HO^- ions from the inner $Ca(OH)_2/CaSO_3{\cdot}(1/2)H_2O$ interface to the surface of $CaSO_3{\cdot}(1/2)H_2O$ could take place together with the deactivation of the surface of $Ca(OH)_2$. In fact, the studies done by *Hsia et al. (1995)*, already pointed out in section 1.5.4., reported evidence of an outward solid-state diffusion mechanism at least at high temperatures.

As has been explained in the section 1.5.4., because of the much lower activation energy for boundary diffusion, this mechanism is dominant at lower temperatures, while lattice diffusion mechanism is more relevant as temperature rises. Consequently, it should be considered that the contribution of boundary diffusion mechanism to the ionic diffusion through the $CaSO_3{\cdot}(1/2)H_2O$ layer is predominant at lower temperatures. On the other hand, as solid-state diffusion is related to the nature of the involved compounds, the ion transfer mechanism should be altered by the presence of adsorbed substances or impurities. In this way, it can be proposed that the adsorbed water both on the grain boundaries and in the bulk of the crystals might reduce the activation energy of the jumps, and therefore adsorbed water might enhance the ion diffusion, as it is illustrated in Fig. 4.29.

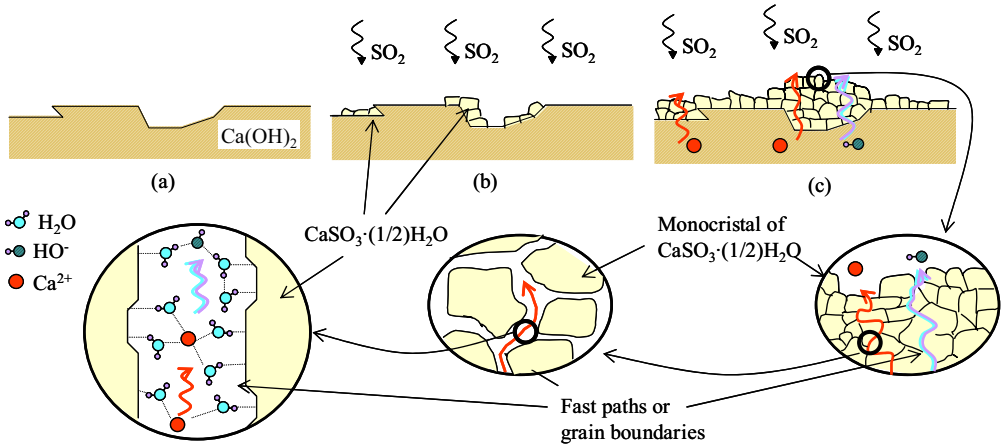

Fig. 4.29: Schematic representation of the evolution of the surface.

(a) Unreacted surface; (b) surface partially deactivated by the covering of product crystals; (c) deactivated surface and predominance of outward solid-state diffusion of Ca^{2+} and HO^- ions. Diffusion through grain boundaries is likely promoted by the effect of adsorbed water.

The ionic mass transfer through a layer can be modeled by means of the Nernst-Planck equation (*Philibert, 1991*), which considers that the driving force for ionic diffusion is on the grounds of two main contributions: (1) the ionic concentration gradient through the layer, and (2) the electrical field gradient in the layer, which should be caused by a net charge in each side of the layer. The general formulation of this equation for the transfer of the ion **i** through the product layer (P) neglecting any coupling phenomenon with the transfer of other ions **j** is the following one:

$$\vec{J}_i = -\left[D_i^P \vec{\nabla} C_i^P + z_i D_i^P C_i^P \frac{F}{RT} \vec{\nabla} \phi^P \right], \qquad (4.29)$$

where C_i^P, D_i^P, and z_i correspond to the concentration, the solid-state diffusion coefficient and the electric charge of ion **i** in the product layer, respectively; ϕ^P is the electric field in the product layer; and F is the Faraday constant. The condition of electrical neutrality requires the following relation to be fulfilled:

$$\vec{J} = \sum_i z_i \vec{J}_i = 0, \qquad (4.30)$$

where $\vec{J}_i$ are the surface flow of the ion **i** [mol g^{-1} s^{-1}], yields (see Appendix G):

$$\vec{J}_i = -\overline{D}_i^P \vec{\nabla} C_i^P, \qquad (4.31)$$

which is analogous to the Fick's first law, with a diffusion coefficient for species **i** ($\overline{D}_i^P$) that includes the drift of all the ionic species, defined as follows for two of them:

$$\overline{D}_i^P = \overline{D}_j^P = \frac{\left(z_i^2 x_i + z_j^2 x_j \right) D_i^P D_j^P}{z_i^2 x_i D_i^P + z_j^2 x_j D_j^P}, \qquad (4.32)$$

where x_i and x_j are the molar fraction of species **i** and **j**, respectively. Under the assumption that the concentration of both ions (Ca^{2+}, HO^-) is null on the outer surface of the solid product, derived from considering ionic transfer control, the electric field gradient in the product layer should be also null. Eq (4.31) can be solved by taking into account the following assumptions:

1. The product layer is approximately continuous (see Fig. 4.29c) and uniform
2. Aggregation between particles is negligible
3. The particles are spherical
4. The concentration of free Ca^{2+} and HO^- ions in the $Ca(OH)_2/CaSO_3{\cdot}(1/2)H_2O$ interface is considered to correspond, respectively, to their values in the crystalline lattice of $Ca(OH)_2$

Then, the surface flow of both ions, $J_{Ca^{2+}}$ and J_{HO^-}, may be described by the following expression:

$$J_{Ca^{2+}} = \frac{1}{2} J_{HO^-} = \frac{3}{R_P^2 \rho_S} \frac{\overline{D}_{Ca}^P C_{Ca}^R}{(1-X_S)^{-1/3} - 1} \ [\text{mol g}^{-1}\ \text{s}^{-1}], \tag{4.33}$$

where C_{Ca}^R is the concentration of Ca^{2+} ions in the crystalline lattice of $Ca(OH)_2$ ($3.2\text{x}10^{-2}$ mol cm^{-3}), and R_p is the radius of the spherical particles. A detailed deduction of eq. (4.33) can be found in Appendix G. Eq. (4.33) is analogous to a SCM, which has been traditionally proposed for an inward controlling diffusion of a gas reagent (*Ginstling and Borunshtein, 1950*). Finally, the combination of eqs. (4.26) and (4.33) gives the final general expression for r_S for the DM-ISCM:

$$r_S = \frac{\varepsilon_b}{\rho_S (1-\varepsilon_b)} k_S C_g^n a_S + \frac{3}{R_P^2 \rho_S} \frac{\overline{D}_{Ca}^P C_{Ca}^R}{(1-X_S)^{-1/3} - 1} \tag{4.34}$$

Eq. (4.34) can be rewritten in the following way:

$$r_S = \Phi k_S C_g^n a_S + \Psi \overline{D}_{Ca}^P \left[\frac{1}{(1-X_S)^{-1/3} - 1} \right], \tag{4.35}$$

where $\Phi = \dfrac{\varepsilon_b}{\rho_S (1-\varepsilon_b)}$ and $\Psi = \dfrac{3}{R_P^2 \rho_S} C_{Ca}^R$.

In case **m**=0, the combination of eqs. (4.28) and (4.33) and the substitution of Φ and Ψ leads to the following expression:

$$r_S = \Phi k_S C_g^n \exp(-\beta t) + \Psi \overline{D}_{Ca^{2+}}^P \left[\frac{1}{(1-X_S)^{-1/3} - 1} \right] \tag{4.36}$$

As a result, the model contains three adjustable parameters to be fitted to the experimental results: k_S, β and $\overline{D}_{Ca}^P$

To sum up, the equations employed to fit to experimental data involving the DM-ISCM are:

- For **n**=0 or **n**=1 and **m**=0 $\Rightarrow$ Eqs. (4.36)
- For **n**=0 or **n**=1 and **m**=1 $\Rightarrow$ Eqs. (4.27) + (4.35)

4.3.2.3.2. Results and discussion of the model fitting

- ***Results of model fitting to experimental breakthrough curves***

Some examples of the fittings of the DM-ISCM to the experimental breakthrough curves both in the absence and in the presence of NO_2 are displayed in Figs. 4.30(a-d). The fitted curves of the DM have been also included to show that the DM-ISCM provides better fittings than the DM, which is confirmed by their lower values of calculated SQ (Table 4.9) and by the residual analyses shown in Appendix F.

Table 4.9: SQ of the fittings with the DM and DM-ISCM

% RH	*T (K)*	*C_{SO_2} (ppm)*	*C_{NO_2} (ppm)*	*Reaction time (h)*	*SQ of DM*	*SQ of DM-ISCM*		
0	333	2000	0	1	0.23	0.04		
30	333	2000	0	1	0.29	0.08		
30	333	2000	175	2	1.86	0.18		
50	333	2000	0	1	0.17	0.10		
50	333	2000	175	2	0.70	0.14		
70	333	5000	0	1	1.41	0.04		
60	333	5000	175	1	0.56	0.15		
					SQ of DM-ISCM			
					n=0; m=0	*n=1; m=0*	*n=0; m=1*	*n=1; m=1*
70	353	2000	0	1	0.052	0.042	0.049	0.061

The fittings of the parameters **n** and **m** corresponding to DM-ISCM show that in almost all experimental curves no significant differences have been found for the tested values of 0 and 1, as can be observed in the breakthrough curve plotted in Fig. 4.31. The values of SQ included in Table 4.9 also confirm that the experimental results are not conclusive to discern between different values of **n** and **m.** Furthermore, an analysis of residuals of several curves, which is shown in Appendix F, also leads to the same conclusions.

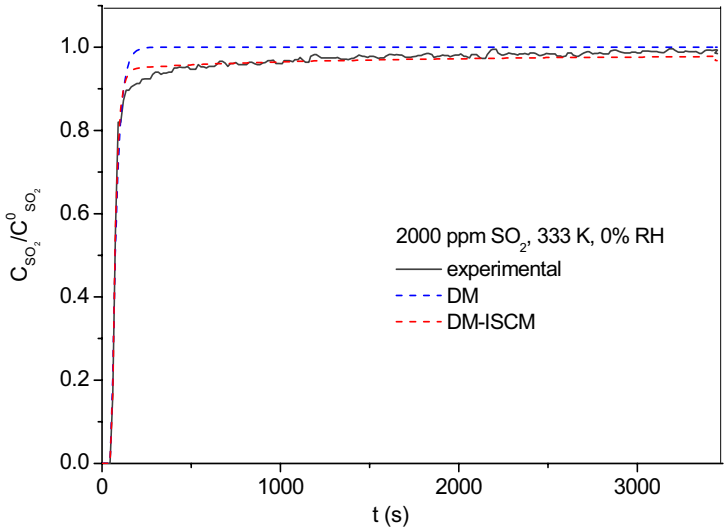
2000 ppm SO2, 333 K, 0% RH
experimental
DM
DM-ISCM
C_SO2/C^0_SO2
t (s)

(a)

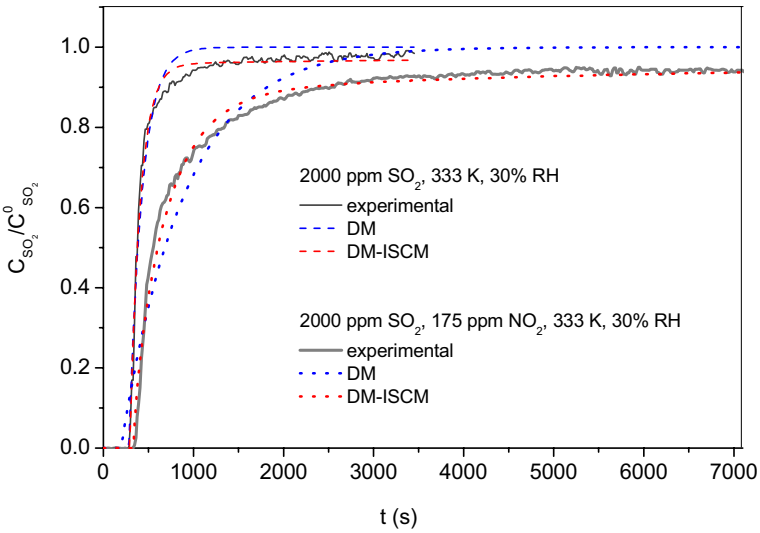
2000 ppm SO2, 333 K, 30% RH
experimental
DM
DM-ISCM
2000 ppm SO2, 175 ppm NO2, 333 K, 30% RH
experimental
DM
DM-ISCM
C_SO2/C^0_SO2
t (s)

(b)

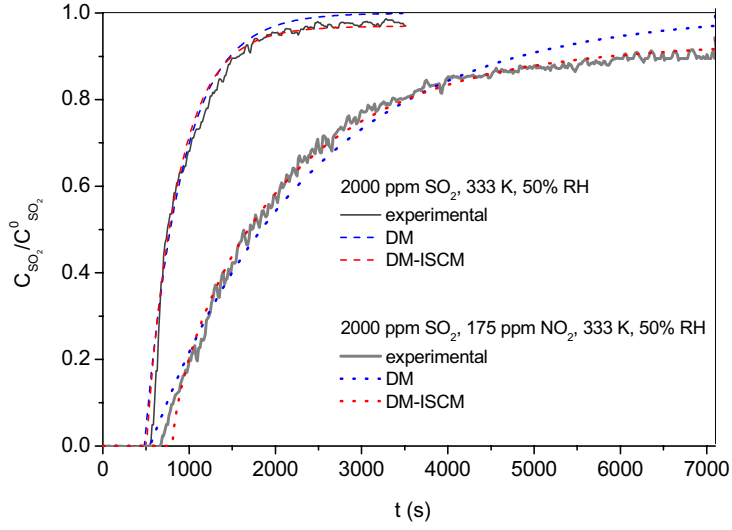
2000 ppm SO2, 333 K, 50% RH
experimental
DM
DM-ISCM
2000 ppm SO2, 175 ppm NO2, 333 K, 50% RH
experimental
DM
DM-ISCM
C_SO2/C^0_SO2
t (s)

(c)

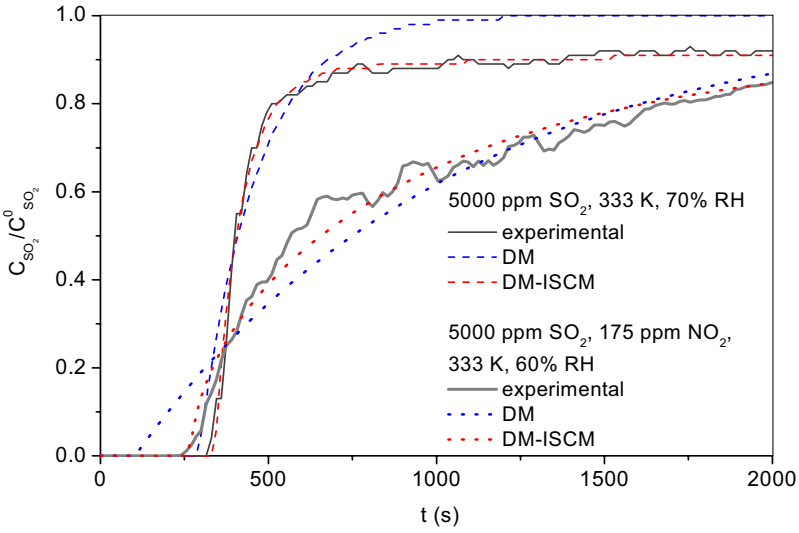

(d)

Fig. 4.30: Experimental and fitted breakthrough curves to DM and DM-ISCM.

The effect of the RH on the parameters k_S, β and $\overline{D}^P_{Ca}$ are shown in Figs. 4.32-34. The confidence interval of the parameters was found to be for almost all curves lower than 13% (97.5% confidence level). As can be seen in Fig. 4.32, the rate constant, k_S, does not appear to depend on the RH at 313 K, whereas a positive influence of the RH is detected beyond this temperature. Moreover, Fig. 4.33 seems to indicate a decreasing exponential trend of the deactivation parameter, β, with the RH. Finally, the representation of $\overline{D}^P_{Ca}$ with respect to the RH depicted in Fig. 4.34 reveals a positive dependence of Ca^{2+} and HO^- solid-state diffusivities through the product layer on this parameter.

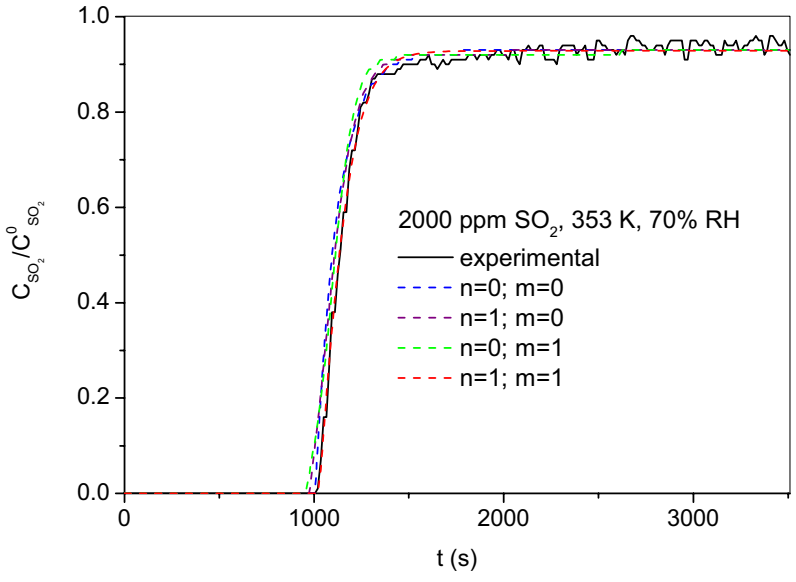

Fig. 4.31: Experimental and fitted breakthrough curves to DM and DM-ISCM.

In Figs. 4.32-34, some values of the adjustable parameters obtained from the experiments done in the presence of the NO_2 are also included. It can be observed that meanwhile the presence of 175 ppm of NO_2 appears to moderately decrease the values of the rate constant, parameters β and $\overline{D}_{Ca}^{P}$ seem to be strongly reduced and increased, respectively. Furthermore, both the exponential trend of β with the RH and the positive influence of the RH on $\overline{D}_{Ca}^{P}$ are stressed.

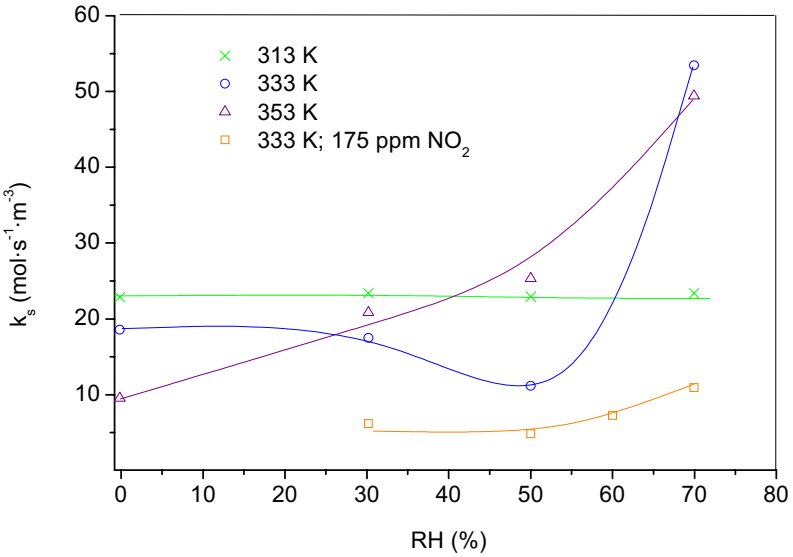

Fig. 4.32: Influence of RH on k_S at 2000 ppm of SO_2.

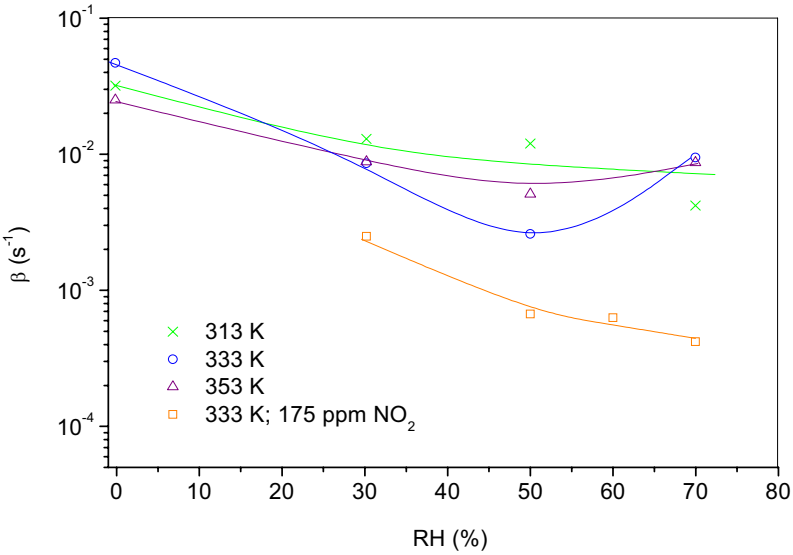

Fig. 4.33: Influence of RH on β at 2000 ppm of SO_2.

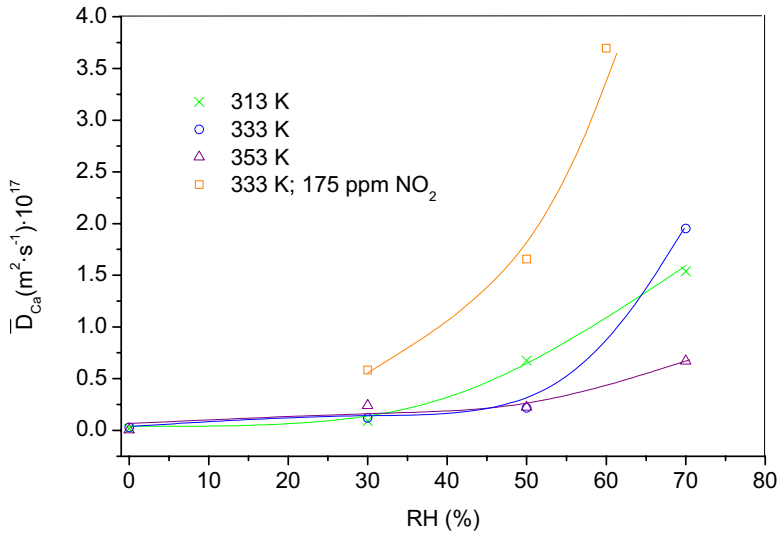

Fig. 4.34: Influence of RH on $\overline{D}_{Ca}^{P}$ at 2000 ppm of SO_2.

Regarding the influence of the temperature on the three parameters of the model, no concluding results have been found. As an instance, the values of k_S at all tested conditions at 2000 ppm of SO_2 are collected in Table 4.10.

Table 4.10: k_S fitted at all conditions tested at 2000 ppm of SO_2

% HR	*T (K)*	*k_S (mol s^{-1} m^{-3})*	*% HR*	*T (K)*	*k_S (mol s^{-1} m^{-3})*
0	313	21.8	50	313	23.0
	333	18.6		333	11.2
	353	9.5		353	25.3
30	313	23.6	70	313	22.6
	333	17.5		333	53.4
	353	20.8		353	49.4

- ***Checking of the external mass transfer (EMT)***

One of the hypotheses of the kinetic model proposed before its resolution is that EMT does not exert any control to the overall reaction. This assumption can now be verified by comparing the reaction rate calculated with those that would be achieved if EMT was the limiting step. As initial reaction rates obtained from our simulations are much lower than those calculated from eq. (4.6) ($1.5\text{-}3.0\times10^{-14}$ mol s^{-1} $particle^{-1}$ and $0.06\text{-}2.0\times10^{-10}$ mol s^{-1} $particle^{-1}$ for 2000 ppm of SO_2 concentration, respectively), which

considers ETM controlling of the overall reaction, it can be concluded that the hypothesis outlined was correct.

- ***Discussion***

Even though a DM seems to predict reasonably well the rupture points and the sharp slope of the curves, the introduction of the contribution of the ISCM to the kinetic equation appears to be necessary to predict successfully the evolution of the curves at long times. Excluding values of 0% RH, calculated values of initial reaction rate in terms of dX_S/dt are in the range $3.5x10^{-4}$-$1.7x10^{-3}$ s^{-1}, which corresponds to the range found experimentally by *Klingspor et al. (1984)* (0-$2x10^{-4}$ s^{-1}) and by *Krammer et al. (1997)* (around 10^{-2} s^{-1}) for the range of RHs tested.

The DM-ISCM is consistent with the reaction mechanism proposed in section 4.3.2.1., which takes into account an adsorption of water on the reactant surface as first followed by the hydration of SO_2 and further reaction. A physical interpretation for the adjustable parameters β and k_S of the model can be proposed. On the one hand, the deactivation constant, β, could be regarded as a structural parameter, because it might be related to the distribution of the product layer on the reactant surface during the progress of the reaction. On the other hand, the rate constant, k_S, could be considered to be basically dependent on the hydration of SO_2 on the surface of the reagent. Moreover, the parameter k_S might include three contributions:

1. Intrinsic kinetic constant, $k_T(T)$, related to the reaction between the adsorbed complex $SO_2 \cdot zH_2O$ and $Ca(OH)_2$, i.e. the intrinsic reaction rate of the reaction (4.12).

2. Equilibrium constant of SO_2 hydration, K_C (see eq. 4.11)

$$K_C(T) = \frac{\theta_{SO_2 zH_2O}}{C_{SO_2}\theta_{H_2O}^z} \tag{4.37}$$

3. Water adsorption isotherm (see eq. 4.10)

$$\theta_{H_2O} = f(p_{H_2O}, T) \tag{4.38}$$

yielding the final expression:

$$k_S = k_T(T)\left[K_C(T)\left(f(p_{H_2O}, T)\right)^z\right]^n \tag{4.39}$$

According to the reaction mechanism discussed, the effect of RH observed in all parameters of the DM-ISCM might be explained as follows:

1. **Effect on k_S**: This parameter depends experimentally on the RH (see Fig. 4.32), which is in agreement with the dependence found in eq. (4.39) with the water partial pressure. This effect

can be interpreted by considering that higher amounts of water might be adsorbed onto the reactant surface as RH increases, which would lead to a higher retention of SO_2.

2. **Effect on β**: The value of β decreases with the RH. This behavior could be ascribed to the way the reaction product deposits on the surface of $Ca(OH)_2$. A deeper study of the effect of the RH on the structure of the product on the reactant surface will be the subject of discussion of section 4.4.3.

3. **Effect on** $\overline{D}_{Ca}^{P}$: The RH enhances the value of $\overline{D}_{Ca}^{P}$. The increase of the amount of water adsorbed on the product layer as the RH increases might lead to an improvement of the ionic movement across it due to a better stabilization of migrating ions.

The aforementioned positive effect of NO_2 on the kinetics of the reaction could be related to the formation of $Ca(NO_3)_2$ and $Ca(NO_2)_2$ species as products of its reaction with $Ca(OH)_2$ (see section 4.2.2.3.). Because nitrate and nitrite species are very hygroscopic, the amount of water retained on the reagent surface at a specific RH would be expected to rise. Hence, the trends with the RH outlined for the parameters β and $\overline{D}_{Ca}^{P}$ would be stressed. However, a slight negative effect for the parameter k_S is observed, which could be explained by considering the competition between SO_2 and NO_2 species for their retention on the reagent surface.

The unclear dependence of parameters k_S and $\overline{D}_{Ca}^{P}$ with temperature can be explained by means of two opposite effects: on the one hand, they should be activated with temperature, but on the other hand, as the temperature increases, the amount of adsorbed water might decrease, as has been reported by *Liu et al. (2002)* for the study of the adsorption of water on $Ca(OH)_2$/fly ash sorbents, which could lead to a reduction of the value of these parameters. As a result, depending on the contribution of each factor, a different evolution with temperature would be expected.

The values of $\overline{D}_{Ca}^{P}$ obtained from the fittings are in the range 0.004-3.70x10^{-17} m^2 s^{-1} (including the values obtained from the experiments with NO_2). No available values of Ca^{2+} and HO^- solid-state diffusion coefficients (D_{Ca}^{P} and D_{HO}^{P}) through $CaSO_3 \cdot (1/2)H_2O$ at temperatures in the range 313-353 K have been found in the literature. However, the values obtained in this work can be compared with the diffusion coefficients values of around 3x10^{-20} m^2 s^{-1} for Ca^{2+} at 1173 K through different solid lattices (*Landolt-Börnstein, 1968*). As can be seen, those found in this work are higher, even though they were determined at much lower temperature. The ionic diffusion is thought to be increased due to the effect of hydration mainly through the grain boundaries, which could act as fast diffusion paths, as the atomic structure of these defects is more open than that of the product lattice.

4.4. AFM STUDY OF THE DESULFURIZATION REACTION: EFFECT OF WATER EXPOSURE ON SURFACE MORPHOLOGY

4.4.1. VISUALIZATION OF THE SURFACE OF REACTED COMMERCIAL $Ca(OH)_2$ CRYSTALS BY SEM

The examination of reacted commercial $Ca(OH)_2$ crystals by SEM (not shown) indicates that the desulfurization reaction at RH<70% leave almost unchanged their shape and surface. Nevertheless, the surface of the particles reacted beyond 70% RH are covered by small needle-shaped grains (see Fig. 4.35-36).

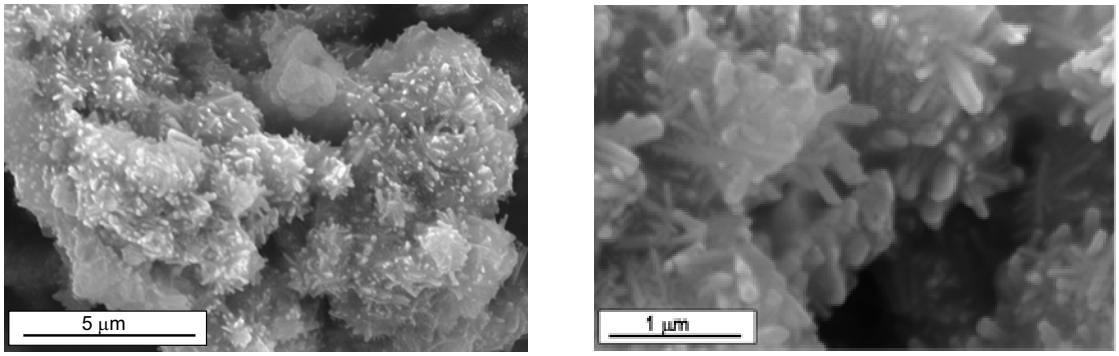

(a) **(b)**

Fig. 4.35: SEM micrograph of an agglomerate of crystals reacted at 333 K, 70% RH and 2000 ppm of SO_2 after 2 hours of exposure time.

Moreover, some EDS analyses done on commercial $Ca(OH)_2$ crystals reacted at different RHs reveal the presence of significant amounts of sulfur on their surface. The analyses done at different regions of the particles seem to indicate that the product is quite well-dispersed over the entire surface. However, as the resolution of EDS analysis is around 1 μm^3, this technique appears to be unsuitable for these crystals to evaluate the degree of localization of the product on their surface for regions lower than 1 μm^2.

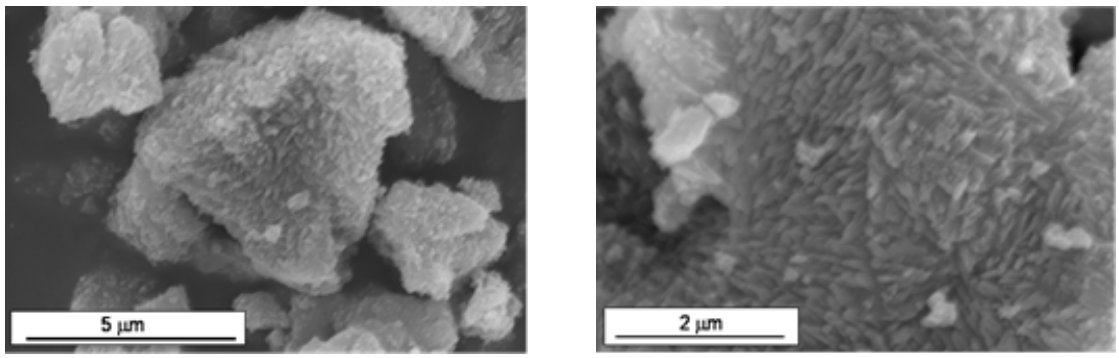

(a) **(b)**

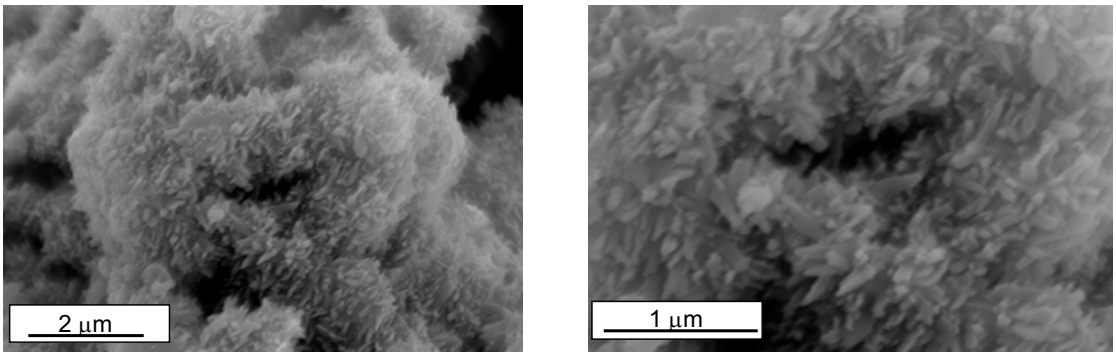

(c) **(d)**

Fig. 4.36: SEM micrograph of an agglomerate of crystals reacted at 333 K, 75% RH and 2000 ppm of SO_2 after 5 hours of exposure time. Fig. (b) and (d) are magnifications of Fig. (a) and (c), respectively.

4.4.2. EFFECT OF WATER VAPOR ON THE SURFACE MORPHOLOGY OF REACTED $Ca(OH)_2$ SINGLE CRYSTALS

To visualize reacted surfaces at higher resolution, further explorations for single crystals by AFM have been done. The AFM images confirm the formation of needle-like features -presumably of $CaSO_3 \cdot (1/2)H_2O$- for the RH range 15-70%. Furthermore, as can be seen in Fig. 4.37, the size of the product features, and therefore the surface roughness (Rms), seems to be strongly dependent on the RH at which the reaction takes place. In order to go deeply into this subject, further crystal samples have been reacted in the range 0-80% of RH. The dependence of the Rms on the RH is plotted in Fig. 4.38.

Blank experiments have been performed to confirm that the increase of surface roughness is exclusively caused by product formation and not due to changes of the $Ca(OH)_2$ surface induced by water vapor. These experiments have been undertaken at 313 K and 50% of RH, but without the presence of SO_2 in the gas phase. The results indicate that water vapor does not exert significant changes on the surface of the cleaved crystals.

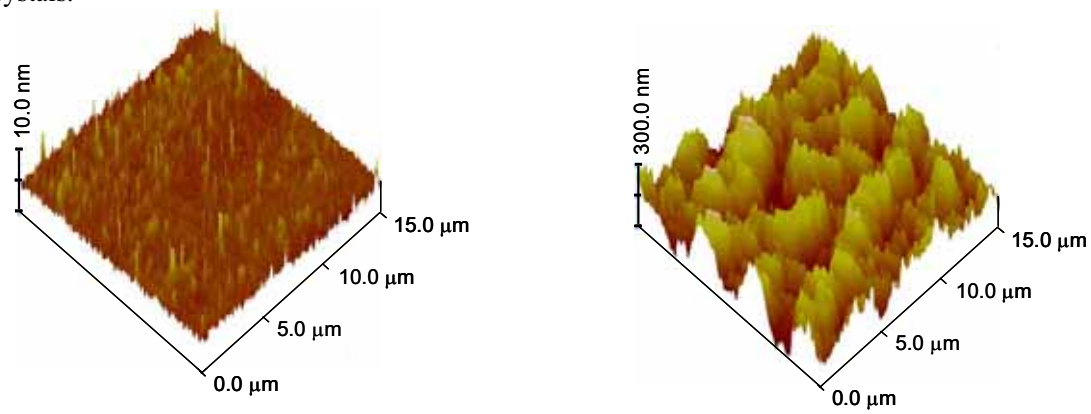

(a) **(b)**

Fig. 4.37: AFM image of surface of two $Ca(OH)_2$ single crystals reacted 313 K and 5500 ppm of SO_2 at different RHs. (a) 15% RH, Rms: 0.8 nm; (b) 70 % RH, Rms: 59.6 nm.

Assuming that the entire product is distributed on the surface as needle-like features -i.e. no continuous layer is formed- a similar trend of the Rms and solid conversion (X_S) with the RH might be expected. Unfortunately, no values of X_S for the reaction between the cleaved $Ca(OH)_2$ crystals and SO_2 are available. Nevertheless, the trend outlined in this section for the Rms vs. RH can be compared with that between X_S and RH for commercial crystals at the same experimental conditions found in section 4.2.1.1. In both cases, an exponential trend with the RH is observed, thus confirming the above assumption.

As can be observed in Fig. 4.38, the Rms values determined at each RH corresponding to different regions of one or more crystals are dispersed, especially at high RHs. In Fig. 4.39, an AFM image of a reacted cleaved crystal is shown, where two adjacent regions with different Rms can be distinguished. The fact that different regions of a crystal show different Rms suggests the presence of regions of different reactivity. This aspect might be related to the solid activity (a_S) defined in the deactivation model (DM) used to fit kinetic experimental data. The different reactivity of different regions on the solid surface might be stressed at higher reaction rates, which takes place at higher RHs.

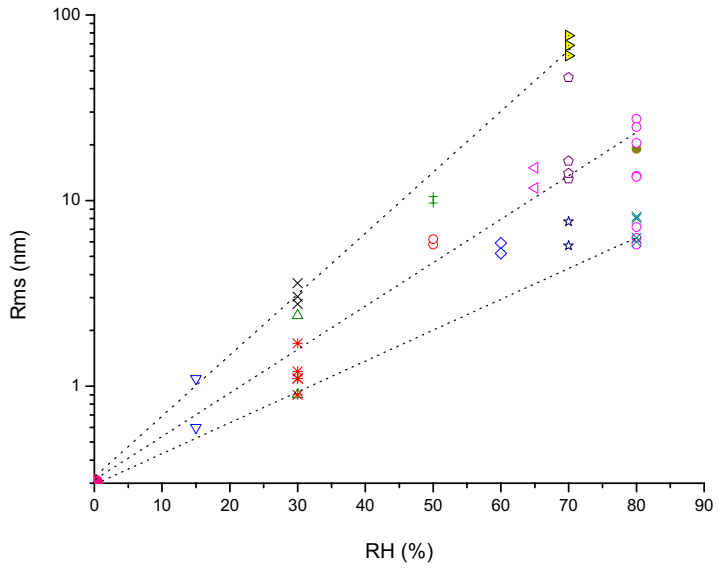

Fig. 4.38: Dependence of the Rms of $Ca(OH)_2$ cleaved single crystals on the RH of the gas phase after 30 min of reaction. Other conditions as in Fig. 4.37. Each symbol indicates different regions of the same crystal.

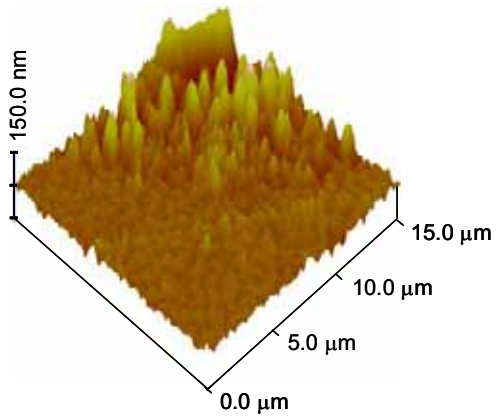

Fig. 4.39: AFM image of a surface reacted at 80% of RH after 30 min, where two adjacent regions with different Rms (5.2 and 26.7 nm) can be distinguished. Other conditions as in Fig. 4.37.

4.4.3. CHANGES IN SURFACE MORPHOLOGY OF REACTED CRYSTALS DUE TO EXPOSURE TO WATER VAPOR

Some experiments have been devoted to study the effect of water on the product structure. Because no product can be formed without the presence of water vapor, the experiments have been carried out in two successive steps: (1) reaction of a cleaved crystal with SO_2 in the presence of water vapor and AFM imaging of the surface just reacted; (2) treatment of the same crystal with certain amount of water vapor and further AFM imaging of the surface. Regarding the second step, three procedures were followed, which results are described below.

4.4.3.1. Short time addition at high water vapor pressure

Some 2D and 3D AFM images of the evolution of a reacted surface and afterwards humidified for 2 hours at 313 K and 80% of RH are shown in Fig. 4.40. The surface is displayed just after being cleaved (Figs. 4.40a1-a2), after being reacted (Figs. 4.40b1-b2) and after the humidification period (Figs. 4.40c1-c2), being all the regions imaged different, but quite close. Furthermore, 2D and 3D AFM images of the same reacted surface but covering much more area (50x50 μm^2) is also shown in Fig. 4.41. The high uniformity observed in this particular region suggests that the size of the area imaged in the range of the apparatus is not significant.

The comparison between the surface before and after the humidification period (Fig. 4.40b and Fig. 4.40c) reveals that the presence of water vapor has induced a clear change of the surface. The roughness has increased dramatically, from 8 to 21 nm. The 3D figures show that the highest features have grown in height from 40 nm to 100 nm and the 2D show that their width has also increased significantly. These changes lead to conclude that water induces crystal rearrangement in such a manner that product features are grouped and as a result larger features are built up.

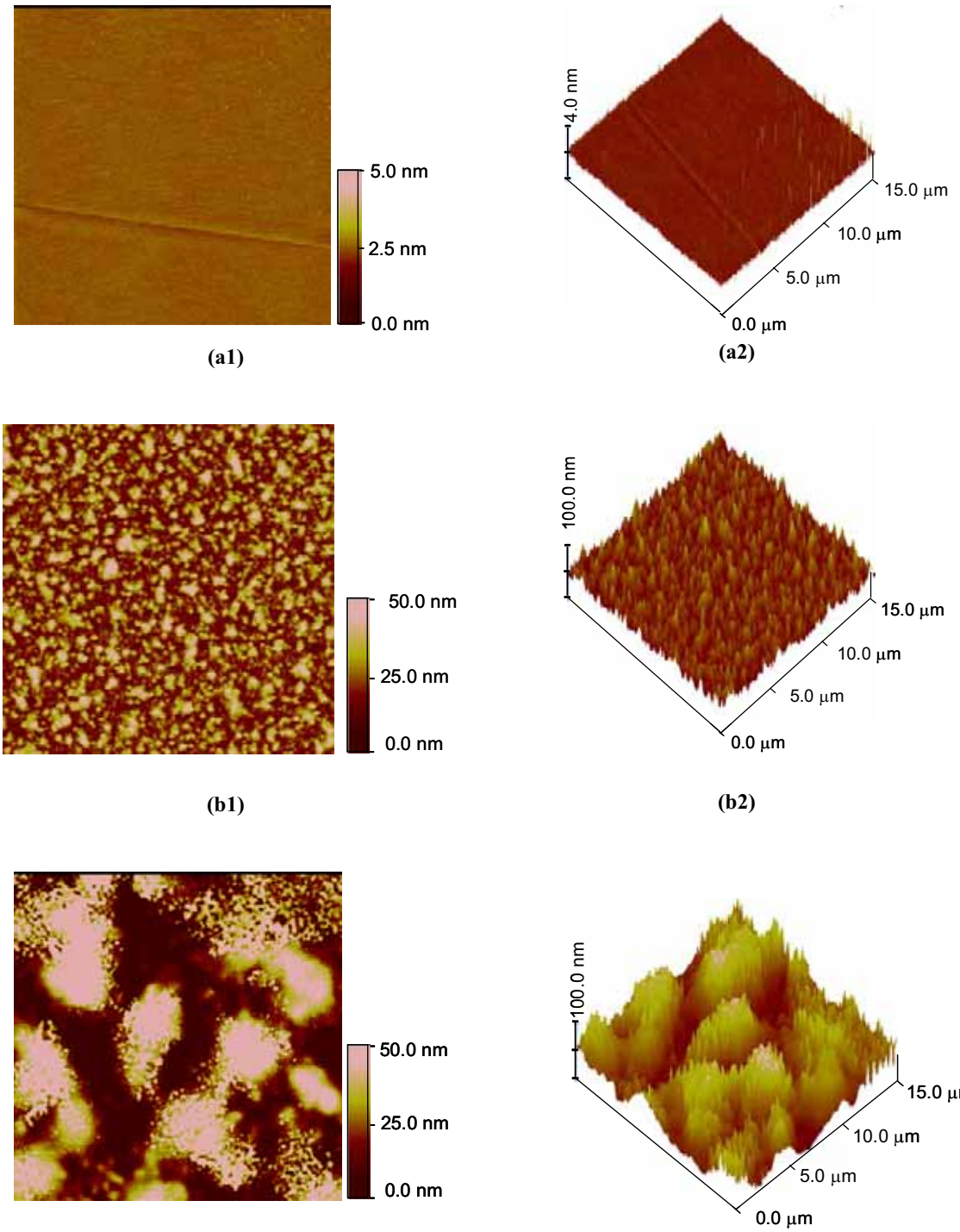

Fig. 4.40: 15x15 μm^2 AFM images of a crystal surface reacted at 313 K, 50% of RH and 5500 ppm of SO_2 for 30 min and afterwards humidified during 2 hours at 313 K and 80% of RH. (a) freshly cleaved surface. Rms: 0.1 nm; (b) surface just reacted, Rms: 7.8 nm; (c) reacted surface after being humidified, Rms: 20.7 nm.

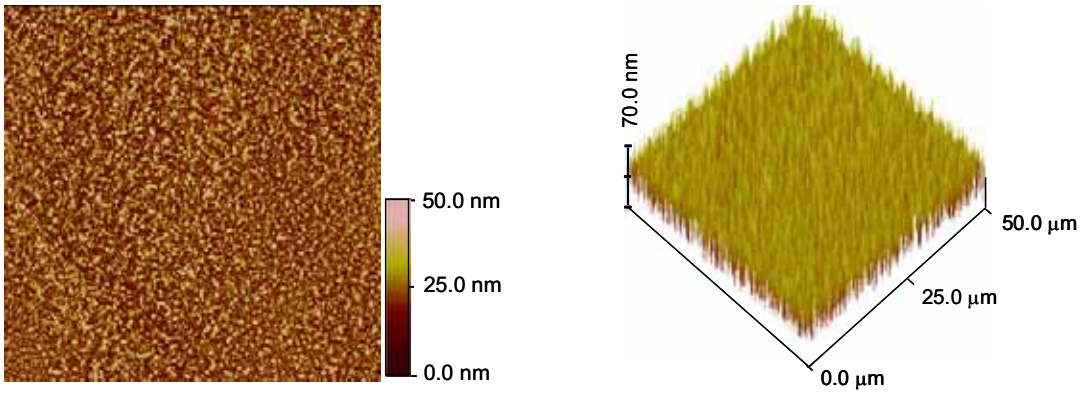

(a1) **(a2)**

Fig. 4.41: 50x50 μm^2 AFM images of a surface just reacted at 313 K, 50% of RH and 5500 ppm of SO_2 for 30 min. Rms: 9.5 nm.

4.4.3.2. Long time addition at room conditions

In order to study the temporal evolution of a reacted surface, a crystal reacted at 30% of RH has been left for some days at room conditions (288-298 K and 60-80% of RH) (see Fig. 4.42). In this figure, the freshly cleaved surface is not shown. The comparison of the images of the surface just reacted at 30% of RH (Fig. 4.42a) and after 3 days (Fig. 4.42b) reveals an extraordinary change of its morphology, raising the Rms from 3 to 14-17 nm. Furthermore, the images taken after 6 days seem to indicate that the Rms has still increased to 17-25 nm (Fig. 4.42c). Finally, no difference in terms of Rms is observed when the crystal is imaged after 9 and 17 days, which indicates that a stationary value has been achieved. This trend is confirmed by another sample reacted at 50% of RH (not shown here). Its Rms increased from 5.8 to 12.0 nm after leaving the sample for 1 day at room conditions. A further image after 6 days does not reveal any change in the Rms, which seems to indicate that a constant value has been achieved.

In order to assure that the observed effects are only related to changes of the product, a blank experiment has been undertaken. A cleaved $Ca(OH)_2$ single crystal has been imaged after being left for 7 days at room conditions. In Fig. 4.43, a surface image together with one of its profiles is shown. As can be seen, small agglomerates or nodules up to 8 nm height and 0.5 μm width are present on the surface. Comparing the evolution of the surface features in reacted crystals with the appeared features of the unreacted one after approximately the same period of time, it can be observed than the formers grew up much more than the latters. As a consequence, it can be concluded that surface changes of reacted crystals must be mainly caused by product changes.

On the other hand, if we assume that 1 layer of water has a thickness of approximately 0.25 nm (*Cantrell and Ewing, 2001*), it seems that the features built on unreacted crystals cannot be water-clusters or water islands, since their size is too large. Consequently, the formation of the nodules seems to be due to a rearrangement of the $Ca(OH)_2$ surface, which should be enhanced owing to the role of adsorbed water, which might cause a certain mobility of the surface.

In order to assure that the changes of the surface are only related to water effect, other two reacted samples at 30% of RH were left in a dessicator at 293 K for 3 and 13 days, respectively. The images of the first sample taken before and after this period are displayed in Fig. 4.44. As can be observed, no significant differences are observed, which seems to reinforce the idea that water is the active agent that promotes surface rearrangement.

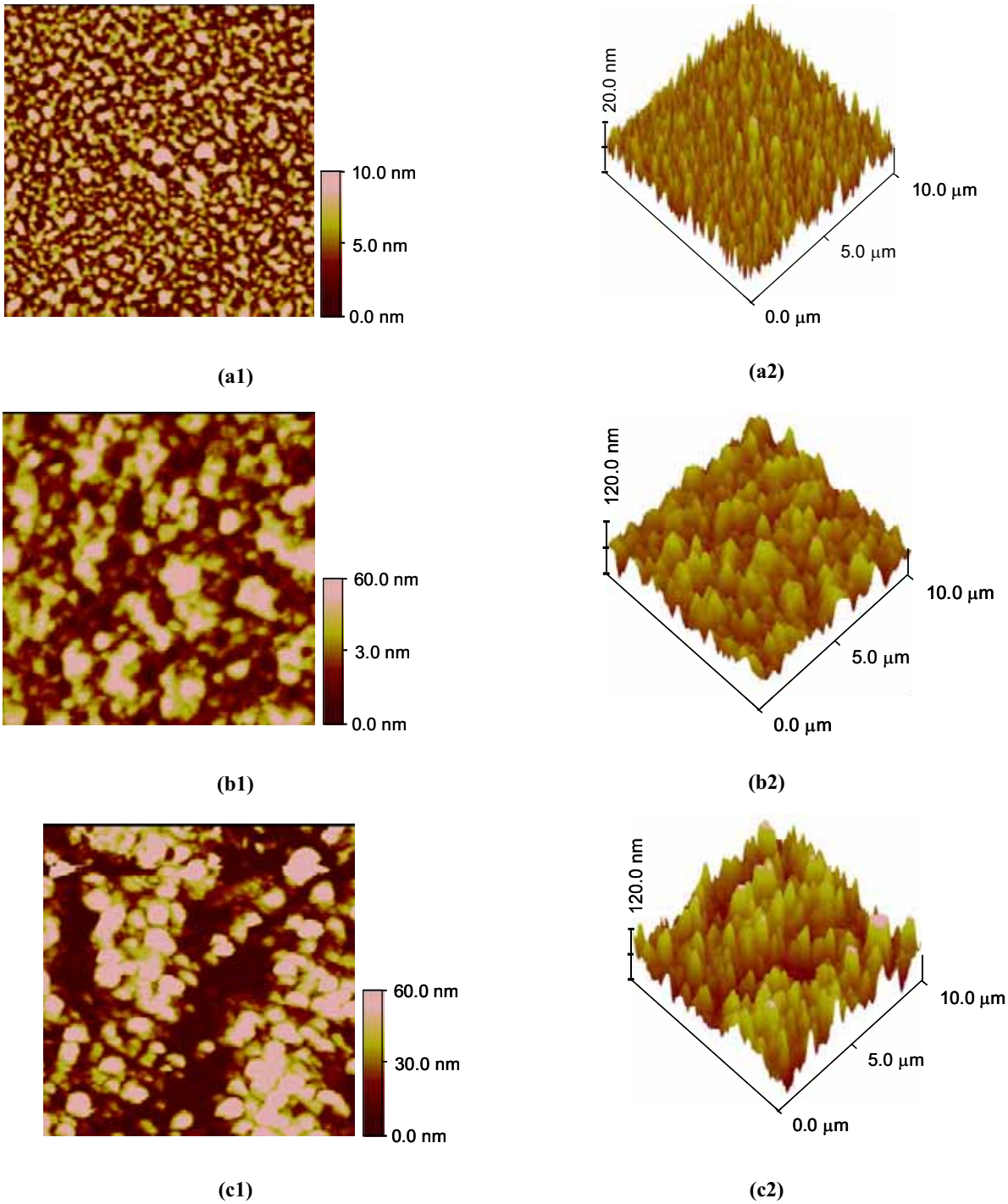

Fig. 4.42: 10x10 μm^2 AFM images of the temporal evolution of a crystal surface reacted at 313 K, 30% of RH and 5500 ppm of SO_2 for 30 min left in contact with the atmosphere at room conditions (288-298 K, 60-80% RH). (a) Surface just reacted, Rms: 2.9 nm; (b) Reacted surface after 3 days, Rms: 14.4 nm; (c) Reacted surface after 6 days, Rms: 25.0 nm.

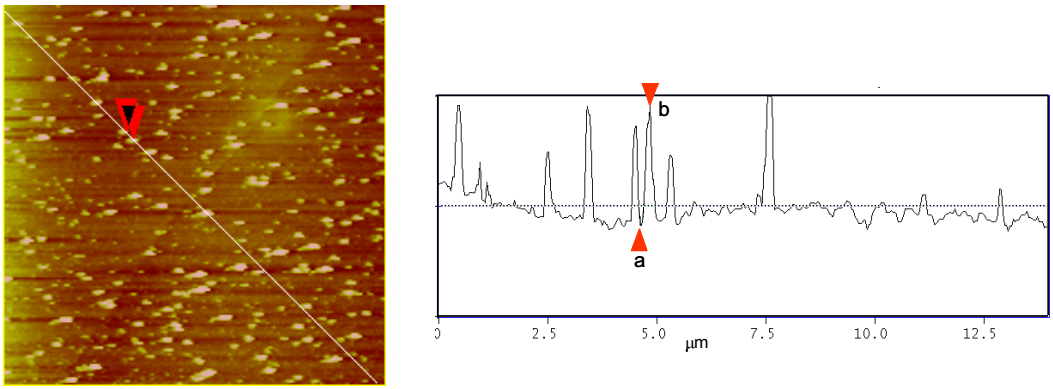

Fig. 4.43: 10x10 µm^2 AFM images of a crystal surface left in contact with the atmosphere at room conditions (288-298 K and 60-80% RH). a-b: 7.9 nm; Rms: 1.3 nm.

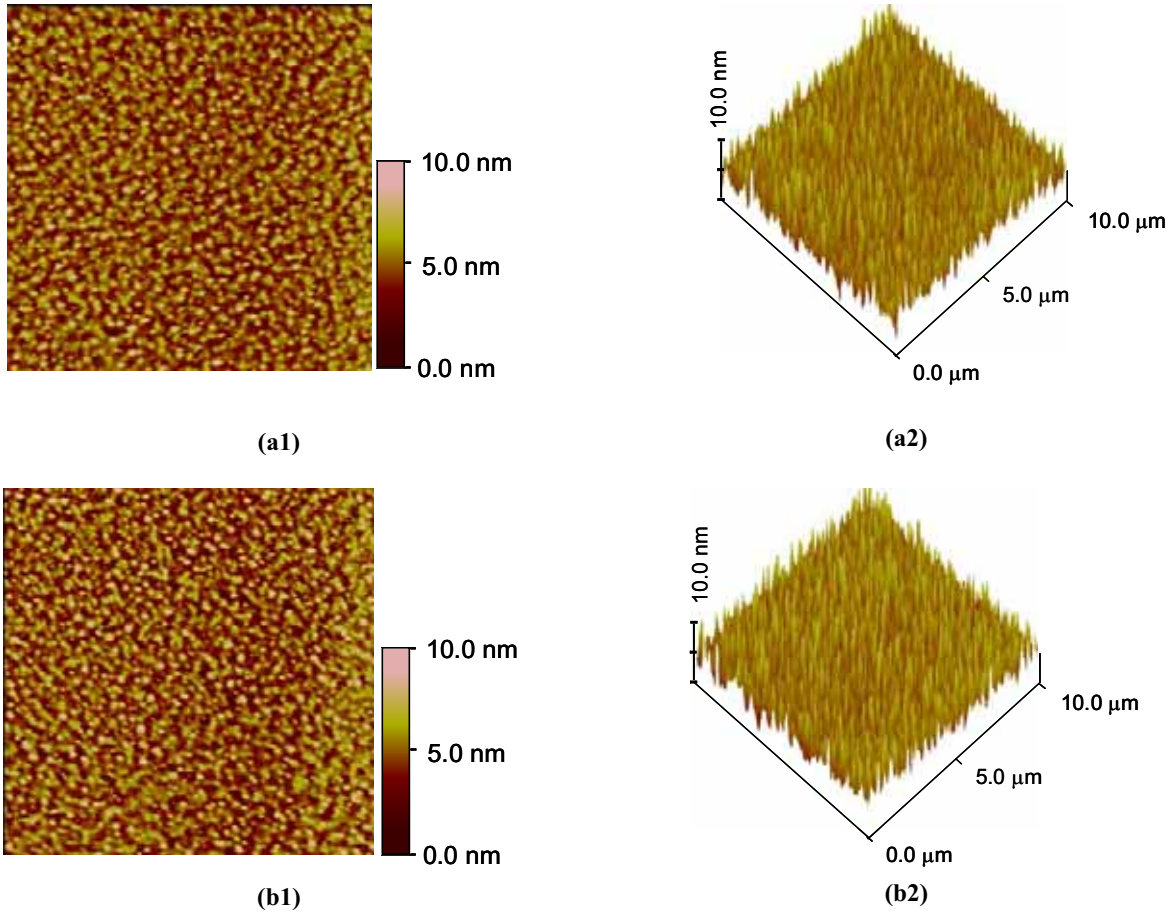

Fig. 4.44: 10x10 µm^2 AFM images of the temporal evolution of a crystal surface reacted at 313 K, 30% of RH and 5500 ppm of SO_2 for 30 min left in contact with a dry atmosphere in a dessicator (293 K). (a) Surface just reacted, Rms: 1.1 nm; (b) Reacted surface after 3 days, Rms: 1.1 nm. No significant changes can be observed.

4.4.3.3. In-situ humidification

As the experiments described above show that the reacted surface tends to be modified by water vapor after one day of being reacted, other experiments have been performed to study its effect at shorter times, specifically for two hours. The study has been done with two reacted samples (30% and 50% of RH). After the reaction, they have been placed in a controlled humidity chamber at 293 K. AFM images have been continuously acquired (every 2.5-2.75 min) while the RH of the chamber is increased from 20 to 75% in a period of ca. 10 min and for an additional period of 90 min keeping the RH constant at 75%. In Fig. 4.45, the evolution of the surface of the sample reacted at 30% of RH during 10 min of humidification is displayed. The image of the surface after having been left for three days at room conditions (293K and 60-80% of RH) is also included (see Fig. 4.45e). No substantial changes have been observed for a similar experiment carried out with a cleaved $Ca(OH)_2$ crystal, which was placed in the controlled humidity chamber at 70% of RH and was continuously imaged (every 5 min) by AFM for two hours.

As can be seen in Fig. 4.45, an increase of RH causes an initial vertical growth of some features from 10 to 45 nm height (Rms: from 3.0 to 4.8 nm). However, this feature growth seems to be unstable due to a further relaxation of the surface (Rms: 2.9 nm). Moreover, the images taken during the following 90 min (not shown) do not show any variation, in contrast to those taken after 3 days (see Fig. 4.45e), where product aggregation is observed again. Similar results have been obtained with the sample reacted at 50% of RH (not shown).

Comparing the temporal evolution of the surface of these experiments with that described in section 4.1.3.1 at 313 K and 80% of RH for 2 h, which involve higher water vapor pressures, it can be again concluded that water vapor pressure might play a key role in the kinetics of product aggregation on the surface of $Ca(OH)_2$ single crystals.

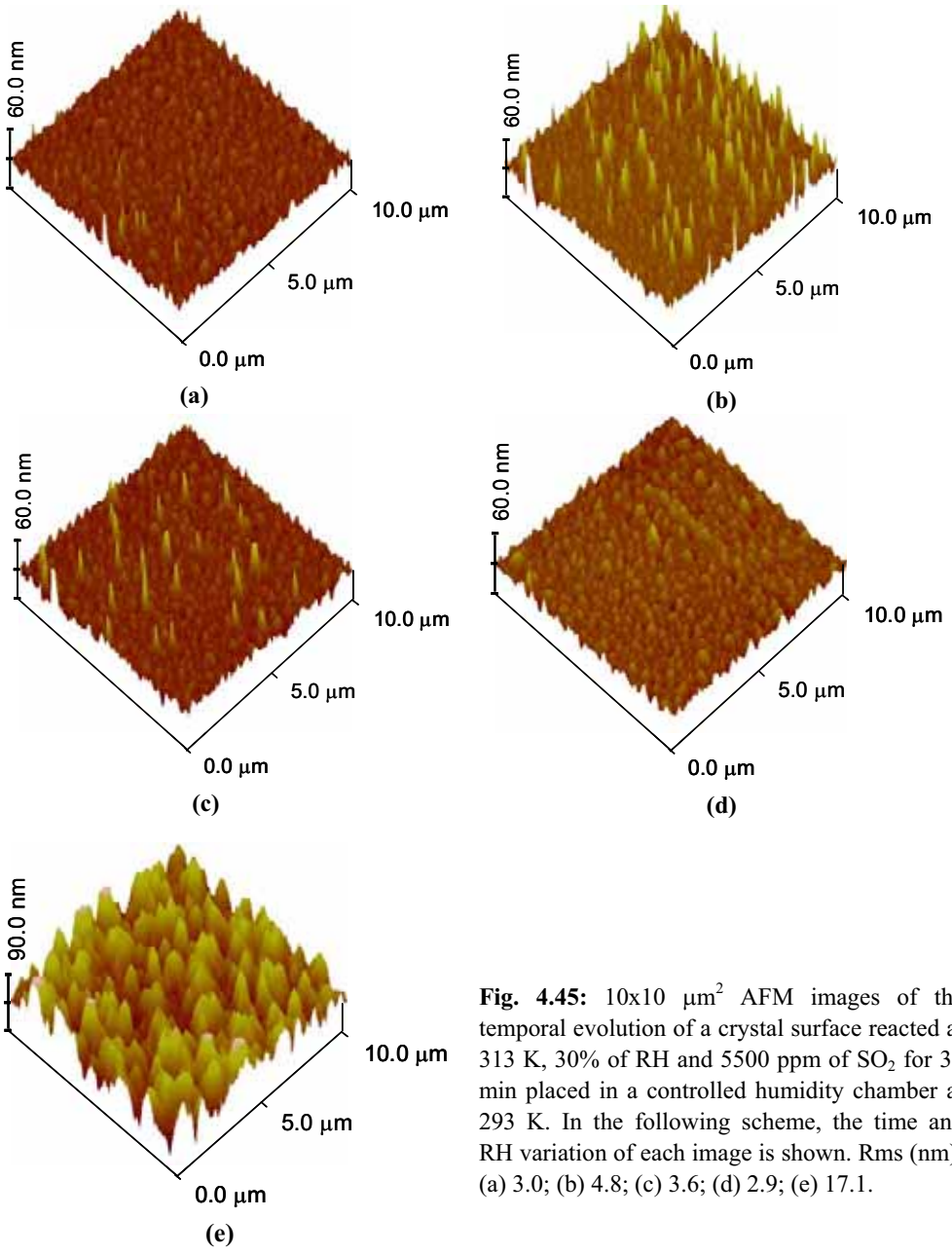

Fig. 4.45: 10x10 μm^2 AFM images of the temporal evolution of a crystal surface reacted at 313 K, 30% of RH and 5500 ppm of SO_2 for 30 min placed in a controlled humidity chamber at 293 K. In the following scheme, the time and RH variation of each image is shown. Rms (nm): (a) 3.0; (b) 4.8; (c) 3.6; (d) 2.9; (e) 17.1.

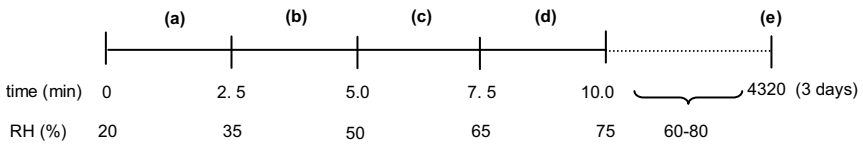

4.4.3.4. EDS analyses: Evidence of solid aggregation

According to the results exposed in sections 4.4.3.1-2, water vapor seems to play a key role on the morphology of the product onto the reacted surface of $Ca(OH)_2$ single crystals and on its further ability to rearrange along the time. Once $Ca(OH)_2$ surface is almost covered by needle-like features, the presence of water seems to enhance crystal mobility and allows crystal aggregation, which is faster at higher vapor pressures.

In can be hypothesized that while product aggregation takes place, a fresh active surface of $Ca(OH)_2$ available for further reaction might be generated. In order to elucidate this point, further EDS elemental analyses of the surface have been done. Because the resolution of EDS analyses is ca. 1 μm^3, a sample has been prepared at conditions which provided features of wider dimensions, that is, reacted at 50% of RH and further humidification for 4 h at 313 K and 80% of RH (see Fig. 4.46a-b).

The comparison of the EDS spectrum in the center of the nodule or aggregate with other four spectra in its nearby shows higher signal of sulfur in the nodule than in its surroundings. This result indicates that the product is localized preferentially in the nodule as $CaSO_3 \cdot (1/2)H_2O$, while the surface that surrounds it is mainly $Ca(OH)_2$. This result seems to confirm the aforementioned hypothesis, which allows to conclude that the presence of water enhances product mobility and opens up fresh $Ca(OH)_2$ reactive sites. A schematic representation of the evolution of features when the surface is exposed to a high vapor pressure is depicted in Fig. 4.47. It can be proposed that adsorbed water might form a non-rigid surface layer that could allow product microcrystals to move by the formation of H-bonds to subsequently aggregate one another.

The phenomenon of crystal mobility on a surface has been reported in other systems that concern the formation of a product on a crystal host in the presence of adsorbed water. In this way, *Allen et al. (1996)*, by means of TEM analysis, found experimental evidence of the reorganization of $NaNO_3$ layers on the surface of NaCl into separate microcrystallites of $NaNO_3$ on a NaCl crystal host when the solid samples were exposed to 45-71% of RH. Moreover, *Zangmeister et al. (1998)* also found a rearrangement of $NaNO_3$ layers to form well-defined $NaNO_3$ “towers”, when they studied by AFM the effect of water saturated atmosphere on the surface of NaCl (100) single-crystal previously reacted with HNO_3.

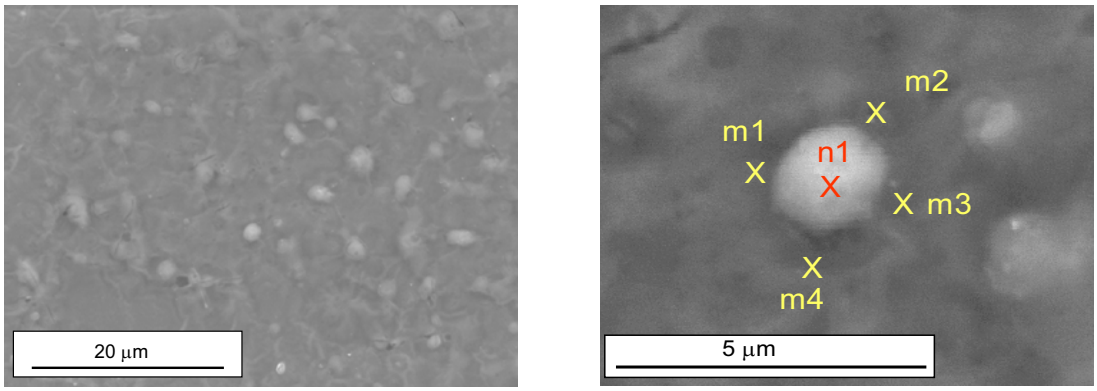

(a) **(b)**

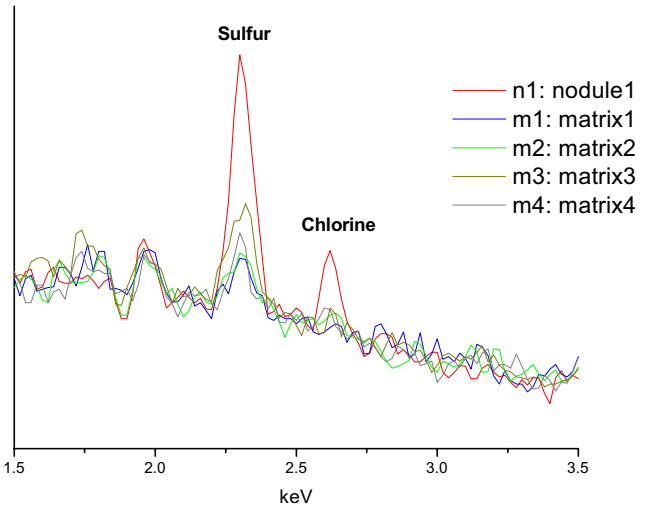

(c)

Fig 4.46: SEM and EDS analyses of a crystal reacted at 313 K, 50% of RH and 5500 ppm of SO_2 for 30 min and after being humidified at 313 K and 80% of RH for 4 h. (a) SEM micrograph, where some aggregates or nodules can be seen; (b) SEM micrograph of one nodule with EDS analyses (n and m denote the nodule and its nearby, respectively; (c) EDS elemental spectra, where the amount of sulfur is practically localized in the nodule.

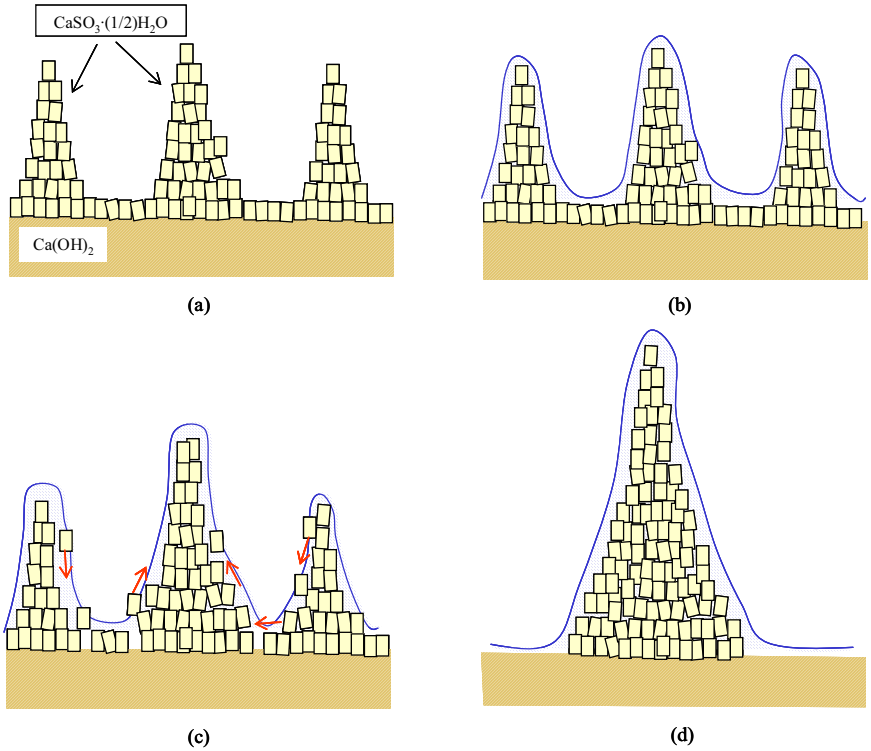

Fig. 4.47: Schematic representation of the evolution of $CaSO_3 \cdot (1/2)H_2O$ features onto the surface of a $Ca(OH)_2$ single crystal when they are in contact with a high water vapor pressure. (a) Close needle-like features of $CaSO_3 \cdot (1/2)H_2O$ formed by $CaSO_3 \cdot (1/2)H_2O$ single crystals; (b) water adsorption on $CaSO_3 \cdot (1/2)H_2O$ crystallites; (c) diffusion of $CaSO_3 \cdot (1/2)H_2O$ crystallites by the interaction with water molecules; (d) needle-like feature grown by the agglomeration of other smaller features.

4.5. PROPOSAL OF A REACTION MECHANISM

A reaction mechanism that might be consistent with the proposed kinetic model (DM-ISCM) in section 4.3.2.3 and the experimental results concerning the effect of water on product morphology described in section 4.4.3 would consist of the following steps (see Fig. 4.48):

1. Water adsorption

Water could be adsorbed on the solid surface -both reactant and product- to form an adsorbed water multilayer at high RHs. This multilayer might show a liquid-like behavior for water coverages>2, which might be achieved for RH>70% (for more detailed information see section 4.3.2.1.).

2. Hydration of SO_2

Hydration of SO_2 with adsorbed water molecules could take place on the solid surface to form $SO_2 \cdot zH_2O$ complexes (for more detailed information see section 4.3.2.1.).

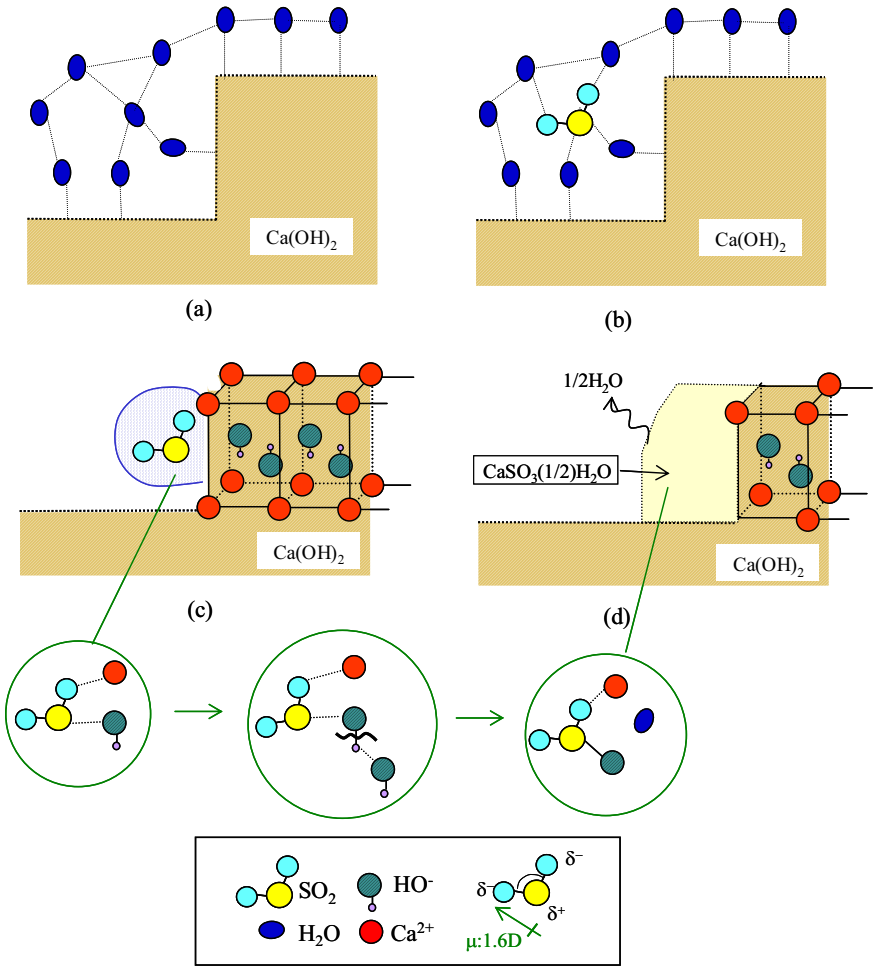

Fig. 4.48: Reaction mechanism proposed for the desulfurization reaction. (a) Water adsorption on the surface of $Ca(OH)_2$; (b) Formation of $SO_2 \cdot zH_2O$ complex; (c) Orientation of SO_2 complex on the surface in such a way that the sulfur interacts with HO^- ions and the oxygen interacts to Ca^{2+} ions and formation of a complex; (d) Formation of $CaSO_3 \cdot (1/2)H_2O$ from the latter complex, formation of 1/2 H_2O molecule and reaction of one H+ ion released from the complex and one HO^- released from the lattice.

3. Reaction of $SO_2 \cdot zH_2O$ with $Ca(OH)_2$

The complexes $SO_2 \cdot zH_2O$ might react with $Ca(OH)_2$ to form the reaction product $CaSO_3 \cdot (1/2)H_2O$. This reaction could take place by two possible ways:

- Hydration of Ca^{2+} and HO^- ions and product precipitation
- Solid-state mechanism

3.1. Hydration of Ca^{2+} and HO^- ions and product precipitation

This mechanism involves a partial dissolution of $Ca(OH)_2$ with the formation of hydrated Ca^{2+} and HO^- ions in the adsorbed water layer. The reaction would take place between the hydrated HO^- and $SO_2 \cdot zH_2O$ with the formation of hydrated SO_3^{2-} ions according to eq. (4.39). The species $CaSO_3 \cdot (1/2)H_2O$ might then precipitate when the water layer covering the solid surface becomes saturated of SO_3^{2-} and Ca^{2+} ions according to eq. (4.40) (Kps in aqueous solution: $5x10^{-5}$).

$$SO_2 \cdot zH_2O + 2HO^- \longrightarrow SO_3^{2-} \cdot (z-1)H_2O + 2H_2O \qquad (4.39)$$

$$SO_3^{2-} \cdot (z-1)H_2O + Ca^{2+} \longrightarrow CaSO_3 \cdot (1/2)H_2O \downarrow + (z-3/2)H_2O \qquad (4.40)$$

3.2. Solid-state mechanism

This mechanism might involve a direct interaction between the hydrated SO_2 complex and Ca^{2+} and HO^- ions placed on the surface of a $Ca(OH)_2$ crystal. Because the ions are in specific positions of the crystal, only some orientations of the hydrated SO_2 complex respect to the crystal might lead to reaction. Two $Ca(OH)_2$ unit cells are depicted as the edge of a crystalline lattice in Fig. 4.48c (see section 4.1.3 for the description of the $Ca(OH)_2$ crystalline lattice). Due to sterical reasons -the size of the ions and lattice parameters are not drawn at real scale in Fig. 4.48c- and the requirement of orientation of the S-O dipole, it seems that the hydrated SO_2 complex can only react with the ions in the crystalline lattice in a tangential direction ("tangential attack or etching") (see Fig. 4.48c). The hydrated SO_2 complex might subsequently proceed to the formation of a covalent bond between the sulfur and the oxygen atom of HO^- ion, thus leading to a new complex. The remaining proton in this complex might be stabilized by another HO^- ion released from the lattice with the ultimate formation of one molecule of H_2O, which would equal stoichiometrically the global reaction (eq. 1.1). Eventually, a new crystal of $CaSO_3 \cdot (1/2)H_2O$ would be formed from the interaction of the final complex with a Ca^{2+} ion of the lattice.

Comparing both mechanisms outlined in this section, it should be stressed that the one related to ion dissolution and precipitation seems to be less favored than the solid-state mechanism because of two outstanding facts: (1) $Ca(OH)_2$ is very insoluble (Kps: $5.02x10^{-6}$), which makes it very difficult to dissolve HO^- and Ca^{2+} ions in the water layer covering the solid surface and (2) the first mechanism requires high water coverages, which, according to the water adsorption isotherm, do only occur at very high RHs. Furthermore, the first mechanism would likely involve the formation of an amorphous product, which seems to be in disagreement with the XRD patterns of reacted commercial crystals (see Fig. 4.16) and, in addition, the product seems to be strongly adhered to the surface -no changes were found on the reacted crystal surfaces after immersion in an ultrasound bath.

The importance of the surface morphology on solid-state reactions should be also emphasized. It is known that chemical reactivity of this kind of reactions is frequently determined by the arrangement of chemical species in crystals and their defects rather than by the intrinsic chemical reactivity of the species (see section 1.5.4.). In a crystal surface, regions with surface defects are energetically more favorable than terraces to establish interactions with adsorbed molecules. Regarding the reaction under study, because water

adsorption strongly depends on the nature of defects, and because the attack seems to be preferably tangential, the presence of defects might be especially important in the progress of the reaction. It should be highlighted that the difference of reactivity was already taken into account in the definition of the surface activity (a_s). Furthermore, the role of defects could also explain the different Rms values found in different regions of reacted $Ca(OH)_2$ single crystals in AFM studies.

4. Diffusion of product crystallites and rearrangement of the reacted surface

When a product crystal is formed, it can be removed from its position to be aggregated with other product crystals with the subsequent formation of needle-like features. This crystal movement, which seems to be subjected to the presence of adsorbed water, liberates or opens up new surface of $Ca(OH)_2$ for further reaction, as it was discussed in section 4.4.3.4. This process could be involved in β parameter of the DM. According to the hypothesis set out in the DM-ISCM model, a reduction of the value of β parameter implies a lower deactivation of the reactant surface (eq. 4.27). A raise of the RH might enhance the mobility of product crystallites on the surface, thus providing a lower deactivation and lower values of β parameter, as was found to occur by fitting experimental kinetic data to the DM-ISCM model (section 4.3.2.3.2). Therefore, this parameter might be regarded as a structural parameter in the DM, as was already suggested in section 4.3.2.3.2.

The role of water on product crystallite mobility might also sustain the possibility of reaction (4.1) to take place when NO_2 is also present in the gas phase (see section 4.2.2.3.). Although this reaction involves two solid reactants, which might be quite unlikely, it might be enhanced because water might promote the contact between both solid reactants.

5. Ionic solid-state diffusion + reaction and/or reaction with residual active surface

According to the results exposed in this section, two mechanisms can be proposed to account for the progress of the reaction after a product layer has been formed. Both of them are consistent with the experimental observation that reaction goes on for a long time at very low reaction rates.

5.1. Ionic outward solid-state diffusion

Even though crystallite diffusion provides free or new $Ca(OH)_2$ surface for further reaction, it could be suggested that this process declines with time until the surface becomes deactivated. At this moment, or even when the surface is partially deactivated, certain amount of SO_2 can continue reacting with Ca^{2+} and HO^- ions that attain the outer surface by diffusion from the $Ca(OH)_2/CaSO_3{\cdot}(1/2)H_2O$ interface (see Fig. 4.49).

According to the fittings of experimental kinetic data to the DM-ISCM model, the ionic diffusion process might be improved due to adsorbed water (see section 4.1.2.2.2). A mechanism for the ionic outward solid-state diffusion consistent with this effect might proceed as follows:

1. Hydration of Ca^{2+} and HO^- ions from the crystalline lattice of $Ca(OH)_2$ at the $Ca(OH)_2/CaSO_3 \cdot (1/2)H_2O$ interface with adsorbed or condensed water in the boundaries between two consecutive $CaSO_3 \cdot (1/2)H_2O$ crystals due to capillary forces.

2. Preferential diffusion of the ions through crystal boundaries. The presence of condensed or adsorbed water might enhance ionic diffusion, especially HO^- diffusion, where a mechanism based on H^+ transfer between water molecules with an inward direction can be proposed (*Levine, 1994*).

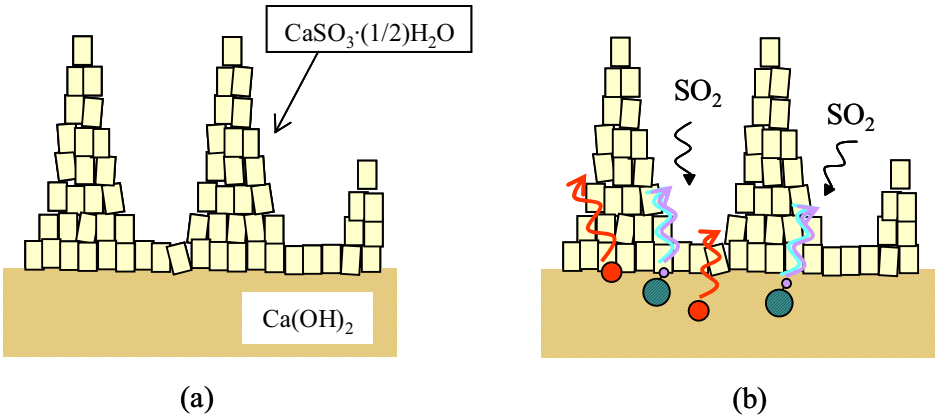

Fig. 4.49: Schematic representation of the *outward solid-state diffusion* mechanism (a) Deactivated surface: any $Ca(OH)_2$ is available for further reaction; (b) Ca^{2+} and HO^- ionic outward solid-state diffusion: the ions attaining the surface can react with SO_2.

5.2. Residual active surface

This mechanism is based on assuming a final steady state where the amount of product crystal is removed from the surface at the same rate that is formed, as it is schematically represented in Fig. 4.50. As a result, the reactant surface might show some partially deactivated or residual areas where the desulfurization reaction can take place, but at very low rates.

Both mechanisms would be consistent with the reported studies (see Table 1.5) that showed no dependence of the reaction rate at long times (after a few minutes) on the SO_2 concentration. While the rate of the outward solid-state diffusion mechanism is controlled by ionic diffusion, the residual active surface mechanism must be limited by the rate of product removal from the surface.

No experimental evidence has been found to discern between the outward solid-state diffusion and the residual surface active mechanisms. Although both mechanisms might take place simultaneously, the prevailing one might depend on the ratio between the rate at which crystal product is removed from the surface and the reaction rate. It can be suggested that the solid-state diffusion mechanism might govern the reaction at lower ratios, while the former might do so at ratios tending to one.

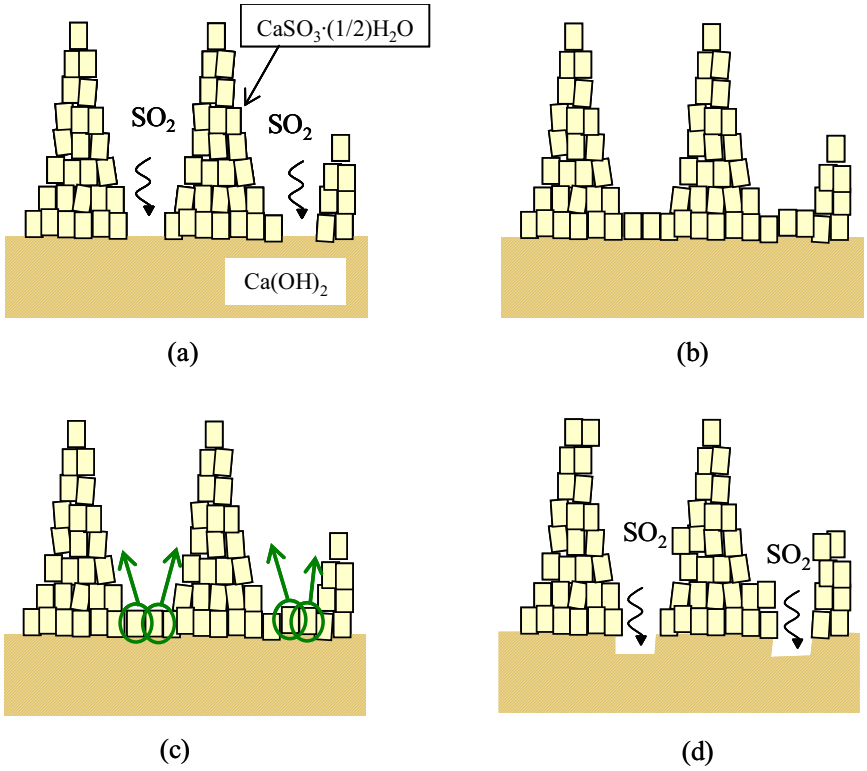

Fig. 4.50: Schematic representation of the *residual active surface* mechanism (a) residual active surface, which can react with SO_2; (b) $CaSO_3 \cdot (1/2)H_2O$ formation; (c) removal of product crystals from the surface by diffusion; (d) new generation of residual active surface.

5. Conclusions

The results obtained in this work lead to the following conclusions:

1. The experimental breakthrough curves of SO_2 obtained in a $Ca(OH)_2$ bed reactor at low temperature in the presence of water vapor reveal that the desulfurization reaction does not stop at long exposure times (higher than 1 h), going on at very low reaction rates. This reaction period can be explained by an outward ionic solid-state diffusion step and/or by the establishment of a steady residual active surface. Both mechanisms are consistent with the experimental observation that the reaction rate at long times strongly depends on the RH.

2. The experimental breakthrough curves have been successfully simulated by a semi-empirical kinetic model (DM-ISCM). This model takes into account the reduction of the active surface of $Ca(OH)_2$ while the reaction progresses and an outward solid-state diffusion of hydrated Ca^{2+} and HO^- ions from the inner $Ca(OH)_2/CaSO_3{\cdot}(1/2)H_2O$ interface to the outer $CaSO_3(1/2){\cdot}H_2O$/gas one. This model predicts a sharp decrease of the reaction rate, after which a long period with a low reaction rate is established.

3. The role of water vapor in the kinetics of the system is reflected in the parameters of the DM-ISCM model (k_S, β and D_{Ca}^{P}). β parameter might be regarded as a structural parameter which accounts for the product crystal mobility. The k_S parameter depends on the hydration of SO_2 on the surface of the reagent. It includes three contributions: the intrinsic kinetic constant of the reaction ($k_T(T)$), the equilibrium constant of SO_2 hydration (K_C) and the water adsorbed (θ_{H_2O}).

4. The AFM technique has shown to be an appropriate tool to provide a new insight into the reaction between SO_2 and $Ca(OH)_2$ crystals at low temperature. It has allowed to visualize the evolution of the surface morphology of crystals after being reacted and after being in contact with a humid atmosphere. This evolution has been crucial to understand the role of water on the reaction, to propose a reaction mechanism and to provide evidence of the importance of the crystal surface features on the desulfurization reaction.

5. The AFM results show evidence of product crystal ($CaSO_3{\cdot}(1/2)H_2O$) mobility on the surface of the reactant crystal ($Ca(OH)_2$) and further product crystal aggregation, but just when the crystal is in contact with water vapor. This finding suggests that once a product crystal is formed during the desulfurization reaction, it is removed from its position, and consequently, new surface of $Ca(OH)_2$ is opened up for further reaction. The widely reported experimental observation concerning the high influence exerted by the relative humidity (RH) on the ability of the $Ca(OH)_2$ to retain SO_2 might be attributed to this phenomenon.

6. A feasible pathway related to the reaction between NO_2 and $Ca(OH)_2$, which is consistent with the results of reacted solid analyses and the effect of water on them, implies two consecutive reactions: (1) NO_2 reacts with $Ca(OH)_2$ to give $Ca(NO_3)_2$ and $Ca(NO_2)_2$; (2) the formed $Ca(NO_2)_2$ further reacts with the adsorbed water to form NO and $Ca(NO_3)_2$:

$$4NO_{2(g)} + 2Ca(OH)_{2(s)} \leftrightarrow Ca(NO_2)_{2(s)} + Ca(NO_3)_{2(s)} + 2H_2O$$

$$3Ca(NO_2)_{2(s)} + 2H_2O_{(ads)} \leftrightarrow Ca(NO_3)_{2(s)} + 4NO_{(g)} + 2Ca(OH)_{2(s)}$$

Both reactions seem to be analogous to those occurring in aqueous solutions. However, the second one in an aqueous system seems to occur only in acidic conditions, while for solid-phase, it seems to be promoted by the presence of adsorbed water. Because both $Ca(NO_3)_2$ and $Ca(NO_2)_2$ readily dissolve in water, its formation might lead to environmental problems when the reacted solid is withdrawn to be disposed of in landfills.

7. When SO_2 and NO_2 coexist in the gas phase, additionally, a redox reaction between the $CaSO_3$ and the NO_2 can also take place, which is consistent with the XRD results obtained in this work. This reaction, which is analogous to that in aqueous solution, appears to be feasible provided that adsorbed water might promote the contact between the two involved solids ($CaSO_3$ and $Ca(OH)_2$).

$$2NO_{2(g)} + CaSO_{3(s)} + Ca(OH)_{2(s)} \leftrightarrow Ca(NO_2)_{2(s)} + CaSO_{4(s)} + H_2O_{(ads)}$$

8. The presence of NO_2 strongly enhances the ability of $Ca(OH)_2$ to capture SO_2. This effect can be explained by considering the formation of $Ca(NO_3)_2$ and $Ca(NO_2)_2$ hygroscopic salts that promote water adsorption, thus enhancing the desulfurization reaction. The DM-ISCM model has been successfully fitted to the SO_2 experimental breakthrough curves in the presence of NO_2. The effect of the RH on the model parameters (k_S, β and $D^P_{Ca^{2+}}$) has been stressed under its presence.

9. The reaction between HCl and $Ca(OH)_2$ forms Ca(OH)Cl, although in certain conditions the final product of the reaction is $CaCl_2$. It has been found that Ca(OH)Cl is an hygroscopic compound, and therefore, the amount of water that might be retained in a in-duct application can be significant. On the other side, it has been found that CaClOH is a stable compound in contact with the atmosphere, so that in principle, it can be settled in landfills. On the contrary, $CaCl_2$ should not be disposed of due to its unsuited properties (it is a deliquescent compound that is transformed into a liquid phase when it gets in contact with the atmosphere, being dripped towards the earth when it is settled).

10. A possible mechanistic pathway of the reaction between HCl and $Ca(OH)_2$ consistent with the formation Ca(OH)Cl as reaction product and various seemingly diverse results from literature concerns two consecutive reactions: (1) the formation of Ca(OH)Cl, and (2) the final formation of $CaCl_2$ from the reaction between Ca(OH)Cl and HCl.

$$Ca(OH)_{2(s)} + HCl_{(g)} \leftrightarrow Ca(OH)Cl_{(s)} + H_2O_{(ads)}$$

$$Ca(OH)Cl_{(s)} + HCl_{(g)} \leftrightarrow CaCl_{2(s)} + H_2O_{(ads)}$$

A kinetic control of these reactions might be suggested, so that, depending on the experimental conditions, the second reaction does not take place. The second reaction could only be promoted at high HCl concentrations and high temperatures, and at higher reaction times.

6. Recommendations

Thoughts and proposals for focusing future efforts to clarify uncompleted aspects or to solve new issues are suggested below:

1. Study of the SO_2 hydration on the adsorbed water by IR techniques. The vibrational bands of species are influenced by the interactions with those surrounding them. Hence, in-situ IR studies of the reaction between SO_2 and $Ca(OH)_2$ in the presence of water vapor could provide information related to the reaction mechanism.

2. Application of AFM and EDS techniques to evaluate the role of water in other gas-solid reactions which have been shown to be highly dependent on water vapor. Systems such as NO_2 ($+SO_2$) or $HCl+(SO_2)$ with $Ca(OH)_2$ or even with other alkaline sorbents (e.g., $NaHCO_3$ or $CaCO_3$) could be tempting issues.

3. Study of the influence of waste gases accompanying SO_2 in incinerators on desulfurization by Ca-based sorbents at low temperature. Experience to date show that efficiencies on SO_2 uptake in incinerator plants are significantly higher than in power plants. The role of other gases emitted simultaneously with SO_2 in incinerators such as HCl or HF could be the subject of further research.

4. Evaluation of the ability of the Ca-sorbents to retain NO_2 at low temperature. Analogously to the study addressed to SO_2 retention, the removal of NO_2 could be also monitored with time.

5. Scope of methods for NO oxidation for further retention of the NO_2 formed by dry scrubbing technologies. Simultaneous NO_x and SO_x retention is still a subject of general interest.

7. Glossary

Latin symbols

a, **b**: fitting parameters of the kinetic models

a_S : active surface [-]

A_b : area of the bed [m^2]

A_{bl} : area drawn by a blank breakthrough curve [s]

A_{exp} : area drawn by a reaction breakthrough curve [s]

A_p : external particle surface [m^2]

A_r : actual area of the particle involved in the empirical model proposed by *Ruiz-Alsop and Rochelle (1997)* [$m^2 g^{-1}$]

A_ϕ : area of spherical particles of equal mass than real particles [$m^2 g^{-1}$]

C_g : concentration of the gas in the bed [$mol\ m^{-3}$]

C_{Ca}^R : Ca^{2+} concentration in the crystalline lattice of $Ca(OH)_2$ [$mol\ m^{-3}$]

d_p : mean particle size [m]

D_a : effective axial dispersion coefficient [$m^2 s^{-1}$]

D_b : bed diameter [m]

D_g^P : diffusion coefficient of gaseous reactant through the product layer [$m^2 s^{-1}$]

$D_{g,0}^P$: D_g^P at $X_S = 0$ [$m^2 s^{-1}$]

D_i^P : solid-state diffusion coefficient of ion i [$m^2 s^{-1}$]

$\overline{D}_i^P$: diffusion coefficient for species **i** that includes the drift of all the ionic species, defined according to eq. (4.32)

E_{ads} : adsorption activation energy [$J\ mol^{-1}$]

E_{ads}° : adsorption activation energy for an ideal surface[$J\ mol^{-1}$]

f : fraction of inert solid [-]

F : Faraday constant, 96487 [C mol^{-1}]

$J_{Ca^{2+}}$: surface flow of Ca^{2+} ions [$mol\ kg^{-1} s^{-1}$]

J_{HO^-} : surface flow of HO^- ions [$mol\ kg^{-1} s^{-1}$]

k_{ads} : kinetic constant of adsorption [s^{-1}]

k_g : external mass transfer coefficient [m s^{-1}]

k_S : rate constant of each kinetic model [$m_g^3 m_S^{-2} s^{-1}$ for SCM and modifications], [$m^{3(n-1)} mol^{(1-n)} s^{-1}$ for DM]

L_b : bed length [m]

L_{wd} : bed length without dilution [m]

m : order of the deactivation process with respect to gas concentration [-]

m_S : amount of solid loaded in the reactor [g]

$mol\ SO_2 / mol\ Ca$: mol of SO_2 retained by mol of $Ca(OH)_2$ [-]

n : reaction order with respect to SO_2 concentration in the DM [-]

n_{Cl} : amount of Cl retained by the solid in HCl experiments [mol]

M_S : molecular weight [kg mol^{-1}]

MWth: unit of capacity heat (equivalent to MW)

N: parameter of the Avrami model, which takes the values 1, 2, 3 or 4

N_{Pe} : Peclet Number for axial dispersion [-]

ppm: parts per million

ppmdv: parts per million by dry volume

r : reaction rate [mol $kg^{-1}s^{-1}$]

$r_{S,p}$: reaction rate per particle [mol $s^{-1}particle^{-1}$]

R : Gas constant, 8.314 [J K^{-1} mol^{-1}]

R_p : particle radius [m]

RH: relative humidity [%]

Rms: root mean square roughness, defined according to eq. (3.3)

SQ: sum of squares of residuals between experimental and calculated breakthrough curves (defined in Appendix F, eq. F.5)

T: temperature [K]

x_i : mol fraction of **i** in the gas phase

X_M: maximum solid conversion [-]

X_S : solid conversion [-]

z_i : electric charge of ion **i** [-]

Greek symbols

β : deactivation constant [$(m^3 mol^{-1})^m s^{-1}$, where **m** is the parameter defined above]

γ : parameter related to the non-ideality of surfaces (adsorption model) [J mol^{-1}]

Δm_{Wt} : total increasing weight of the sample after the drying period in TGA experiments (see Fig. 3.7)

Δm_{Ws} : amount of strongly bound water [g]

Δm_{Wl} : amount of loosely bound water [g]

ε_b : porosity of the bed [-]

ε_L : relative error of the solid conversion [-]

θ : surface coverage [-]

ρ_S : solid density [kg m^{-3}]

σ^p : roughness parameter [-], defined in eq. (4.17) (empirical model proposed by *Ruiz-Alsop and Rochelle, 1997*)

$\sigma_{100\%}$: 100% of solid conversion, defined as eq. (4.7) [-].

Φ_V : volumetric flow rate of the gas flow [$m^3 s^{-1}$]

ϕ^P : electric field [V]

Φ , Ψ : kinetic parameters in eqs. (4.35-36)

subindex

S: solid

g: gas

superindex

0: inlet of the bed

P: product layer

Acronyms

ADVACATE: Advanced silicate process

AFM: Atomic force microscopy

CFB: Circulating fluidized bed reactor

CZD: Confined Zone Dispersion

DM: Deactivation model

DM-ISCM: deactivation model combined with the inverse shrinking core model

EDS: Energy dispersive spectroscopy

EMT: External mass transfer

EPA: Environmental Protection Agency

EPRI: Electric Power Research Institute

FGD: Flue gas desulfurization

GE IDS: General Electric In-Duct Scrubbing

HALT: Hydrate Addition at Low Temperature

IC: ion chromatography

IMT: Internal mass transfer

SCM: Shrinking core model

SEM: Scanning electron microscopy

TGA: Thermogravimetric analyzer

TP: Tapping mode

XRD: X-ray diffraction

XRF: X-ray fluorescence

8. References

BOOKS, JOURNALS AND REPORTS

Aichinger, G.; Brunner, Ch.; Khinast, J. Kinetic studies on low temperature, dry flue gas desulphurization. Coal Science *(1995), 1859-1862.*

Allal, K.M.; Dolignier, J.C.; Martin, G. Reaction mechanism of calcium hydroxide with gaseous hydrogen chloride. Revue de l´institut français du pétrole *(1998), 53(6): 871-880.*

Allen, H.C.; Laux, J.M.; Vogt. R.; Finlayson-Pitts, B.J.; Hemminger, J.C. Water-induced reorganization of ultrathin nitrate films on NaCl: Implications for the tropospheric chemistry of sea salt particles. J. Phys. Chem. *(1996), 100(16): 6371-6375.*

Anderson, J.R.; Bourdart, M. (editors) Catalysis, Science and technology, Vol. 2. Springer-Verlag, Berlin (1981).

Avrami, M. Kinetics of phase change. II. Transformation-time relations for random distribution of nuclei. *J. Chem. Phys.* (1940), 8: 212-224.

Bhatia, SK.; Perlmutter, D.D. The effect of pore structure on fluid-solid reactions: application to the SO_2-lime reaction. AIChE J. *(1981), 27(2): 226-234.*

Blythe, G.M.; Smityh, R.; McElroy, M.; Rhudy, R.; Bland, V.; Martin, C. EPRI pilot testing of SO_2 removal by calcium injection upstream of a particulate control device. Proc. of the 1986 Joint Symposium on dry SO_2/NO_x control technologies, Raleigh, NC, June, 1986, EPRI CS-4966, Vol. 2.

Borgwardt, R.H.; Bruce, KR. Effect of specific surface area on the reactivity of CaO with SO_2. AIChE J *(1986), 32 (2): 239-246.*

Brauer, G. Química inorgánica preparative. Reverte, Barcelona (1958).

Brown, C. Pick the best acid-gas emission controls for your plant. Chem. Eng. Prog*., October (1998), 63.*

Brownell, F. W.; Antonson, R.S.; Fast, K.L.; Fichtorn, N.W.; Freeman, L. E. et al. Clean Air Handbook, 3rd ed., Hunton & Williams, Washington DC (1998).

Brunauer, S.; Emmet, P.M.; Teller, E. Adsorption of gases in multi molecular layers. *J. Am. Chem. Soc.* (1938), 60: 309-319.

Buonicore, A.J.; Davis, W.A (Editors). Air Pollution Engineering Manual. Van Nostrand Reinhold, New York (1992).

Carberry, J.J. Chemical and catalytic reaction engineering. McGraw-Hill, New York (1976).

Cantrell, W.; Ewing, G.E. Thin film water on muscovite mica. *J. Phys. Chem. B* (2001), 105(23): 5434-5439.

Chaix-Pluchery, O.; Pannetier, J.; Bouillot, J.;, Niepce, J.C. Strusctural prereactional transformations in $Ca(OH)_2$. *J. Solid State Chem.* (1987), 67: 225-234.

Chang, J.C.S.; Sedman, C.B. Scale-up testing of the ADVACATE damp solids injection process, Proc. of the First Combined FGD and Dry SO_2 Control Symposium, St. Louis, MO, October, 1988.

Chisholm, P.N.; Rochelle, G.T. Absorption of HCl and SO_2 from humidified flue gas with calcium silicate solids. *Ind. Eng. Chem. Res.* (2000), 39(4): 1048-1060.

Chisolm, P.N.; Rochelle, G.T. Dry absorption of HCl and SO_2 with hydrated lime from humidified flue gas. *Ind. Eng. Chem. Res.* (1999), 38: 4068-4080.

Christman, P.G.*;* Edgar, T.F. Distributed pore-size model for sulfation of limestone. *AIChEJ* (1983), 29(3): 388-395.

Chu, P.; Rochelle,G.T. Removal of SO_2 and NO_x from stack gas by reaction with calcium hydroxide solids. *JAPCA* (1989), 39: 175-179.

Cliffton, C.L.; Alstein, N.; Hule, R.E. Rate Constant for the Reaction of NO_2 with Sulfur (IV) over the pH Range 5.3-13. *Environ. Sci. Technol*. (1988), 22: 586-589.

Colls, J. Air Pollution: an introduction. E & FN Spon, London (1997).

Cussler, E.L. Diffussion: mass transfer in fluid systems, 2nd ed., Cambridge University Press, New York (1987).

Dahlin, R.; Vann Busch, P.; Snyder, T. Fundamental Mechanism in flue gas conditioning. Literature review and assembly of theories on the interactions of ash and FGD sorbents, Per. by Southern Research Institute,. Birmingham, Alabama. Prep. for U.S. Department of Energy of Pittsburgh Energy Technology Center. January 1992.

Damle, A.S.; Ramanathan, K.; Harmon, D.L. Kinetics of reaction between hydrated lime and sulfur dioxide. Proc. of the 6th Symp. Transfer Util. Control Technol. EPRI CS-4918. 1986, vol.1, 18/1-18/20.

Daoudi, M.; Walters, J.K. A thermogravimetric study of the reaction of hydrogen chloride gas with calcined limestone: determination of kinetic parameters. Chem. Eng. J*. (1991), 47: 1-9.*

Deister, U.; Warneck, P. Photooxidation of SO_3^{2-} in aqueous solution. *J. Phys. Chem.* (1990), 94: 2191-2198.

De Nevers, N. Ingeniería de control de la contaminación del aire. Mc Graw Hill Interamericana Editores, S.A. de C.V., Méjico (1998).

Doğu, G.; Doğu, T. Kinetics of capture of sulfur dioxide and applications to flue gas desulfurization. H. I. de Lasa et al. (eds). Chemical Reactor technology for environmentally safe reactors and products. Kluwer Academic Publishers, Netherland, (1993), 467-498.

Doğu, T. The importance of pore structure in the kinetics of gas solid non-catalytic reactions. *Chem. Eng. J.* (1981), 21: 213-222.

Doraiswamy, L.K.; Kulkarni, B.D. Gas-Solid noncatalytic reactions. Carberry, J.J.; Varma, A. Chemical reactor and reactor engineering. Marcel Dekker, New York (1987).

Downing, R.J.; Ramankutty, R.; Shah J. RAINS-ASIA: An Assessment Model for Acid Deposition in Asia, The World Bank, Washington, D.C. (1997).

Engkvist, O.; Stone, A.J. Adsorption of water on the NaCl(001) surface. III. Monte Carlo simulations at ambient temperature. *J. Chem. Phys.* (2000), 112(15): 6827-6833.

Eriksen, T.E. pH Effects on the pulse radiolysis of deoxygenated aqueous solutions of sulfur dioxide. *Journal of the Chemical Society, Faraday Transactions 1: Physical Chemistry in Condensed Phases* (1974), 70(2): 208-215.

European Directive 80/779/CEE of the Council of 15 July 1980 on air quality limit values and guide values for sulphur dioxide and suspended particulates.

European Directive 82/884/CEE of the Council of 3 December 1982 on a limit value for lead in the air.

European Directive 85/203/CEE of the Council of 7 March 1985 on air quality standards for nitrogen dioxide.

European Directive 88/609/EEC of the Council of 24 November 1988 on the limitation of emissions of certain pollutants into the air from Large Combustion Plants.

European Directive 89/427/CEE of the Council of 21 June 1989 amending Directive 80/779/EEC on air quality limit values and guide values for sulphur dioxide and suspended particulates.

European Directive 96/62/CEE of the Council of September 1996 on ambient assessment and management.

European Directive 2000/76/EC of the European Parliament and of the Council of 4 December 2000 on the incineration of waste.

European Directive 2001/80/EC of the European Parliament and of the Council of 23 October 2001 on the limitation of emissions of certain pollutants into the air from Large Combustion Plants

Fonseca, A.M.; Órfão, J.J.; Salcedo, R.L. Kinetic modeling of the reaction of HCl and solid lime at low temperatures. *Ind. Eng. Chem. Res.* (1998), 37: 4570-4576.

Foster, M.C.; Ewing, G.E. Adsorption of water on the NaCl(001) surface. II. An infrared study at ambient temperatures. *J. Chem. Phys.* (2000), 112(15): 6817-6826.

Froment, G.F.; Bischoff, K.B. Chemical reactor analysis and design, 2nd ed., John Wiley & Sons, Inc., Singapor (1990).

Garea, A.; Herrera, J.L.; Renedo, M.J.; Fernández, J.; Irabien, A. Thermogravimetric determination of the influence of water vapor in the FGD in-duct injection at low temperatures. *J. Chem. Technol. Biotechnol.* (2000), 75: 484-490.

Georgakis, C.; Chang, C.W.; Szekely, J. A changing grain size model for gas-solid reactions. *Chem. Eng. Sci* (1978), 34: 1072.

Girifalco, L.A. Atomic migration in crystals. Blaisdell, New York (1964).

Ginstling, A.M.; Brounshtein, B.I. Concerning the diffusion kinetics of reactions in spherical particles. *J. Appl. Chem. USSR*. (1950), 23: 1327-1338.

Gmelin Handbuch der Anorganischen Chemie, 28, Verlag Chemie, Berlin (1956-1957).

Golesworthy, T. A review of industrial flue gas cleaning (3). *Filtration & Separation*, July/August (1999), 16.

Goodman, A.L.; Underwood, G.M.; Grassian, V.H. A laboratory study of the heterogeneous reaction of nitric acid on calcium carbonate particles. *J. Geophys. Res.* (2000), 105(D23): 29053-29064.

Gottstein, G. Grain boundary migration in metals: thermodynamics, kinetics, application. CRC Press, Boca Raton (Florida) (1999).

Greenwood, N.N., Earnshaw, A. Chemistry of the elements. Pergamon Press, Oxford, 1986.

Gutiérrez, F.J.; Ollero, P. Flue-Gas desulfurization in an Advanced in-Duct Desulfurization Process: an empirical model from an experimental pilot-plant study. *Ind. Eng. Chem. Res.* (2003), 42: 6625-6637.

Hartman, M.; Coughlin, R.W. Reaction of sulfur dioxide with limestone and the grain model. *AIChE J*. (1976), 22(3): 490-498.

Hartman, M.; Trnka, O. Influence of temperature on the reactivity of limestone particles with sulfur dioxide. *Chem. Eng. Sci.* (1980), 35: 1189-1194.

Hayon, E.; Treinin, A.; Wilf, J. Electronic spectra, photochemistry, and autoxidation mechanism of the sulfite-bisulfite-pyrosulfite systems. The SO_2^-, SO_3^-, SO_4^-, and SO_5^- radicals. *J. Am. Chem. Soc.* (1972), 94(1): 47-57.

Himmelblau, D. Process Analysis by Statistical Methods. Wiley & Sons, Inc., USA (1970).

Ho, C.; Shih, S.; Liu, C.; Chu, H.; Lee, C. Kinetics of the sulfation of $Ca(OH)_2$ at low temperatures. Ind. Eng. Chem. Res. *(2002), 41: 3357-3364.*

Hsia, C.; St. Pierre, G.R.; Fan, L.S. Isotope study on diffusion in $CaSO_4$ formed during sorbent-flue-gas reaction. *AIChE J*. (1995), 41(10): 2337-2340.

Hsia, C.; St. Pierre, G.R.; Raghunathan, K.; Fan, L.S. Diffusion through $CaSO_4$ formed during the reaction of CaO with SO_2 and O_2. *AIChE J.* (1993), 39(4): 698-700.

Irabien, A.; Cortabitarte, F.; Ortiz, M.I. Kinetics of flue gas desulfurization at low temperatures: non-ideal surface adsorption model. Chem. Eng. Sci. *(1992), 47(7): 1533-1543.*

Jorgensen, C.; Chang, J.C.S.; Brna, T.G. Evaluation of sorbents and additives for dry SO_2 removal. Environmental Progress. *(1987), 6(2): 26-32.*

Jozewicz, W.; Gullett, B.K. Reaction mechanisms of dry Ca-based sorbents with gaseous HCl. Ind. Eng. Chem. Res. *(1995), 34: 607-612.*

Jozewicz, W.; Jorgensen, C.; Chang, J.C.S. Development and pilot plant evaluation of silica-enhanced lime sorbents for Dry Flue Gas Desulfurization, Proc. of the 10th symposium on FGD, Atlant, GA; U.S. Environmental Protection Agency. U.S. Government Printing Office: Washington, D.C., 1986.

Karatepe, N.; Ersoy-Meriçboyu, A.; Yavuz, R. Kinetic model for desulphurization at low temperatures using hydrated sorbent. *Thermochimica Acta* (1999), 127-134.

Karlsson, H.T.; Klingspor, J.; Bjerle, I. Adsorption of hydrochloric acid on solid slaked lime for flue gas clean up. *JAPCA* (1981), 31(11): 1177-1180.

Karlsson, H.T.; Klingspor, J. Tentative modeling of spray-dry scrubbing of SO_2. *Chem. Eng. Technol.* (1987), 10: 104-112.

Klingspor, J.; Strömberg, A.M.; Karlsson, H.T.; Bjerle, I. Similarities between lime and limestone in Wet-Dry Scrubbing. *Chem. Eng. Process*. (1984), 18: 239-247.

Kobayashi, H.; Takezawa, N.; Niki, T. Removal of nitrogen oxides with aqueous solutions of inorganic and organic reagents. *Environ. Sci. Technol*. (1977), 11(2), 190-192.

Koch, M. Raktionsmechnismen von sauren Gasen mit Kalziumhydroxid. Diploma Thesis, University of Technology, Graz, Austria, 2004.

Krammer, G.; Brunner, Ch.; Khinast, J.; Staudinger, G. Reaction of $Ca(OH)_2$ with SO_2 at low temperature. *Ind. Eng. Chem. Res.* (1997), 36: 1410-1418.

Krammer, G.; Reissner, H.K.; Staudinger, G. Cyclic activation of calcium hydroxide for enhanced desulfurization. *Chem. Eng. Proc.* (2002), 41: 463.

Landolt-Börnstein, 5. Teil Bandteil b. Springer- Verslag, Berlin (1968).

Levenspiel, O. Chemical reaction engineering. 3rd ed., Wiley, cop., New York (1999).

Levine, I. N. Fisicoquimica. 3rd ed., McGraw-Hill, Madrid (1991).

Li, G.G.; Keener, T.C.; Wang, J. A two-stage reactor for studying sorbent reactivities in flue gas desulfurization systems utilizing a fabric filter collector. *Environmental Technology* (1998), 19: 475-482.

Littlejohn, D.; Wang, Y.; Chang, S.-H. Oxidation of aqueous sulfite ion by nitrogen dioxide. *Environ. Sci. Technol*. (1993), 27: 2162-2167.

Liu, C.F.; Shih, S.M.; Lin, R.B. Kinetics of the reaction of $Ca(OH)_2$/fly ash sorbent with SO_2 at low temperatures. *Chem. Eng. Sci.* (2002), 57: 93-104.

Loerting, T.; Kroemer, R.T.; Liedl, K.R. On the competing hydrations of sulfur dioxide and sulfur trioxide in our atmosphere. *Chem. Commun.* (2000), 999-1000.

Manahan, S. E. Environmental Chemistry, 6th ed., Lewis, Boca Raton (Florida) (1994).

Martinez, J.C.; Izquierdo, J.F.; Cunill, F.; Tejero, J.; Querol, J. Reactivation of fly ash and $Ca(OH)_2$ mixtures for SO_2 removal of flue gas. *Ind. Eng. Chem. Res.* (1991), 30: 2143-2147.

Maziuk, J.; Kumm, J.H. Comparison of dry injection acid-gas control technologies. Proc. of Air & Waste Management Association (2002), 560-570.

Millikan, J. Die oxyhaloide der alkalischen erden. Z. Phys. Ch. *(1918), 92: 496.*

Moreno, J.A.; Mizrachi, S.; Oppeltz, V. Proton dynamics in calcium hydroxide. A NMR study. *Solid StateCommunications* (1984), 51(8): 597-601.

Mura, G.; Lallai, A. Reaction kinetics of gas hydrogen chloride and limestone. *Chem. Eng. Sci.* (1994), 49: 4491-4500.

Muzio, L.J.; Offen, G.R. Assessment of Dry sorbent emission control technologies. Part I. Fundamental Processes. *JAPCA* (1987), 37(5): 642-54.

Mycock, J.C.; McKenna, J.D.; Theodore, L. Handbook of air pollution control engineering and technology. CRC Press, Boca Raton (Florida) (1995).

Nelli, C.H.; Rochelle, G.T. Simultaneous sulfur dioxide and nitrogen dioxide removal by calcium hydroxide and calcium silicate solids. *J. Air & Waste Manage. Assoc.* (1998), 48: 819-828.

O'Dowd, W.J.; Markussen, J.M.; Pennline, H.W.; Resnik, K.P. Characterization of NO_2 and SO_2 removals in a spray dryer/baghouse system. *Ind. Eng. Chem. Res*. (1994), 33: 2749-2756.

Ollero, P.; Gutiérrez Ortiz, F.J.; Cabanillas, A.; Otero, J. Flue-Gas desulfurization in circulating fluidized beds: an empirical model from an experimental pilot-plant study. *Ind. Eng. Chem. Res.* (2001), 40: 5640-5648.

Ortiz, M.I.; Garea, A.; Irabien, A.; Cortabitarte, F. Flue gas desulfurization at low temperatures. Characterization of the structural changes in the solid sorbent. Powder Technology *(1993), 75: 167-172.*

Pauling, L. The nature of the chemical bond and the structure of molecules and crystals: and introduction to modern structural chemistry, 3rd ed., Cornell University Press, Ithaca (New York) (1960).

Peters, S.J.; Ewing, E. Water on salt: An infrared study of adsorbed H_2O on NaCl(100) under ambient conditions. J. Phys. Chem. B *(1997), 101: 10880-10886.*

Peterson, J.R.; Durhan, M.D.; Vlachos, N.S. Fundamental Investigation of Duct/ESP Phenomena. Prep. by Radian Corporation, Austin, Texas for U.S. Department of Energy of Pittsburgh Energy Technology Center. May 1989.

Philibert, J. Atom movements. Diffusion and mass transport in solids, Les Éditions de Physique, cop. (1991).

Ramachandran, P.A.; Smith, J.M. Effect of sintering and porosity changes on rates of gas-solid reactions. *Chem. Eng. J.* (1977), 14: 137.

Rao, C.N.R. Gopalakrishnan, J. New Directions in solid state chemistry, 2nd ed., Cambridge University Press., Grat Britain (1997).

Rase, H.F. Chemical reactor design for process plants. John Wiley & Sons, Inc., USA (1977).

Reid, R.C.; Prausnitz, J.M.; Poling, B.E. The properties of gases and liquids, 4th ed., Mc Graw-Hill, New York (1996).

Rochelle, G.T.; Jozewicz, W. Reaction of hydrated lime with SO_2 in humidified fue gas. Proc. of SO_2 Control Symposium, New Orleans, Lousiana, May 1990.

Rosenberg, H.S.; Grotta, H.M. NO_x Influence on sulfite oxidation and scaling in lime/limestone Flue Gas Desulfurization systems. *Environ. Sci. Technol*. (1980), 14(4): 470-473.

Ruiz-Alsop, R.; Rochelle, G.T. Effect of Relative Humidity and Additives on the Reaction of Sulfur Dioxide with Calcium Hydroxide. Prep. for U.S. EPA Office of Research and Development, Washington. 1987.

Schwartz, C.E.; Smith, J.M. Flow distribution in packed beds. *Ind. Eng. Chem.* (1953), 45(6): 1209-1218.

Sedman, C.B. Controlling emissions from fuel and waste combustion. *Chem. Eng.,* (1999), 106(1): 82-88.

Seeker, W.R.; Chen, S.L.; Kramlich, J.C.; Greene, S.B.; Overmoe, B.J. Fundamental studies of low-temperature sulphur capture by dry calcitic sorbent injection. Proc. of Joint Symp. Dry SO_2 and simultaneous SO_2/NO_x control technol. Washington (1986).

Sharpe, A.G. Inorganic chemistry. Longman, London (1992).

Shriver, D.F.; Atkins, P.W.; Langford, C.H. Inorganic chemistry, 2nd ed., Oxford University Press., Great Britain (1994).

Simons, G.A.; Garman, A.R.; Boni, A.A. The kinetic rate of SO_2 sorption by CaO. *AIChE J.* (1987), 33(2): 211-217.

Sohn, H.Y.; Szekely, J. The effect of reaction order in non-catlytic gas-solid reaction. *Can. J. Chem. Eng.* (1972), 50: 674.

Sotirchos, S.V.; Yu, H. Overlapping grain models for gas-solid reactions with solid product. *Ind. Eng. Chem. Res.* (1988), 27: 836-845.

Stouffer, M.R.; Ion, H.; Burke, F.P. An investigation of the mechanisms of flue gas desulfurization by In-Duct Dry Sorbent Injection. *Ind. Eng. Chem. Res.* (1989), 28: 20-27.

Strömberg, A.M. Prospects form Further Development of Spray-Dry Scrubbing. Doctoral Dissertation, Lund (1992).

Takeuchi, H.; Ando, M.; Kizawa, N. Absorption of nitrogen oxides in aqueous sodium sulfite and bisulfite solutions. *Ind. Eng. Chem. Process Des. Dev.* (1977), 16(3): 303-308.

Ullmann´s Encyclopedia of Industrial Chemistry, 6th ed., Wiley-VCH, Weinheim (2003).

Van den Bleek, C.M.; Van der Wiele, K.; Van den Berg, P.J. Effect of dilution on the degree of conversión in fixed bed catalytic reactors. *Chem. Eng. Sci.* (1969), 24(4): 681-694.

Vesilind, P.A.; Peirce, J.J.; Weiner, R. Environmental Engineering, 2nd ed., Butterworth, Boston (1988).

Waygood, S.J.; Mc.Elroy, W.J. Spectroscopy and decay kinetics of the sulfite radical anion in aqueous solution". *J. Chem. Soc. Faraday Trans.* (1992), 88(11): 1525-1530.

Weinell, C.E.; Jensen, P.I.; Dam-Johansen, K.; Livbjerg, H. "Hydrogen chloride reaction with lime and limestone: kinetics and sorption capacity". *Ind. Eng. Chem. Res.* (1992) 31, 164-171.

Withum, J.A.; Maskew, J.T.; Rosenhoover, W.A.; Stouffer, M.R.; Wu, M.M. Development of the Advanced Coolside Sorbent Injection Process for SO_2 Control. Proc. of SO_2 Control Symposium, Miami, 1995.

Yagi, S.; Kunii, D. *Chem. Eng. Sci.* (1961), 16: 364-380.

Yoon, H.; Stouffer, M.R.; Burke, F.P. Coolside desulfurization reactions and mechanisms. Proc. of 194th American Chemical Society National Meeting, 1987.

Yoon, H.; Stouffer, M.R.; Rosenhoover, W.A.; Statnick, R.M. Laboratory and field development of Coolside SO_2 abatement technology, 2nd Annual Pittsburgh Coal Conference, 1985.

Yoon, H.; Stouffer, M.R.; Rosenhoover, W.A.; Withum, J.A.; Burke, F.P. Pilot process variable study of Coolside desulfurization. Environmental Progress (1988), 7(2): 104-111.

Zamansky, V. M.; HO, L.; Maly, P.M.; Seeker, W.R. Oxidation of NO to NO_2 by hydrogen peroxide and its mixtures with methanol in natural gas and coal combustion gases. *Combust. Sci. and Tech.* (1996), 120: 255-272.

Zangmeister, C.D.; Pemberton, J.E. In-situ monitoring of the NaCl + HNO_3 surface reaction: The observation of mobile surface strings. J. Phys. Chem. B. *(1998), 102(45): 8950-8953.*

WEB SITES

[www.radford.edu]: Environmental history timeline. In Radford University Homepage. Consulted on 6th July 2004. Available in <http://www.radford.edu/~wkovarik/hist1/timeline.new.html>

[www.ametsoc.org]: History of the Clean Air Act. In American Meteorological Society Homepage. Consulted on 6th July 2004. Available in <http://www.ametsoc.org/sloan/cleanair/cleanairlegisl.html>

[www.eeb.org]: Air pollution. In European Environmental Bureau Homepage. Consulted on 6th July 2004. Available in <http://www.eeb.org/activities/air/main.htm>

[www.epa.gov]: Air Pollution. In US Environmental Protection Agency Homepage. Consulted on 6th July 2004. Available in <http://www.epa.gov/ebtpages/airairpollution.html>

[www.wri.org]: Acid Rain. Downpour in Asia?. In World Resources Institute Homepage. Consulted on 6th July 2004. Available in: <http://www.wri.org/wri/trends/acidrain.html>

[www.bp.com]: Statistical Review of World Energy 2004. In British Petrol Homepage. Consulted on 6th July 2004. Available in: <http://www.bp.com/subsection.do?categoryId=95&contentId=2006480>

[fossil.energy.gov]: Gasification Technologies. In Office of Fossil Energy Homepage. Consulted on 6th July 2004. Available in: <http://fossil.energy.gov/programs/powersystems/gasification>

[www.worldbank,org/…/aqsowet]: Wet Flue Gas Desulfurization. In The World Bank Group Homepage. Consulted on 6th July 2004.
Available in: <http://www.worldbank.org/html/fpd/em/power/EA/mitigatn/aqsowet.stm>

[www.worldbank,org/…/aqsosoij]: Sorbent Injection. In The World Bank Group Homepage. Consulted on 6th July 2004. Available in:
<http://www.worldbank.org/html/fpd/em/power/EA/mitigatn/aqsosoij.stm>

9. Appendices

APPENDIX A

DETERMINATION OF THE SO_2 RETAINED PER MOL OF Ca FROM EXPERIMENTAL BREAKTHROUGH CURVES

The procedure to determine the total amount of SO_2 retained per mol of Ca from an experimental breakthrough curve is explained in detail below. As an instance, the values obtained at 2000 ppm of SO_2, 353 K, 50% of RH and 1 hour of reaction have also been included (see Fig. A.1). The procedure consists of evaluating the difference between the amount of SO_2 that is fed to the reactor and the amount that is not retained during the experimental time, which are evaluated from the blank and the reaction curve, respectively, as follows:

1. Calculation of the amount of SO_2 that is not retained in the bed during the experimental time. As the ordinate of the experimental breakthrough curve corresponds to the ratio between the SO_2 concentration at the outlet and inlet of the reactor measured by the analyzer system [ppm], ($C_{SO_2}/C^0_{SO_2}$), the amount of SO_2 not retained is given by:

$$\text{mol } SO_2 \text{ not retained} = A_{exp}\, C^0_{SO_2(f)}\, 10^{-6}\, \frac{\phi_v}{22400} \qquad \text{(A.1)}$$

   where $C^0_{SO_2(f)}$ denotes the SO_2 concentration fed to the reactor calculated from the gas flow ratios [ppm], A_{exp} denotes the area of the reaction curve [s^{-1}] and ϕ_V is the volumetric total flow in the bed [mL(STP) s^{-1}].

2. Calculation of the amount of SO_2 fed to the reactor during 1 hour. This value has been obtained in an analogous way but considering the blank experimental breakthrough curve obtained at the same conditions:

$$\text{mol}\, SO_2 \text{ fed} = A_{bl}\, C^0_{SO_2(f)}\, 10^{-6}\, \frac{\phi_v}{22400} \qquad \text{(A.2)}$$

3. Calculation of total amount of SO_2 retained per mol of Ca. Considering the stoichiometry of reaction (1.1), it is given by:

$$\text{mol } SO_2 \text{ retained}/\text{mol Ca} = \left(\text{mol } SO_2 \text{ fed} - \text{mol } SO_2 \text{ not retained}\right)\frac{M_{Ca(OH)_2}}{m_{Ca(OH)_2}} \qquad \text{(A.3)}$$

   Substituting eqs. (A.1-2) in (A.3) and rearranging, yields eq. (A.4):

$$\text{mol } SO_2 \text{ retained}/\text{mol}\,Ca = \left(A_{bl} - A_{exp}\right) C^0_{SO_2(f)}\, 10^{-6}\, \frac{\phi_v}{22400}\, \frac{M_{Ca(OH)_2}}{m_{Ca(OH)_2}} \qquad \text{(A.4)}$$

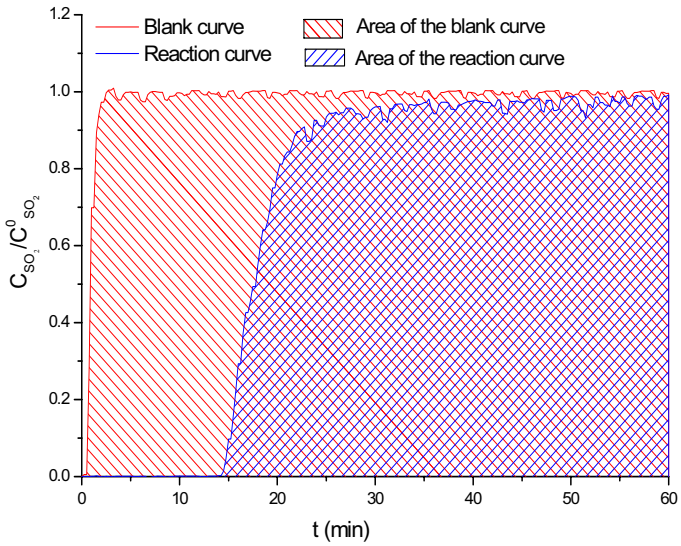

Fig A.1. Blank and reaction experimental breakthrough curves obtained at 2000 ppm SO_2, 353 K and 50% of RH.

For experiment of Fig. A.1, A_{exp} and A_{bl} are drawn in blue and red, respectively:

$$A_{exp} = 3494.6\ \text{s}$$

$$A_{bl} = 2466.0\ \text{s}$$

$$C^0_{SO_2(f)} = \frac{3\,\text{mL}\,(\text{STP})\,\text{min}^{-1}}{1500\,\text{mL}\,(\text{STP})\,\text{min}^{-1}} \cdot 10^6 = 2000\ \text{ppm}$$

$$\phi_V = 25\,\text{mL}\,(\text{STP})\,\text{s}^{-1}$$

$\xrightarrow{\text{(eq.A.4)}}$ **0.170 mol SO_2 retained by mol Ca**

APPENDIX B

ATOMIC FORCE MICROSCOPY (AFM)

Atomic Force Microscopy (AFM) is included within the family of Scanning Probe Microscopies (SPMs). Likewise optical and electron microscopies, SPM techniques enable imaging of sample surfaces. Among the advantages of SPMs techniques are its high resolution (nanometric or atomic), they are non-destructive and they can operate in practically any environment –air, liquid and vacuum. AFM does not only provide the topography of the surface, but also information concerning its softness or hardness, its stickiness or slipperiness, or the springiness of the material.

AFM was designed by G. Binning in 1986. This technique is based on placing a small probe, which is constituted by a sharp *tip* attached to a *cantilever* (see Fig. B.1), on the sample surface in such a way that "almost touches" it. This approach causes a force interaction between them, causing a deflection of the cantilever. As the probe tracks the sample, the variations of the deflections are sensed, thus configuring the topographic image of the scanned area.

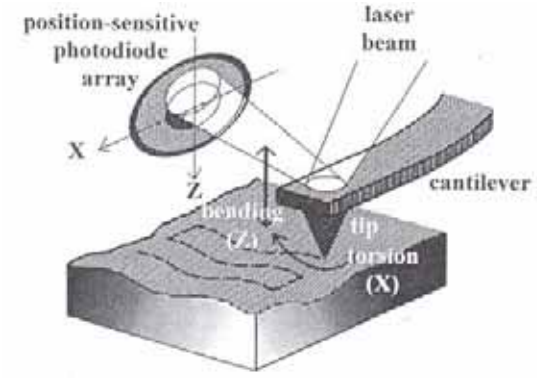

Fig B.1. Schematic representation of the laser beam detection mechanism.

The heart of AFM is the tip since this is the part which interacts with the sample. The sharpness of the tip determines the AFM resolution: the sharper it is, the tinier the interaction area of the surface is and, as a result, the higher the resolution. The *scanning mechanism* is also a key feature of the AFM. The sample is mounted on top of a cylindrical piezoelectric transducer that enables the AFM to accurately positioning the tip relative to the sample surface. The final feature of the AFM to mention is the *detection mechanism*. One of the most common is laser beam detection. It is based on measuring, by a photodiode system, the deflection of the laser beam reflected off the rear side of the cantilever caused by a cantilever displacement (schematically represented in Fig. B.1). AFM enables to imaging in different modes, which are generally classified as follows:

1. *Contact mode.* The tip is brought into direct contact with the surface of the sample, and consequently, the tip-sample interaction involved is repulsive in nature. The entire scanning is

performed by setting an imaging force, that is, the cantilever is bent to a small but fixed amount. The larger the amount the cantilever is bent, the higher the imaging force that the sample experiences.

2. *Non-contact modes.* These operating modes use the range of attractive forces involved in the tip-sample interaction. It allows for reasonably high scan speeds. They can be mainly classified as: *tapping mode* (in air or under liquid) and true *non-contact mode*. When imaging in tapping mode, the cantilever is deliberately excited by an electrical oscillator, bouncing it effectively up and down as it travels over the sample. In true non-contact mode, the oscillating cantilever never actually touches the surface of the sample.

APPENDIX C

EVALUATION OF THE AXIAL DISPERSION IN A FIXED-BED REACTOR

The axial dispersion can be neglected for gases in a fixed-bed reactor when the following relation is fulfilled (*Rase, 1977*):

$$\frac{1}{2} N_{Pe} \frac{L_b}{d_p} \geq 100 , \qquad (C.1)$$

where L_b and d_p are the height of the bed and the mean particle size, respectively, and N_{Pe} (Peclet Number for axial dispersion) is given by:

$$N_{Pe} = \frac{v_i d_p}{D_a} \qquad (C.2)$$

where D_a is the effective axial dispersion coefficient [$m^2\ s^{-1}$]. N_{Pe} is a function of the particle Reynolds number (Re_p) (*Levenspiel, 1972*), which is defined as:

$$Re_p = \frac{d_p v \rho}{\mu} \qquad (C.3)$$

where μ and ρ correspond, respectively, to the viscosity and density of the gas phase, and v is the superficial velocity [$m\ s^{-1}$], which is related to the interstitial velocity (v_i) by the bed porosity (ε_b) according to the following expression:

$$v_i = \frac{v}{\varepsilon_b} , \qquad (C.4)$$

The values of v, v_i and Re_p for all experimental conditions tested in this work are listed in Table C.1. The parameters μ and ρ have been estimated at different gas phase compositions and temperatures. Moreover, the following assumptions have been taken into account:

1. The reactor is assumed to operate at isobaric conditions, since the pressure difference between its inlet and outlet are lower than 15%.

2. The pressure of the gas phase in the reactor is sufficiently low (1.2 bars) to consider ideal gas behavior.

3. The amount of SO_2 is negligible compared to N_2 and H_2O concentration ($8x10^3$ ppm respect to $9.7x10^5$ and $1.9x10^4$ ppm, respectively, in the worst case).

4. The porosity of the bed, ε_b, has been assumed to be constant in the whole bed, which has been experimentally estimated as 28.6% ± 0.8%.

Table C.1: Hydrodynamic properties of the gas mixture in the reactor.

T (K)	*RH (%)*	X_{N_2}	X_{H_2O}	*μ (kg m^{-1} s^{-1})*	*v (m s^{-1})*	v_i *(m s^{-1})*	Re_p *[-]*
313	30	0.98	0.02	1.79E-05	0.21	0.74	4.7
	50	0.97	0.03	1.77E-05	0.21	0.74	4.8
	70	0.96	0.04	1.75E-05	0.21	0.74	4.8
333	30	0.95	0.05	1.81E-05	0.22	0.79	4.6
	50	0.92	0.08	1.75E-05	0.22	0.79	4.7
	70	0.88	0.12	1.69E-05	0.22	0.79	4.8
353	30	0.88	0.12	1.78E-05	0.24	0.83	4.6
	50	0.80	0.20	1.54E-05	0.24	0.83	5.1
	70	0.72	0.28	1.40E-05	0.24	0.83	5.5

According to *Levenspiel (1972)*, the N_{Pe} of the gas flow of this study (with $Re_p \sim 5$ for all the situations tested) is ca. 2. Taking into account that d_p is 0.308 mm (see section 3.1.1.1.) and that $L_b > 30$ mm, the application of criterion (C.1) assures that **axial dispersion can be rejected in the reactor under study**.

APPENDIX D

ESTIMATION OF EXTERNAL MASS TRANSFER (EMT) COEFFICIENTS

1. Estimation of SO_2 diffusion coefficients (D_{SO_2-m})

The estimation of the molecular diffusion coefficient of a dilute species **i** in a multicomponent gas mixture (D_{i-m}) can be reduced to the estimation of the binary diffusion coefficients (D_{ij}), where **j** corresponds to the other species present in the mixture. Assuming that D_{ij} does not depend on the composition of the gas mixture, $D_{i\text{-}m}$ can be found from the following expression (*Reid et al.1996*):

$$D_{i-m} = \left(\sum_{\substack{j=1 \\ j \neq i}}^{n} \frac{x_j}{D_{ij}} \right)^{-1} \qquad (D.1)$$

where x_j is the molar fraction of the species **j** in the gas mixture. Because the SO_2 concentration is very low compared to that of N_2 and H_2O ($8x10^3$ ppm respect to $9.7x10^5$ and $1.9x10^4$ ppm, respectively, for the worst condition), D_{SO_2-m} is given by the expression:

$$D_{SO_2-m} = \left(\frac{x_{N_2}}{D_{SO_2,N_2}} + \frac{x_{H_2O}}{D_{SO_2,H_2O}} \right)^{-1} \qquad (D.2)$$

D_{ij} diffusion coefficients can be estimated by the Chapman- Enskog equation. For an ideal gas, this equation is reduced to the following one (*Levine, 1991*):

$$D_{ij} = \frac{0.00266T^{3/2}}{PM_{ij}^{1/2}\sigma_{ij}^2\Omega_D} \qquad (D.3)$$

where σ_{ij} is the characteristic Lennard-Jones length [Å], but Ω_D is the diffusion collision integral [-], T [K] and P [atm] are the temperature and pressure, respectively, and M_{ij} corresponds to the average molecular weight. Equation (D.3) is suitable for dilute gases at low pressures consisting of non-polar spherical molecules with molecular weight that do not differ significantly.

However, because SO_2 and H_2O are polar molecules, eq. (D.3) is in principle inappropriate to estimate their molecular diffusion coefficients. Brokaw suggested an alternative method, where eq. (D.3) is still used, where Ω_D and σ_{ij} are now re-estimated. First, Ω_D is estimated from a modification of the Neufield equation, which is finally given by:

$$\Omega_D = \frac{A}{(T^*)^B} + \frac{C}{\exp(DT^*)} + \frac{E}{\exp(FT^*)} + \frac{G}{\exp(HT^*)} + \frac{0{,}19\delta_{ij}^2}{T^*} \qquad (D.4)$$

where A,…,H are constant parameters with values A=1.06036, B=0.15610 C=0.19300, D=0.47635, E=1.03587, F=1.52996, G=1.76474 and H=3.89411, and T* is the so-called characteristic temperature:

$$T^* = \frac{k_{Bol}T}{\varepsilon_{ij}} \qquad (D.5)$$

where ε_{ij} is the characteristic Lennard-Jones energy and k_{Bol} is the Boltzmann's constant. Both ε_{ij}, δ_{ij} and σ_{ij} are estimated, respectively, from the geometric average of the pure parameters ε_i, δ_i and σ_i, which are defined as

$$\delta_i = \frac{1.9410^3 \mu_{p_i}^2}{V_{b_i}\, T_{b_i}} \qquad (D.6)$$

$$\frac{\varepsilon_i}{k} = 1.18\,(1+1.3\,\delta_i^2)\,T_{b_i} \qquad (D.7)$$

$$\sigma_i = \left(\frac{1.585\,V_{b\,i}}{1+1.3\,\delta_i^2}\right)^{1/3} \qquad (D.8)$$

where μ_{p_i}, V_{b_i} and T_{b_i} are the dipole moment, liquid molar volume at boiling point and normal boiling point, respectively, of the pure component **i**. All of them, which have been found in the literature, are shown in the Table D.1.

Table D.1: Parameters of the pure components to estimate $D_{i,j}$ by the Brokaw's method

Parameter	*SO_2*	*N_2*	*H_20*
μ_{p_i} (D)*	1.6	0.0	1.8
V_b ($cm^3\ mol^{-1}$)**	44.8	31.2	18.9
T_b (K)*	263.1	77.35	373.15

* *Reid (1996),* ** *Perry (1973)*

The obtained values of D_{SO_2-m} for the temperatures tested are shown in Table D.2. The influence of gas composition at different RHs was proved to be negligible on the estimation of D_{SO_2-m} diffusion coefficients.

Table D.2: D_{SO_2-m} estimated by the Brokaw's method.

T (K)	*D_{SO_2-m} x10^4 ($m^2\ s^{-1}$)*
313	0.121 ± 0.006
333	0.135 ± 0.006
353	0.151 ± 0.005

2. Determination of the EMT coefficients (k_g)

Different empirical correlations are available in the literature for fixed-bed reactors, which have been applied to determine k_g. These correlations are developed in terms of the Sherwood number (N_{Sh}), Schmidt number (N_{Sc}), Re_p (Eq. C.3) or $\overline{Re}$ and "j" factor of Colburn (j_D), which are defined, respectively, as follows:

$$N_{Sh} = \frac{k_g\, d_p}{D_{SO_2-m}}, \quad N_{Sc} = \frac{\mu}{\rho\, D_{SO_2-m}}, \quad \overline{Re} = \frac{Re_p}{(1-\varepsilon_b)}, \quad j_D = \frac{N_{Sh}}{Re_P\ N_{Sc}^{1/3}} \qquad (D.9\text{-}12)$$

It should be noted that N_{Sh} numbers were determined from the mean size of the reagent particles, since it is directly related to the mass transfer through the gas film surrounding the reagent particles. However, because $\overline{Re}$ is related to the hydrodynamics of the gas phase, this number has been

calculated from the mean size of the inert particles, which is actually the major solid species in the packed bed.

The correlations used in our estimations are the following ones:

i. Correlation of Gliddon & Cranfield (1970) (Doraiswamy and Sharma, 1984)

k_g coefficients can be estimated from N_{Sh}, which can be obtained from j_D. In its turn, j_D is related to the heat transfer factor j_H by the following equation:

$$j_D = 0.8 j_H , \qquad \text{(D.13)}$$

where

$$j_H = 0.41\, Re_P^{-0,06} \quad (2<Re_p<100) \qquad \text{(D.14)}$$

ii. Correlation of Wakao & Funazkri (1978) (Doraiswamy and Sharma, 1984)

k_g coefficients can be estimated from N_{Sh}, which is calculated from the following semi-empirical correlation:

$$N_{Sh} = 2 + 1.1\, N_{Sc}^{1/3}\, Re_p^{0,6} \quad (3 < Re_p < 10.000) \qquad \text{(D.15)}$$

iii. Correlation of Chu, Kalil and Wetteroth (Chu et al.,1953)

This correlation is valid for both fixed-bed and fluidized-bed reactors and for a wide range of N_{Sc} values (from 0.6 to 1400) and for ε_b values in the range 25-97%. For very small Re_p numbers, the following correlation is suggested:

$$j_D = 5.7\left(\overline{Re}\right)^{-0,78} \qquad (1 < \overline{Re} < 30) \qquad \text{(D.16)}$$

The estimation of j_D allows to estimate N_{Sh} and consequently, k_g.

The results for obtained values of k_g by the three correlations are summarized in Table D.3. It can be observed that the values differ substantially, especially when comparing the first and second methods with the third one. In fact, these differences reflect the great dispersion of data available in the literature, which are even more evident for low Re_p numbers (*Dwivedi and Upadhyay, 1977*).

Table D.3: EMT coefficients estimated by three empirical correlations.

T (K)	*RH (%)*	N_{Sc}	Re_P	$\overline{Re}$	*Glidon & Cranfield*		*Wakao & Funazkri*		*Chu, Kalil & Wetteroth*	
					j_D	k_g ($m\ s^{-1}$)	N_{Sh}	k_g ($m\ s^{-1}$)	j_D	k_g ($m\ s^{-1}$)
313	30	1.1	4.7	6.6	0.47	2.96	5.3	6.79	1.3	0.25
	50	1.1	4.8	6.7	0.47	2.97	5.2	6.74	1.3	0.25
	70	1.1	4.8	6.7	0.47	2.97	5.2	6.69	1.3	0.25
333	30	1.1	4.6	6.5	0.47	3.20	5.1	7.31	1.3	0.28
	50	1.1	4.7	6.6	0.47	3.23	5.0	7.17	1.3	0.28
	70	1.0	4.8	6.8	0.47	3.26	4.9	7.03	1.3	0.29
353	30	1.0	4.6	6.4	0.47	3.46	4.8	7.71	1.3	0.32
	50	0.9	5.1	7.2	0.46	3.66	4.5	7.20	1.2	0.32
	70	0.8	5.5	7.7	0.46	3.76	4.3	6.87	1.2	0.32

APPENDIX F

STATISTIC ANALYSIS

1. **Estimation of confidence intervals for fitted parameters for nonlinear models** (*Himmelblau, 1970*).

The individual confidence interval for each parameter δ_i of a nonlinear model for a significance level α can be estimated by the following equation:

$$\delta_i = d_i \pm t_{1-\alpha/2}\, S_{\overline{Y}_i} C_{ii}^{0.5}; \qquad \text{(F.1)}$$

where d_i is the estimated value of the parameter δ_i, t is the Student-t used in the t-test, $S^2_{\overline{Y}_i}$ is the estimated variance of $\overline{Y}_i$, which is the sample average of observed Y´s at x_i points, and C_{ii} is the value of the diagonal of the matrix C, given by:

$$C = \left(X^T \times X\right)^{-1} \qquad \text{(F.2)}$$

where X is an $(n \times m)$ matrix defined as:

$$[X_{ij}] = \frac{\partial \eta_i(x_i)}{\partial \delta_j} \qquad \text{(F.3)}$$

with

i: experimental point index i: 1,..., n

j: fitting parameter index j: 1,..., m

where $\eta_i(x_i)$ is the nonlinear model evaluated at the x_i point. The application of this method to determine the confidence intervals of the m=3 parameters of the DM-ISCM fitted to the experimental breakthrough curves at 1 hour leads to a (234×3) matrix, where 234 is the number of experimental points of each curve. The function $\eta_i(x_i)$ corresponds to the fitted breakthrough curve. An estimation of the partial derivates to obtain $[X_{ij}]$ has been performed varying ±1% each d_i parameter while the rest are constant. The 1% variations have been found satisfactory as the same results were obtained for variations in the range of ±0.1-5% of each parameter d_i. The value of $t_{1-\alpha/2}$ was taken as 1.96, which corresponds to that of a infinite number of degrees of freedom with a 95% of confidence interval. The variance $S_{\overline{Y}_i}$ was estimated by the following expression:

$$S^2_{\overline{Y}_i} = S_r^2 + S_e^2 \qquad \text{(F.4)}$$

where S_r^2 and S_e^2 are, respectively, the residual and error mean squares, which are defined by the following equations:

$$S_r^2 = \frac{\sum_{i=1}^{n} p_i (\overline{Y_i} - \hat{Y}_i)^2}{n-2} = \frac{SQ}{n-2} \qquad S_e^2 = \frac{\sum_{i=1}^{n} \sum_{j=1}^{p_i} (Y_{i,j} - \overline{Y}_i)^2}{\sum_{i=1}^{n} p_i - n} \qquad \text{(F.5 - 6)}$$

where $Y_{i,j}$ is the j^{th} observation of Y at x_i, $\hat{Y}_i$ is the estimated value at x_i, $\mathbf{p_i}$ is the number of replicate measurements (in case that no replicate values are available, p_i takes the value 1) and **n** is the number of

data points, which is 234 for curves of 1 hour. The variance S_e^2 was estimated using Eq. (F.6) for those experimental conditions where replicates were available (see Table 4.5). An average value of the resulting S_e^2 for each replicate conditions was considered for the rest of experimental conditions.

2. Analysis of residuals

For several experimental conditions, the deviation between the experimental and predicted $C_{SO_2} / C^0_{SO_2}$ values, that is $\left(\overline{Y_i} - \hat{Y_i}\right) \Big/ \overline{Y_i}$, for the models tested vs. time was plotted. Figs. F.1-2 show two examples of the analysis of residuals to compare the results of the DM with those of DM-ISCM. As can be seen, deviations of the DM are larger than those of the DM-ISCM. Furthermore, the distribution of the points with respect to the 0% of deviation is biased in the DM, while most of those of the DM-ISCM are randomly distributed.

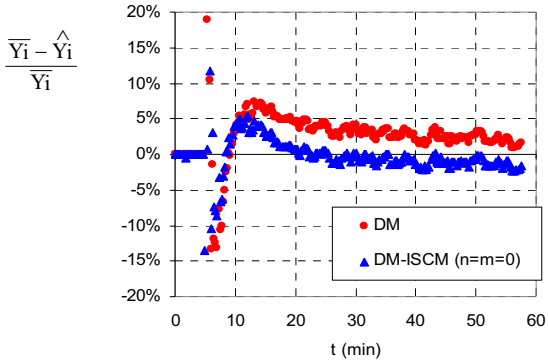

Fig. F.1: Analyses of residuals of data at 2000 ppm of SO_2, 333 K, 30% RH.

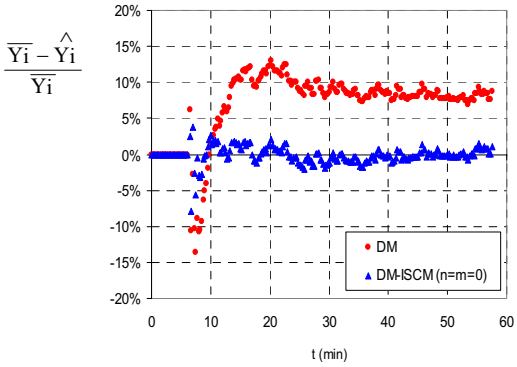

Fig. F.2: Analyses of residuals of data at 5000 ppm of SO_2, 333 K, 70% RH.

In Figs. F.3-4, the analyses of residuals of the DM-ISCM for the different values tested of **n** and **m** (n = 0, 1 and m = 0, 1) for two different experimental conditions is displayed. The results indicate that there are no significant differences between the tested models.

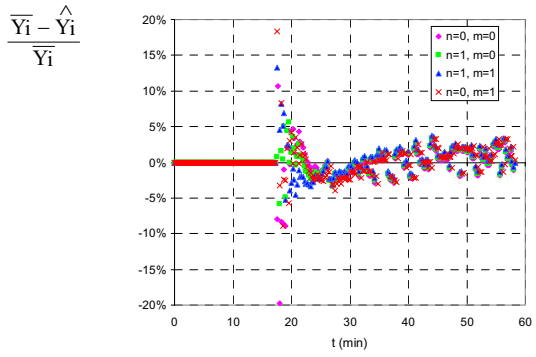

Fig. F.3: Residuals for different combinations of n, m values at 2000 ppm of SO_2, 353 K, 70% of RH.

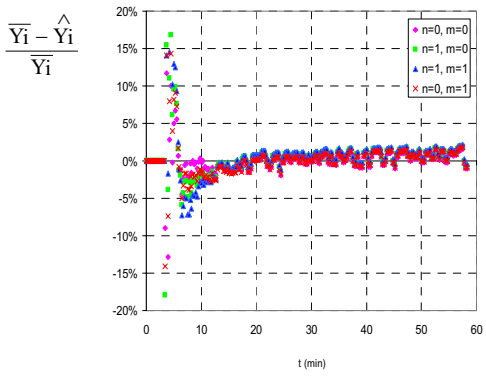

Fig. F.4: Residuals for different combinations of n, m values at 5000 ppm of SO_2, 353 K, 50% of RH.

APPENDIX G

MODELING OF INVERSE SHRINKING CORE MODEL (ISCM)

The flux equations of two ionic species A (cation) and B (anion) that diffuse through a lattice P is given by (see Fig. G.1):

$$\vec{J}_A = -\left[D_A^P \vec{\nabla} C_A^P + z_A D_A^P C_A^P \frac{F}{RT} \vec{\nabla}\phi^P \right] \tag{G.1}$$

$$\vec{J}_B = -\left[D_B^P \vec{\nabla} C_B^P + z_B D_B^P C_B^P \frac{F}{RT} \vec{\nabla}\phi^P \right] \tag{G.2}$$

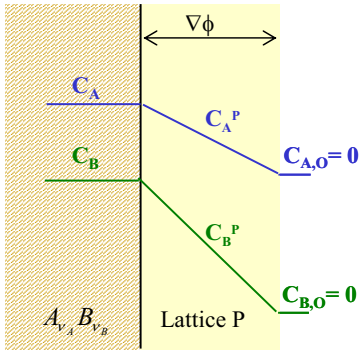

Fig. G.1: Diffusion of A and B species through a lattice P from the lattice $A_{\nu_A} B_{\nu_B}$

The condition of electrical neutrality requires the following relation to be accomplished:

$$z_A \vec{J}_A + z_B \vec{J}_B = 0 \tag{G.3}$$

The substitution of eq. (G.1) and (G.2) for each species to eq. (G.3) and rearranging yields:

$$\vec{\nabla}\phi^P = -\frac{RT}{F}\left[\frac{z_A D_A \vec{\nabla} C_A^P + z_B D_B \vec{\nabla} C_B^P}{z_A^2 D_A C_A^P + z_B^2 D_B C_B^P} \right] \tag{G.4}$$

According to the stoichiometry of the solid reagent, the following expression should be accomplished:

$$\frac{1}{\nu_A}\vec{\nabla} C_A^P = \frac{1}{\nu_B}\vec{\nabla} C_B^P \tag{G.5}$$

The substitution of eq. (G.5) to eq. (G.4) leads to the following equation:

$$\vec{\nabla}\phi^P = -\frac{RT}{F}\left[\frac{z_A D_A + z_B \frac{\nu_B}{\nu_A} D_B}{z_A^2 D_A C_A^P + z_B^2 D_B C_B^P} \right] \vec{\nabla} C_A^P \tag{G.6}$$

Substituting eq. (G.6) to eq. (G.1), and taking into account the following relation:

$$z_A \nu_A = -z_B \nu_B \tag{G.7}$$

and further rearranging, it is found that the driving force of the ionic flux of each species is proportional to the concentration gradient, as follows:

$$\vec{J}_A = -\bar{D}_A^P \vec{\nabla} C_A^P \tag{G.8}$$

$$\vec{J}_B = -\bar{D}_B^P \vec{\nabla} C_B^P \tag{G.9}$$

where

$$\bar{D}_A^P = \bar{D}_B^P = \frac{\left(z_A^2 x_A + z_B^2 x_B\right) D_A^P D_B^P}{z_A^2 x_A D_A^P + z_B^2 x_B D_B^P} \tag{G.10}$$

For $Ca(OH)_2$, eq. (G.10) is transformed into:

$$\bar{D}_{Ca}^P = \bar{D}_{OH}^P = \frac{\left(4x_{Ca} + x_{OH}\right) D_{Ca}^P D_{OH}^P}{4x_{Ca} D_{Ca}^P + x_{OH} D_{OH}^P} \tag{G.11}$$

For spherical particles of radius R, the flux of each species, for instance A, is given by:

$$\vec{J}_A = -\frac{dn_A}{dt}\frac{1}{4\pi r^2} \quad \left[\text{mol m}^{-2}\ \text{s}^{-1}\right] \tag{G.12}$$

where r is the radius of any spherical surface and n_A the amount of A in the lattice P (see Fig. G.2)

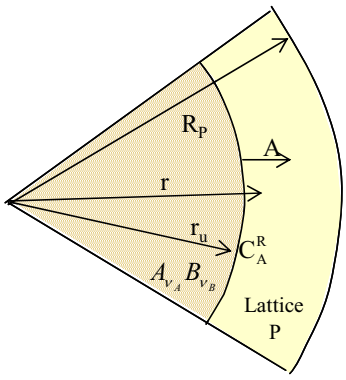

Fig. G.2: Diffusion of A species through a lattice P from the lattice $A_{\nu_A} B_{\nu_B}$

Equaling eq. (G.8) with eq. (G.12), assuming that the concentration of A is null at radius R_P and rearranging, the following expression is obtained:

$$\frac{dn_A}{dt} = \frac{4\pi \overline{D}_i^P C_A^R}{\left(\frac{1}{r_u} - \frac{1}{R_P}\right)} \tag{G.13}$$

where C_A^R is the concentration of A in the lattice $A_{\nu_A} B_{\nu_B}$ and r_u corresponds to its radius.

Taking into account that the lattice $A_{\nu_A} B_{\nu_B}$ are spherical particles of solid reagent which react to give a product P (lattice P) by the outward diffusion of the ions A and B through it, the solid conversion can be related to r_u by the following expression:

$$1 - X_S = \frac{\frac{4}{3}\pi r_u^3}{\frac{4}{3}\pi R_P^3} \tag{G.14}$$

Substituting eq. (G.14) to eq. (G.13) and rearranging yields:

$$\frac{dn_A}{dt} = \frac{4\pi \overline{D}_i^P C_A^R R_P}{(1 - X_S)^{-1/3} - 1} \tag{G.15}$$

Finally,

$$J_A = \frac{1}{\frac{4}{3}\pi R_P^3 \rho_S} \frac{4\pi \overline{D}_i^P C_A^R R_P}{(1 - X_S)^{-1/3} - 1} = \frac{3}{R_P^2 \rho_S} \frac{\overline{D}_i^P C_A^R}{(1 - X_S)^{-1/3} - 1} \quad \left[\text{mol g}^{-1}\ \text{s}^{-1}\right] \tag{G.16}$$

10. Abstract in Catalan language

1. INTRODUCCIÓ

1.1. GASOS ÀCIDS: CONTAMINANTS ATMOSFÈRICS

En les últimes dècades, la contínua i creixent demanda de qualitat de vida, juntament amb un progressiu i sostingut increment de la població mundial, ha generat un fort creixement de l'activitat industrial i del transport. Aquesta situació ha originat una emissió massiva de contaminants a l'atmosfera, alterant-ne la seva composició i causant així efectes nocius en el medi ambient i en la salut humana.

Malgrat l'existència de referències des del segle XIV que constaten la preocupació per l'efecte de les activitats humanes sobre la salut, no va ésser fins del segle XX, i amb molta més força fins als anys 70-90, que els dirigents europeus i nord-americans es van ocupar seriosament dels seus efectes globals sobre el medi ambient. Tradicionalment, tant la legislació nord-americana com l'europea s'han centrat en la contaminació causada per la pluja àcida i per l'anomenat smog fotoquímic. La pluja àcida pot originar-se a partir de l'emissió directa de gasos àcids forts, com el HCl, però la major part és produïda indirectament per l'emissió d'altres gasos com el SO_2 i el NO_2 –els quals poden oxidar-se i formar, respectivament, H_2SO_4 i HNO_3 en presència d'aigua. El H_2SO_4 constitueix la principal contribució a la pluja àcida, essent el HNO_3 i el HCl contaminants secundaris a causa de la seva menor presència a l'atmosfera. D'altra banda, el smog fotoquímic es troba constituït per una mescla de centenars de compostos potencialment perillosos i la seva formació es troba determinada per la presència de NO_x, VOCs i radiació solar (Vesilind et al. 1988; Manahan, 1994).

El SO_2 i el HCl atmosfèrics s'originen bàsicament a partir de la combustió de materials sòlids que contenen sofre o clor, respectivament. En aquest sentit, la principal font d'emissió del SO_2 són les centrals tèrmiques de combustió de carbó –el petroli també pot contenir sofre-, però també se'n pot generar a partir d'altres processos com el refinat del petroli i les plantes incineradores. El HCl també es pot emetre en centrals tèrmiques de combustió de combustibles fòssils, però la seva font principal són les incineradores, tant de residus urbans com d'industrials o perillosos. Finalment, el NO_2 es pot emetre directament mitjançant fonts estacionàries i mòbils, però bona part del NO_2 present a l'atmosfera prové de l'oxidació fotoquímica del NO amb ozó (O_3). El NO_2 emès directament a l'atmosfera prové bàsicament de l'oxidació del N_2 que acompanya l'aire en les combustions, encara que una petita fracció també pot originar-se en la combustió de combustibles que contenen nitrogen. En general, les combustions produeixen una mescla de NO i NO_2, coneguda com NO_x, amb una composició típica de 90-95% NO i 10-5% NO_2.

1.2. MÈTODES POST-COMBUSTIÓ PER AL CONTROL D'EMISSIONS DE GASOS ÀCIDS

Una de les alternatives més utilitzades per a reduir les emissions de gasos àcids generats en fonts estacionàries són les tecnologies de control post-combustió, que es basen en retenir els contaminants un cop ja formats i retirats dels forns de combustió mitjançant l'ús de columnes de rentat *(scrubbers)*.

Aquests mètodes es van desenvolupar inicialment per a desulfurar els gasos emesos en centrals tèrmiques –anomenats genèricament processos *Flue Gas Desulfurization* (FGD)-, que actualment s'han extès a d'altres aplicacions, per exemple els incineradors, per a retenir diferents tipus de gasos contaminants com el HCl. Contràriament com succeeix amb el NO_2, el NO no pot ésser eficientment retingut mitjançant aquestes tecnologies, almenys en les seves formes més bàsiques, la qual cosa implica que aquestes no es puguin considerar eficients per al control d'emissions de NO_x *(Brown, 1998)*.

En línies generals, les tecnologies post-combustió consisteixen en l'addició de sòlids alcalins en el corrent gasós per a neutralitzar els seus components gasosos àcids. Aquest procés genera productes sòlids (sulfits, sulfats i clorurs) amb un potencial contaminant molt menor que l'associada als seus precursors gasosos. Els sòlids utilitzats amb més freqüència són el $CaCO_3$ i $Ca(OH)_2$, el primer dels quals presenta un cost menor que el segon, però, en contrapartida, és menys reactiu.

En moltes d'aquestes tecnologies s'afegeix aigua de diferents formes en el procés, ja que la reacció de neutralització dels gasos àcids s'afavoreix en la seva presència. Depenent de la quantitat d'aigua i forma que s'introdueixi en el procés i del punt d'inserció del sòlid adsorbent en les centrals tèrmiques, les tecnologies es poden classificar de la següent forma (veure Fig. 1.2 [(1)] de la memòria) *(Golesworthy, 1999)*:

- mètodes humits
- mètodes secs, que es poden dividir en:
  - Injecció al forn
  - *Spray dry scrubbing*
  - Injecció d'adsorbent sec

En termes generals, els mètodes humits són els mes utilitzats en centrals tèrmiques de gran capacitat, a causa principalment de la seva major eficiència en la retenció dels contaminants. Tanmateix, aquests processos també són els més costosos, presenten gran complexitat d'operació i generen grans quantitats de residus en forma de pasta que cal estabilitzar abans d'ésser dipositats en abocadors [(2)]. Entre els mètodes secs, el *spray dry scrubber* és el més extès perquè és força eficient, però en contrapartida també opera amb pastes *(slurries)*, fet que dificulta la seva manipulació tant en la fase d'operació com en la de tractament i deposició dels residus (*Vesilind, 1988; Buonicore and Davis, 1992; De Nevers, 1992; Brown, 1998; Golesworthy, 1999*).

De la resta de tecnologies seques, les tecnologies d'injecció de sòlid en els conductes -in-duct sorbent injection with humidification-, que es basen en introduir les partícules d'adsorbent i l'aigua en forma d'esprai directament als conductes de sortida dels corrents de gasos, semblen una opció

[(1)] Totes les figures, taules i equacions referenciades en aquest resum es refereixen a la memòria.

[(2)] A la Taula 1.2 de la memòria es recopilen les dades més destacables de cadascuna de les tecnologies post-combustió indicades.

tecnològica força atractiva, ja que són processos molt simples, requereixen poc espai, presenten baixos costos d'inversió i d'operació i generen residus sòlids pràcticament secs (veure Fig. 1.3 de la memòria). Aquesta tecnologia presenta eficiències elevades en la retenció de gasos en plantes incineradores -90% i 50% per al HCl i SO_2, respectivament. Altrament, la seva aplicació en centrals tèrmiques de combustió de carbó és molt limitada, ja que els nivells de retenció de SO_2 són menors que els dels mètodes anteriorment mencionats –en general, s'assoleixen retencions del 40-80%- i presenten baixes conversions dels sòlids adsorbents -menors al 35%- (*Muzio and Offen, 1987; Chu and Rochelle, 1989; Golesworthy, 1999*).

En els darrers anys s'ha dut a terme una recerca intensiva a escala de laboratori i de planta pilot per a la determinació de l'efecte de les diferents variables de procés en els processos "in-duct" -temperatura, humitat relativa, àrea superficial del sòlid adsorbent i relació calci/sofre- sobre la capacitat dels sòlids per a retenir SO_2. En canvi, s'han publicat pocs estudis centrats en la cinètica i mecanismes de reacció que intervenen en aquests processos. La manca d'estudis de les reaccions implicades és més acusada en aquelles parts dels processos on l'aigua intervé en forma vapor, com és en els col·lectors de partícules de les centrals tèrmiques –normalment filtres de mànigues- i en els conductes on les temperatures són suficientment elevades per a què l'aigua es trobi en forma vapor.

1.3. REACTIVITAT QUÍMICA DELS SISTMES SO_2, NO_2 i HCl + $Ca(OH)_2$

1.3.1. Reactivitat química del sistema SO_2 + $Ca(OH)_2$.

La reacció química que té lloc entre el SO_2 i el $Ca(OH)_2$ en presència de vapor d'aigua a temperatures baixes -333-413 K, pròpies dels col·lectors de partícules- és la següent (*Manahan,1994*):

$$Ca(OH)_2 + SO_2 \xrightarrow{H_2O(vap)} CaSO_3 \cdot (1/2)H_2O + (1/2)H_2O, \qquad (1.1)$$

essent una part del sulfit de calci oxidat a sulfat. Un gran nombre d'estudis previs han posat de manifest que la humitat relativa (RH) és la variable més influent del procés a temperatures baixes (veure Taula 1.2 de la memòria). Aquest efecte suggereix que l'aigua adsorbida a la superfície dels sòlids adsorbents juga un paper determinant en la cinètica de la reacció, però encara avui dia aquest paper no ha estat desentrellat.

En comparació a la RH, la temperatura i la concentració no tenen un paper tan rellevant en la reacció i es presenten contradiccions en relació als resultats de diferents investigadors. D'una banda, mentre *Rochelle i Jozewicz (1990)* i *Krammer et al. (1997)* no troben un efecte significatiu de la temperatura en la velocitat de reacció, *Jorgensen et al. (1987), Ruiz-Alsop i Rochelle (1987), Aichinger et al. (1995)* i *Ho et al. (2002)* indiquen una lleugera o moderada influència de la temperatura en la conversió del sòlid (veure Taula 1.4). Respecte a la concentració de SO_2, la majoria dels estudis indiquen que aquesta variable no afecta a la conversió del sòlid ni a la velocitat de reacció a temps llargs (més d'una hora de reacció). No obstant, els resultats de *Ruiz-Alsop i Rochelle (1987)* semblen revelar que aquesta hi presenta un efecte en funció del valors de RH i de la concentració de SO_2. Tanmateix, els investigadors *Krammer et al. (1997)* troben que és funció de la conversió de sòlid, de tal forma que la

reacció solament depèn de la concentració de SO_2 a baixes conversions de sòlid, però no a d'altes ni a conversió zero (veure Taula 1.5).

1.3.2. Reactivitat química del sistema NO_2 +(SO_2) + $Ca(OH)_2$.

La reacció química entre el NO_2 i sòlids alcalins de calci en presència de vapor d'aigua està molt poc referida a la literatura, però en canvi sí que aquesta és més extensa per a les reaccions que es produeixen en fase aquosa. Segons *Schriver et al. (1994)*, el NO_2 dismuta en absorbir-se en aigua (reacció 1.9), i, en cas que el medi sigui àcid, els ions nitrit poden dismutar altre cop i formar ions nitrat i molècules de NO gasós segons la reacció (1.10):

$$2NO_{2(aq)} + 2OH^-_{(aq)} \leftrightarrow NO^-_{2(aq)} + NO^-_{3(aq)} + H_2O_{(l)} \quad (1.9)$$

$$3NO^-_{2(aq)} + 2H^+_{(aq)} \rightarrow NO^-_{3(aq)} + 2NO_{(g)} + H_2O_{(l)} \quad (1.10)$$

En els sistemes en que el NO_2 i el SO_2 coexisteixen en fase gasosa s'ha suggerit que es produeix una reacció redox entre el NO_2 gasós i els ions sulfit presents en la fase aquosa resultants de la retenció de SO_2 d'acord amb la reacció (1.11):

$$2NO_{2(g)} + SO^{2-}_{3(aq)} + H_2O_{(l)} \leftrightarrow 2NO^-_{2(aq)} + SO^{2-}_{4(aq)} + 2H^+_{(aq)} \quad (1.11)$$

Els estudis realitzats per *Nelli i Rochelle (1998)* a escala de laboratori sobre la reactivitat d'aquest sistema en presència de vapor d'aigua amb adsorbents alcalins de calci suggereixen que, a una RH > 50%, la quantitat d'aigua que cobreix la superfície és suficient per absorbir NO_2 i SO_2, i que les reaccions que es produeixen són anàlogues a les proposades en fase aquosa.

O'Dowd et al. (1994) i *Nelli i Rochelle (1998)* van analitzar, respectivament, els sòlids reaccionats a escala de planta pilot i de laboratori, però els seus resultats revelen certes discrepàncies. En aquest sentit, mentre que *O'Dowd et al. (1994)* van trobar que els ions nitrit són les espècies predominants tant en presència com en absència de SO_2, *Nelli i Rochelle (1998)* solament van detectar la presència d'ions nitrat. Aquests últims expliquen els seus resultats suposant la formació d'una capa de producte impermeable sobre els sòlid reaccionat, de forma que la superfície s'acidificaria per la retenció del SO_2 i com a conseqüència s'eliminarien els ions nitrit del medi mitjançant la reacció (1.10). En resum, sembla necessari continuar estudiant el sistema NO_2 + SO_2 amb $Ca(OH)_2$ per intentar clarificar-ne els camins de reacció que s'hi poden presentar.

1.3.3. Reactivitat química del sistema HCl + $Ca(OH)_2$.

Millikan (1918) va suggerir que la reacció global entre el HCl i el $Ca(OH)_2$ en fase aquosa és la següent:

$$Ca(OH)_2 + 2HCl \longrightarrow CaCl_2 + 2H_2O \qquad (1.15)$$

Els estudis posteriors referits a la retenció de HCl mitjançant tecnologies seques *(Karlsson et al., 1981; Weinell et al., 1992; Fonseca et al., 1998)*, a baixes i altes temperatures assumeixen que té lloc la reacció (1.15), de forma que el $CaCl_2$ és el producte de la reacció. No obstant, pocs estudis s'han centrat en la identificació dels productes de la reacció i en els possibles camins de reacció. *Karlsson et al. (1981), Weinell et al. (1992)*, *Fonseca et al. (1998) i Chisholm i Rochelle (1999)* van trobar relacions finals de Cl/Ca entre 1 i 2 operant a temperatures entre 323 i 493 K en presència de vapor d'aigua. Aquest resultat és coherent amb la reacció (1.15) i indica que almenys una part del producte pot ésser efectivament $CaCl_2$.

A altes temperatures (583-943 K), *Daoudi i Walters (1991)* van realitzar anàlisis dels sòlids reaccionats i van detectar $CaCl_2$ com a únic producte de reacció. També van verificar que la màxima variació de massa del sòlid després de reaccionar corresponia a la total transformació del reactant en $CaCl_2$. Posteriorment, *Jozewicz i Gullet (1995)* van detectar la presència no solament de $CaCl_2 \cdot 2H_2O$ sinó també de Ca(OH)Cl a l'analitzar els sòlids que havien estat en contacte amb el HCl durant 1 minut a 773 K i en condicions seques. No obstant, únicament van observar la presència de l'espècie Ca(OH)Cl a 473 K, en coherència amb els resultats d'*Allal et al. (1998)* per a temps de residència de 0.5 s a 523 K i en condicions seques.

La comparació entre l'estequiometria del Ca(OH)Cl i del $CaCl_2$ indica que ambdós compostos provenen a partir, respectivament, de la substitució d'un o dos grups hidroxil del $Ca(OH)_2$ per àtoms de Cl. Aquest fet suggereix que la reacció (1.15) pot tenir lloc a través de l'intermedi Ca(OH)Cl, tal com van proposar *Jozewicz and Gullet (1995)*:

$$Ca(OH)_2 + HCl \longleftrightarrow Ca(OH)Cl + H_2O \qquad (1.16)$$

$$Ca(OH)Cl + HCl \longleftrightarrow CaCl_2 + H_2O\,, \qquad (1.17)$$

A partir de les consideracions ressaltades, l'estequiometria de la reacció entre el HCl i el $Ca(OH)_2$ sembla que encara no estigui del tot aclarida, malgrat ésser essencial per a la determinació de la capacitat màxima de retenció de HCl pel sòlid adsorbent. A més, el producte de reacció també condiciona la capacitat de retenció d'aigua dins dels conductes de les centrals tèrmiques i la seva estabilitat química a l'hora d'ésser dipositats en abocadors.

2. RESULTATS

2.1. REACTIVITAT DELS SISTEMES SO_2 (+NO_2)/HCl + $Ca(OH)_2$

2.1.1. Reactivitat del sistema SO_2 + $Ca(OH)_2$.

En aquest apartat s'ha estudiat l'efecte de la RH, temperatura i concentració de SO_2 -en els rangs 0-70%, 313-353 K i 2000-8000 ppm de SO_2, respectivament- sobre la capacitat del $Ca(OH)_2$ per a retenir SO_2 durant 1 hora de reacció. Per dur a terme aquest estudi s'han emprat partícules comercials de $Ca(OH)_2$ d'una mida mitjana de 9.4 μm [(3)]. Els resultats obtinguts a partir de l'anàlisi de corbes de ruptura de SO_2 mostren un fort efecte de la RH, amb tendències exponencials a temperatures de 313-333 K i lineals a 353 K. En canvi, la influència de la temperatura i la concentració de SO_2 és molt menor que la de la RH, essent en molts casos pràcticament negligible en ambdós casos. També s'ha observat que les conversions de sòlid després d'1 hora de reacció són menors del 30% en totes les condicions assajades. Tots aquest resultats semblen confirmar les conclusions a què s'ha arribat en diferents estudis previs (*Damle et al. 1986, Jorgensen et al., 1987, Ruiz-Alsop and Rochelle, 1987, Aichinger et al. 1995, Karatepe et al. 1999, Garea et al., 2000).*

A més, també s'han dut a terme alguns experiments a temps llargs -4 i 6 hores a 50% i 70%, respectivament-, els resultats dels quals semblen indicar que la reacció no s'atura després d'una hora, sinó que es continua al llarg de tot el període de temps estudiat. Aquesta etapa es caracteritzaria per presentar una velocitat de reacció molt baixa i seria potenciada per la RH.

2.1.2. Reactivitat del sistema NO_2 + SO_2 + $Ca(OH)_2$.

Els resultats obtinguts a partir de corbes de ruptura experimentals manifesten que la presència de NO_2 (75-250 ppm) incrementa sensiblement la capacitat del $Ca(OH)_2$ per a retenir SO_2, amb un augment de la retenció de fins el 200% després de 2-3 h de reacció. Aquesta increment de la reactivitat sembla trobar-se potenciat per la concentració de NO_2 fins a 175 ppm, però a majors concentracions no se n'observen augments significatius. D'altra banda, també s'ha observat que la presència de NO_2 sembla accentuar l'efecte positiu de la RH en la retenció de SO_2 i incrementar sensiblement la velocitat de reacció a l'etapa corresponent a temps llargs.

Per tal d'intentar clarificar els camins de reacció que tenen lloc quan ambdós gasos coexisteixen en la fase gasosa s'han realitzat diverses anàlisis dels sòlids reaccionats. Les anàlisis de DRX (difracció de raigs X) mostren la presència d'una senyal principal de $CaSO_3 \cdot (1/2)H_2O$ i d'altres molt menors, però

(3) A la Taula 4.1 de la memòria es poden trobar les dades més rellevants sobre les característiques del sòlid emprat.

apreciables, corresponents a sulfat de calci (veure Fig. 4.16). La presència d'ions sulfat podria explicar-se a partir d'una reacció redox (4.1), que seria anàloga a la que ocorre en fase aquosa (reacció 1.11):

$$2NO_{2(g)} + CaSO_{3(s)} + Ca(OH)_{2(s)} \leftrightarrow Ca(NO_2)_{2(s)} + CaSO_{4(s)} + H_2O_{(ads)} \qquad (4.1)$$

Aquesta reacció, que en un principi caldria pensar que es trobi desafavorida cinèticament, ja que implica la reacció entre dos sòlids, podria produir-se a causa de la presència de nitrit i nitrat de calci. Ja que aquestes espècies són molt higroscòpiques, aquestes podrien potenciar la formació d'una capa d'aigua adsorbida a la superfície del sòlid, de tal manera que els ions implicats (HO^-, SO_3^{2-} i Ca^{2+}) hi podrien reaccionar molt més lliurement.

D'altra banda, les anàlisis d'ions nitrit i nitrat en els sòlids reaccionats (veure Fig. 4.17), tant en experiments en què es presentaven ambdós gasos com en d'altres on s'hi presentava únicament NO_2, indiquen que la relació nitrat/nitrit és major que 1 pràcticament per a tots els casos. La presència d'ions nitrat sembla ésser incoherent amb la reacció (4.1), a més que aquesta reacció sigui òbviament inconsistent amb el sistema que únicament conté NO_2. Aquests fets donen lloc a proposar la reacció (4.2), anàloga a la reacció (1.9) per a solucions aquoses, que podria tenir lloc tant en absència com en presència de SO_2:

$$4NO_{2(g)} + 2Ca(OH)_{2(s)} \leftrightarrow Ca(NO_2)_{2(s)} + Ca(NO_3)_{2(s)} + 2H_2O \qquad (4.2)$$

La major presència d'ions nitrat respecte a ions nitrit podria explicar-se a partir de la reacció (4.3), que seria anàloga a la reacció (1.10) en fase aquosa:

$$3Ca(NO_2)_{2(s)} + 2H_2O_{(ads)} \leftrightarrow Ca(NO_3)_{2(s)} + 4NO_{(g)} + 2Ca(OH)_{2(s)} \qquad (4.3)$$

En aquest sentit, l'aigua adsorbida podria retirar els ions nitrit formats d'acord amb les reaccions (4.1) i (4.2). Altre cop, aquesta reacció podria explicar-se mitjançant la formació d'espècies higroscòpiques. Aquesta reacció és consistent amb l'observació experimental que la relació nitrat/nitrit tendeix a créixer amb la RH (veure Fig. 4.17).

Finalment, es podria proposar que la reacció (4.1) justifica l'increment de la capacitat del sòlid per a retenir SO_2 quan el NO_2 es troba present al sistema. No obstant, les dades experimentals no semblen ésser coherents amb aquesta hipòtesi. Una altra explicació més factible podria considerar altre cop la formació de $Ca(NO_3)_2$ i $Ca(NO_2)_2$ a la superfície sòlid, de tal manera que la seva presència tindria un efecte similar a un augment de la RH de la fase gasosa. Amb l'objectiu de validar aquesta hipòtesi s'ha realitzat un experiment utilitzant $Ca(NO_3)_2$ com a additiu sòlid i sense alimentar el reactor amb NO_2. Els resultats semblen suggerir que, efectivament, la presència d'additius higroscòpics millora enormement les retencions de SO_2, els quals són coherents amb les isotermes d'adsorció d'aigua sobre partícules de $CaCO_3$ que contenen certes quantitats de $Ca(NO_3)_2$ obtingudes per *Goodman et al.(2000)*.

2.1.3. Reactivitat del sistema HCl + $Ca(OH)_2$.

L'anàlisi de DRX realitzada sobre una mostra acabada de reaccionar a 393 K i 18% de RH mostra la presència de Ca(OH)Cl com a únic producte de reacció. La presència d'aquest compost ja havia estat identificada prèviament a altes temperatures (523-773 K), però en canvi, sembla contradir els resultats d'altres estudis a temperatures més baixes que troben relacions Cl/Ca majors d'1. D'altra banda, les anàlisis d'EDS de Cl i Ca realitzats en monocristalls reaccionats mostren la presència de regions del cristall amb relacions Cl/Ca majors d'1.

L'aparent discrepància entre els diferents resultats referits als productes de reacció es pot resoldre considerant que tenen lloc les reaccions (1.16) i (1.17), és a dir una primera etapa en què el $Ca(OH)_2$ reacciona amb HCl per a formar Ca(OH)Cl, i una segona etapa on aquest darrer reacciona amb HCl per formar $CaCl_2$. No obstant, per tal de que aquest camí de reacció sigui consistent amb tots els resultats experimentals obtinguts –tant en el present treball com per part d'altres investigadors- cal proposar la restricció que la reacció (1.16) solament ocorre sempre i quan el $Ca(OH)_2$ no estigui disponible, bé localment o bé en tota la partícula. Aquesta situació es donaria preferencialment en les següents situacions: (1) reaccions a temps llargs; (2) presència de velocitats de reacció elevades –altes temperatures o concentracions de HCl elevades.

Finalment també cal destacar que s'ha realitzat un estudi per avaluar la capacitat del sòlid per retenir aigua a mesura que aquest va reaccionant. Aquesta mesura pot tenir implicacions tant en l'operativa dels processos com en la deposició dels residus sòlids en abocadors. En aquest sentit, s'ha obtingut que aproximadament es retenen 1.2 mols d'aigua per cada mol de clor retingut en les condicions en què es forma únicament Ca(OH)Cl. Aquest resultat indica que aquest compost és higroscòpic, però en molt menor grau que el $CaCl_2$. També s'ha trobat que de la quantitat d'aigua retinguda, pràcticament la meitat s'elimina amb facilitat –en concret, a 393 K en sec.

2.2. MODEL CINETIC DEL SISTEMA SO_2 (+NO_2) + $Ca(OH)_2$

En aquest apartat s'ha procedit a la determinació d'un model cinètic que expliqui les dades experimentals obtingudes. La seva determinació inclou les següents etapes:

1. *Proposta d'un model cinètic*

2. *Modelització del reactor*: Introducció del model cinètic proposat en els balanços microscòpics de matèria dels reactants en el reactor de llit fix i posterior integració a través de tot el llit i de tot el temps de reacció, de forma que s'obtiguin corbes de ruptura simulades.

3. *Ajust del model*: Ajust de les corbes de ruptura simulades a les experimentals mitjançant un mètode d'optimització dels paràmetres basat en l'algoritme Levenberg-Marquardt.

Per a la modelització del llit, en primer lloc s'han aplicat alguns criteris descrits en la literatura per a assegurar que el model de flux correspongui al de flux en pistó. Respecte al model cinètic, s'ha

comprovat que les etapes de transferència externa de matèria (EMT) i interna (IMT) no contribueixen significativament a la cinètica de la reacció.

La determinació del model cinètic ha consistit en dues etapes: (1) assaig de diferents models, la major part dels quals havien estat aplicats prèviament per altres investigadors; (2) proposta d'un model cinètic basat en el que millor s'ajusta dels anteriors. Els models cinètics que s'han assajat han estat: model de nucli sense reaccionar (SCM); SCM amb dues correlacions empíriques, una de les quals considera una reducció del coeficient de difusió amb la conversió del sòlid, i l'altre proposa una reducció de la rugositat de la superfície a mesura que la reacció progressa; model d'adsorció que considera una superfície heterogènia; model de nucleació i creixement d'Avrami; i model de desactivació (DM).

Les corbes de ruptura simulades amb els diferents models assajats no s'ajusten satisfactòriament a les experimentals en tot el tram estudiat. No obstant, el model DM prediu correctament el primer tram de les corbes, malgrat que subestima les velocitats de reacció a temps llargs corresponents al període de baixes velocitats descrit prèviament (veure Fig. 4.28).

El model DM assumeix que la reacció depèn de la concentració de molècules de gas a la superfície del sòlid i de la superfície activa d'aquest darrer (a_S). A mesura que la reacció avança, el producte sòlid s'aniria dipositant sobre la superfície del sòlid reactant, de manera que es reduiria la superfície activa d'aquest darrer, és a dir la seva superfície es *desactivaria*. Simultàniament a la desactivació de la superfície i a la formació d'una capa de producte, la reacció podria continuar, però essent controlada per un procés difusiu. Alguns resultats experimentals semblen suggerir la possibilitat d'un procés de difusió en estat sòlid d'ions Ca^{2+} i HO^- des de la interfase $Ca(OH)_2/CaSO_3{\cdot}(1/2)H_2O$ fins a la superfície, el qual seria més probable que la difusió de molècules de SO_2 cap a l'interior de la partícula no reaccionada. Certament, la difusió en estat sòlid és molt lenta i s'afavoreix a temperatures molt altes. No obstant, és factible suposar que la presència d'aigua adsorbida en la partícula pugui afavorir la difusió iònica a les temperatures de treball (313-353 K), especialment en els seus límits de gra o *grain boundaries*, hipòtesi que seria coherent amb l'efecte observat que l'etapa de reacció que s'assoleix a temps llargs és funció de la RH.

La difusió iònica s'ha modelat mitjançant l'equació de Nernst-Planck (*Philibert, 1991*). S'ha assumit que la capa de producte és pràcticament contínua, que l'agregació de partícules és negligible, que aquestes són esfèriques i que la concentració d'ions Ca^{2+} i HO^- lliures per difondre correspon a la seva concentració en la xarxa cristal·lina. S'obté finalment una equació per descriure aquest procés formalment anàloga a la del SCM per la difusió d'un gas reactant cap a l'interior de les partícules, amb la diferència que l'expressió obtinguda depèn de la concentració d'ions dins la xarxa en lloc de la concentració de SO_2. El model definitiu que considera el model DM i la difusió en estat sòlid d'ions (ISCM-DM) correspon a l'equacio (4.35).

$$r_S = \Phi\, k_S\, C_g^n\, a_S + \Psi\, \overline{D}^P_{Ca^{2+}} \left[\frac{1}{\left(1-X_S\right)^{-1/3} - 1} \right], \qquad (4.35)$$

on $\Phi = \dfrac{\varepsilon_b}{\rho_S \left(1-\varepsilon_b\right)}$ i $\Psi = \dfrac{3}{R_P^2 \rho_S} C^R_{Ca}$.

Els paràmetres ajustables del model són k_S (constant cinètica del DM), β (constant de desactivació) i $\overline{D}^{P}_{Ca}$ (coeficient de difusió d'estat sòlid dels ions Ca^{2+}).

Com es pot veure a les Figs. 4.30, els ajustos de les corbes simulades a les experimentals són excel·lents. Per tant, es pot concloure que el model DM-ISCM prediu satisfactòriament les dades cinètiques per a totes les condicions experimentals assajades, tant en presència com en absència de NO_2. Els paràmetres del model ajustats depenen fortament de la RH. Les dependències amb la RH són les següents:

- k_S augmenta amb la RH. Aquest paràmetre inclou tres contribucions d'acord amb la següent expressió:

$$k_S = k_T(T)\left[K_C(T)\left(f\left(p_{H_2O}, T\right)\right)^z\right]^n \qquad (4.39)$$

  on $k_T(T)$ correspon a la constant cinètica intrínseca de la reacció del complex $SO_2 \cdot zH_2O$ adsorbit a la superfície del sòlid reactant i el $Ca(OH)_2$, K_C és la constant d'equilibri de formació del complex $SO_2 \cdot zH_2O$, i $f\left(p_{H_2O}, T\right)$ és la isoterma d'adsorció de l'aigua en $Ca(OH)_2$.

- β disminueix amb la RH. Aquesta disminució estaria relacionada amb la forma en que el sòlid es diposita sobre la superfície del reactant.

- $\overline{D}^{P}_{Ca}$ augmenta amb la RH, la qual cosa és coherent amb la hipòtesi formulada prèviament referida a l'efecte de l'aigua adsorbida sobre la difusió iònica a través dels límits de gra del reactant.

2.3. ESTUDI MITJANÇANT MICROSCÒPIA DE FORÇA ATÒMICA (AFM) DE LA REACCIÓ DE DESULFURACIÓ: EFECTE DEL VAPOR D'AIGUA SOBRE LA MORFOLOGIA DE LA SUPERFÍCIE REACCIONADA

En les reaccions heterogènies on hi ha cristalls implicats, la superfície d'aquests normalment juga un paper molt important en l'avanç de les reaccions. La visualització de les superfícies reaccionades requereix l'ús de tècniques de microscòpia d'elevada resolució. Algunes proves preliminars van mostrar que la microscòpia de força atòmica (AFM) és una tècnica adequada per a l'estudi de la reacció entre el $Ca(OH)_2$ i el SO_2. Els monocristalls de $Ca(OH)_2$ emprats en aquest estudi es van preparar al laboratori.

Les imatges de superfícies reaccionades amb SO_2 obtingudes mitjançant la tècnica AFM mostren la formació d'estructures de $CaSO_3 \cdot (1/2)H_2O$ en forma d'agulla. La dimensió d'aquestes estructures, i per tant la rugositat de la superfície (Rms), augmenta amb la RH a les quals s'ha produït la reacció. Una representació de Rms amb la RH mostra una relació pràcticament exponencial de la rugositat mitja dels cristalls reaccionats amb la RH, que coincideix amb la tendència trobada de la capacitat del sòlid per retenir SO_2 amb la RH emprant $Ca(OH)_2$ comercial (apartat 2.1.1 del resum). Aquest fet sembla indicar que tot el producte generat a la superfície del reactant no es diposita de forma contínua, tal com s'havia suposat tradicionalment. D'altra banda, en certes ocasions, les imatges de regions diferents d'una mateix monocristall reaccionat mostren importants variacions de Rms, la qual cosa sembla reflectir que la

morfologia inicial de la superfície no reaccionada sigui probablement determinant en la seva reactivitat. Aquest resultat seria coherent amb la definició de superfície activa en el model de desactivació (DM).

També s'ha estudiat l'evolució de superfície reaccionades amb la RH mitjançant tres procediments: (1) exposició de la mostra a pressions de vapor altes (313 K i 80% de RH) i temps curts (2 hores); (2) exposició a condicions atmosfèriques (293-298 K, 60-80% de RH) a temps llargs (fins a 20 dies); (3) seguiment in-situ de l'evolució de la superfície del reactant en una atmosfera d'humitat controlada. Els resultats dels procediments (1) i (2) evidencien canvis substancials de la superfície dels sòlids reaccionats amb la RH, de tal manera que les estructures en forma d'agulla inicials s'agrupen formant estructures similars però de major mida (veure Fig. 4.40, 4.42). Comparant els resultats dels experiments corresponents als tres procediments es pot concloure que la quantitat d'aigua present a la fase gas podria tenir un efecte important sobre la cinètica d'aquest procés. Cal mencionar que s'han realitzat estudis per assegurar que el moviment dels cristalls és causat exclusivament a la presència d'aigua i que aquests moviments afecten principalment a les estructures en forma d'agulla del producte de reacció, és a dir que les estructures finals observades no són causades a partir de modificacions del monocristall de $Ca(OH)_2$.

Finalment, els resultats d'EDS sobre cristalls reaccionats tractats durant 4 h a 313 K i 80% de RH (veure Fig. 4.46) suggereixen que el procés d'agregació retira parcialment el producte dipositat sobre la superfície i genera nova superfície del reactant que estarà disponible per a què la reacció continuï.

2.4. PROPOSTA D'UN MECANISME DE REACCIÓ

Un mecanisme de reacció consistent amb el model DM-ISCM i amb els resultats experimentals obtinguts referits a l'efecte de l'aigua sobre la morfologia del reactant $Ca(OH)_2$ podria consistir en les següents etapes (veure Fig. 4.48):

1. Adsorció d'aigua sobre la superfície del sòlid

   D'acord amb la isoterma d'adsorció d'aigua sobre $Ca(OH)_2$, l'aigua tendeix a adsorbir-se formant multicapes –amb recobriments aproximats de 1.0, 1.3, 1.5, 2.0 i 3.0 per a valors de RH de 20, 30, 50, 70 i 90%, respectivament. Per a recobriments d'aigua superiors a 2.0 (RH>70%), la multicapa es podria comportar de forma similar a una capa d'aigua líquida.

2. Hidratació de SO_2 amb molècules d'aigua adsorbides a la superfície

   Tant en fase gasosa (*Loerting et al., 2000*) com en fase líquida (*Greenwood i Earnshaw, 1984*), el SO_2 es pot hidratar formant espècies $SO_2 \cdot zH_2O$ amb diferents valors de z. En aquest sentit, el SO_2 també podria hidratar-se amb molècules d'aigua adsorbides a la superfície del $Ca(OH)_2$. Aquesta proposta ve reforçada per la naturalesa quasi-líquida de la multicapa d'aigua formada, especialment a elevades RHs.

3. Reacció entre $SO_2 \cdot zH_2O$ i $Ca(OH)_2$

El mecanisme de la reacció implicaria probablement una orientació específica del dipol de les molècules de SO_2 hidratat a la superfície del $Ca(OH)_2$ enfront del cristall. A partir de l'estructura cristal·lina del $Ca(OH)_2$ i dels seus paràmetres de xarxa, juntament amb la distància S-O del SO_2, sembla que l'única disposició del SO_2 que condueixi a la reacció sigui la que implica un atac tangencial (veure Fig. 4.48c). Aleshores, el SO_2 podria evolucionar amb la formació d'un enllaç covalent entre el sofre del SO_2 i l'oxigen d'un HO^- de la xarxa cristal·lina del $Ca(OH)_2$, formant-se així un nou complex. El protó del HO^- que quedaria lliure es podria estabilitzar amb un altre io HO^- de la xarxa cristal·lina amb la formació d'una molècula de H_2O.

4. Difusió dels cristalls de productes i reestructuració de la superfície reaccionada.

   Els resultats obtinguts mitjançant les tècniques d'AFM i d'EDS mostren que un cop format el producte, aquest es pot desplaçar per la superfície i agregar-se amb d'altres cristalls amb la posterior formació d'estructures en forma d'agulla. Aquest moviment, que sembla trobar-se subjecte a la presència d'aigua, alliberaria nova superfície del $Ca(OH)_2$ que podria continuar reaccionant. Aquest procés podria venir representat pel paràmetre β del model DM, podent ésser conseqüentment considerat com a un paràmetre estructural.. A més, aquest paper de l'aigua sembla reforçar la possibilitat que tingui lloc la reacció (4.1) quan es presenta NO_2 a la fase gasosa.

5. Difusió en estat sòlid + reacció i/o reacció amb superfície activa residual del $Ca(OH)_2$

   Es poden proposar 2 mecanismes que podrien tenir lloc un cop formada una capa de producte. Ambdós són consistents amb l'observació experimental de que la reacció continua a temps llargs a baixes velocitats de reacció. El primer d'ells consistiria en la difusió d'ions Ca^{2+} i HO^- proposat en el model DM-ISCM (secció 2.2 d'aquest resum). El segon es basaria en considerar l'assoliment d'una etapa estacionària en què el producte es retiraria de la superfície a la mateixa velocitat que es generaria. D'aquesta forma, la superfície del $Ca(OH)_2$ presentaria algunes petites àrees parcialment desactivades on la reacció podria avançar, però a velocitats molt petites.

   Cal destacar que ambdós mecanismes també serien consistents amb els resultats d'alguns investigadors que indiquen que la velocitat de reacció a temps llarg no depèn de la concentració de SO_2. Mentre que la velocitat de reacció del primer mecanisme estaria controlada per la difusió iònica, la del segon es trobaria limitada per la velocitat d'eliminació del producte de la superfície.

   No s'han trobat evidències experimentals que permetin discernir entre ambdós mecanismes. Malgrat que ambdós podrien tenir lloc simultàniament, el predominant podria dependre de la relació entre la velocitat de la reordenació superficial i la velocitat de reacció. Així, la difusió iònica podria governar el procés a baixes relacions, mentre que el segon mecanisme ho faria a relacions properes a 1.

3. CONCLUSIONS

Les conclusions que es deriven d'aquest treball són les següents:

1. Les corbes de ruptura de SO_2 experimentals indiquen que la reacció de desulfuració no finalitza a elevats temps d'exposició (1-6 h), sinó que continua a velocitats molt baixes. Aquest període es podria explicar a partir del mecanisme de difusió iònica en estat sòlid o per la presència d'una superfície activa residual pràcticament constant. Ambdós mecanismes són consistents amb l'observació experimental que la cinètica d'aquest període depèn fortament de la humitat relativa.

2. Les dades cinètiques experimentals s'han simulat satisfactòriament amb el model semiempíric DM-ISCM. Aquest model té en compte la reducció de la superfície activa de $Ca(OH)_2$ amb l'avanç de la reacció i la difusió en estat sòlid dels ions Ca^{2+} i HO^- hidratats des de la interfase interna $Ca(OH)_2/CaSO_3{\cdot}(1/2)H_2O$ fins a l'externa de $CaSO_3(1/2){\cdot}H_2O$/gas.

3. El paper de l'aigua en la cinètica del sistema es reflecteix en els paràmetres del DM-ISCM (k_S, β i $\overline{D}^{P}_{Ca}$). El paràmetre β es pot considerar un paràmetre estructural relacionat amb la mobilitat del producte. El paràmetre k_S depèn de la hidratació de SO_2 en la superfície del reactant i inclou tres contribucions: la constant cinètica intrínseca de la reacció ($k_T(T)$), la constant d'equilibri d'hidratació de SO_2 (K_C) i la quantitat d'aigua adsorbida (θ_{H_2O}).

4. La microscòpia AFM és una eina apropiada per a l'estudi de la reacció entre el SO_2 i monocristalls de $Ca(OH)_2$ a baixa temperatura i en presència de vapor d'aigua. Ha permès visualitzar l'evolució de la morfologia de la superfície dels cristalls després d'haver reaccionat i després d'estar en contacte amb una atmosfera humida. Aquesta evolució ha estat essencial per entendre el paper de l'aigua en la reacció i proposar un mecanisme de reacció.

5. Els resultats obtinguts a partir de la tècnica d'AFM mostren evidències de la mobilitat i reordenació del producte cristal·lí de la reacció -$CaSO_3{\cdot}(1/2)H_2O$- sobre la superfície del cristall reactant -$Ca(OH)_2$- i de la posterior agregació dels cristalls de producte. Aquest procés estaria subjecte a la presència d'aigua adsorbida a la superfície del reactant. Aquest resultat suggereix que després de la generació del cristall de producte durant la reacció de desulfuració, aquest es retiraria de la seva posició i conseqüentment es podria generar nova superfície de $Ca(OH)_2$ que seria responsable del progrés de la reacció. Aquest procés podria justificar el paper del vapor d'aigua en la potenciació la reacció de desulfuració.

6. Un camí de reacció factible per a la reacció entre el NO_2 i $Ca(OH)_2$ implicaria dues reaccions consecutives: (1) reacció del NO_2 amb $Ca(OH)_2$ per a donar $Ca(NO_3)_2$ i $Ca(NO_2)_2$; (2) el $Ca(NO_3)_2$ format continuaria reaccionant amb l'aigua adsorbida i dismutaria a $NO_{(g)}$ i $Ca(NO_3)_2$. Ambdues reaccions són anàlogues a les que ocorren en fase aquosa (reaccions 1.9 i 1.10, respectivament). No obstant, en fase aquosa, la segona solament ocorre en condicions àcides, mentre que en fase sòlida sembla que únicament requereixi la presència d'aigua adsorbida.

7. Quan el SO_2 i NO_2 coexisteixen en fase gasosa es pot produir una reacció redox entre el $CaSO_3$ -producte de la retenció de SO_2- i el NO_2. Aquesta reacció, anàloga a la que es produeix en fase aquosa, podria ésser factible en presència d'aigua adsorbida, la qual podria facilitar el contacte entre els sòlids implicats -$CaSO_3$ i $Ca(OH)_2$.

8. La presència de NO_2 millora fortament la capacitat del $Ca(OH)_2$ per a capturar SO_2. Aquest resultat es podria explicar per la formació de $Ca(NO_3)_2$ i $Ca(NO_2)_2$, ja que presenten un caràcter higroscòpic que podria potenciar l'efecte de l'aigua sobre la reacció. Les corbes de ruptura de SO_2 obtingudes en presència de NO_2 s'ajusten satisfactòriament al model DM-ISCM.

9. La reacció entre el HCl i el $Ca(OH)_2$ forma preferentment l'espècie Ca(OH)Cl, malgrat que en certes condicions –no assajades en aquest treball- el producte final sembla ésser $CaCl_2$. S'ha obtingut que el Ca(OH)Cl és un compost higroscòpic, propietat que podria ésser rellevant en les aplicacions dels processos "in-duct". En qualsevol cas, ja que el $CaCl_2$ és molt més higroscòpic, si aquest darrer s'obté com a producte principal de reacció, els problemes operacionals podrien ésser molt més importants. D'altra banda, també s'ha obtingut que el Ca(OH)Cl és un compost estable en contacte amb l'atmosfera, de manera que en principi es podria dipositar en abocadors, contràriament al cas del $CaCl_2$, el qual pot filtrar-se fàcilment cap als subsòls.

10. Un camí de reacció factible per la reacció entre el HCl i el $Ca(OH)_2$ consistent amb tots els resultats experimentals obtinguts podria consistir en dues reaccions consecutives: (1) formació de l'espècie Ca(OH)Cl i (2) formació de $CaCl_2$ a partir de la reacció entre el Ca(OH)Cl i el HCl. Es podria suggerir un control cinètic d'aquestes reaccions, de forma que, depenent de les condicions de treball, la segona reacció no tindria lloc. La segona reacció es trobaria afavorida a elevades concentracions de HCl, altes temperatures i temps de reacció llargs.